NOVEL INSIGHTS INTO ALGAL BIOLOGY AND BIOTECHNOLOGY

EDITED BY: Yuval Kaye, Yandu Lu, Jianhua Fan, Haojie Jin, Youn-Il Park, Peer Schenk and Jianfeng Niu

PUBLISHED IN: Frontiers in Plant Science and Frontiers in Bioengineering and Biotechnology

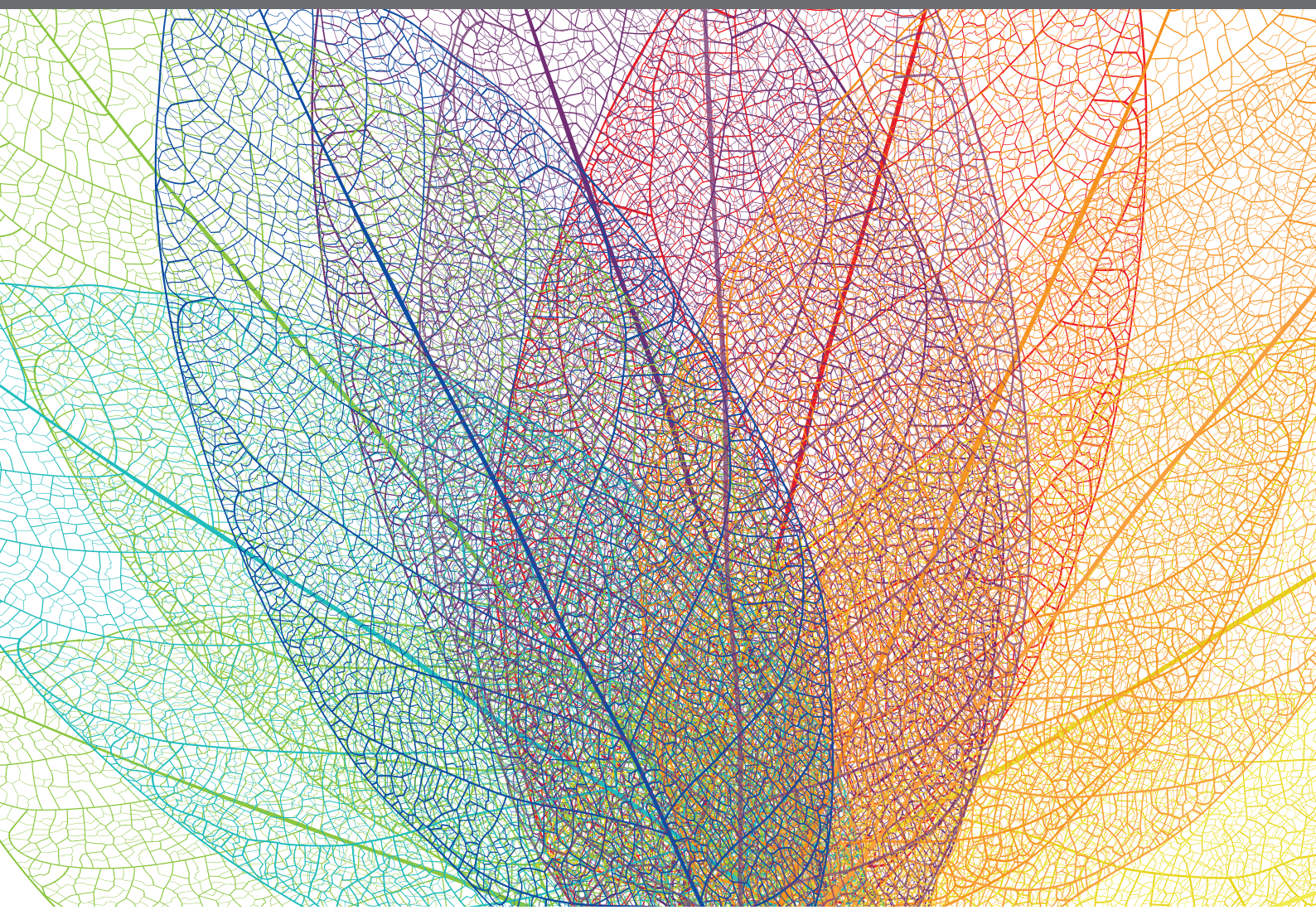

frontiers Research Topics

ISSN 1664-8714
ISBN 978-2-88945-867-7
DOI 10.3389/978-2-88945-867-7

About Frontiers

Frontiers is more than just an open-access publisher of scholarly articles: it is a pioneering approach to the world of academia, radically improving the way scholarly research is managed. The grand vision of Frontiers is a world where all people have an equal opportunity to seek, share and generate knowledge. Frontiers provides immediate and permanent online open access to all its publications, but this alone is not enough to realize our grand goals.

Frontiers Journal Series

The Frontiers Journal Series is a multi-tier and interdisciplinary set of open-access, online journals, promising a paradigm shift from the current review, selection and dissemination processes in academic publishing. All Frontiers journals are driven by researchers for researchers; therefore, they constitute a service to the scholarly community. At the same time, the Frontiers Journal Series operates on a revolutionary invention, the tiered publishing system, initially addressing specific communities of scholars, and gradually climbing up to broader public understanding, thus serving the interests of the lay society, too.

Dedication to Quality

Each Frontiers article is a landmark of the highest quality, thanks to genuinely collaborative interactions between authors and review editors, who include some of the world's best academicians. Research must be certified by peers before entering a stream of knowledge that may eventually reach the public - and shape society; therefore, Frontiers only applies the most rigorous and unbiased reviews.
Frontiers revolutionizes research publishing by freely delivering the most outstanding research, evaluated with no bias from both the academic and social point of view. By applying the most advanced information technologies, Frontiers is catapulting scholarly publishing into a new generation.

What are Frontiers Research Topics?

Frontiers Research Topics are very popular trademarks of the Frontiers Journals Series: they are collections of at least ten articles, all centered on a particular subject. With their unique mix of varied contributions from Original Research to Review Articles, Frontiers Research Topics unify the most influential researchers, the latest key findings and historical advances in a hot research area! Find out more on how to host your own Frontiers Research Topic or contribute to one as an author by contacting the Frontiers Editorial Office: researchtopics@frontiersin.org

NOVEL INSIGHTS INTO ALGAL BIOLOGY AND BIOTECHNOLOGY

Topic Editors:
Yuval Kaye, Carnegie Institution for Science (CIS), United States
Yandu Lu, Hainan University, China
Jianhua Fan, East China University of Science and Technology, China
Haojie Jin, Carnegie Institution for Science (CIS), United States
Youn-Il Park, Chungnam National University, South Korea
Peer Schenk, University of Queensland, Australia
Jianfeng Niu, Institute of Oceanology (CAS), China

Citation: Kaye, Y., Lu, Y., Fan, J., Jin, H., Park, Y.-I., Schenk, P., Niu, J., eds. (2019). Novel Insights into Algal Biology and Biotechnology. Lausanne: Frontiers Media. doi: 10.3389/978-2-88945-867-7

Table of Contents

frontiers in Plant Science

ORIGINAL RESEARCH
published: 31 October 2018
doi: 10.3389/fpls.2018.01532

A Stepwise $NaHSO_3$ Addition Mode Greatly Improves H_2 Photoproduction in *Chlamydomonas reinhardtii*

*Lanzhen Wei†, Xin Li†, Baoqiang Fan†, Zhaoxing Ran and Weimin Ma**

College of Life and Environment Science, Shanghai Normal University, Shanghai, China

$NaHSO_3$ addition greatly increases the yield of H_2 photoproduction in a unicellular green alga *Chlamydomonas reinhardtii* through removing O_2 and activating hydrogenase but significantly impairs the activity of PSII, an electron source for H_2 photoproduction. Here, a stepwise addition mode of total 13 mM $NaHSO_3$, an optimal concentration for H_2 photoproduction of *C. reinhardtii* identified in a previous one step addition method, significantly improved H_2 photoproduction. Such improvement was believed to be the result of increased residual PSII activity in an anaerobic background, but was at least independent of two alternative electron sinks for H_2 photoproduction, cyclic electron transport around PSI and CO_2 assimilation. Based on the above results, we propose that increased residual PSII activity in an anaerobic environment is an efficient strategy to enhance H_2 photoproduction in *C. reinhardtii*, and the stepwise $NaHSO_3$ addition mode is a case study in the strategy.

Keywords: $NaHSO_3$, stepwise mode, anaerobic environment, PSII activity, H_2 photoproduction, *Chlamydomonas reinhardtii*

OPEN ACCESS

Edited by:
Yandu Lu,
Hainan University, China

Reviewed by:
Emilio Fernandez,
Universidad de Córdoba, Spain
Hongmin Qin,
Texas A&M University, United States
Weichao Huang,
Carnegie Institution for Science (CIS), United States

****Correspondence:***
Weimin Ma
wma@shnu.edu.cn

† These authors have contributed equally to this work

Specialty section:
This article was submitted to Plant Biotechnology, a section of the journal Frontiers in Plant Science

Received: *27 February 2018*
Accepted: *28 September 2018*
Published: *31 October 2018*

Citation:
Wei L, Li X, Fan B, Ran Z and Ma W (2018) A Stepwise $NaHSO_3$ Addition Mode Greatly Improves H_2 Photoproduction in Chlamydomonas reinhardtii. Front. Plant Sci. 9:1532. doi: 10.3389/fpls.2018.01532

INTRODUCTION

With the increasing awareness of fossil fuel depletion and global warming, efforts have been undertaken to develop clean and sustainable energy sources (McKendry, 2002). Molecular hydrogen (H_2) is one of the potential future energy sources (Hansel and Lindblad, 1998; Momirlan and Veziroglu, 2002). *C. reinhardtii*, a unicellular green alga, has been recognized as an ideal system for sustainable H_2 photoproduction under anaerobic conditions; however, this alga cannot efficiently and continuously produce H_2 in an aerobic environment because its H_2ase is extremely sensitive to O_2 (Ghirardi et al., 1997). To activate H_2ase for sustainable and efficient H_2 photoproduction in *C. reinhardtii*, therefore, numerous strategies have been extensively developed mainly through engineering O_2 tolerance in H_2ase (Flynn et al., 2002; Liebgott et al., 2011; Wu et al., 2011) or decreasing O_2 content around H_2ase (Melis et al., 2000; Kruse et al., 2005; Surzycki et al., 2007; Wu et al., 2010; Xu et al., 2011; Jurado-Oller et al., 2015; Xiong et al., 2015; Shu et al., 2018).

Abbreviations: AA, antimycin A; CET, cyclic electron transport around PSI; Chl, chlorophyll; *C. reinhardtii*, *Chlamydomonas reinhardtii*; DCMU, 3-(3,4-dichlorophenyl)-1,1-dimethylurea; DO, dissolved oxygen; F_v/F_m, maximal quantum yield of PSII; GA, glycolaldehyde; H_2ase, hydrogenase; Lin, lincomycin; MV, methyl viologen; one step method, a one step addition method of $NaHSO_3$; stepwise mode, a stepwise addition mode of $NaHSO_3$; TAP, Tris-acetate-phosphate.

Meanwhile, our studies demonstrate that $NaHSO_3$ addition strategy is capable of decreased the O_2 content around H_2ase, thereby activating the enzyme activity and promoting H_2 photoproduction (Wang et al., 2010; Ma et al., 2011; Wei et al., 2017). This strategy can result in an approximately 10-fold or 200-fold increase in H_2 photoproduction in the nitrogen-fixing cyanobacterium *Anabaena* sp. strain PCC 7120 (Wang et al., 2010) or the unicellular green alga *C. reinhardtii* (Ma et al., 2011; Wei et al., 2017), respectively. Despite these increases, this yield is still not sufficient to meet the requirements of industrial applications. Thus, extensive optimization of this $NaHSO_3$ addition strategy is necessary to increase H_2 photoproduction in *C. reinhardtii* further.

The yield of H_2 photoproduction caused by sulfur deprivation is also not sufficient to meet the requirements of industrial applications. Under sulfur deprivation conditions, therefore, many strategies have been developed to improve the yield of H_2 photoproduction in *C. reinhardtii* via metabolic and genetic engineering (for review, see Esquível et al., 2011; Dubini and Ghirardi, 2015). Among them, increased residual photosystem II (PSII) activity was found to play a vital role in efficient H_2 photoproduction (Zhang et al., 2002; Kosourov et al., 2005; Kim et al., 2010; Volgusheva et al., 2013; Grewe et al., 2014; Steinbeck et al., 2015; Chen et al., 2016), since the PSII activity is significantly impaired by sulfur deprivation (Melis et al., 2000). Similarly, in the $NaHSO_3$ addition background, the PSII activity is also significantly impaired (Wang et al., 2010). To test whether increased residual PSII activity in the $NaHSO_3$ addition background can also enhance H_2 photoproduction, we monitored the accumulated H_2 level and residual PSII activity in the stepwise mode of total 13 mM $NaHSO_3$, an optimal concentration for H_2 production of *C. reinhardtii* identified in a previous one step addition method (Ma et al., 2011). We also measured the content of dissolved O_2 and activities of two alternative electron sinks for H_2 photoproduction, CET and CO_2 assimilation, in the stepwise $NaHSO_3$ addition mode. Our results demonstrate that the stepwise $NaHSO_3$ addition mode evidently enhances the yield of H_2 photoproduction in *C. reinhardtii*; such enhancement is mostly the result of increased residual PSII activity in an anaerobic environment, but is at least independent of two alternative electron sinks for H_2 photoproduction.

MATERIALS AND METHODS

Culture Conditions

Cells of *C. reinhardtii* (CC-503 strain) were cultured at 25°C in TAP medium (Harris, 1989). The medium was buffered with Tris–HCl (20 mM; pH 7.3), bubbled with air under continuous illumination with cool-white fluorescent lamps (40 μmol photons $m^{-2}s^{-1}$), and inoculated with approximately 8.1×10^4 cells mL^{-1} of *C. reinhardtii* (inoculum size, 1%).

Sample Preparation and $NaHSO_3$ Addition

Cells of *C. reinhardtii* were continuously illuminated by growth light of 40 μmol photons $m^{-2}s^{-1}$ and were cultured in 0.5 L of TAP medium for 2 days with bubble aeration (A_{750} = 0.8–1.0), after which a fixed volume of cells containing 300 μg of Chl was transferred to 60 mL serum bottles (30 mL head space and 30 mL cells) with rubber seals. After cells were statically pre-cultured under continuous illumination of 200 μmol photons $m^{-2}s^{-1}$ for 36 h, total 13 mM of $NaHSO_3$ was directly or step by step added to the serum bottles, as indicated in **Figures 1**, **2**, **Supplementary Figure S1**, and described in **Table 1**, with Lin of 5 mM (final concentration) or AA of 10 μM (final concentration) or GA of 2 mM (final concentration) or DCMU of 20 μM (final concentration) or not. Subsequently, the

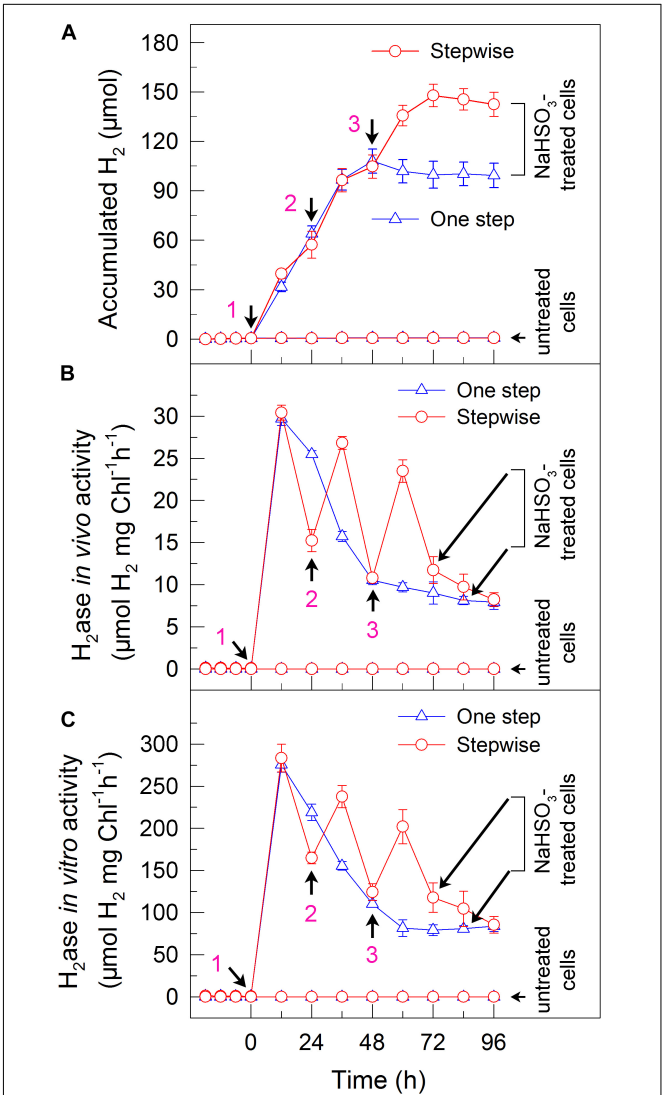

FIGURE 1 | A stepwise $NaHSO_3$ addition mode significantly increases **(A)** H_2 photoproduction, and **(B)** *in vivo* and **(C)** *in vitro* H_2ase activity in *C. reinhardtii*. After cells were statically pre-cultured under continuous illumination of 200 μmol photons $m^{-2}s^{-1}$ for 36 h, total 13 mM of $NaHSO_3$ was directly or step by step added to the serum bottles, as indicated by arrows 1–3 and described in **Table 1**. Values are means ± SD (n = 5).

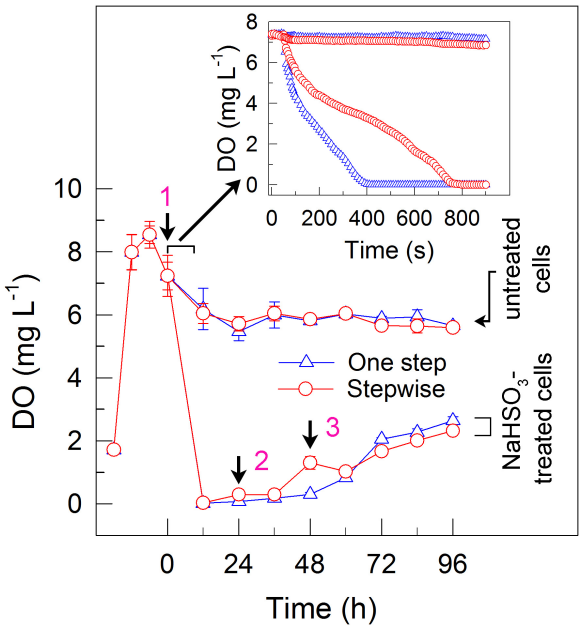

FIGURE 2 | A stepwise $NaHSO_3$ addition mode influences the content of dissolved oxygen (DO) in *C. reinhardtii*. Pre-culture conditions of cells and addition modes of $NaHSO_3$ are shown in the legend of **Figure 1**. Values are means ± SD (n = 5).

TABLE 1 | A table schematically represents one step method and stepwise mode of total 13 mM $NaHSO_3$.

$NaHSO_3$ addition	$NaHSO_3$ (mM)			
	Arrow 1	Arrow 2	Arrow 3	Total
One step method	13	0	0	13
Stepwise mode	9	2	2	13

*Arrows 1–3 shown in **Figures 1–5** and both arrows have a 24 h interval.*

cells were still illuminated at 200 μmol photons $m^{-2}s^{-1}$ or were incubated in the dark to induce the production of H_2.

Monitoring H_2 Photoproduction

At predetermined time intervals, 200 μL of gas samples were withdrawn from the bottles using a gas-tight syringe and injected into a gas chromatograph (Agilent 7890A; Agilent Technologies Inc., United States) with a thermal conductivity detector for determining the concentrations of H_2, O_2, and N_2 simultaneously. The column of the gas chromatograph was a molecular sieve column (type 5Å; 2 m × 1/8 mm), and argon was used as the carrier gas.

H_2ase Activity Assay

In vivo and *in vitro* H_2ase activity was monitored as described earlier (Ma et al., 2011; Wei et al., 2013, 2017) with some modifications. In brief, 1 mL cell suspension samples upon exposure to 200 μmol photons $m^{-2}s^{-1}$ were anaerobically withdrawn from the 60 mL serum bottles at designated time points (see **Figures 1B,C**) and then injected into 10 mL glass vials. To measure *in vivo* H_2ase activity, the cell suspension samples were immediately purged with argon gas for 1 min to eliminate the inhibitory effect of O_2 on the H_2ase activity. The cell suspension samples were then placed in a 25°C water bath for 1 h and shaken continuously (150 rpm) whilst exposed to a constant light of 200 μmol photons $m^{-2}s^{-1}$. To measure *in vitro* H_2ase activity, we used vials containing 1 mL of 10 mM oxidized MV prepared in O_2-free 50 mM Tris buffer (for pH 7.1–9.0) and 0.2% (*w*/*v*) Triton X-100. The reaction was started when MV was reduced by the addition of 100 μL of 100 mM anaerobic sodium dithionite in 0.03 N NaOH. This assay was performed at 37°C in the dark for 20 min. We determined the amount of H_2 produced in the headspace of the glass vial by gas chromatography, and the rate of H_2 production was calculated on the basis of the total Chl content in the glass vial, unless otherwise indicated.

Dissolved Oxygen Measurement

Dissolved oxygen was monitored as described earlier (Wei et al., 2017). In brief, a DO meter (Orion Star A213, Thermo Scientific, Untied States) was used to monitor the DO attenuation process after the addition of $NaHSO_3$ to the cell suspension cultures of *C. reinhardtii*. The DO meter was corrected before each measurement. The DO meter probe was placed in the middle of the cell suspension cultures and the data were recorded at several designated time points.

Chl Fluorescence and P700 Analysis

The yields of Chl fluorescence at a steady-state of electron transport were measured at room temperature using a Dual-PAM-100 monitoring system (Walz, Effeltrich, Germany) equipped with an ED-101US/MD unit (Schreiber et al., 1986; Ma et al., 2008; Wei et al., 2013, 2017). Minimal fluorescence at open PSII centers in the dark-adapted state (F_o) was excited by a weak measuring light (650 nm) at a photon flux density of 0.05–0.15 μmol photons $m^{-2}s^{-1}$. A saturating pulse of red light (600 ms, 10,000 μmol photons $m^{-2}s^{-1}$) was applied to determine the maximal fluorescence at closed PSII centers in the dark-adapted state (F_m). F_v/F_m was evaluated as $(F_m-F_o)/F_m$ (Kitajima and Butler, 1975; Wei et al., 2013, 2017).

The reduction of $P700^+$ in darkness was measured with the aforementioned Dual-PAM-100 fluorometer by monitoring absorbance changes at 830 nm and using 875 nm as a reference. Cells were kept in the dark for 2 min, and 10 μM of DCMU was added to the cell suspension cultures prior to the measurement. The P700 was oxidized by far-red light with a maximum at 720 nm from a light-emitting diode lamp for 30 s, and the subsequent re-reduction of $P700^+$ in the dark was monitored and its half-time was calculated.

Oxygen Evolution Activity

Oxygen production in intact *C. reinhardtii* cells by photosynthesis was determined at 25°C by monitoring the changes in O_2 levels with a Clark-type oxygen electrode (Hansatech Instruments, King's Lynn, United Kingdom). Prior to the measurements, 10 mM of $NaHCO_3$ was added to the

cell suspension cultures. The intensity of light used for the measurements was 1,000 μmol photons $m^{-2}s^{-1}$.

RESULTS

A Stepwise $NaHSO_3$ Addition Mode Significantly Increases the Yield of H_2 Photoproduction in *C. reinhardtii*

To test whether a stepwise $NaHSO_3$ addition mode can enhance the yield of H_2 photoproduction, we monitored accumulated H_2 amounts in the one step addition method and stepwise mode of total 13 mM $NaHSO_3$ (hereafter one step method and stepwise mode, respectively; see **Table 1**), an optimal concentration for H_2 photoproduction of *C. reinhardtii* identified in a previous one step method (Ma et al., 2011). Compared to the one step method, stepwise mode evidently enhanced the yield of H_2 photoproduction (**Figure 1A** and **Table 2**). The H_2 level in stepwise mode was approximately 1.5 times greater than that in one step method and, approximately 350 times greater than that in untreated cells (**Figure 1A** and **Table 2**). This was confirmed by the results of *in vivo* (**Figure 1B**) and *in vitro* (**Figure 1C**) H_2ase activity. We therefore conclude that the stepwise mode considerably improves H_2 photoproduction in the green alga *C. reinhardtii*.

The Stepwise Mode Can Also Establish an Anaerobic Environment

To elucidate the mechanism underlying the increase in the H_2 yield under stepwise mode, we monitored the dissolved O_2 (DO) content in the cell suspension cultures of *C. reinhardtii*. The results indicated that addition of total 13 mM $NaHSO_3$ to the cell suspension cultures in both the one step method and stepwise mode can similarly create an anaerobic environment (**Figure 2**), although the stepwise mode was slightly slow to generate an anaerobic environment when compared to the one step method (insert in **Figure 2**). It is worthy of note that, when an initial concentration of $NaHSO_3$ in stepwise mode was less than or equal to 7 mM, the cell suspension cultures did not enter or maintain an anaerobic environment, which evidently suppressed the increase of H_2 photoproduction in the stepwise mode (data not shown). Based on the above results, we propose that the stepwise mode is necessary to operate in an anaerobic environment as an efficient strategy for H_2 photoproduction in *C. reinhardtii*.

TABLE 2 | Comparison of H_2 photoproduction characteristics in *C. reinhardtii* between one step method and stepwise mode.

$NaHSO_3$ addition	Vmax (μmol H_2 mg $Chl^{-1}h^{-1}$)[1]	Amax (relative; %)[2]	Time (day)[3]
One step method	11.8 ± 0.7	100 ± 6.9	50.2 ± 3.2
Stepwise mode	14.7 ± 1.2	145.6 ± 5.1	76.1 ± 2.8

*[1]Vmax indicates the maximum velocity of H_2 photoproduction. [2]Amax indicates the maximum accumulated H_2 (calculated from **Figure 1A**) and its value in one step method was taken as 100%. [3]Time represents the time of continuous H_2 production, which was calculated from **Figure 1A**.*

The Stepwise Mode Maintains a Relatively High Residual Activity of Electron Source for H_2 Photoproduction

To understand why the stepwise mode can increase the yield of H_2 photoproduction, we measured the activity of PSII, an electron source for H_2 photoproduction. After the addition of total 13 mM $NaHSO_3$ to the cell suspension cultures, the residual activity of PSII was much higher in stepwise mode than that in one step method, as evaluated by the F_v/F_m values (**Figure 3**). This was supported by the results that the stepwise mode maintained a slightly high DO content at an efficient H_2 production stage when compared to the one step method (**Figure 2**). This implies that the relatively high PSII activity under anaerobic conditions is an important reason for improved H_2 photoproduction in the stepwise mode.

The Stepwise Mode Slightly Enhances the Activities of Two Alternative Electron Sinks for H_2 Photoproduction

We also measured the activities of CET and CO_2 assimilation, two alternative electron sinks for H_2 photoproduction. The rates of CET and CO_2 assimilation were slightly faster in the stepwise mode than those in the one step method, as estimated by the rate of re-reduction of $P700^+$ (**Figure 4**), and photosynthetic production of O_2 with $NaHCO_3$ as an artificial electron acceptor (**Figure 5**), respectively. It appears plausible that at least the two alternative electron sinks for H_2 photoproduction do not contribute to enhance the photoproduction of H_2 in the stepwise mode. If this possibility is true, an increase in H_2 photoproduction caused by impaired the activity of either CET or CO_2 assimilation will be higher in the stepwise mode than that in the one step method. The results shown in **Figure 6** support our hypothesis that the increase in H_2 photoproduction

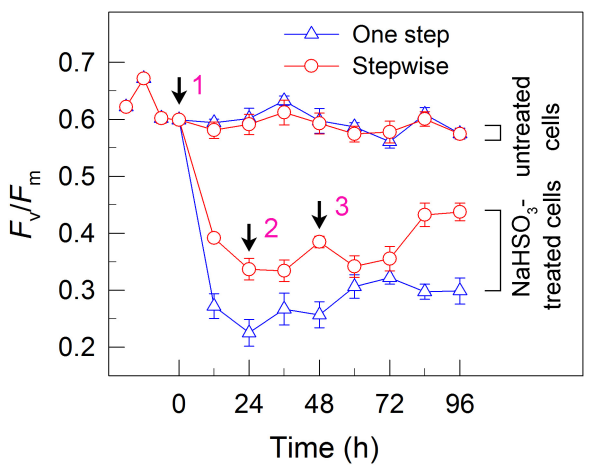

FIGURE 3 | A stepwise addition mode alleviates the inhibitory effects of $NaHSO_3$ on PSII activity in *C. reinhardtii*. The Chl concentration was adjusted to 10 μg mL^{-1} before measurement. PSII activity was evaluated by the F_v/F_m values. Values are means ± SD (n = 5).

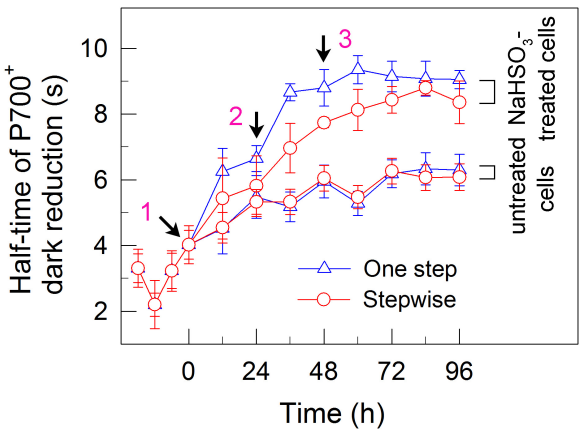

FIGURE 4 | A stepwise addition mode slightly alleviates the inhibitory effects of $NaHSO_3$ on cyclic electron transport around PSI in *C. reinhardtii*. The rate of cyclic electron transport around PSI was judged by half-time of $P700^+$ dark reduction. Values are means ± SD (n = 5).

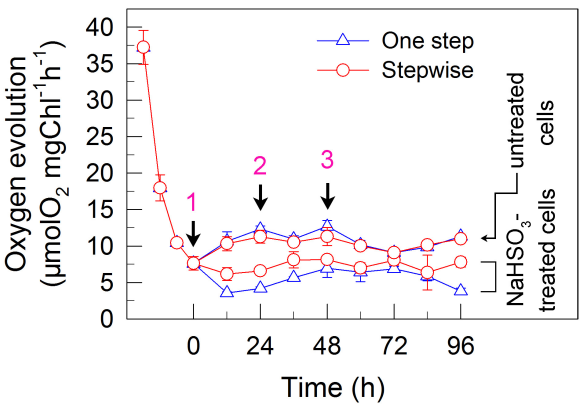

FIGURE 5 | A stepwise addition mode slightly alleviates the inhibitory effects of $NaHSO_3$ on CO_2 assimilation in *C. reinhardtii*. Activity of CO_2 assimilation was assessed by photosynthetic production of O_2 with $NaHCO_3$ as an artificial electron acceptor. Values are means ± SD (n = 5).

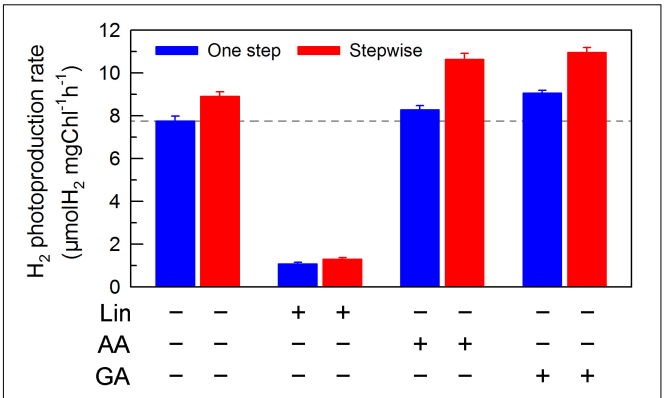

FIGURE 6 | Comparison of the H_2 photoproduction in *C. reinhardtii* between one step method and stepwise mode with multiple inhibitors. After cells were statically pre-cultured under continuous illumination of 200 μmol photons $m^{-2}s^{-1}$ for 36 h, $NaHSO_3$ was added as described in the legend for **Figure 1**, as well as several inhibitors, lincomycin (Lin; 5 mM), antimycin A (AA; 10 μM), and glycolaldehyde (GA; 2 mM) were also added to the serum bottles, respectively. Values are means ± SD (n = 5).

was slightly higher in the stepwise mode than that in the one step method in the presence of either AA that specifically inhibits the CET activity (Tagawa et al., 1963) or GA that disrupts the Calvin–Benson cycle activity via inhibiting the phosphoribulokinase (Rühle et al., 2008). Taking all these results together, we may conclude that in the anaerobic background, increased residual PSII activity can significantly enhance the yield of H_2 photoproduction in *C. reinhardtii*.

If this conclusion is true, impaired PSII activity in an anaerobic environment created by $NaHSO_3$ addition will inevitably decrease the yield of H_2 photoproduction in *C. reinhardtii* at a significant level. As expected, the H_2 photoproduction rate was significantly decreased in the presence of Lin, which impairs the PSII activity via inhibiting the D1 protein synthesis (Vavilin et al., 1995), regardless of either one step method or stepwise mode (**Figure 6**). This consolidates our conclusion that increased residual PSII activity in an anaerobic environment is an efficient strategy to improve H_2 photoproduction in *C. reinhardtii* and the stepwise $NaHSO_3$ addition mode is a case study in this strategy.

DISCUSSION

Whether $NaHSO_3$ addition promotes photosynthesis or H_2 photoproduction depends on its concentrations: $NaHSO_3$ in a low amount improves photosynthesis (Wang et al., 2003) but in a moderate amount can enhance H_2 photoproduction (Wang et al., 2010; Ma et al., 2011). Wang et al. (2003) demonstrate that a low amount (100 μM) of $NaHSO_3$ increases cyclic photophosphorylation and consequently improves photosynthesis via optimizing the ATP/NADPH ratio. By contrast, Wei et al. (2017) demonstrate that a moderate amount (13 mM) of $NaHSO_3$ can remove O_2 efficiently through the reaction of bisulfite with superoxide anion produced at the acceptor side of PSI, especially under sufficient light conditions, consequently activates H_2ase and promotes H_2 photoproduction. The results of this study indicate that a moderate amount of $NaHSO_3$ under a stepwise addition mode can quickly establish an anaerobic environment (**Figure 2**) and significantly improves H_2 photoproduction in a unicellular green alga *C. reinhardtii* (**Table 1** and **Figure 1**). Such improvement is at least independent of two alternative electron sinks for H_2 photoproduction, CET (**Figures 4**, **6**), and CO_2 assimilation (**Figures 5**, **6**) and, most likely the result of maintained a relatively high electron source for H_2 photoproduction, PSII activity (**Figures 3**, **6**).

Under a photon flux density of 200 μmol photons $m^{-2}s^{-1}$, the Mehler reaction is usually considered to also be an important alternative electron sink for H_2 photoproduction. However, we found that the Mehler reaction is almost absent in $NaHSO_3$ addition strategy, regardless of either one step method or stepwise mode (data not shown), possibly because addition of $NaHSO_3$ to

the cell suspension cultures quickly results in entering of cells to an anaerobic environment (less than 800 s) (**Figure 2**). Therefore, the improvement of H_2 photoproduction in *C. reinhardtii* by a moderate amount of $NaHSO_3$ under a stepwise addition mode is also independent of a third alternative electron sink for H_2 photoproduction, Mehler reaction, and consolidating the above mentioned possibility that such improvement is the result of increased residual PSII activity, an electron source for H_2 photoproduction.

Based on different sources of electrons to H_2ase, three pathways for H_2 production have been identified in *C. reinhardtii*. Their sources of electrons to H_2ase come from water photolysis via PSII (Melis et al., 2000; Kosourov et al., 2003), NADPH through type II NAD(P)H dehydrogenase (Baltz et al., 2014) and the fermentative degradation of endogenous compounds (Gfeller and Gibbs, 1985), respectively. We observed that production of H_2 under photon flux densities of 200 μmol photons $m^{-2}s^{-1}$ by $NaHSO_3$ addition was almost completely suppressed in cells incubated in the dark (**Supplementary Figures S1A,B**) or treated with DCMU (**Supplementary Figures S1A,C**). A quick establishment of anaerobic environment by $NaHSO_3$ addition (**Figure 2**) suppresses the acetate uptake (Jurado-Oller et al., 2015) and impairs the mitochondrial respiratory electron transport chain function. Taking all these results together, we propose that in the $NaHSO_3$ addition strategy, the source of electrons for H_2 production predominantly, if not totally, comes from water photolysis via PSII, regardless of either the one step method or the stepwise mode.

The results of this study further indicate that the stepwise mode increased the maximum accumulated H_2 levels, produced a higher maximum velocity of H_2 photoproduction, and prolonged the time length of H_2 photoproduction when compared to the one step method (**Table 2**). We thus propose that the stepwise mode developed in this study is an efficient and sustained strategy for improving H_2 photoproduction in the green alga *C. reinhardtii*.

Although a moderate amount of $NaHSO_3$ can remove efficiently O_2, the activity of PSII, an electron source for H_2 photoproduction, is also significantly impaired (Wang et al., 2010; Ma et al., 2011; Wei et al., 2017). The results of this study observe that in the anaerobic background, a stepwise mode maintains a relatively high PSII activity (**Figure 3**) and consequently promotes H_2 photoproduction (**Figure 1**). The cause and effect of PSII activity and H_2 photoproduction is also present in the sulfur-deprived strategy (Zhang et al., 2002; Kosourov et al., 2005; Kim et al., 2010; Volgusheva et al., 2013; Grewe et al., 2014; Steinbeck et al., 2015; Chen et al., 2016) but the reasons why H_2 photoproduction is terminated in sulfur deprivation and $NaHSO_3$ addition strategies are distinctly different. It is known that H_2 photoproduction is terminated in the sulfur deprivation strategy because of cell death (Nguyen et al., 2008) and in the $NaHSO_3$ addition strategy because of conversion of too much bisulfite to sulfate (Wei et al., 2017). It is worthy of note that the relationship between H_2 production and biomass accumulation in sulfur deprivation and $NaHSO_3$ addition strategies is also distinctly different. Regardless of either one step method or stepwise mode, the simultaneous production of H_2 and biomass is present in $NaHSO_3$ addition strategy, as observed in mixotrophic nutrient-replete cultures under low light conditions (Jurado-Oller et al., 2015), but is absent in sulfur deprivation strategy. Therefore, it appears reasonable that improved PSII activity in the $NaHSO_3$ background is considered to be a better strategy to meet future application requirements in comparison with that in the sulfur-deprived background.

AUTHOR CONTRIBUTIONS

WM designed and supervised the experiments. XL, BF, and ZR performed the experiments and analyzed the data. LW and WM analyzed and interpreted the data and wrote the article.

FUNDING

This work was supported by the Shanghai Science and Technology Committee (Grant No. 17070502900) and National Natural Science Foundation of China (Grant Nos. 31570235 and 31770259).

SUPPLEMENTARY MATERIAL

The Supplementary Material for this article can be found online at: https://www.frontiersin.org/articles/10.3389/fpls.2018.01532/full#supplementary-material

REFERENCES

Baltz, A., Dang, K. V., Beyly, A., Auroy, P., Richaud, P., Cournac, L., et al. (2014). Plastidial expression of type II NAD(P)H dehydrogenase increases the reducing state of plastoquinones and hydrogen photoproduction rate by the indirect pathway in *Chlamydomonas reinhardtii*. *Plant Physiol.* 165, 1344–1352. doi: 10.1104/pp.114.240432

Chen, M., Zhang, J., Zhao, L., Xing, J., Peng, L., Kuang, T., et al. (2016). Loss of algal proton gradient regulation 5 increases reactive oxygen species scavenging and H_2 evolution. *J. Integr. Plant Biol.* 58, 943–946. doi: 10.1111/jipb.12502

Dubini, A., and Ghirardi, M. L. (2015). Engineering photosynthetic organisms for the production of biohydrogen. *Photosynth. Res.* 123, 241–253. doi: 10.1007/s11120-014-9991-x

Esquível, M. G., Amaro, H. M., Pinto, T. S., Fevereiro, P. S., and Malcata, F. X. (2011). Efficient H_2 production via *Chlamydomonas reinhardtii*. *Trends Biotechnol.* 29, 595–600. doi: 10.1016/j.tibtech.2011.06.008

Flynn, T., Ghirardi, M. L., and Seibert, M. (2002). Accumulation of O_2-tolerant phenotypes in H_2-producing strains of *Chlamydomonas reinhardtii* by sequential applications of chemical mutagenesis and selection. *Int. J. Hydrogen Energy* 27, 1421–1430. doi: 10.1016/S0360-3199(02)00117-9

Gfeller, R. P., and Gibbs, M. (1985). Fermentative metabolism of *Chlamydomonas reinhardtii*: II. Role of plastoquinone. *Plant Physiol.* 77, 509–511. doi: 10.1104/pp.77.2.509

Ghirardi, M. L., Togasaki, R. K., and Seibert, M. (1997). Oxygen sensitivity of algal H_2 production. *Appl. Microbiol. Biotechnol.* 63, 141–151. doi: 10.1007/BF02920420

Grewe, S., Ballottari, M., Alcocer, M., D'Andrea, C., Blifernez-Klassen, O., Hankamer, B., et al. (2014). Light-harvesting complex protein LHCBM9 is critical for photosystem II activity and hydrogen production in *Chlamydomonas reinhardtii*. *Plant Cell* 26, 1598–1611. doi: 10.1105/tpc.114.124198

Hansel, A., and Lindblad, P. (1998). Towards optimization of cyanobacteria as biotechnologically relevant producers of molecular hydrogen, a clean and renewable energy source. *Appl. Microbiol. Biotechnol.* 50, 153–160. doi: 10.1007/s002530051270

Harris, E. H. (1989). *The Chlamydomonas Sourcebook: A Comprehensive Guide to Biology and Laboratory Use*. San Diego, CA: Academic Press.

Jurado-Oller, J. L., Dubini, A., Galván, A., Fernández, E., and González-Ballester, D. (2015). Low oxygen levels contribute to improve photohydrogen production in mixotrophic non-stressed *Chlamydomonas* cultures. *Biotechnol. Biofuels* 8:149. doi: 10.1186/s13068-015-0341-9

Kim, J. P., Kim, K. R., Choi, S. P., Han, S. J., Kim, M. S., and Sim, S. J. (2010). Repeated production of hydrogen by sulfate re-addition in sulfur deprived culture of *Chlamydomonas reinhardtii*. *Int. J. Hydrogen Energy* 35, 13387–13391. doi: 10.1016/j.ijhydene.2009.11.113

Kitajima, M., and Butler, W. (1975). Quenching of chlorophyll fluorescence and primary photochemistry in chloroplasts by dibromothymoquinone. *Biochim. Biophys. Acta* 376, 105–115. doi: 10.1016/0005-2728(75)90209-1

Kosourov, S., Makarova, V., Fedorov, A. S., Tsygankov, A., Seibert, M., and Ghirardi, M. L. (2005). The effect of sulfur re-addition on H_2 photoproduction by sulfur-deprived green algae. *Photosynth. Res.* 85, 295–305. doi: 10.1007/s11120-005-5105-0

Kosourov, S., Seibert, M., and Ghirardi, M. L. (2003). Effects of extracellular pH on the metabolic pathways in sulfur-deprived, H_2-producing *Chlamydomonas reinhardtii* cultures. *Plant Cell Physiol.* 44, 146–155. doi: 10.1093/pcp/pcg020

Kruse, O., Rupprecht, J., Bader, K. P., Thomas-Hall, S., Schenk, P. M., Finazzi, G., et al. (2005). Improved photobiological H_2 production in engineered green algal cells. *J. Biol. Chem.* 280, 34170–34177. doi: 10.1074/jbc.M503840200

Liebgott, P. P., Dementin, S., Léger, C., and Rousset, M. (2011). Towards engineering O_2-tolerance in [Ni–Fe] hydrogenases. *Energy Environ. Sci.* 4, 33–41. doi: 10.1039/C0EE00093K

Ma, W., Chen, M., Wang, L., Wei, L., and Wang, Q. (2011). Treatment with $NaHSO_3$ greatly enhances photobiological H_2 production in the green alga *Chlamydomonas reinhardtii*. *Bioresour. Technol.* 102, 8635–8638. doi: 10.1016/j.biortech.2011.03.052

Ma, W., Wei, L., and Wang, Q. (2008). The response of electron transport mediated by active NADPH dehydrogenase complexes to heat stress in the cyanobacterium *Synechocystis* 6803. *Sci. China C Life Sci.* 51, 1082–1087. doi: 10.1007/s11427-008-0139-0

McKendry, P. (2002). Energy production from biomass (Part 1): overview of biomass. *Bioresour. Technol.* 83, 37–46. doi: 10.1016/S0960-8524(01)00118-3

Melis, A., Zhang, L., Forestier, M., Ghirardi, M. L., and Seibert, M. (2000). Sustained photobiological hydrogen gas production upon reversible inactivation of oxygen evolution in the green alga *Chlamydomonas reinhardtii*. *Plant Physiol.* 122, 127–136. doi: 10.1104/pp.122.1.127

Momirlan, M., and Veziroglu, T. N. (2002). Current status of hydrogen energy. *Renew. Sustain. Energ. Rev.* 6, 141–179. doi: 10.1016/S1364-0321(02)00004-7

Nguyen, A. V., Thomas-Hall, S. R., Malnoë, A., Timmins, M., Mussgnug, J. H., Rupprecht, J., et al. (2008). Transcriptome for photobiological hydrogen production induced by sulfur deprivation in the green alga *Chlamydomonas reinhardtii*. *Eukaryot. Cell* 7, 1965–1979. doi: 10.1128/EC.00418-07

Rühle, T., Hemschemeier, A., Melis, A., and Happe, T. (2008). A novel screening protocol for the isolation of hydrogen producing *Chlamydomonas reinhardtii* strains. *BMC Plant Biol.* 8:107. doi: 10.1186/1471-2229-8-107

Schreiber, U., Schliwa, U., and Bilger, W. (1986). Continuous recording of photochemical and non-photochemical chlorophyll fluorescence quenching with a new type of modulation fluorometer. *Photosynth. Res.* 10, 51–62. doi: 10.1007/BF00024185

Shu, L., Xiong, W., Shao, C., Huang, T., Duan, P., Liu, K., et al. (2018). Improvement in the photobiological hydrogen production of aggregated *Chlorella* by dimethyl sulfoxide. *Chembiochem* 19, 669–673. doi: 10.1002/cbic.201700637

Steinbeck, J., Nikolova, D., Weingarten, R., Johnson, X., Richaud, P., Peltier, G., et al. (2015). Deletion of Proton Gradient Regulation 5 (PGR5) and PGR5-Like 1 (PGRL1) proteins promote sustainable light-driven hydrogen production in *Chlamydomonas reinhardtii* due to increased PSII activity under sulfur deprivation. *Front. Plant Sci.* 6:892. doi: 10.3389/fpls.2015.00892

Surzycki, R., Cournac, L., Peltier, G., and Rochaix, J. D. (2007). Potential for hydrogen production with inducible chloroplast gene expression in *Chlamydomonas*. *Proc. Natl. Acad. Sci. U.S.A.* 104, 17548–17553. doi: 10.1073/pnas.0704205104

Tagawa, K., Tsujimoto, H. Y., and Arnon, D. I. (1963). Role of chloroplast ferredoxin in the energy conversion process of photosynthesis. *Proc. Natl. Acad. Sci. U.S.A.* 49, 567–572. doi: 10.1073/pnas.49.4.567

Vavilin, D. V., Tyystjärvi, E., and Aro, E. M. (1995). In search of a reversible stage of photoinhibition in a higher plant: no changes in the amount of functional photosystem II accompany relaxation of variable fluorescence after exposure of lincomycin-treated *Cucurbita pepo* leaves to high light. *Photosynth. Res.* 45, 239–247. doi: 10.1007/BF00015564

Volgusheva, A., Styring, S., and Mamedov, F. (2013). Increased photosystem II stability promotes H_2 production in sulfur-deprived *Chlamydomonas reinhardtii*. *Proc. Natl. Acad. Sci. U.S.A.* 110, 7223–7228. doi: 10.1073/pnas.1220645110

Wang, H., Mi, H., Ye, J., Deng, Y., and Shen, Y. (2003). Low concentrations of $NaHSO_3$ increase cyclic photophosphorylation and photosynthesis in cyanobacterium *Synechocystis* PCC6803. *Photosynth. Res.* 75, 151–159. doi: 10.1023/A:1022813402265

Wang, L., Chen, M., Wei, L., Gao, F., Lv, Z., Wang, Q., et al. (2010). Treatment with moderate concentrations of $NaHSO_3$ enhances photobiological H_2 production in the cyanobacterium *Anabaena* sp. strain PCC 7120. *Int. J. Hydrogen Energy* 35, 12777–12783. doi: 10.1016/j.ijhydene.2010.08.115

Wei, L., Li, X., Yi, J., Yang, Z., Wang, Q., and Ma, W. (2013). A simple approach for the efficient production of hydrogen from Taihu Lake *Microcystis* spp. blooms. *Bioresour. Technol.* 139, 136–140. doi: 10.1016/j.biortech.2013.04.026

Wei, L., Yi, J., Wang, L., Huang, T., Gao, F., Wang, Q., et al. (2017). Light intensity is important for hydrogen production in $NaHSO_3$-treated *Chlamydomonas reinhardtii*. *Plant Cell Physiol.* 58, 451–457. doi: 10.1093/pcp/pcw216

Wu, S., Huang, R., Xu, L., Yan, G., and Wang, Q. (2010). Improved hydrogen production with expression of *hemH* and *lba* genes in chloroplast of *Chlamydomonas reinhardtii*. *J. Biotechnol.* 146, 120–125. doi: 10.1016/j.jbiotec.2010.01.023

Wu, X., Liang, Y., Li, Q., Zhou, J., and Long, M. (2011). Characterization and cloning of oxygen-tolerant hydrogenase from *Klebsiella oxytoca* HP1. *Res. Microbiol.* 162, 330–336. doi: 10.1016/j.resmic.2010.12.003

Xiong, W., Zhao, X., Zhu, G., Shao, C., Li, Y., Ma, W., et al. (2015). Silicification-induced cell aggregation for the sustainable production of H_2 under aerobic conditions. *Angew. Chem. Int. Ed. Engl.* 54, 11961–11965. doi: 10.1002/anie.201504634

Xu, F. Q., Ma, W. M., and Zhu, X. G. (2011). Introducing pyruvate oxidase into the chloroplast of *Chlamydomonas reinhardtii* increases oxygen consumption and promotes hydrogen production. *Int. J. Hydrogen Energy* 36, 10648–10654. doi: 10.1016/j.ijhydene.2011.05.130

Zhang, L., Happe, T., and Melis, A. (2002). Biochemical and morphological characterization of sulfur-deprived and H_2-producing *Chlamydomonas reinhardtii* (green alga). *Planta* 214, 552–561. doi: 10.1007/s004250100660

Conflict of Interest Statement: The authors declare that the research was conducted in the absence of any commercial or financial relationships that could be construed as a potential conflict of interest.

frontiers in Plant Science

ORIGINAL RESEARCH
published: 13 July 2018
doi: 10.3389/fpls.2018.00947

Purification and Characterisation of Malate Dehydrogenase From *Synechocystis* sp. PCC 6803: Biochemical Barrier of the Oxidative Tricarboxylic Acid Cycle

*Masahiro Takeya, Shoki Ito, Haruna Sukigara and Takashi Osanai**

School of Agriculture, Meiji University, Tokyo, Japan

Cyanobacteria possess an atypical tricarboxylic acid (TCA) cycle with various bypasses. Previous studies have suggested that a cyclic flow through the TCA cycle is not essential for cyanobacteria under normal growth conditions. The cyanobacterial TCA cycle is, thus, different from that in other bacteria, and the biochemical properties of enzymes in this TCA cycle are less understood. In this study, we reveal the biochemical characteristics of malate dehydrogenase (MDH) from *Synechocystis* sp. PCC 6803 MDH (*Sy*MDH). The optimal temperature of *Sy*MDH activity was 45–50°C and *Sy*MDH was more thermostable than MDHs from other mesophilic microorganisms. The optimal pH of *Sy*MDH varied with the direction of the reaction: pH 8.0 for the oxidative reaction and pH 6.5 for the reductive reaction. The reductive reaction catalysed by *Sy*MDH was activated by magnesium ions and fumarate, indicating that *Sy*MDH is regulated by a positive feedback mechanism. The K_m-value of *Sy*MDH for malate was approximately 210-fold higher than that for oxaloacetate and the K_m-value for NAD^+ was approximately 19-fold higher than that for NADH. The catalytic efficiency of *Sy*MDH for the reductive reaction, deduced from k_{cat}-values, was also higher than that for the oxidative reaction. These results indicate that *Sy*MDH is more efficient in the reductive reaction in the TCA cycle, and it plays key roles in determining the direction of the TCA cycle in this cyanobacterium.

Keywords: biochemistry, cyanobacteria, malate dehydrogenase, metabolic enzyme, TCA cycle

OPEN ACCESS

Edited by:
Peer Schenk,
The University of Queensland,
Australia

Reviewed by:
Martin Hagemann,
University of Rostock, Germany
Shuyi Zhang,
Massachusetts Institute of Technology, United States

***Correspondence:**
Takashi Osanai
tosanai@meiji.ac.jp

Specialty section:
This article was submitted to Plant Biotechnology, a section of the journal Frontiers in Plant Science

Received: *28 November 2017*
Accepted: *12 June 2018*
Published: *13 July 2018*

Citation:
Takeya M, Ito S, Sukigara H and Osanai T (2018) Purification and Characterisation of Malate Dehydrogenase From Synechocystis sp. PCC 6803: Biochemical Barrier of the Oxidative Tricarboxylic Acid Cycle. Front. Plant Sci. 9:947. doi: 10.3389/fpls.2018.00947

INTRODUCTION

Cyanobacteria performing oxygenic photosynthesis synthesise various compounds from carbon dioxide using light energy. Cyanobacteria are widely used as hosts in metabolic engineering to produce renewable resources. *Synechocystis* sp. PCC 6803 (hereafter *Synechocystis* 6803) is one of the most highly studied cyanobacteria because it has many advantageous features, such as rapid proliferation and ease of transformation. Besides genetics, biochemical analyses of enzymes related to oxaloacetate metabolism proceed using *Synechocystis* 6803 enzymes (Ito et al., 2017; Takeya et al., 2017), and thus this cyanobacterium is widely used for basic studies of primary carbon metabolism.

The tricarboxylic acid (TCA) cycle is one of the most important biochemical reactions in aerobic energy production, and is common among most respiring organisms. Reductants are generated by oxidation of metabolites through the TCA cycle, leading to ATP production through the process of respiration, which uses these reductants. Metabolites in the TCA cycle, such as oxaloacetate and 2-oxoglutarate, are precursors of various metabolites, including amino acids, sugars, and lipids (Owen et al., 2002). The cyanobacterial TCA cycle is also involved in various metabolic systems, which can lead to the production of useful materials, such as succinate (Osanai et al., 2015), amino acids (Matsunaga et al., 1991), ethylene (Xiong et al., 2015) via acetyl-CoA, and TCA cycle derivatives from fixing carbon dioxide by oxygenic photosynthesis using light energy.

Compared to studies on enzymes in the Calvin cycle, biochemical analysis of enzymes of the TCA cycle in cyanobacteria is limited. The cyanobacterial TCA cycle was once thought to be an incomplete cycle owing to the lack of 2-oxoglutarate dehydrogenase (OGDH); however, it has been demonstrated that 2-oxoglutarate decarboxylase and succinate semialdehyde dehydrogenase produce succinate from 2-oxoglutarate (Zhang and Bryant, 2011; Steinhauser et al., 2012). In addition, the γ-aminobutyric acid (GABA) shunt produces succinate from glutamate in *Synechocystis* 6803 (Xiong et al., 2014), and the glyoxylic acid shunt is found in the cyanobacterium *Chlorogloeopsis fritschii* strain PCC 9212 (Zhang and Bryant, 2015). Thus, the cyanobacterial TCA cycles are potentially closed with these alternative shunts. However, these studies only analysed the first half of the TCA cycle, from citrate to succinate. The latter half of the TCA cycle has been studied by *in silico* analysis (Knoop et al., 2013; Rubin et al., 2015). Kinetic values, such as k_{cat} and K_m, of cyanobacterial TCA cycle enzymes have not been determined, except for isocitrate dehydrogenase (Muro-Pastor and Florencio, 1992, 1994). Biochemical analysis of phosphoenolpyruvate carboxylase (PEPC), which produces oxaloacetate from phosphoenolpyruvate, reveals that *Synechocystis* 6803 PEPC is uniquely tolerant to feedback inhibition by malate and aspartate (Takeya et al., 2017). In addition to the oxidative cycle, the cyanobacterial TCA cycle reverses to a reductive reaction (called the reductive branch of the TCA cycle) under dark, anaerobic conditions (Hasunuma et al., 2016).

Malate dehydrogenase (MDH) is an enzyme that catalyses the interconversion between malate and oxaloacetate using NAD(P)H. MDHs are largely conserved in most species, irrespective of variation in the TCA cycle (Huynen et al., 1999; Minárik et al., 2002). MDH catalyses the oxidative reaction in the TCA cycle (malate to oxaloacetate) *in vivo*, although MDH thermodynamically prefers the reductive reaction (oxaloacetate to malate) *in vitro* (Molenaar et al., 1998). Thus, MDH is a unique enzyme that prefers the reductive reaction in the TCA cycle; however, the biochemical parameters of *Synechocystis* 6803 MDH (*Sy*MDH) have not been determined. MDH functions to protect against oxidative stress in *Escherichia coli* (Wu et al., 2007; Singh et al., 2008), also suggesting the physiological importance of MDHs in bacteria. In this study, *Sy*MDH was purified, and its biochemical functions were demonstrated for the first time, revealing unique regulatory mechanisms of *Sy*MDH.

MATERIALS AND METHODS

Construction of Cloning Vectors for Recombinant Protein Expression

A *Bam*HI-*Xho*I DNA fragment of the *citH* (sll0891) ORF from the *Synechocystis* 6803 genome was amplified by PCR using KOD Plus Neo polymerase (Toyobo, Osaka, Japan) with the primers: forward, GAAGGTCGTGGGATCATGAATATTTT GGAGTATGCTC and reverse, GATGCGGCCGCTCGAGT TAACCGTCGCTAACCAT. The resultant fragments were excised with *Bam*HI-*Xho*I (Takara Bio, Shiga Japan) and cloned into the *Bam*HI-*Xho*I site of pGEX5X-1 (GE Healthcare Japan, Tokyo, Japan) using the In-Fusion HD Cloning Kit (Takara Bio, Shiga, Japan). Sequence integrity was confirmed by sequencing.

Affinity Purification of Recombinant Proteins

Expression vectors were transformed into *E. coli* BL21 (DH5α, Takara Bio). Two litres of *E. coli* containing the vectors were cultivated at 30°C with shaking (150 rpm), and protein expression was induced overnight by adding 0.01 mM isopropyl β-D-1-thiogalactopyranoside (Wako Chemicals, Osaka, Japan).

Affinity chromatography was performed for protein purification as described in a previous study (Osanai et al., 2009). Two litres of *E. coli* cell culture were disrupted by sonication VC-750 (EYELA, Tokyo, Japan) for 5 min with 30% intensity and centrifuged at 5,800 × *g* for 2 min at 4°C. The supernatant was transferred to a new 50-mL plastic tube on ice and 640 μL of glutathione-Sepharose 4B resin (GE Healthcare Japan) was mixed into the supernatant. After gentle rotating for 30 min, 1 mM ATP and 1 mM $MgSO_4{\cdot}7H_2O$ were added and samples were incubated with gentle shaking for 30 min to remove intracellular chaperons. After centrifugation (5,800 × *g* for 2 min at 4°C), the supernatant was removed and resins were re-suspended in 700 μL of PBS-T (1.37 M NaCl, 27 mM KCl, 81 mM $Na_2HPO_4{\cdot}12H_2O$, 14.7 mM KH_2PO_4, 0.05% Tween-20) with 1 mM ATP/1 mM $MgSO_4{\cdot}7H_2O$. The resin was washed with 500 μL of PBS-T (1.37 M NaCl, 27 mM KCl, 81 mM $Na_2HPO_4{\cdot}12H_2O$, 14.7 mM KH_2PO_4, 0.05% Tween-20) and eluted three times with 500 μL of GST elution buffer (50 mM Tris–HCl, pH 8.0, 10 mM reduced glutathione). Proteins were concentrated with VivaSpin 500 MWCO 50,000 spin columns (Sartorius, Göttingen, Germany) and protein concentration was measured with a PIERCE BCA Protein Assay Kit (Thermo Fisher Scientific, Rockford, IL, United States). Protein purification was validated by SDS-PAGE, including staining using InstantBlue (Expedion Protein Solutions, San Diego, CA, United States).

Enzyme Assays

7.8 μg or 10 μg of *Sy*MDHs were used to measure oxidative or reductive reactions, respectively. The purified protein was

mixed with 1 mL of assay solution (100 mM potassium phosphate buffer [pH 8.0 or pH 6.5], 0.1–32 mM nicotinamide adenine dinucleotide (NAD^+), 0.01–0.64 mM nicotinamide adenine dinucleotide hydride (NADH), 0.2–32 mM malate, 0.02–0.4 mM oxaloacetate). The optimal temperature and the optimal pH were measured at the concentration exhibiting maximum activity (NAD^+: 8.0 mM, NADH: 0.1 mM, malate: 4.0 mM, oxaloacetate: 0.1 mM). For the cell extract assay, cells from 1 L culture were collected by centrifugation and resuspend in 100 mM potassium phosphate buffer (pH7.0). The cells were disrupted by sonication and centrifuged at 5,800 × *g* for 30 min at 4°C. The protein concentration was quantified with BCA Protein Assay Kit (Thermo) and 420 μg of total proteins was added to 1 mL assay solution. Absorbance was measured at 340 nm using a UV-1850 spectrophotometer (Shimadzu, Tokyo, Japan). V_{max} and K_m-values were determined using a Lineweaver–Burk double reciprocal plot. Results were plotted as a graph of the rate of reaction against the concentration of substrate and coenzyme using Kaleida Graph ver. 4.5 software. When the data did not show substrate inhibition, we performed curve fitting used the Michaelis–Menten equation (Eq. 1). When the data exhibited substrate inhibition, we performed curve fitting using the modified Michaelis–Menten equation (Eq. 2) (Eszes et al., 1996).

$$v = V_{max}[S]/([S] + K_m) \quad (1)$$

$$v = V_{max}[S]/([S] + K_m + [S]^2/K_i) \quad (2)$$

v and V_{max} indicate reaction velocity and maximum reaction velocity, respectively. [S], K_m, and K_i indicate substrate concentration, the half-maximum concentration giving rise to 50% V_{max} and an inhibition constant, respectively.

RESULTS

Measurement of Kinetic Parameters

To determine the kinetic parameters of *Sy*MDH, glutathione *S*-transferase (GST)-tagged *Sy*MDH (GST-*Sy*MDH) proteins were expressed in *E. coli* and purified by affinity chromatography (**Figure 1A**). *Sy*MDH activity in the oxidative reaction (malate to oxaloacetate) was the highest at pH 8.0 and at a temperature of 50°C (**Figures 1B,C**). *Sy*MDH activity in the reductive reaction (oxaloacetate to malate) was the highest at pH 6.5 and at 45°C (**Figures 1B,C**). Kinetic parameters of *Sy*MDH were determined by a Lineweaver–Burk double reciprocal plot using the specific activity values in **Figures 2**, **3**. These results are summarised in **Tables 1**, **2**. *Sy*MDH displayed approximately 1.7-fold (k_{cat}) and 350-fold (k_{cat}/K_m) preferences for oxaloacetate reduction over malate oxidation and approximately 4.7-fold (k_{cat}) and 89.5-fold (k_{cat}/K_m) preferences for NADH oxidation over NAD^+

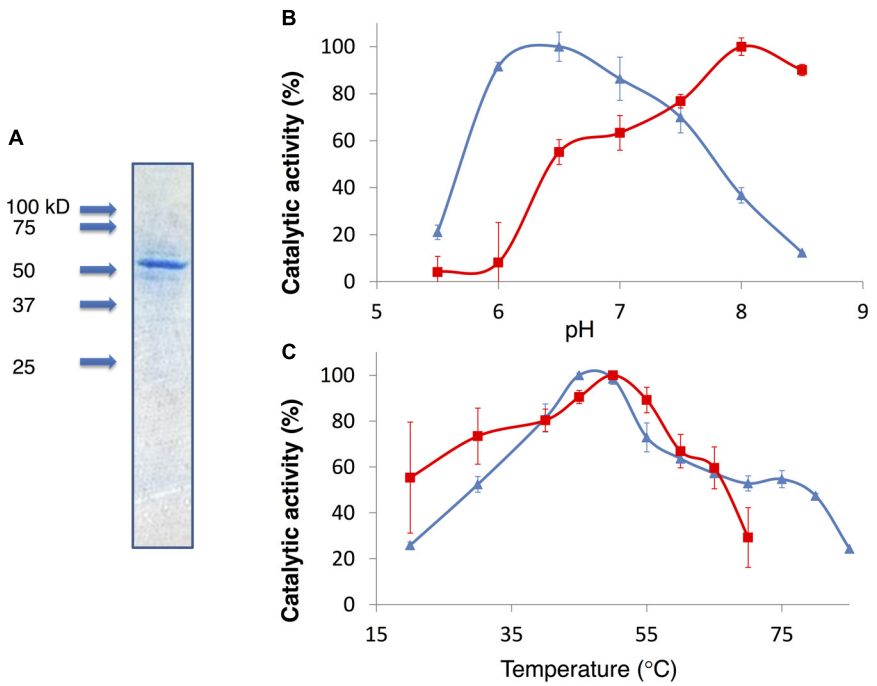

FIGURE 1 | (A) Purification of GST-tagged *Sy*MDH. Proteins were electrophoresed on a 12% SDS-PAGE gel. The gel was stained with InstantBlue. Arrowheads indicate the molecular weight. **(B)** The effect of pH on *Sy*MDH activity. Red square represents the specific activity in the oxidative reaction (malate to oxaloacetate). Blue triangle represents the specific activity in the reductive reaction (oxaloacetate to malate). Data represent the relative values of the mean from three independent experiments. **(C)** The effect of temperature on *Sy*MDH activity. Red square represents the specific activity in the oxidative reaction (malate to oxaloacetate). Blue triangle represents the specific activity in the reductive reaction (oxaloacetate to malate). Data represent the relative values of the mean from three independent experiments.

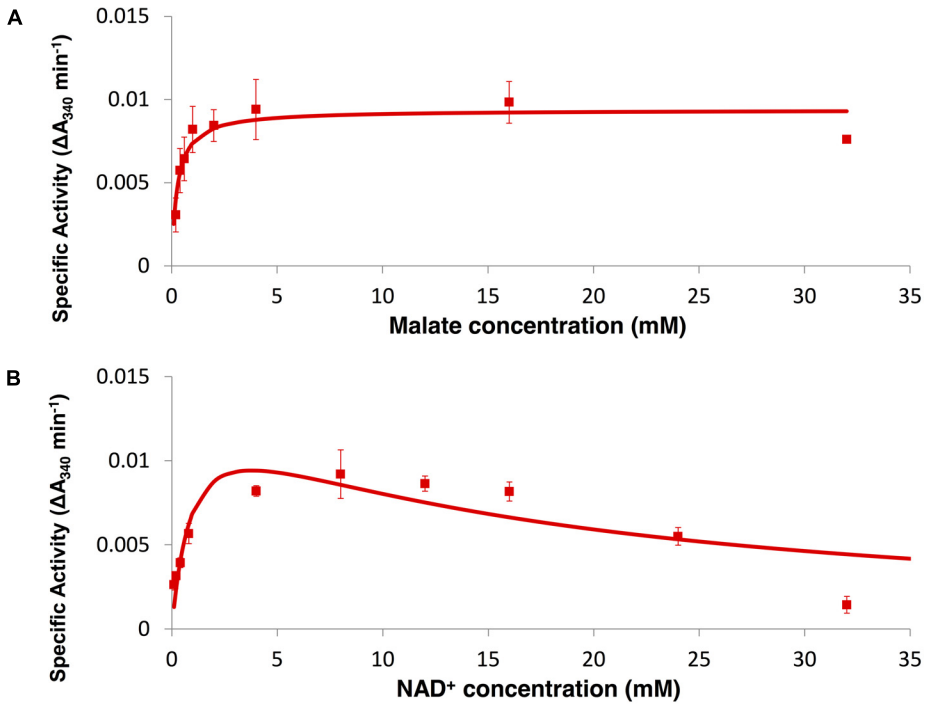

FIGURE 2 | Enzyme assay of *Sy*MDH in the oxidative reaction *in vitro*. **(A)** Activity was measured by varying the malate concentration at a fixed NAD^+ concentration (8.0 mM). The graphs show the mean ± SD obtained from three independent experiments. **(B)** Activity was measured by varying the NAD^+ concentration at a fixed malate concentration (4.0 mM). The graphs show the mean ± SD obtained from three independent experiments.

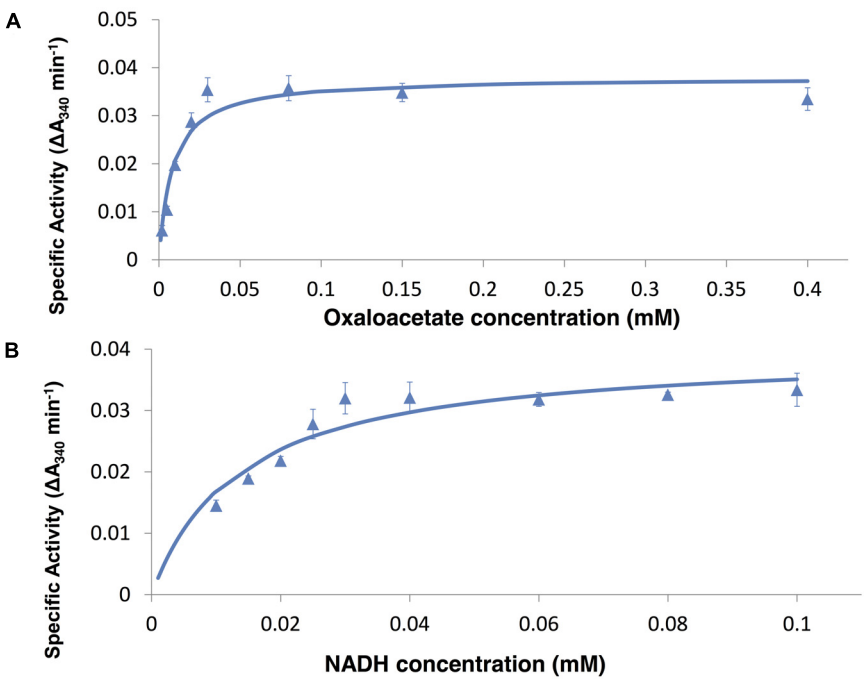

FIGURE 3 | Enzyme assay of *Sy*MDH in the reductive reaction *in vitro*. **(A)** Activity was measured by varying the oxaloacetate concentration at a fixed NADH concentration (0.1 mM). The graphs show the mean ± SD obtained from three independent experiments. **(B)** Activity was measured by varying the NADH concentration at a fixed oxaloacetate concentration (0.1 mM). The graphs show the mean ± SD obtained from three independent experiments.

TABLE 1 | Kinetic parameters of *Sy*MDH.

	V_{max} (units·mg^{-1})	k_{cat} (S^{-1})	k_{cat}/K_m (S^{-1}·mM^{-1})
Malate	0.412	1.58×10^5	0.618×10^5
OAA	0.685	2.63×10^5	216×10^5
NAD^+	0.199	0.765×10^5	1.33×10^5
NADH	0.931	3.58×10^5	119×10^5

The oxidative reaction (malate to oxaloacetate) was assayed in 100 mM potassium phosphate buffer (pH 8.0) by varying the malate concentration at a fixed NAD^+ concentration (8.0 mM) or by varying the NAD^+ concentration at a fixed malate concentration (4.0 mM). The reductive reaction (oxaloacetate to malate) was assayed in 100 mM potassium phosphate buffer (pH 6.5) by varying the oxaloacetate concentration at a fixed NADH concentration (0.1 mM) or by varying the NADH concentration at a fixed oxaloacetate concentration (0.1 mM). The kinetic parameters were calculated by the Lineweaver–Burk plot.

reduction (**Table 1**). The catalytic efficiency of the reductive reaction was higher than that of the oxidation reaction for both the substrate and the coenzyme. The K_m-value for malate was approximately 210-fold higher than that for oxaloacetate, and the K_m-value for NAD^+ was approximately 19-fold higher than that for NADH (**Table 2**). *Sy*MDH appeared to prefer oxaloacetate and NADH as substrate and coenzyme, respectively, *in vitro*. *Sy*MDH had enzymatic activity toward NAD^+ and NADH, but no activity toward $NADP^+$ and NADPH both *in vitro* and *in vivo* (Supplementary Figures S1, S2). We also determined kinetic parameters of *Sy*MDH using the Michaelis–Menten equation. These results are summarised in Supplementary Tables S1, S2. These calculations showed that *Sy*MDH prefers oxaloacetate and NADH as substrate and coenzyme, respectively; the K_m-value for malate was approximately 84.4-fold higher than that for oxaloacetate, and the K_m-value for NAD^+ was approximately 71.4-fold higher than that for NADH (Supplementary Table S2). *Sy*MDH exhibited substrate inhibition by NAD^+ (**Figure 2B**), and the value of K_i was 14.5 mM (Supplementary Table S1).

Effect of Various Effectors on *Sy*MDH Activity

The reductive reaction catalysed by bacterial MDHs is inhibited by TCA cycle metabolites, such as excess oxaloacetate and divalent metal ions (Takahashi-Íñiguez et al., 2016). Therefore, we measured the activity of *Sy*MDH in the reductive reaction in the presence of various effectors. *Sy*MDH was inhibited by excess NAD^+ in the reductive reaction (**Figure 2B**). With the exception of cobalt, magnesium, and copper ions, all other metal ions showed little effect on *Sy*MDH (**Figure 4**). *Sy*MDH activity increased approximately 140 and 160% with the addition of 1 mM $Co(NO_3)_2{\cdot}6H_2O$ and 1 mM $MgCl_2$, respectively (**Figure 4**). In the presence of 10 mM $MgCl_2$, the activity of *Sy*MDH increased to approximately 190% (**Figure 4**). Among the metal ions tested, only copper ions reduced the activity of *Sy*MDH. In the presence of 1 mM $CuSO_4{\cdot}5H_2O$, *Sy*MDH activity decreased to approximately 40% of normal activity (**Figure 4**). *Sy*MDH activity could not be measured in the presence of 10 mM calcium, manganese, cobalt, zinc, or copper ions due to the formation of a precipitate (**Figure 4**). *Sy*MDH activity rose approximately 170 and 190% with the addition of 1 and 10 mM fumarate, respectively (**Figure 4**). *Sy*MDH activity with oxaloacetate at a concentration of 0.01–0.6 mM was measured in the presence of 10 mM magnesium and fumarate, and the kinetic parameters were calculated by Lineweaver–Burk plots (**Figure 5A**). Both the K_m and V_{max}-values of this substrate and reaction, respectively, increased with the addition of 10 mM $MgCl_2$ and fumarate (**Figures 5B,C**). To strengthen the validity of our results, we also performed biochemical assays using cell extracts (Supplementary Figure S3a). Unlike *in vitro*, the K_m-value did not change *in vivo* in the presence of 10 mM $MgCl_2$ and fumarate (Supplementary Figure S3b). The V_{max}-value increased *in vivo* similar to *in vitro* in the presence of 10 mM $MgCl_2$ and fumarate (Supplementary Figure S3c).

Thermal Properties of *Sy*MDH Activity

Synechocystis 6803 MDH activity was measured by varying temperature (20–50°C). The K_m and the V_{max} were calculated by both a Lineweaver–Burk double reciprocal plot (**Figures 5**, **6**) and curve fitting used the Michaelis–Menten equation (Supplementary Figures S4, S5). The K_m and the V_{max}-values for malate tend to decrease as the temperature rise, although the V_{max}-values less dependent on the temperature (**Figure 6** and Supplementary Figure S4). On the contrary, the K_m and the V_{max}-values for oxaloacetate increased as the temperature

TABLE 2 | Comparison of K_m-values of MDHs in various microorganisms.

K_m (μM)	Malate	OAA	NAD^+	NADH	Malate/OAA	NAD^+/NADH	Reference
Nitrosomonas europaea	5000	20	24	22	250	1.1	Deutch, 2013
Synechocystis sp. PCC 6803	2600	12	580	30	216.7	19.3	This study
Syntrophic propionate-oxidising *bacterium strain MPOB*	4000	50	1100	30	80	36.7	van Kuijk and Stams, 1996
Methanobacterium thermoautotrophicum	400	30	90	90	13.3	1	Thompson et al., 1997
Bacillus subtilis B1	260	22	100	14	11.8	7.1	Wynne et al., 1996
Haemophilus parasuis	550	72	120	17	7.6	7.1	Wise et al., 1997
Streptomyces coelicolor	490	190	150	83	2.6	1.8	Ge et al., 2010
Pseudomonas stutzeri	63	32	340	36	2	9.4	Labrou and Clonis, 1997
Helicobacter pylori	180	130	160	65	1.4	2.5	Pitson et al., 1999
Methanothermus fervidus	150	200	140	5	0.8	28	Honka et al., 1990

K_m-values are listed in ascending order of K_m for malate/K_m for oxaloacetate. K_m-values were calculated by the Lineweaver–Burk plot.

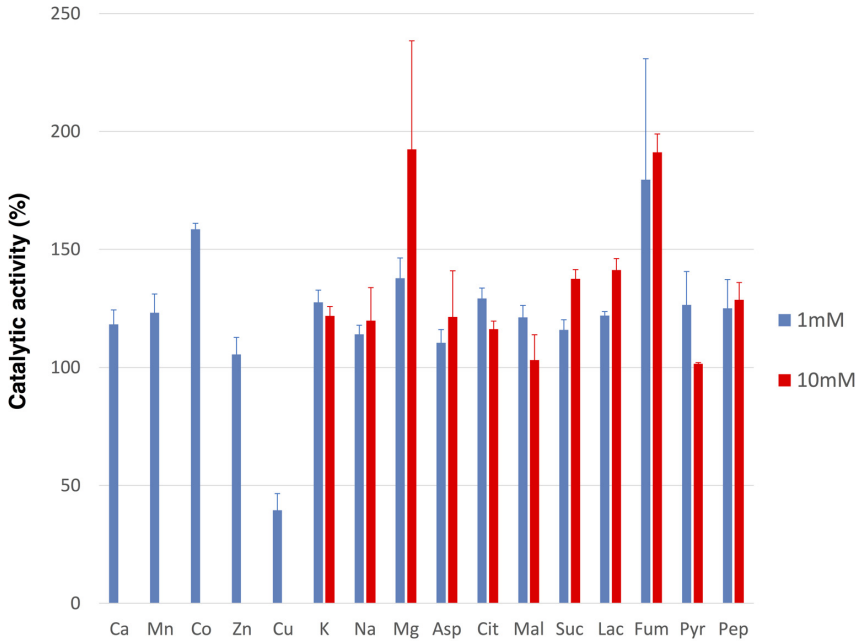

FIGURE 4 | Effects of various metal ions and compounds on the *Sy*MDH in the reductive reaction *in vitro*. 10 μg of *Sy*MDH was pre-incubated with 100 mM potassium phosphate (pH 6.5), 0.1 mM NADH, 0.1 mM oxaloacetate and effectors, at 45°C. The graphs show the mean ± SD obtained from three independent experiments. Activity of *Sy*MDH in the absence of effectors was set at 100%. Ca, $CaCl_2$; Mn, $MnCl_2{\cdot}4H_2O$; Co, $Co(NO_3)_2{\cdot}6H_2O$; Zn, $ZnSO_4{\cdot}7H_2O$; Cu, $CuSO_4{\cdot}5H_2O$; K, KCl; Na, NaCl; Mg, $MgCl_2$; Asp, L-Aspartate; Cit, Citrate; Mal, L-Malate; Suc, Succinate; Lac, L-lactate; Fum, Fumarate; Pyr, Pyruvate; Pep, Phosphoenolpyruvate.

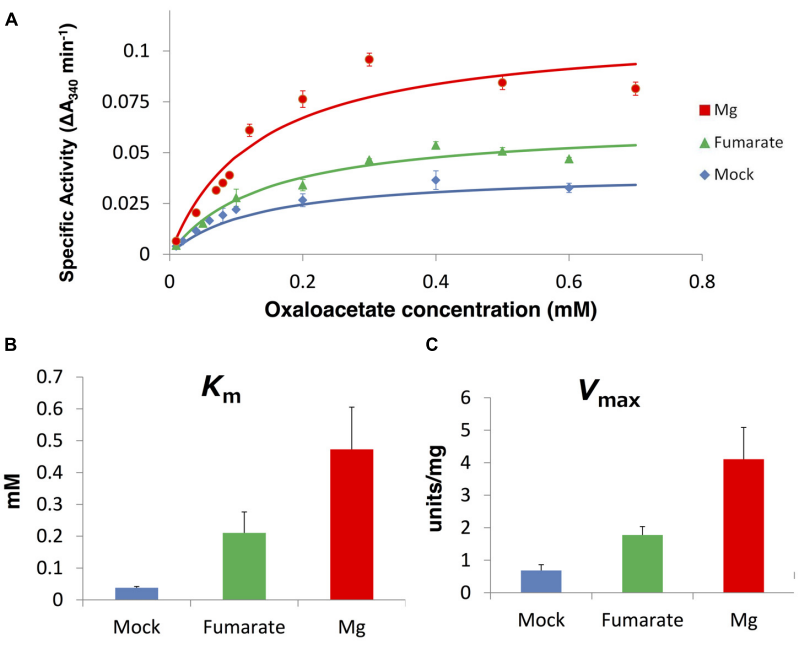

FIGURE 5 | The K_m and V_{max}-values for oxaloacetate in the presence of 10 mM fumarate and 10 mM magnesium ion *in vitro*. **(A)** Saturation curves of the activity of *Sy*MDH. Blue line indicates mock, green line indicates presence of fumarate, and red line indicates the presence of magnesium. The graph shows the mean of three independent experiments. **(B)** K_m (mean ± SD) (units/mg protein) values in the presence of 10 mM fumarate and 10 mM magnesium ion, obtained from three independent experiments. **(C)** V_{max} (mean ± SD) values for oxaloacetate, obtained from three independent experiments. Mock indicates the enzymatic activity in the absence of additional compounds.

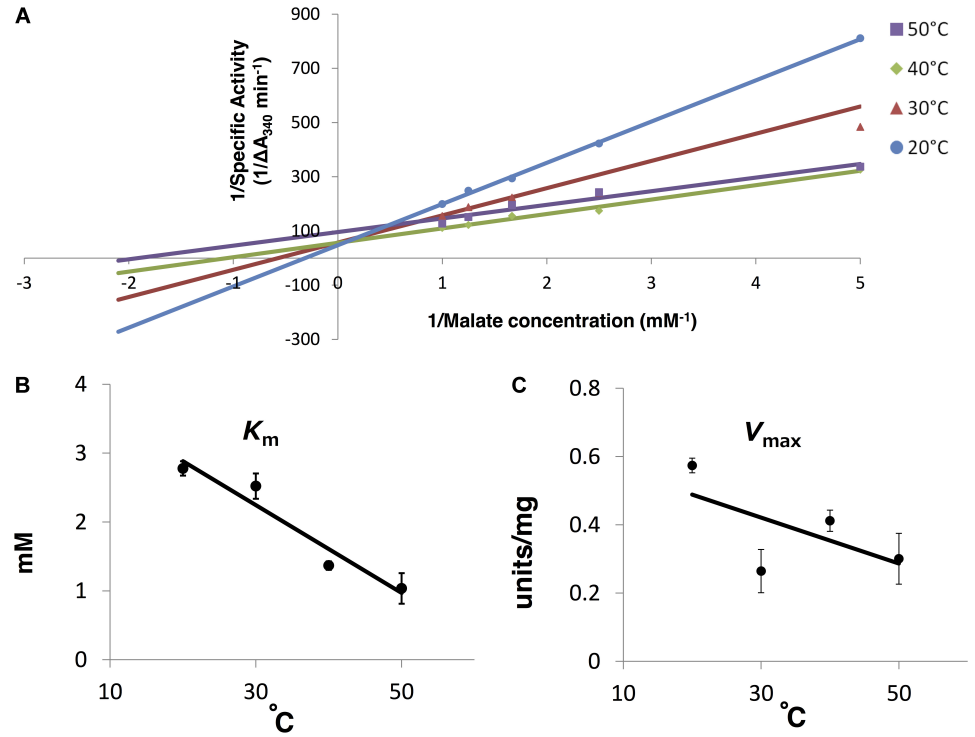

FIGURE 6 | Thermal profiles of *Sy*MDH in the oxidative reaction *in vitro*. **(A)** Lineweaver–Burk plot of the *Sy*MDH activity in the oxidative reaction at 20–50°C. Blue, red, green, and purple lines indicate condition at 20, 30, 40, and 50°C, respectively. The graph shows the mean of three independent experiments. **(B)** K_m (mean ± SD) values for malate were obtained from three independent experiments by varying the temperature (20–50°C). **(C)** V_{max} (mean ± SD) (units/mg protein) values for malate were obtained from three independent experiments by varying the temperature (20–50°C).

rise (**Figure 7** and Supplementary Figure S5). The K_m and the V_{max} for malate at 20°C were approximately 2.7-fold and 1.9-fold higher than that at 50°C, respectively (**Figure 6**). The K_m and V_{max} for oxaloacetate at 20°C were approximately 0.19- and 0.13-fold higher than that at 50°C, respectively (**Figure 7**). The K_m and V_{max} of *Sy*MDH demonstrated its temperature dependency.

DISCUSSION

We purified recombinant *Sy*MDH protein and revealed the biochemical properties of cyanobacterial MDH for the first time. The optimal pH of *Sy*MDH was different for the oxidative reaction and the reductive reaction (**Figure 1B**). Cyanobacteria utilise a reductive branch of TCA cycle and excrete succinate under dark anaerobic conditions (Hasunuma et al., 2016). The intracellular pH of cyanobacteria decreases during the transition from light to dark conditions (Coleman and Coleman, 1981; Mangan et al., 2016). Therefore, to adapt to the drastic changes in primary metabolism during the light and dark cycle, *Sy*MDH is thought to shift its substrate affinity according to the intracellular pH. *Sy*MDH was stable at a wide range of temperature, being particularly tolerant to high temperatures (**Figure 1C**). Among the mesophilic microorganisms, MDHs from *Streptomyces avermitilis*, *Streptomyces coelicolor*, and *Nitrosomonas europaea* maintain their activity at 50°C (Mikulášová et al., 1998; Ge et al., 2010; Deutch, 2013), but these MDHs are completely inactivated at 60–70°C (Mikulášová et al., 1998; Ge et al., 2010; Deutch, 2013). *Sy*MDH maintains its activity in both oxidative and reductive reactions at 60–70°C (**Figure 1C**). Therefore, *Sy*MDH is the most thermostable enzyme among MDHs from the mesophilic microorganisms investigated thus far. The optimal temperatures of *Sy*MDH were 50 and 45°C, for the oxidative and reductive reaction, respectively (**Figure 1C**). Thus, optimal temperature of *Sy*MDH (45–50°C) and optimal growth temperature of *Synechocystis* 6803 (30–35°C) were different. Generally, an enzymatic reaction is promoted by increasing temperature, because the kinetic energy of the reactants increases. However, an enzyme denature at high temperatures. Since *Sy*MDH is a heat-stable enzyme (**Figure 1B**), the enzyme activity became the highest at around 50°C, which is higher than the optimal growth temperature in *Synechocystis* 6803. Besides *Synechocystis* 6803, microorganisms having the MDHs with the optimal temperature much higher than the optimal growth temperature are *S. avermitilis* and *S. coelicolor*, *N. europaea* (Mikulášová et al., 1998; Ge et al., 2010; Deutch, 2013). *Sy*MDH activity was suppressed by copper (**Figure 4**), as was observed for the MDH from *Pseudomonas stutzeri* (Labrou and Clonis, 1997). *P. stutzeri* MDH is also inhibited by citrate (Labrou and Clonis, 1997), but *Sy*MDH was slightly activated by citrate (**Figure 4**). The only reported activators

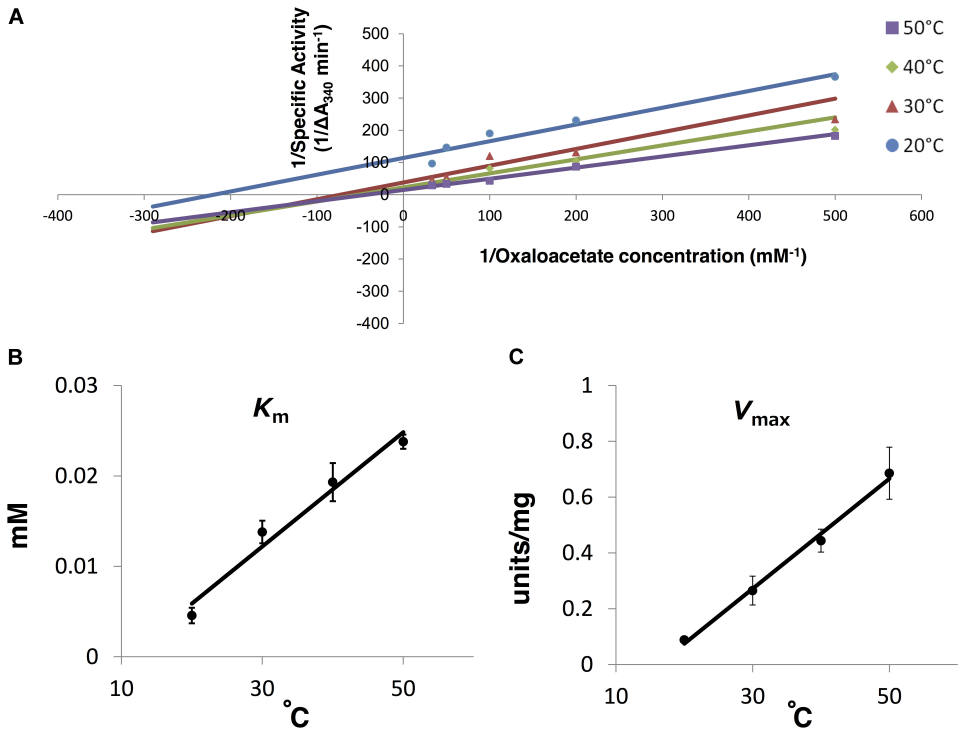

FIGURE 7 | Thermal profiles of *Sy*MDH in the reductive reaction *in vitro*. **(A)** Lineweaver–Burk plot of the *Sy*MDH activity in the reductive reaction at 20–50°C. Blue, red, green, and purple lines indicate condition at 20, 30, 40, and 50°C, respectively. The graph shows the mean of three independent experiments. **(B)** K_m (mean ± SD) values for oxaloacetate were obtained from three independent experiments by varying the temperature (20–50°C). **(C)** V_{max} (mean ± SD) (units/mg protein) values for oxaloacetate were obtained from three independent experiments by varying the temperature (20–50°C).

of bacterial MDHs are >0.18 mM malate and 3 M NaCl (Cendrin et al., 1997; Labrou and Clonis, 1997), but *Sy*MDH was significantly activated by magnesium ions and fumarate (**Figure 5** and Supplementary Figure S3), suggesting that *Sy*MDH is regulated by a positive feedback mechanism. These results are indicative of the diversity of regulation among MDHs. Intracellular concentrations of malate and fumarate in *E. coli* cells are 1.7 and 0.11 mM, respectively (Bennett et al., 2009). Since *Sy*MDH showed maximum activity at 5 mM malate (**Figure 2**) and was activated with 1 mM fumarate (**Figure 4**), it is plausible that *Sy*MDH activity was regulated by the TCA cycle metabolites. Excess NAD^+ (>4 mM) caused substrate inhibition in *Sy*MDH (**Figure 2B**). MDHs from *Methanobacterium thermoautotrophicum* and *P. stutzeri* are also inhibited by excess NAD^+ (>0.5 mM) and NAD^+ (>250 mM), respectively (Labrou and Clonis, 1997; Thompson et al., 1997). Intracellular concentrations of NAD^+ in *E. coli* cells is 2.6 mM (Bennett et al., 2009), thus, *Sy*MDH activity is thought to inhibited by NAD^+ present in *Synechocystis* 6803.

The affinity of oxaloacetate and NADH for *Sy*MDH was higher than the affinity of malate and NAD^+, respectively (**Table 1**). Generally, bacterial MDHs show higher affinity for oxaloacetate than malate (Takahashi-Íñiguez et al., 2016), and *Sy*MDH was consistent with this. When comparing the substrate affinity among bacterial MDHs, the K_m (malate)/K_m (oxaloacetate) ratio in descending order is as follows: *N. europaea* (250), *Synechocystis* 6803 (210), Syntrophic propionate-oxidising bacterium strain MPOB (80.0), and *Methanobacterium thermoautotrophicum* (13.3) (**Table 2**). The previous study demonstrated that the NAD^+ concentration is approximately 500 times higher than NADH concentration in *Synechocystis* 6803 (Osanai et al., 2014). Therefore, although our biochemical analysis showed that *Sy*MDH has higher coenzyme specificity toward NADH than NAD^+, *Sy*MDH can catalyse both reductive and oxidative reactions *in vivo*. The K_m (NAD^+)/K_m (NADH) ratio in descending order is as follows: Syntrophic propionate-oxidising bacterium strain MPOB (36.7), *Methanothermus fervidus* (28.0), and *Synechocystis* 6803 (19.0). These aforementioned microorganisms are thought to have low MDH activity in the oxidation reaction. This is because *N. europaea* is deficient in 2-oxoglutarate dehydrogenase (Beyer et al., 2009) and succinyl-CoA is formed via phosphoenolpyruvate and oxaloacetate using a reductive branch of TCA cycle (Deutch, 2013). In addition, syntrophic propionate-oxidising bacterium strain MPOB, *Methanobacterium thermoautotrophicum*, and *Methanothermus fervidus* are anaerobic microorganisms (Harmsen et al., 1996; Thompson et al., 1997; Stetter et al., 1981), and therefore, their oxidative TCA cycles are barely functioning. As with microorganisms in which the oxidative TCA cycle does not appear to function, the K_m (for malate)/K_m (for

oxaloacetate) ratio and the K_m (NAD^+)/K_m (NADH) ratio of *Sy*MDH were very high. Therefore, *Sy*MDH is likely to have low activity in the oxidative reaction. This conclusion is supported by flux analyses. Previous studies measured metabolic flow by estimating the flux rates of metabolites per dry cell weight (DCW) per unit hour in *Synechocystis* 6803 under mixotrophic conditions and found that all fluxes in TCA cycle reactions were clockwise (0.02–0.11 mmol $gDCW^{-1}$ h^{-1}), except for the interconversion between malate and oxaloacetate, which was anticlockwise (0.13 mmol $gDCW^{-1}$ h^{-1}; Nakajima et al., 2014). Similar results were observed under photoheterotrophic, nitrogen-limited, and dark conditions (Nakajima et al., 2014, 2017; Wan et al., 2017). *In vivo* studies have shown that many genes of the cyanobacterial TCA cycle are unnecessary for normal growth (Broddrick et al., 2016). Even if expression of fumarase, which catalyses the reversible hydration/dehydration of fumarate to malate, is blocked, growth of cyanobacteria under continuous light is not affected (Rubin et al., 2015). Therefore, the oxidative reaction of *Sy*MDH is also thought to be unnecessary in cyanobacteria, because fumarase-deficient cyanobacteria grow normally. These studies support our biochemical studies suggesting that the oxidative reaction of *Sy*MDH is very weak and almost non-functional. The kinetic parameters of *Sy*MDH were affected by temperature (**Figures 6**, **7** and Supplementary Figures S4, S5). K_m-value for oxaloacetate was always lower than that for malate in range of 20–50°C, thus, it is considered that *Sy*MDH always show higher affinity for oxaloacetate than malate within 20–50°C and the reaction direction of *Sy*MDH tends to flow from oxaloacetate to malate within the growth temperature of *Synechocystis* 6803.

Our study revealed that *Sy*MDH shows a higher affinity for substances produced through the reductive reaction than those produced through the oxidative reaction, similar to MDHs derived from anaerobic microorganisms in which the oxidative TCA cycle seems to be barely functioning. Cyanobacteria have been found to close the TCA cycle using various bypasses (Zhang and Bryant, 2011; Steinhauser et al., 2012; Xiong et al., 2014). However, the results in this study indicate that the oxidative TCA cycle of *Synechocystis* 6803 may be functionally linear, and not cyclic in nature, because *Sy*MDH preferentially undergoes a reductive reaction rather than an oxidative reaction and turns off the cyclic process of the oxidative TCA cycle.

AUTHOR CONTRIBUTIONS

MT designed the research, performed the experiments, analysed the data, and wrote the manuscript. SI analysed the data. HS performed the experiments. TO analysed the data and wrote the manuscript.

FUNDING

This work was supported by the Ministry of Education, Culture, Sports, Science and Technology, Japan, by a grant to TO, from ALCA (Project Name "Production of cyanobacterial succinate by the genetic engineering of transcriptional regulators and circadian clocks") (Grant No. JPMJAL1306), from the Japan Science and Technology Agency, and by JSPS KAKENHI Grant-in-Aid for Scientific Research on Innovative Areas (Grant No. 16H06559).

SUPPLEMENTARY MATERIAL

The Supplementary Material for this article can be found online at: https://www.frontiersin.org/articles/10.3389/fpls.2018.00947/full#supplementary-material

REFERENCES

Bennett, B. D., Kimball, E. H., Gao, M., Osterhout, R., Van Dien, S. J., and Rabinowitz, J. D. (2009). Absolute metabolite concentrations and implied enzyme active site occupancy in *Escherichia coli*. *Nat. Chem. Biol.* 8, 593–599. doi: 10.1038/nchembio.186

Beyer, S., Gilch, S., Meyer, O., and Schmidt, I. (2009). Transcription of genes coding for metabolic key functions in *Nitrosomonas europaea* during aerobic and anaerobic growth. *J. Mol. Microbiol. Biotechnol.* 16, 187–197. doi: 10.1159/000142531

Broddrick, J. T., Rubin, B. E., Welkie, D. G., Du, N., Mih, N., Diamond, S., et al. (2016). Unique attributes of cyanobacterial metabolism revealed by improved genome-scale metabolic modeling and essential gene analysis. *Proc. Natl. Acad. Sci. U.S.A.* 113, E8344–E8353. doi: 10.1073/pnas.1613446113

Cendrin, F., Chroboczek, J., Zaccai, G., Eisenberg, H., and Mevarech, M. (1997). Cloning, sequencing, and expression in *Escherichia coli* of the gene coding for malate dehydrogenase of the extremely halophilic archaebacterium *Haloarcula marismortui*. *Biochemistry* 32, 4308–4313. doi: 10.1021/bi00067a020

Coleman, J. R., and Coleman, B. (1981). Inorganic carbon accumulation and photosynthesis in a blue-green alga as a function of external pH. *Plant Physiol.* 67, 917–921. doi: 10.1104/pp.67.5.917

Deutch, C. E. (2013). L-Malate dehydrogenase activity in the reductive arm of the incomplete citric acid cycle of *Nitrosomonas europaea*. *Antonie Van Leeuwenhoek* 104, 645–655. doi: 10.1007/s10482-013-9973-6

Eszes, C. M., Sessions, R. B., Clarke, A. R., Moreton, K. M., and Holbrook, J. J. (1996). Removal of substrate inhibition in a lactate dehydrogenase from human muscle by a single residue change. *FEBS Lett.* 399, 193–197. doi: 10.1016/S0014-5793(96)01317-8

Ge, Y. D., Cao, Z. Y., Wang, Z. D., Chen, L. L., Zhu, Y. M., and Zhu, G. P. (2010). Identification and biochemical characterization of a thermostable malate dehydrogenase from the mesophile *Streptomyces coelicolor* A3(2). *Biosci. Biotechnol. Biochem.* 74, 2194–2201. doi: 10.1271/bbb.100357

Harmsen, H. J., Kengen, H. M., Akkermans, A. D., Stams, A. J., and Vos, W. M. (1996). Detection and localization of syntrophic propionate-oxidizing bacteria in granular sludge by in situ hybridization using 16S rRNA-based oligonucleotide probes. *Appl. Environ. Microbiol.* 62, 1656–1663.

Hasunuma, T., Matsuda, M., and Kondo, A. (2016). Improved sugar-free succinate production by *Synechocystis* sp. PCC 6803 following identification of the limiting steps in glycogen catabolism. *Metab. Eng. Commun.* 3, 130–141. doi: 10.1016/j.meteno.2016.04.003

Honka, E., Fabry, S., Niermann, T., Palm, P., and Hensel, R. (1990). Properties and primary structure of the L-malate dehydrogenase from the extremely thermophilic archaebacterium *Methanothermus*

fervidus. *Eur. J. Biochem.* 188, 623–632. doi: 10.1111/j.1432-1033.1990.tb15443.x

Huynen, M. A., Dandekar, T., and Bork, P. (1999). Variation and evolution of the citric-acid cycle: a genomic perspective. *Trends Microbiol.* 7, 281–291. doi: 10.1016/S0966-842X(99)01539-5

Ito, S., Takeya, M., and Osanai, T. (2017). Substrate specificity and allosteric regulation of a d-lactate dehydrogenase from a unicellular cyanobacterium are altered by an amino acid substitution. *Sci. Rep.* 7:15052. doi: 10.1038/s41598-017-15341-5

Knoop, H., Gründel, M., Zilliges, Y., Lehmann, R., Hoffmann, S., Lockau, W., et al. (2013). Flux balance analysis of cyanobacterial metabolism: the metabolic network of *Synechocystis* sp. PCC 6803. *PLoS Comput. Biol.* 9:e1003081. doi: 10.1371/journal.pcbi.1003081

Labrou, N. E., and Clonis, Y. D. (1997). L-Malate dehydrogenase from *Pseudomonas stutzeri*: purification and characterization. *Arch. Biochem. Biophys.* 337, 103–114. doi: 10.3923/ajbkr.2011.478.485

Mangan, N. M., Flamholz, A., Hood, R. D., Milo, R., and Savage, D. F. (2016). pH determines the energetic efficiency of the cyanobacterial CO_2 concentrating mechanism. *Proc. Natl. Acad. Sci. U.S.A.* 113, E5354–E5362. doi: 10.1073/pnas.1525145113

Matsunaga, T., Takeyama, H., Sudo, H., Oyama, N., Ariura, S., Takano, H., et al. (1991). Glutamate production from CO_2 by marine cyanobacterium *Synechococcus* sp. using a novel biosolar reactor employing light-diffusing optical fibers. *Appl. Biochem. Biotechnol.* 28:157. doi: 10.1007/BF02922597

Mikulášová, D., Kollárová, M., Miginiac-Maslow, M., Decottignies, P., Jacquot, J. P., Kutejová, E., et al. (1998). Purification and characterization of the malate dehydrogenase from *Streptomyces aureofaciens*. *FEMS Microbiol. Lett.* 159, 299–305. doi: 10.1016/S0378-1097(97)00567-3

Minárik, P., Tomásková, N., Kollárová, M., and Antalík, M. (2002). Malate dehydrogenases structure and function. *Gen. Physiol. Biophys.* 21, 257–265.

Molenaar, D., van der Rest, M. E., and Petrović, S. (1998). Biochemical and genetic characterization of the membrane associated malate dehydrogenase (acceptor) from *Corynebacterium glutamicum*. *Eur. J. Biochem.* 25, 395–403. doi: 10.1046/j.1432-1327.1998.2540395.x

Muro-Pastor, M. I., and Florencio, F. J. (1992). Purification and properties of NADP-isocitrate dehydrogenase from the unicellular cyanobacterium *Synechocystis* sp. PCC 6803. *Eur. J. Biochem.* 203, 99–105. doi: 10.1111/j.1432-1033.1992.tb19833.x

Muro-Pastor, M. I., and Florencio, F. J. (1994). NADP(+)-isocitrate dehydrogenase from the cyanobacterium *Anabaena* sp. strain PCC 7120: purification and characterization of the enzyme and cloning, sequencing, and disruption of the icd gene. *J. Bacteriol.* 176, 2718–2726. doi: 10.1128/jb.176.9.2718-2726.1994

Nakajima, T., Kajihata, S., Yoshikawa, K., Matsuda, F., Furusawa, C., Hirasawa, T., et al. (2014). Integrated metabolic flux and omics analysis of *Synechocystis* sp. PCC 6803 under mixotrophic and photoheterotrophic conditions. *Plant Cell Physiol.* 55, 1605–1612. doi: 10.1093/pcp/pcu091

Nakajima, T., Yoshikawa, K., Toya, Y., Matsuda, F., and Shimizu, H. (2017). Metabolic flux analysis of the *Synechocystis* sp. PCC 6803 Δ*nrtABCD* mutant reveals a mechanism for metabolic adaptation to nitrogen-limited conditions. *Plant Cell Physiol.* 58, 537–545. doi: 10.1093/pcp/pcw233

Osanai, T., Imashimizu, M., Seki, A., Sato, S., Tabata, S., Imamura, S., et al. (2009). ChlH, the H subunit of the Mg-chelatase, is an anti-sigma factor for SigE in *Synechocystis* sp. PCC 6803. *Proc. Natl. Acad. Sci. U.S.A.* 106, 6860–6865. doi: 10.1073/pnas.0810040106

Osanai, T., Oikawa, A., Shirai, T., Kuwahara, A., Iijima, H., Tanaka, K., et al. (2014). Capillary electrophoresis-mass spectrometry reveals the distribution of carbon metabolites during nitrogen starvation in *Synechocystis* sp. PCC 6803. *Environ. Microbiol.* 16, 512–524. doi: 10.1111/1462-2920.12170

Osanai, T., Shirai, T., Iijima, H., Nakaya, Y., Okamoto, M., Kondo, A., et al. (2015). Genetic manipulation of a metabolic enzyme and a transcriptional regulator increasing succinate excretion from unicellular cyanobacterium. *Front. Microbiol.* 6:1064. doi: 10.3389/fmicb.2015.01064

Owen, O. E., Kalhan, S. C., and Hanson, R. W. (2002). The key role of anaplerosis and cataplerosis for citric acid cycle function. *J. Biol. Chem.* 277, 30409–30412. doi: 10.1074/jbc.R200006200

Pitson, S. M., Mendz, G. L., Srinivasan, S., and Hazell, S. L. (1999). The tricarboxylic acid cycle of *Helicobacter pylori*. *Eur. J. Biochem.* 260, 258–267. doi: 10.1046/j.1432-1327.1999.00153.x

Rubin, B. E., Wetmore, K. M., Price, M. N., Diamond, S., Shultzaberger, R. K., Lowe, L. C., et al. (2015). The essential gene set of a photosynthetic organism. *Proc. Natl. Acad. Sci. U.S.A.* 112, 6634–6643. doi: 10.1073/pnas.1519220112

Singh, R., Lemire, J., Mailloux, R. J., and Appanna, V. D. (2008). A novel strategy involved in [corrected] anti-oxidative defense: the conversion of NADH into NADPH by a metabolic network. *PLoS One* 3:e2682. doi: 10.1371/journal.pone.0002682

Steinhauser, D., Fernie, A. R., and Araújo, W. L. (2012). Unusual cyanobacterial TCA cycles: not broken just different. *Trends Plant Sci.* 17, 503–509. doi: 10.1016/j.tplants.2012.05.005

Stetter, K. O., Thomm, M., Winter, J. G. W., Juber, H., Zillig, W., Janecovic, D., et al. (1981). *Methanothermus fervidus* sp., a novel extremely thermophilic methanogen isolated from an icelandic hot spring. *Zentralbl. Bakterial. Hyg. I Abt. Orig. C* 2, 166–178. doi: 10.1016/S0721-9571(81)80038-5

Takahashi-Íñiguez, T., Aburto-Rodríguez, N., Vilchis-González, A. L., and Flores, M. E. (2016). Function, kinetic properties, crystallization, and regulation of microbial malate dehydrogenase. *J. Zhejiang Univ. Sci. B* 17, 247–261. doi: 10.1631/jzus.B1500219

Takeya, M., Hirai, M. Y., and Osanai, T. (2017). Allosteric inhibition of phosphoenolpyruvate carboxylases is determined by a single amino acid residue in cyanobacteria. *Sci. Rep.* 24:41080. doi: 10.1038/srep41080

Thompson, H., Tersteegen, A., Thauer, R. K., and Hedderich, R. (1997). Two malate dehydrogenases in *Methanobacterium thermoautotrophicum*. *Arch. Microbiol.* 170, 38–42. doi: 10.1007/s002030050612

van Kuijk, B. L., and Stams, A. J. (1996). Purification and characterization of malate dehydrogenase from the syntrophic propionate-oxidizing bacterium strain MPOB. *FEMS Microbiol. Lett.* 144, 141–144. doi: 10.1111/j.1574-6968.1996.tb08520.x

Wan, N., DeLorenzo, D. M., He, L., You, L., Immethun, C. M., Wang, G., et al. (2017). Cyanobacterial carbon metabolism: fluxome plasticity and oxygen dependence. *Biotechnol. Bioeng.* 114, 1593–1602. doi: 10.1002/bit.26287

Wise, D. J., Anderson, C. D., and Anderson, B. M. (1997). Purification and kinetic characterization of *Haemophilus parasuis* malate dehydrogenase. *Arch. Biochem. Biophys.* 344, 176–183. doi: 10.1006/abbi.1997.0186

Wu, H., Li, Z. M., Zhou, L., and Ye, Q. (2007). Improved succinic acid production in the anaerobic culture of an *Escherichia coli pflB ldhA* double mutant as a result of enhanced anaplerotic activities in the preceding aerobic culture. *Appl. Environ. Microbiol.* 73, 7837–7843. doi: 10.1128/AEM.01546-07

Wynne, S. A., Nicholls, D. J., Scawen, M. D., and Sundaram, T. K. (1996). Tetrameric malate dehydrogenase from a thermophilic *Bacillus*: cloning, sequence and overexpression of the gene encoding the enzyme and isolation and characterization of the recombinant enzyme. *Biochem. J.* 317(Pt 1), 235–245. doi: 10.1042/bj3170235

Xiong, W., Brune, D., and Vermaas, W. F. (2014). The γ-aminobutyric acid shunt contributes to closing the tricarboxylic acid cycle in *Synechocystis* sp. PCC 6803. *Mol. Microbiol.* 93, 786–796. doi: 10.1111/mmi.12699

Xiong, W., Morgan, J. A., Ungerer, J., Wang, B., Maness, P. C., and Yu, J. (2015). The plasticity of cyanobacterial metabolism supports direct CO_2 conversion to ethylene. *Nat. Plants* 1:15053. doi: 10.1038/nplants.2015.53

Zhang, S., and Bryant, D. A. (2011). The tricarboxylic acid cycle in cyanobacteria. *Science* 334, 1551–1553. doi: 10.1126/science.1210858

Zhang, S., and Bryant, D. A. (2015). Biochemical validation of the glyoxylate cycle in the cyanobacterium *Chlorogloeopsis fritschii* strain PCC 9212. *J. Biol. Chem.* 290, 14019–14030. doi: 10.1074/jbc.M115.648170

Conflict of Interest Statement: The authors declare that the research was conducted in the absence of any commercial or financial relationships that could be construed as a potential conflict of interest.

frontiers in Bioengineering and Biotechnology

BOOK REVIEW
published: 13 July 2018
doi: 10.3389/fbioe.2018.00096

Book Review: Algal Green Chemistry Recent Progress in Biotechnology

*Sirisha L. Vavilala, Siddhesh B. Ghag and Jacinta S. D'Souza**

School of Biological Sciences, UM-DAE Centre for Excellence in Basic Sciences, Kalina campus, Mumbai, India

Keywords: algae, cytoprotectants, bioproducts, therapeutics, pigments, biotechnology

A Book Review on
Algal Green Chemistry Recent Progress in Biotechnology

Rajesh Prasad Rastogi, Datta Madamwar and Ashok Pandey (Amsterdam: Elsevier), 2017, 330 pages, ISBN: 978-0-444-64041-3.

An apt for the current issue, the book consists of 14 chapters that provide interesting scientific insights into the vastly rich algal resource. While the book is unstructured, we have divided the review into four scientifically relevant sections (i) Cytoprotectants, (ii) pigments/therapeutics, (iii) bioproducts, and (iv) biomass production.

Chapter one introduces algal osmoprotectants, highlighting the diverse research performed with salinity and its impact on photosynthetic organisms; it specifically focuses on saccharides, glycine betaine, glycerols and dimethylsulfoniopropionate and the accumulation of the last three molecules under abiotic stress. For glycine betaine, the emphasis is on gene expression and enzymatic regulation, while for dimethylsulfoniopropionate the "omics" approach to identify biosynthetic enzymes is elaborated. Further, it expands on the role of Mycosporines and Mycosporine-like amino acids (MAAs) as sunscreen, osmoprotectant, and antioxidants. In chapter two, UV-induced effects on various organisms and the search for algal photoprotectants is discussed. It emphasizes on the role, occurrence, genetic/environmental regulation, and biosynthesis of algal sun protectants (glycosylated MAAs and Scytonemins); further focusing on MAAs that is again described in chapter five. Among cyanobacterial MAAs, the chapter emphasizes upon asterina-330, palythine, palythinol, euhalothece-362, and mycosporine-2-glycine and explains the novel MAAs that exist in algae. It concludes with how UV photoprotectants from nature remain a key exploration area.

Chapter five deals with natural antioxidants with a therapeutic perspective. It begins by highlighting the effect of ROS accumulation on biomolecules; discussing further on oxidative stress-induced mitochondrial irregularities. The occurrence, structure, mode of action, and putative roles in therapeutics of algae-based antioxidants such as phycobiliproteins, phlorotannins, carotenoids, sulfated polysaccharides, Scytonemins, and MAAs is justified. The authors suggest the need for further research to identify high bioactivity molecules. Chapter four deals with the emerging area of nutraceuticals. While microalgae have been a research area for decades, it has only recently served as source of chemicals/pharmaceuticals. It focuses on a variety of nutrients in algae including polyunsaturated fatty acids, vitamins, polysaccharides, and proteins; but, expands on the various categories of polyunsaturated fatty acids, structural chemistry, algal sources, and particularly the health benefits of Omega-3 fatty acids. The authors highlight the types, structural chemistry, algal sources and nutraceutical/biotechnological applications of β-carotene, astaxanthin, and lutein, with a brief mention of the industrial and health applications of algal pigments, vitamins, polysaccharides, Mycosporine and MAAs and bioactive peptides. It concludes with the benefits of nutritionally important algae such as *Haematococcus pluvialis*, *Chlorella*, *Spirulina*,

OPEN ACCESS

Edited by:
Yandu Lu,
Hainan University, China

Reviewed by:
Weiqi Fu,
New York University Abu Dhabi, United Arab Emirates
Kaiyao Huang,
Chinese Academy of Sciences, China

****Correspondence:***
Jacinta S. D'Souza
jacinta@cbs.ac.in

Specialty section:
This article was submitted to Bioenergy and Biofuels, a section of the journal Frontiers in Bioengineering and Biotechnology

Received: *28 March 2018*
Accepted: *25 June 2018*
Published: *13 July 2018*

Citation:
Vavilala SL, Ghag SB and D'Souza JS (2018) Book Review: Algal Green Chemistry Recent Progress in Biotechnology. Front. Bioeng. Biotechnol. 6:96. doi: 10.3389/fbioe.2018.00096

Nannochloropsis. In chapter seven, the authors expand on the factors that influence carotenogenesis like light intensity, temperature, salinity, and nutrient limitation and a description of pigment extraction, applications, and future prospects. In chapter nine, the authors organized the chemical structures, absorbance maxima, and distribution of pigments in a tabular format. It also covers commercialized algal pigments used as skin ointments and cosmetics; however, the application of these pigments in dye/textile industry and as food colorants remains unaddressed. Chapter eight describes the synthesis and catabolism of γ-amino butyric acid and polyamines that accumulate in stress-exposed cells. Accumulation of γ-amino butyric acid in cyanobacteria can be correlated with the nitrogen/carbon source and also supplementation with polyamines (putrescine and spermidine) in the growth medium; the latter accumulate with stress. Variations in the enzymes that synthesize polyamines in cyanobacteria have been observed. Chapter 12 summarizes the occurrence, metabolism and biological significance of polyamines in microalgae and sea grasses. It compiles the investigation of molecular mechanisms of polyamines of macroalgae under stress. However, a comparison between polyamines in macroalgae and higher plants could have been more insightful.

Chapter six discusses several routes ranging from the direct or derivative-based use of microalgal biomass or engineering microalgae to make bioplastics. While the challenge lies in the field of harvesting, innovative cultivation techniques have contributed to its scientific progress. An excellent compilation of the ratios that make use of microalgae producing PHAs blended with petrochemical plastics is provided as a ready-reckoner. Chapter 10 deals with the application of algal species as a biofertilizer that are capable of reclaiming sodic soils and improving the soil microflora. Engineered cyanobacteria have been developed with novel transgenes for upgrading biofertilizer technology. However, translating from lab to field is challenging but worth investing. Chapter 14 deals with algal biofilms that have been visualized as a stress-responsive physiology and a nuisance to the environment. These are now exploited for waste water treatment, nutrient sequestration, as biofertilizers, in the form of biological soil crusts and in the production of biofuels. The authors admit that a thorough understanding of algal biofilms is imminent, a lot needs to be done. Bioenergy derived from algal biomass has been an intensively pursued field and chapter 11 provides an exhaustive overview. It describes ways of optimizing the reactor parameters for increased biomass production. Before standardizing, mathematical simulations are a good starting point. In particular, three models have been put forth for light availability. Added to this issue is, the removal of spent medium and O_2 which inhibit algal growth. Several downstream processes have been provided using single/mixed algal cultures and the challenge in harvesting and extracting the bio-oil remains. It gives the reader a comprehensive account of bio-oil production. Chapter three deals with the proteome-based approach in *Spirulina* for bioproducts production. The authors depict the use of multidiscipline for the implementation of knowledge-to-process implying the need for basic knowledge in biochemical synthesis and regulation in understanding cellular functioning.

Finally, chapter 13 concerns the strategies used in the production of microalgal biomass. Considering their diverse forms, and the potential they exhibit, the nutrients required, growth conditions and the use of appropriate strain is proportionate to the production of biomass; this being equally diverse and heterogeneous.

The research areas covered in this book are rapidly expanding. The authors have comprehensively compiled literature on algal compounds and their applications with depth and clarity. It is handy for students, researchers and industrialists working in the field of algal bioactive compounds. It highlights both recent and past advances in the field presenting the challenges and prospects of translating laboratory research for commercial application.

AUTHOR CONTRIBUTIONS

All authors listed have made a substantial, direct and intellectual contribution to the work, and approved it for publication.

Conflict of Interest Statement: The authors declare that the research was conducted in the absence of any commercial or financial relationships that could be construed as a potential conflict of interest.

frontiers in Plant Science

ORIGINAL RESEARCH
published: 28 June 2018
doi: 10.3389/fpls.2018.00869

A Novel and Convenient Method for Early Warning of Algal Cell Density by Chlorophyll Fluorescence Parameters and Its Application in a Highland Lake

Huan Wang[1,2], Rong Zhu[1,2], Jia Zhang[1,2], Leyi Ni[1], Hong Shen[1] and Ping Xie[1,3]**

[1] Donghu Experimental Station of Lake Ecosystems, State Key Laboratory of Freshwater Ecology and Biotechnology of China, Institute of Hydrobiology, Chinese Academy of Sciences, Wuhan, China, [2] University of Chinese Academy of Sciences, Beijing, China, [3] State Key Laboratory of Plateau Ecology and Agriculture, Qinghai University, Xining, China

OPEN ACCESS

Edited by:
Jianhua Fan,
East China University of Science and Technology, China

Reviewed by:
Raquel Esteban,
University of the Basque Country (UPV/EHU), Spain
Amarendra Narayan Misra,
Khallikote University, India
Taras P. Pasternak,
Albert Ludwigs Universität Freiburg, Germany

***Correspondence:**
Hong Shen
hongshen@ihb.ac.cn
Ping Xie
xieping@ihb.ac.cn

Specialty section:
This article was submitted to Plant Biotechnology, a section of the journal Frontiers in Plant Science

Received: *09 February 2018*
Accepted: *04 June 2018*
Published: *28 June 2018*

Citation:
Wang H, Zhu R, Zhang J, Ni L, Shen H and Xie P (2018) A Novel and Convenient Method for Early Warning of Algal Cell Density by Chlorophyll Fluorescence Parameters and Its Application in a Highland Lake. Front. Plant Sci. 9:869. doi: 10.3389/fpls.2018.00869

The occurrence of algal blooms in drinking water sources and recreational water bodies have been increasing and causing severe environmental problems worldwide, particularly when blooms dominated by *Microcystis* spp. Bloom prediction and early warning mechanisms are becoming increasingly important for preventing harmful algal blooms in freshwater ecosystems. Chlorophyll fluorescence parameters (CFpars) have been widely used to evaluate growth scope and photosynthetic efficiency of phytoplankton. According to our 2-year monthly monitor datasets in Lake Erhai, a simple but convenient method was established to predict *Microcystis* blooms and algal cell densities based on a CFpar representing maximal photochemical quantum yield of Photosystems II (PSII) of algae. Generalized linear mixed models, used to identify the key factors related to the phytoplankton biomass in Lake Erhai, showed significant correlations between Chl *a* concentration and both the light attenuation coefficient and water temperature. We fitted seasonal trends of CFpars (F_v/F_m and $\Delta F/F_m'$) and algal cell densities into the trigonometric regression to predict their seasonal variations and the autocorrelation function was applied to calculate the time lag between them. We found that the time lag only existed between F_v/F_m from blue channel and algal cell densities even both F_v/F_m and $\Delta F/F_m'$ show the significant non-linear dynamics relationships with algal cell densities. The peak values of total algal cell density, cyanobacteria density and *Microcystis* density followed the foregoing peak value of F_v/F_m from blue channel with a time lagged around 40 days. Therefore, we could predict the possibilities of *Microcystis* bloom and estimate the algal cell densities in Lake Erhai ahead of 40 days based on the trends of F_v/F_m values from blue channel. The results from our study implies that the corresponding critical thresholds between F_v/F_m value and bloom occurrence, which might give new insight into prediction of cyanobacteria blooms and provide a convenient and efficient way for establishment of early warning of cyanobacteria bloom in eutrophic aquatic ecosystems.

Keywords: chlorophyll fluorescence, *Microcystis* bloom, generalized linear mixed models, trigonometric regression, Phyto-PAM, algal density, the time lag

INTRODUCTION

Harmful algal blooms (HABs) in freshwater ecosystems are subject of serious concern for ecosystems and human health because they reduce the quality and quantity of habitat for plants and animals, disrupt food web dynamics, create hypoxic zones, and produce toxins (Paerl et al., 2001; Miller et al., 2017). Changing environmental conditions like drought, increased water temperature and low water levels (Paerl et al., 2001; de Figueiredo et al., 2004; Qin et al., 2010; Watson et al., 2017), can increase the intensity and frequency of algal blooms. Further, through its effects on regional and local climatic patterns, climate change is also modifying patterns of HAB (Michalak et al., 2013). Therefore, predicting the HABs has become increasingly important for environmental and public health management.

Many efforts and resources have been devoted to forecasting algal blooms using mathematical modeling through quantitive indicators and environmental drivers. One of the most extensively applied models of predicting blooms are the parametric models (Wong et al., 2007; Gill et al., 2017). For example, the Baltic Operational Oceanographic System (BOOS) is a real-time oceanic observation system combining ecological forecast models for algal bloom in Baltic sea with annual water forecasts for the Baltic sea[1]. Artificial neural networks (ANNs) provide an alternative to parametric forecast models, where several environmental factors act as input variables to estimate the evolution of algal bloom and predict cell densities of freshwater phytoplankton species (Recknagel et al., 1997; Lee et al., 2003; Muttil and Chau, 2006). Statistical methods such as cross-correlation (Trimbee and Prepas, 1987), and generalized additive model (Lamon et al., 1996; Tao et al., 2012), as well as the development of satellite remote sensing forecasting techniques (Stumpf, 2001; Kutser, 2004), are also other possible options for predicting the occurrence of HAB. Despite having good predictive accuracy, all these methods have the major drawback of being time and labor consuming as well as complex in their calculation. Accuracy of these methods also rely on selecting a suitable set of parameters and models according to different lake conditions, nutrient status, and different local meteorological and hydrological conditions. Hence, previous studies have highlighted the need for simple, rapid, and geographically non-restricted approaches to predict algae blooms.

All the methods mentioned above are based on the relationships between algal growth and environmental factors, but rarely use physiological parameters of algae for bloom prediction. Chlorophyll fluorescence parameters (CFpars), F_v/F_m and $\Delta F/F_m'$, can be considered as the main indicators for assessment of the photosystem II efficiency and for the photosynthetic capacity of algae (Misra et al., 2012). The fluorescence ratio F_v/F_m refers to the photosynthetic activity and is taken as an algae viability assessment. Similarly, $\Delta F/F_m'$ reflects the actual physiological activity of PS II (Genty et al., 1990). Previous studies have shown that both F_v/F_m and $\Delta F/F_m'$ respond to changes of environmental factors such as nutrients and light intensity and are directly related to the growth of algae (Boyd et al., 1999; Misra et al., 2012; Shi et al., 2016). Therefore, the use of these CFpars may be suitable candidates for simple predictions of algal blooms. To this end, pulse amplitude modulated (PAM) fluorometry is a promising analytical technique that measures the photochemical efficiency of photosystem II in phytoplankton; one of the most common, non-invasive and rapid existing indicators of the viability condition of phytoplankton in a sample irrespective of their size (Schreiber et al., 1995b; White et al., 2011; Kalaji et al., 2014, 2017). Furthermore, Phyto-PAM fluorometry procedure can distinguish the ratios of fluorescence yields of cyanobacteria, green algae and diatoms/dinoflagellates and output as different channels (blue channel, green channel and brown channel, respectively) (Dorigo and Leboulanger, 2001; Schmitt-Jansen and Altenburger, 2008). In the case of cyanobacteria (blue channel), almost no Chl fluorescence is excited by blue light (470 nm), while excitation at 645 nm is particularly strong due to phycocyanin and allophycocyanin absorption.

Highland lakes are distinctive unique ecosystems because they are subjected to extreme environmental conditions, such as strong radiation, low water temperature, relatively low nutrient conditions, and relatively simple food webs with low species abundance (Tolotti et al., 2006). As a result, these lakes have low buffering capacity and are very sensitive to climate change and other anthropogenic influences (Psenner and Schmidt, 1992; Psenner, 2002). Therefore, this sensitivity and responsiveness of the phytoplankton community in plateau lakes to external environmental stress makes them an ideal system for the purpose of this study. Highland lakes are also increasingly exposed to human activity globally. Common impacts include wastewater discharge from farmlands and households, fish introduction, transport and tourism pollution. These impacts are generating increased eutrophication, disappearance of aquatic vegetation, and algae blooms highland aquatic ecosystems (Tolotti et al., 2006; Huang et al., 2014). Notwithstanding these unfolding environmental problems, few studies have examined bloom forecast in highland lakes.

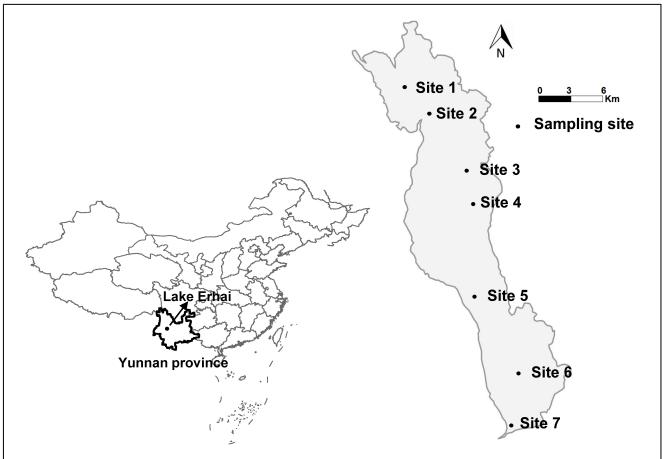

FIGURE 1 | A map of Lake Erhai with the location of the sampling sites.

[1] www.boos.org

Lake Erhai, a typical high altitude lake in the Chinese Yunnan Province, has suffered increasingly frequent cyanobacterial blooms despite the relative lower nutrients and higher illumination characteristic of highland lakes compared to lowland lakes (Xu, 1996; Paerl et al., 2011). These responses are difficult to model explicitly according to conventional models based on quantitive indicators and environmental drivers. Before 1970s, Lake Erhai was an oligotrophic lake (Jin et al., 2005). Since the 80s, however, the lake has been affected by man-made eutrophication resulting from the growing resident population (Jin et al., 2005). This situation exacerbated after the 90s, as district population and human activities continued to increase, resulting in frequent cyanobacterial blooms (Wu and Wang, 1999). Large scale *Anabaena*-dominated cyanobacterial bloom firstly appeared during the summer of 1996 (Dong, 1999). However, the dominant cyanobacterial species during summer shifted to *Microcystis* after 2008 (Wen and Ma, 2011; Wei et al., 2012), coincident with an increase in bloom frequency and intensity. Here, we explore the potential for using multiwavelength Phyto-PAM fluorometry as a simple early warning forecast method for *Microcystis* blooms based on field data collected monthly over 2 years, with a focus on predictive performance and methodological constraints. Our research should give new insight into prediction of cyanobacteria blooms and provide a convenient and efficient way for the establishment of early warning systems of cyanobacterial blooms in eutrophic aquatic ecosystems.

MATERIALS AND METHODS

Study Site and Sampling Method

Data presented in this study correspond to a 2-year (June 2013–May 2015) field survey conducted in Lake Erhai (25°36′–25°58′ N, 100°05′–100°17′ E), the second largest high-altitude freshwater lake of the Yunnan Highlands in China with the normal elevation is 1974 m, to trace algal dynamics and *Microcystis* bloom. Water samples were taken monthly from three water depths (surface, middle, and bottom) at

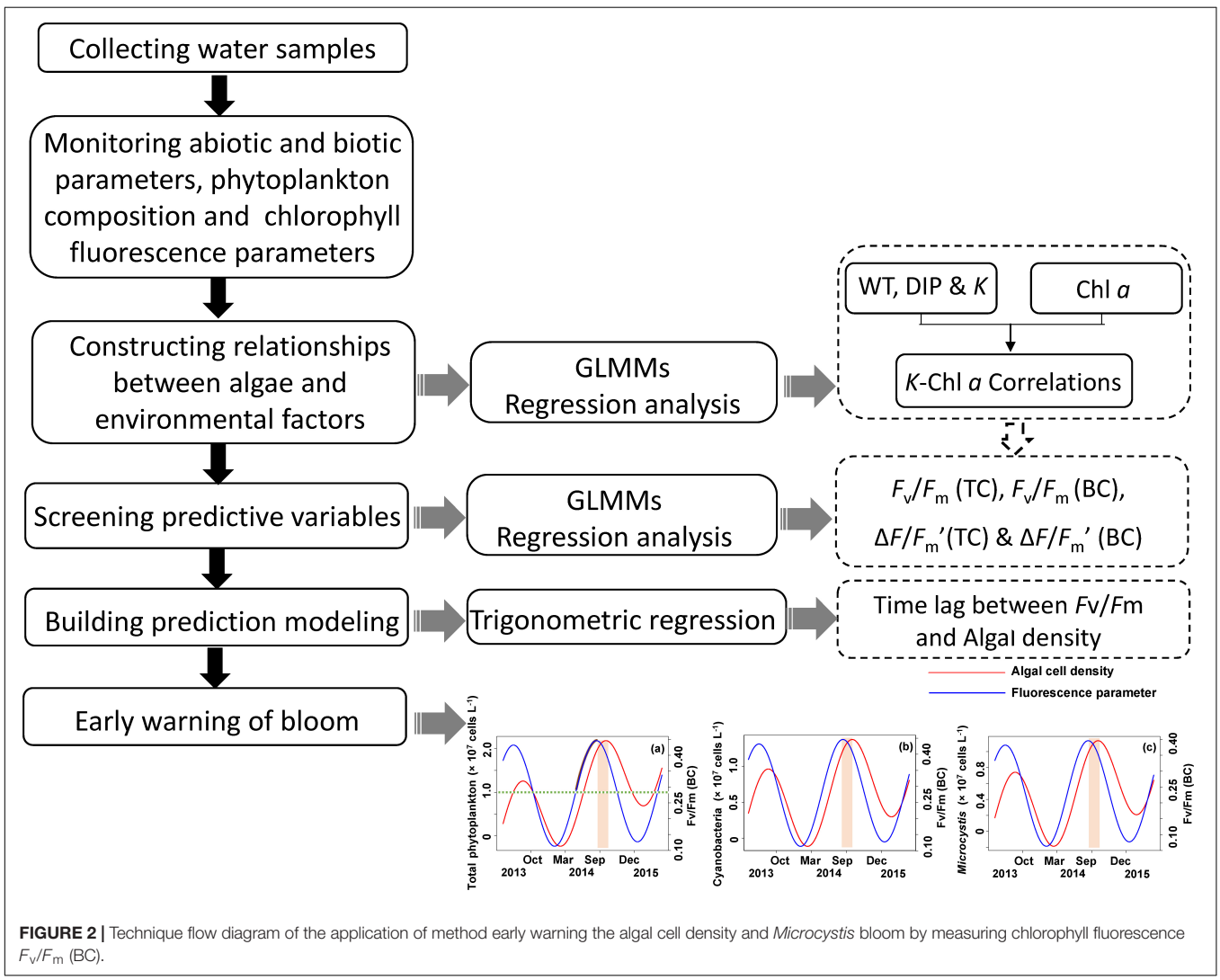

FIGURE 2 | Technique flow diagram of the application of method early warning the algal cell density and *Microcystis* bloom by measuring chlorophyll fluorescence F_v/F_m (BC).

seven sites (**Figure 1**), then pooled for the measurement of physicochemical parameters, physiological indicators, and algal densities at each site. The water samples were stored in transparent glass bottles of 2.5 L and kept bottles half full. After sampling was completed (within 5 h), we measured the CFpars and physicochemical parameters immediately in the laboratory.

Identification of Phytoplankton

One-L water samples were immobilized by 1% Lugol's iodine solution and concentrated to 50 ml by a siphon after sedimentation for 48 h in Utermhol chambers to analyze the phytoplankton composition (Huang et al., 1999). Concentrated samples (0.1 ml) were thereafter counted and measured under 400× magnification using an Olympus microscope (Olympus BX21, Tokyo, Japan) after mixing. Colonial *Microcystis* cells were separated using an ultrasonic device (JY88-II, Scientiz, Ningbo, Zhejiang, China) and their constituent cells counted. Taxonomic identification of the phytoplankton species was performed according to Hu and Wei (Hu, 2006).

Measurements of Physicochemical Parameters

All samples for nutrient and chlorophyll *a* determination were stored in the portable refrigerator (0°C) in the field and analyzed immediately upon returning to the laboratory. Samples for total phosphorus (TP), dissolved total phosphorus (DTP), dissolved inorganic phosphorus (DIP), total nitrogen (TN), nitrate (NO_3^-), ammonium (NO_4^+), and chlorophyll *a* (Chl *a*) concentrations were analyzed following standard preservation and analytical procedures of the Water Environment Federation (Association et al., 1915). The concentrations of Chl *a* was determined by spectroradiometer (SHIMADZU UV-2550, Japan) after appropriate aliquots (200–1000 ml) were filtered through Whatman GF-C glass microfiber filters and 24 h extraction in 90% acetone at 4°C in the dark. The absorbance of the processed samples was recorded at two different wavelengths (665 and 750 nm) following the protocol of Lorenzen (1967) for calculating Chl *a* concentration. Water temperature (T), pH value, dissolved oxygen (DO), and conductivity (COND) were measured onsite at 0.5 m below the water surface with a YSI ProPlus multiparameter water quality meter (Yellow Springs, OH, United States). The Secchi depth (SD) was assessed with a black and white Secchi disk (20 cm in diameter) to determine water transparency. PAR was measured at water depths of 0, 0.5, 1.0, 1.5, and 2.0 m using an underwater radiation sensor (UWQ-8342) connected to a data logger (Li-1400; Li-Cor Company, Lincoln, NE, United States). Light attenuation coefficient of water column (K) was calculated based on the equation: $I_d = I_s(1\text{-}K)/K$, where I_d and I_s are irradiance at the corresponding water depth and water surface, respectively (Duarte et al., 1986).

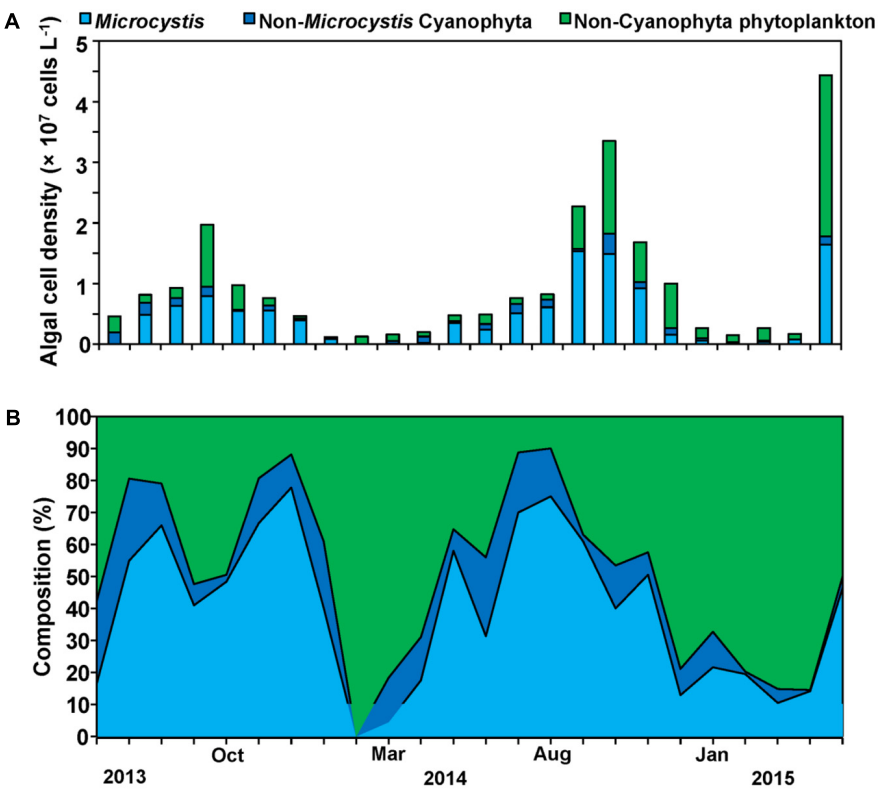

FIGURE 3 | Cell density successions **(A)** and composition successions **(B)** of *Microcystis*, Non- *Microcystis* Cyanophyta and Non-Cyanophyta phytoplankton cell density.

Measurements Chlorophyll Fluorescence Parameters

A Phyto-PAM (PHYTO-PAM Phytoplankton Analyzer, Heinz Walz GMBH, Effeltrich, Germany) was used to measure the maximum quantum yield [$F_v/F_m = (F_m - F_0)/F_m$] and the effective quantum yield [$\Delta F/F_m' = (F_m' - F_0')/F_m'$] (Kühl et al., 2001). PAM fluorometry sensors estimate photosynthetic activity by comparing fluorescence yield of PSII under ambient irradiance (F) and after application of a saturating pulse (F_m) (Bilger et al., 1995; Schreiber et al., 1995a; Schreiber, 2004). F_0 and F_m are the minimum and maximum fluorescence of a dark-adapted sample during a saturating light pulse, respectively. Similarly, F_0' and F_m' are the minimum and maximum fluorescence of a light-adapted sample during a saturating light pulse. Because emission wavelengths (peaking at 470, 520, 645, and 665 nm) do not correspond to the peak wavelengths of absorption of the relevant pigments, the deconvolution procedure requires the ratios of fluorescence yields of cyanobacteria, green algae, and diatoms/dinoflagellates to show pronounced differences upon excitation with these wavelengths.

Statistics and Inferences

The analytical process is schematically shown in **Figure 2**. Generalized linear mixed models (GLMMs) (Bolker et al., 2009) were used to detect the key environment drivers (i.e., light, temperature, and nutrient) correlated to phytoplankton biomass (Chl *a*) during the period of field monitoring. In present study, we used Chl *a* as a measure of algal biomass according to previous studies in both freshwater and marine ecosystems (Carlson, 1977; Barlow et al., 1993; Schlüter et al., 2000; Chen et al., 2003). Sampling site within the lake was introduced as a random effect in the model to avoid pseudoreplication by introducing correlation among species (Hurlbert, 1984). The random effects might also account for some unknown factors that influence the phytoplankton biomass in the lake, such as differences in flow velocity and nutrient concentration among sampling sites. Variables of environment drivers were transformed using square root to normalize the data for analysis.

Generalized linear mixed models (Bolker et al., 2009) was also used to test whether CFpars can predict algae density or biomass. The total phytoplankton cell density (C_t), cyanobacteria cell density (C_c), and *Microcystis* cell density (C_m) were used as response variables. The F_v/F_m from total channel [F_v/F_m (TC)], F_v/F_m from blue channel [F_v/F_m (BC)], $\Delta F/F_m'$ from total channel [$\Delta F/F_m'$ (TC)] and $\Delta F/F_m'$ from blue channel [$\Delta F/F_m'$ (BC)] were used as predictor variables. Site effects were also incorporated as random effect in these models.

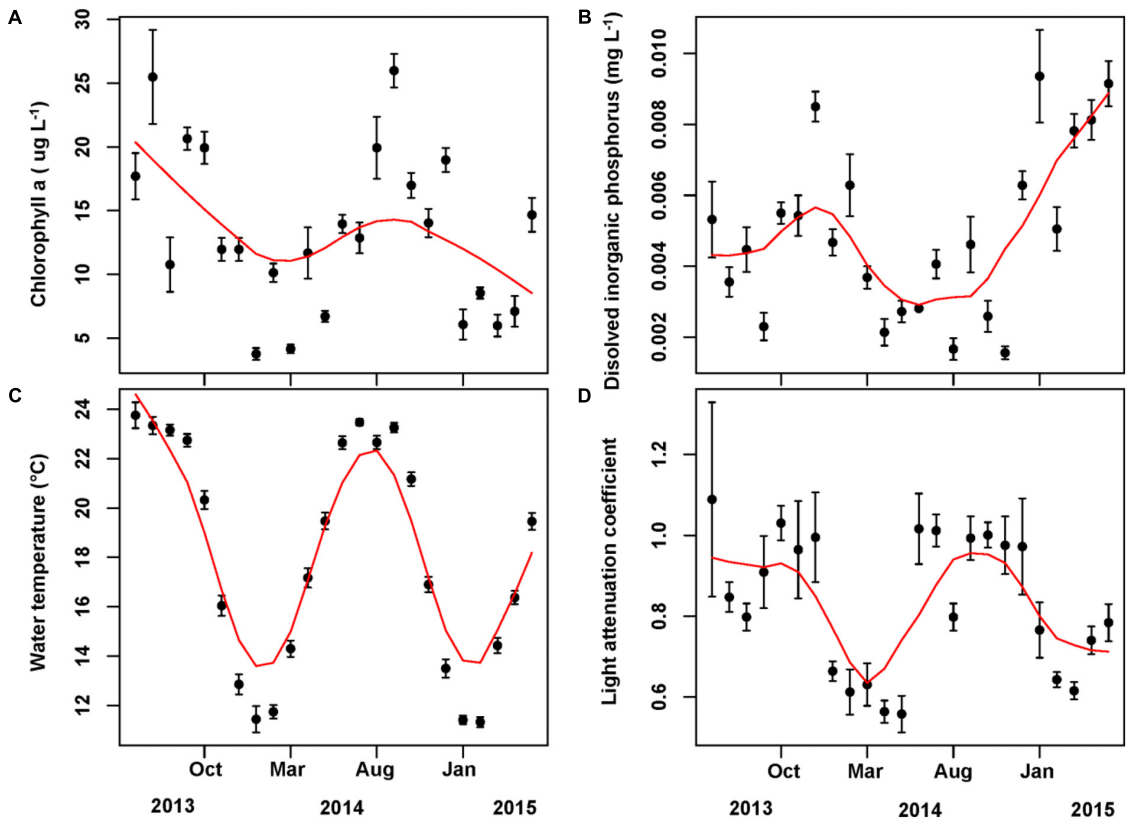

FIGURE 4 | Monthly time series of Chlorophyll *a* **(A)**, dissolved inorganic phosphorus **(B)**, water temperature **(C)**, and light attenuation coefficient **(D)**. The mean value and associated standard deviation among sites is shown in each panel.

Informed by the results from the GLMMs, we built a bloom prediction model by fitting a seasonal trigonometric regression to each cell density parameter (C_t, C_c, and C_m) and the values of F_v/F_m and $\Delta F/F_m'$ according to the following equation (Pollock, 2000):

$$y = \beta_0 + \beta_1 x + \beta_2 sin(2\pi x) + \beta_3 cos(2\pi x) + \varepsilon$$

Where y is cell densities (C_t, C_c, or C_m) or F_v/F_m or $\Delta F/F_m'$, x is time (month), β_0 is the intercept and β_1 is the slope of the regression, which represent stochastic local trend components; β_2 and β_3 are the coefficients of the trigonometric (cyclical) seasonal components [$\sin(2\pi x)$ and $\cos(2\pi x)$]. The error term is represented by ε. The values of x and y were selected at random for running the trigonometric regressions and Each model ran 9999 times for re-randomization tests and the cross correlations between cell density and CFpars were calculated by the autocorrelation function (ACF) with associated confidence intervals at the 0.05 level. Cross-correlation values can be considered as the time lag between cell density and CFpars, which are reported as mean and standard deviation.

All statistical analyses were conducted in R 3.1.0 (R Core Team, 2014) using the packages reshape2 (Wickham, 2007), lme4 (Bates et al., 2011), and ggplot2 (Wickham, 2009).

RESULTS

Phytoplankton Cell Densities

Our sampling campaign lasted 2 years and included two cyanobacteria bloom phases. Cyanophyta was the major phylum of phytoplankton during the whole year with 50% of total phytoplankton cell density, and *Microcystis* was the overwhelming dominant genus during the periods of cyanobacterial blooms with 78% of total cyanobacterial cell density (**Figure 3**). At specific bloom phases *Microcystis* reached up to 80% of all cyanobacterial cell density with the cell densities exceeding 1×10^7 cells L^{-1}, while those of cyanobacterial exceeded 1.5×10^7 cells L^{-1} comprising 60% of all phytoplankton cell density (**Figures 3A,B**).

Driving Factors of Phytoplankton Cell Densities

The mean concentration of Chl *a* during the sampling period (June 2013 to May 2015) was 13.33 ug/L, with a peak value exceeding 30 ug/L. Water temperature and light attenuation coefficient followed similar seasonal variations (**Figure 4**). The maximum level of water temperature encountered in

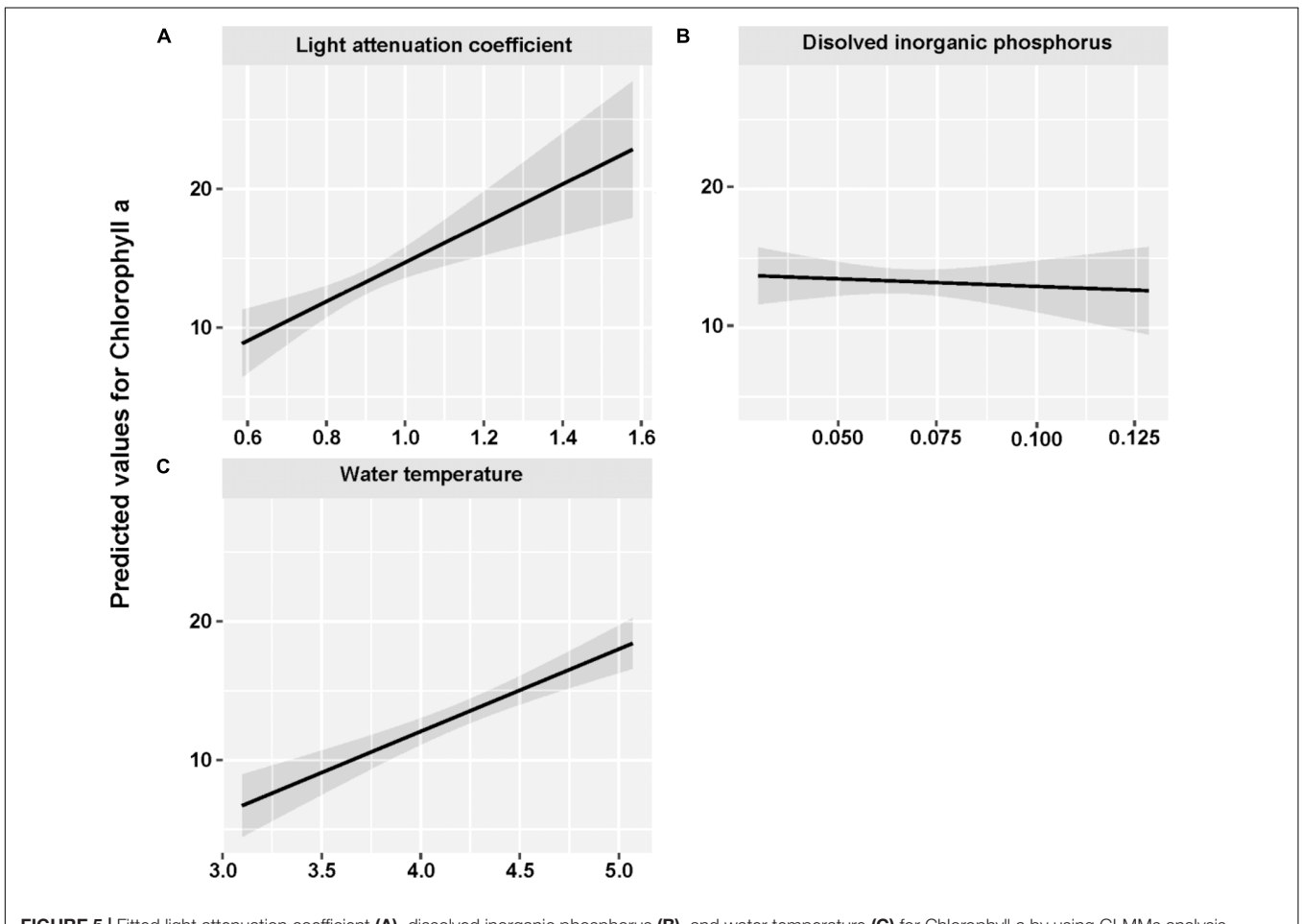

FIGURE 5 | Fitted light attenuation coefficient **(A)**, dissolved inorganic phosphorus **(B)**, and water temperature **(C)** for Chlorophyll *a* by using GLMMs analysis.

TABLE 1 | Values (mean ± SD, ranges in parentheses) of F_v/F_m (TC), F_v/F_m (BC), $\Delta F/F_m'$ (TC), $\Delta F/F_m'$ (BC), C_t, C_c, and C_m using GLMMs with two stochastic (intercept β_0 and slope β_1) local trend components and two trigonometric (cyclical) seasonal components (sin β_2 and cos β_3 pairs).

	β_0	β_1	β_2	β_3	Model adj R^2	Model F	Model *p*-value
F_v/F_m (TC)	0.53 ± 0.01 ($p < 0.001$)	−0.00 ± 0.00 ($p < 0.05$)	0.04 ± 0.01 ($p < 0.001$)	−0.01 ± 0.01 (ns)	0.71	$F_{3,20} = 19.92$	$p < 0.001$
F_v/F_m (BC)	0.27 ± 0.08 ($p < 0.01$)	0.00 ± 0.01 (ns)	0.16 ± 0.05 ($p < 0.01$)	0.04 ± 0.05 (ns)	0.25	$F_{3,20} = 3.56$	$p < 0.05$
$\Delta F/F_m'$ (TC)	0.34 ± 0.023 ($p < 0.001$)	0.00 ± 0.00 (ns)	0.07 ± 0.02 ($p < 0.001$)	−0.01 ± 0.01 (ns)	0.47	$F_{3,20} = 7.75$	$p < 0.05$
$\Delta F/F_m'$ (BC)	0.15 ± 0.06 ($p < 0.05$)	0.00 ± 0.00 ($p < 0.05$)	0.16 ± 0.04 ($p < 0.01$)	0.00 ± 0.04 (ns)	0.34	$F_{3,20} = 4.9$	$p < 0.05$
C_t	22742 ± 4005336 (ns)	770943 ± 285584 ($p < 0.05$)	9190585 ± 2781086 ($p < 0.01$)	−2975061 ± 2584577 (ns)	0.32	$F_{3,20} = 4.69$	$p < 0.05$
C_c	1360317 ± 1656293 (ns)	336873 ± 118095 ($p < 0.01$)	5917219 ± 1150040 ($p < 0.001$)	−2095533 ± 1068779 (ns)	0.54	$F_{3,20} = 10.04$	$p < 0.001$
C_m	541413 ± 1564123 (ns)	330612 ± 111523 ($p < 0.01$)	5211725 ± 1086041 ($p < 0.001$)	−2068081 ± 1009302 (ns)	0.52	$F_{3,20} = 9.17$	$p < 0.001$

Lake Erhai was 25.7°C, and the mean water temperature during sampling period was of 18.0°C (**Figure 4C**). Light attenuation coefficient showed a mean of 0.83 and a maximum of 2.49 (**Figure 4D**). The results from GLMMs model showed a highly significant relationship ($p < 0.0001$) of both water temperature and light attenuation coefficient to Chl *a* concentration (**Figure 5**). In contrast, all nutrient parameters, pH, DO, SD, and COND showed lower non-significant correlations with Chl *a* concentration (data not shown). The annual change of water temperature and the light attenuation coefficient in Lake Erhai, characteristic of a highland lake, and their close relationship to Chl *a*, suggest a potential relationship between algal cell densities, photosynthetic activity and the seasonal succession of algae, which can be predicted directly/indirectly by measuring the fluorescence parameters.

Testing Parameters of GLMMs

To test the practicability of using the CFpars for determining the algal cell density in water columns, we used F_v/F_m (TC), F_v/F_m (BC), $\Delta F/F_m'$ (TC), $\Delta F/F_m'$ (BC), C_t, C_c, and C_m fitting time cycle changes of GLMMs. All parameters were significantly correlated with seasonality ($p < 0.05$). Further, F_v/F_m (TC), F_v/F_m (BC), and C_m were highly significantly correlated with seasonal variation ($p < 0.001$) (**Table 1**). As a result, all these parameters could be potentially selected for model creation to estimate phytoplankton cell density by fluorescence, where model prediction of algal cell density is a function of its Chlorophyll light response.

Time Lag Between Algal Cell Density and Fluorescence Parameters

The relationship between the algal cell density and F_v/F_m or $\Delta F/F_m'$ value was also first identified by GLMMs, then fitted using trigonometric regression. We found significant positive non-linear correlations between fluorescence parameters and cell density (**Figures 6–8**).

No apparent time lag was found between F_v/F_m (TC) and C_t (**Figures 6b,f**) or C_c (**Figures 7b,f**) or C_m (**Figures 8b,f**). However, the time lag between F_v/F_m (BC) and C_t (**Figures 6b,f**) or C_c (**Figures 7b,f**) or C_m (**Figures 8b,f**) was almost 40 days. F_v/F_m (BC) lead on average C_t by 38.9 ± 5.3 days (**Figures 4C,D**). F_v/F_m (BC) lead C_c by 37.8 ± 5.6 days (**Figures 7c,g**). F_v/F_m (BC) forward lead C_m by 39.1 ± 5.5 (**Figures 8c,g**). Similarly, no time lag was found between $\Delta F/F_m'$ (TC) and neither C_t (**Figures 6d,h**), C_c (**Figures 7d,h**), or C_m (**Figures 8d,h**). Time lags were found in the other parameters, with the $\Delta F/F_m'$ (BC) leading total phytoplankton cell density by 0.2 ± 0.9 days (**Figures 6e,i**); $\Delta F/F_m'$ (BC) leading C_c by 0.1 ± 0.6 days (**Figures 7e,i**); and $\Delta F/F_m'$ (BC) leading C_m by 0.5 ± 1.3 days (**Figures 8e,i**).

Application of F_v/F_m (BC) to Early Warning of *Microcystis* Blooms

According to the strong time lag between F_v/F_m and cell density, forecasting *Microcystis* bloom and the cell density in Lake Erhai

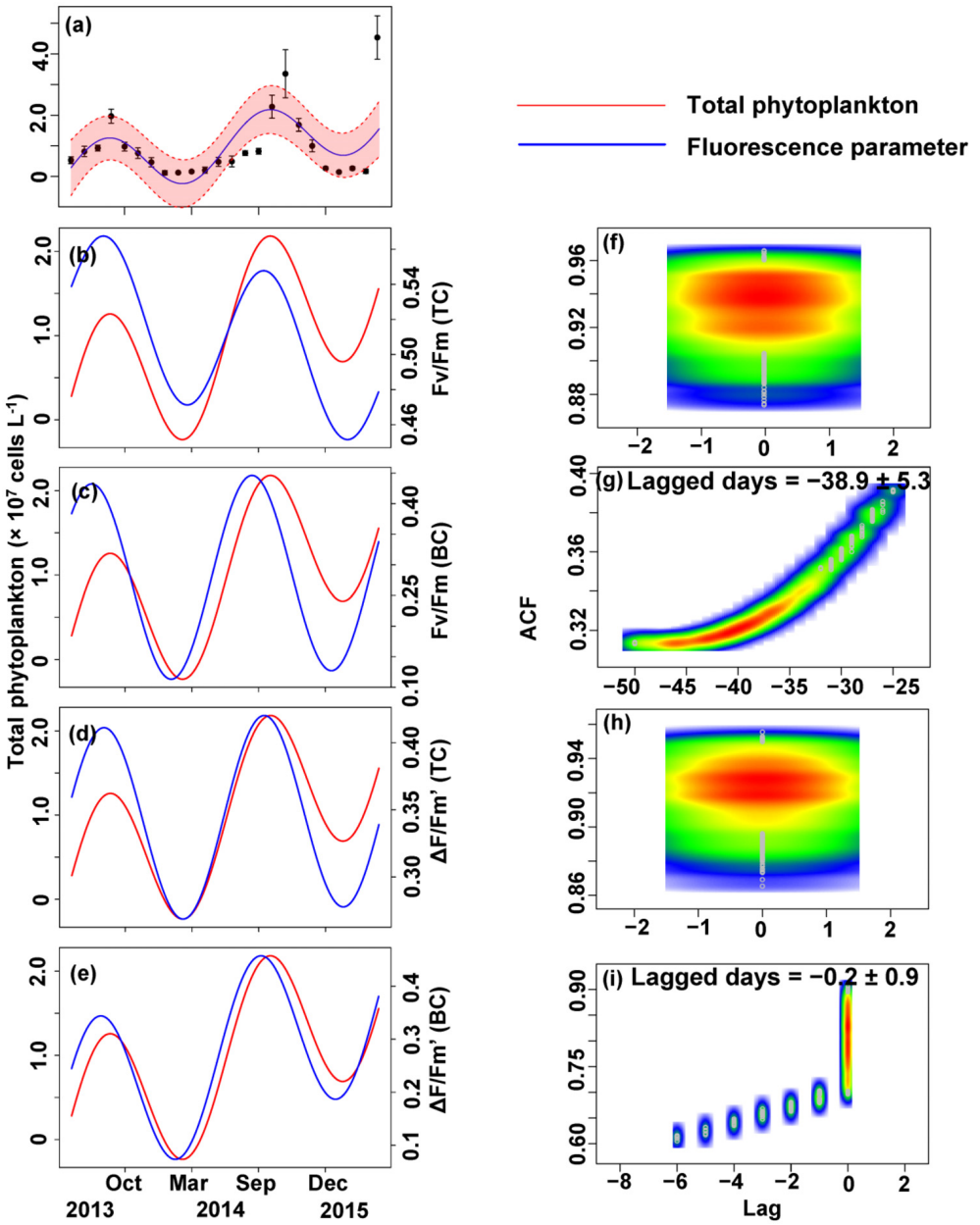

FIGURE 6 | Trigonometric regression of the total phytoplankton cell density ($\times 10^7$ cells L^{-1}) **(a)** and fluorescence measurements [F_v/F_m (TC) **(b)**, F_v/F_m (BC) **(c)**, $\Delta F/F_m'$ (TC) **(d),** and $\Delta F/F_m'$ (BC) **(e)**]. We fitted these seasonal trends with a time-lag analysis [F_v/F_m (TC) **(f)**, F_v/F_m (BC) **(g)**, $\Delta F/F_m'$ (TC) **(h)**, and $\Delta F/F_m'$ (BC) **(i)**]. The legged days and associated standard deviation among sites is shown in each panel.

should be possible by in lake monitoring of the F_v/F_m (BC) value (**Figure 9**). The trigonometric regression (**Figure 9A**) shows that the likelihood of a cyanobacteria bloom can increase when the value of F_v/F_m reach 0.28 and the trend keeps upward. But if the trend decreases, the possibility of cyanobacteria bloom can become low even if the value of F_v/F_m remains higher than 0.28. If the trend of F_v/F_m declines and the F_v/F_m value is lower than 0.28, a cyanobacteria bloom seems unlikely. Here, we define 10^7 cells L^{-1} as the threshold value for a cyanobacteria bloom. The peak value of F_v/F_m (BC) is usually followed by a peak value of phytoplankton after approximately 40 days.

DISCUSSION

In present study, we developed a novel method to predict *Microcystis* bloom via physiological parameters of algae and provided a rapid and simple way of early warning for blooms. Compare to the common approaches (direct physicochemical

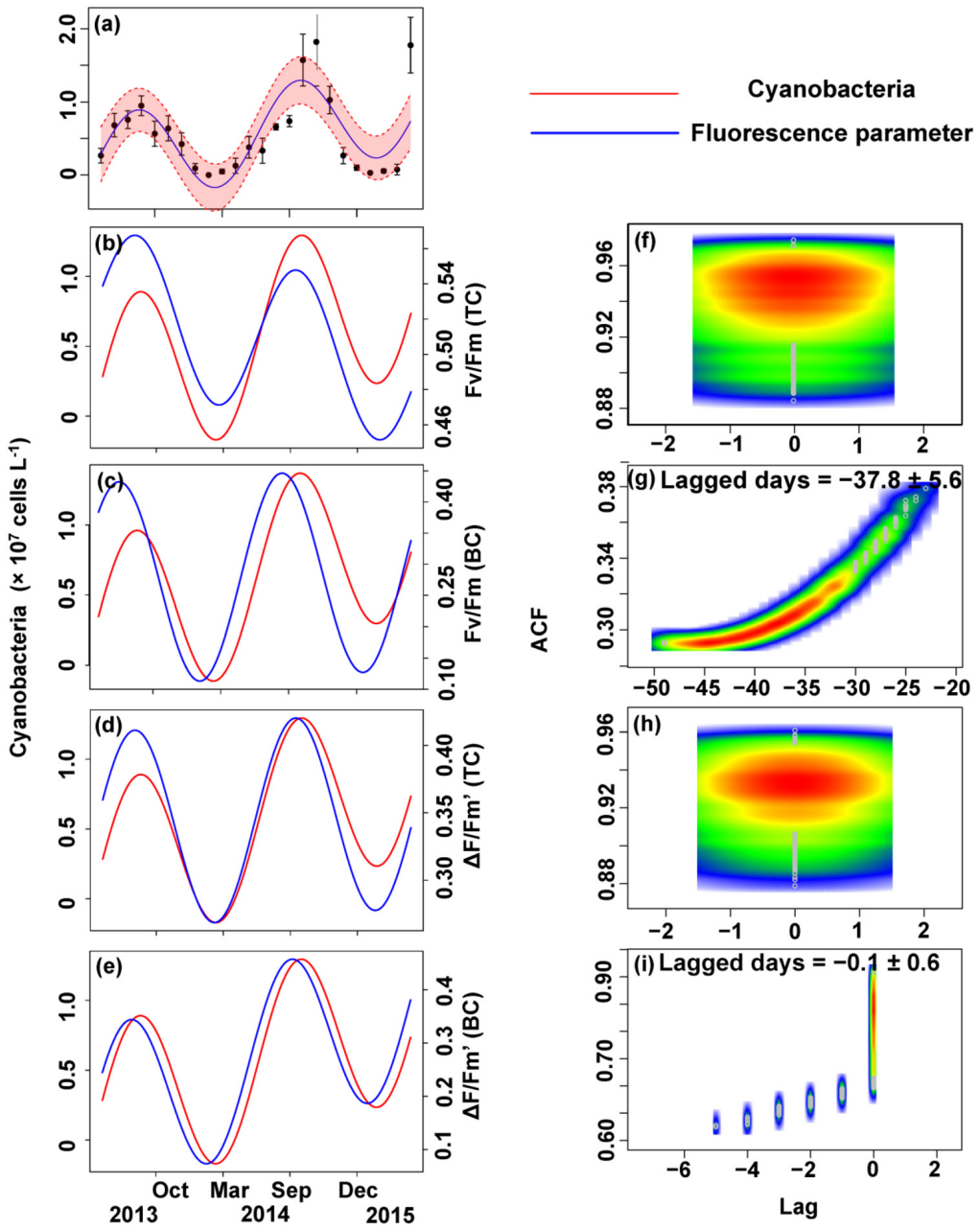

FIGURE 7 | Trigonometric regression of the cyanobacteria cell density **(a)** and fluorescence measurements [F_v/F_m (TC) **(b)**, F_v/F_m (BC) **(c)**, $\Delta F/F_m'$ (TC) **(d)**, and $\Delta F/F_m'$ (BC) **(e)**]. We fitted these seasonal trends with a time-lag analysis [F_v/F_m (TC) **(f)**, F_v/F_m (BC) **(g)**, $\Delta F/F_m'$ (TC) **(h)**, and $\Delta F/F_m'$ (BC) **(i)**]. The legged days and associated standard deviation among sites is shown in each panel.

measurements combined with regular monitoring) of bloom forecast (Trimbee and Prepas, 1987; Recknagel et al., 1997; Wong et al., 2007; Winder and Sommer, 2012; Ruiz-de la Torre et al., 2013; Gill et al., 2017), our method could save both time and labor by handling just one forecast factor through a single operation. Compare to the remote sensing approaches, the effective ways which widely used for short-term bloom forecast by using satellite and airborne measurements of spectral reflectance of water color (Wynne et al., 2013; Gill et al., 2017) even sometimes they were limited to the use of cloudless remote-sensing images and constrained by pixels, our method emphasized on chlorophyll fluorescent parameters (F_v/F_m) instead of monitoring Chl *a* concentrations. A similar method for bloom prediction has not been reported so far. Both abiotic environmental factors (O'neil et al., 2012; Paerl and Paul, 2012; Winder and Sommer, 2012; Ruiz-de la Torre et al., 2013) and biotic factors (Provasoli, 1958; González et al., 2000; Chattopadhayay et al., 2002) could affect the concentrations

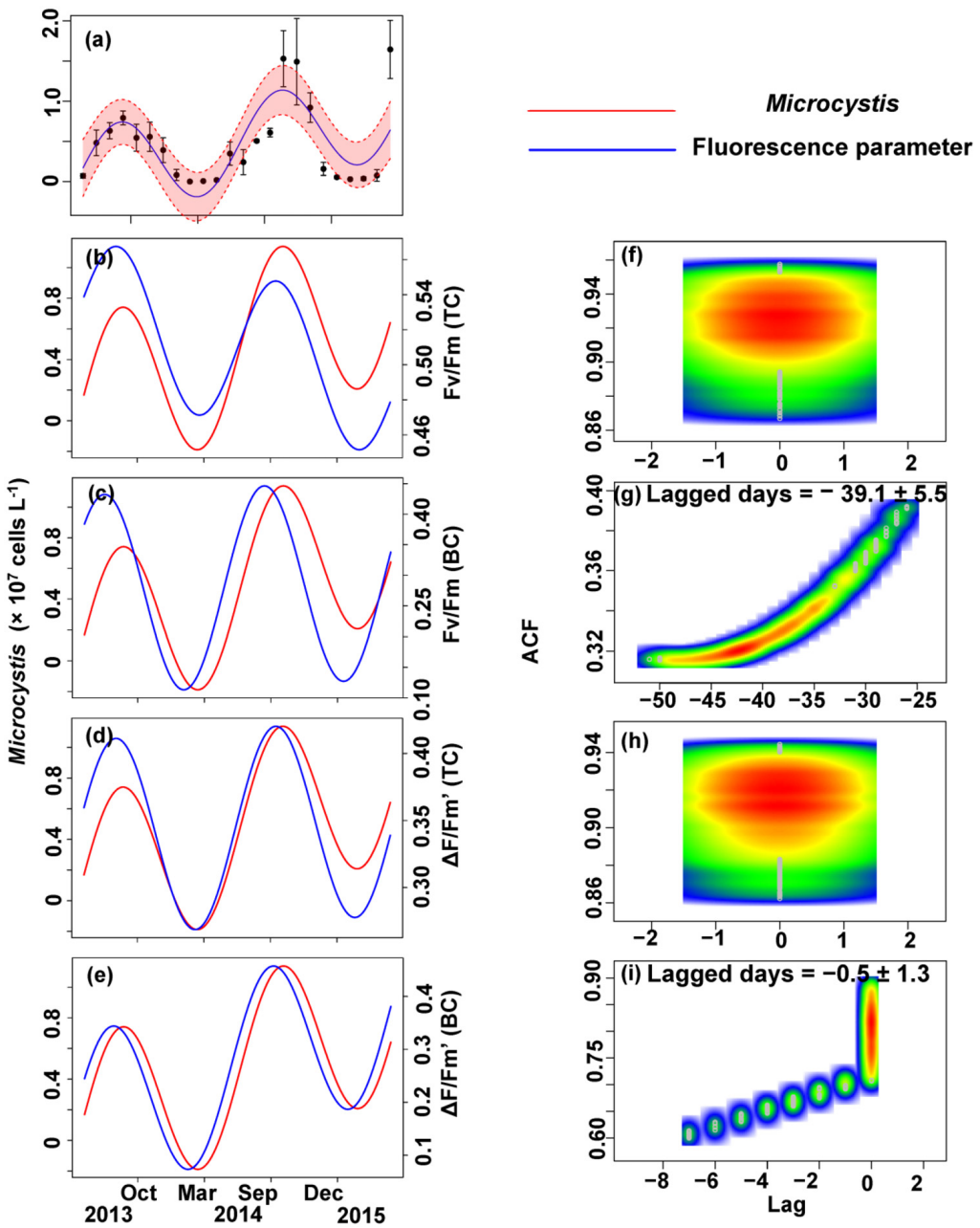

FIGURE 8 | Trigonometric regression of the *Microcystis* cell density **(a)** and fluorescence measurements [F_v/F_m (TC) **(b)**, F_v/F_m (BC) **(c)**, $\Delta F/F_m'$ (TC) **(d)**, and $\Delta F/F_m'$ (BC) **(e)**]. We fitted these seasonal trends with a time-lag analysis [F_v/F_m (TC) **(f)**, F_v/F_m (BC) **(g)**, $\Delta F/F_m'$ (TC) **(h)**, and $\Delta F/F_m'$ (BC) **(i)**]. The legged days and associated standard deviation among sites is shown in each panel.

of Chl *a* and trigger cyanobacterial blooms. Unlike the effects of environmental factors on phytoplankton, the maximum quantum yield (F_v/F_m) indicates directly photosynthetic activity of phytoplankton (Schreiber et al., 1995b; Shi et al., 2016). F_v/F_m can drop significantly when algae in response to changing environmental conditions (Shen and Song, 2007; Shi et al., 2016). Therefore, F_v/F_m can be considered as a sensitive indicator that can reflect algae viability assessment (Genty et al., 1990; Oxborough and Baker, 1997; Boyd et al., 2000).

The GLMMs, trigonometric regression and ACF are the main analytical models used in our method for prediction of time lag responses in dynamics of phytoplankton. GLMMs model are a popular and widely used method for selecting driving factors in fisheries research (Venables and Dichmont, 2004) and plant litter decomposition (Veen et al., 2015), and seemed to successfully determine the dominant factors in our study. The trigonometric regression can effectively reflect and forecast the time series changes and seasonal trends of electricity demand (Harvey and

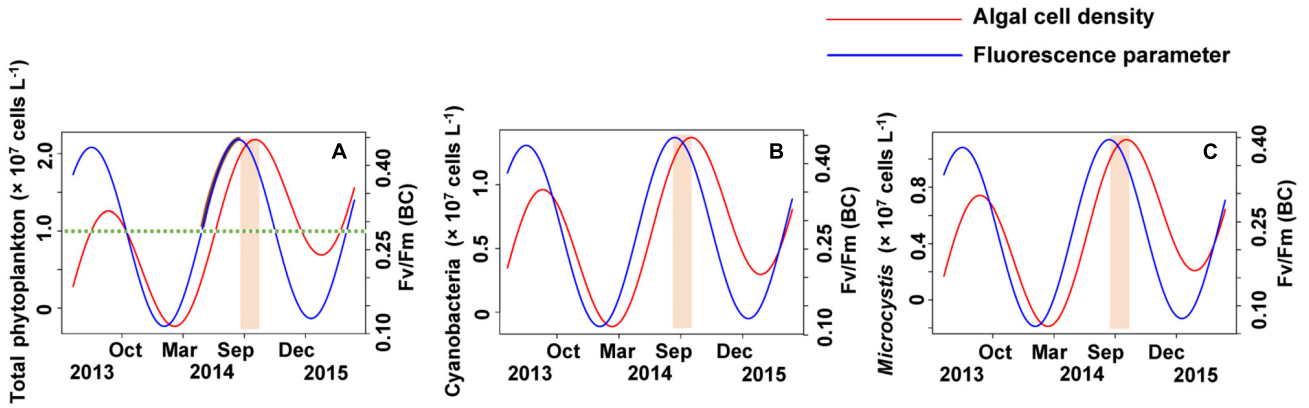

FIGURE 9 | The early warning of algal cell density and *Microcystis* bloom by simulating the time lag between F_v/F_m (BC) and algal cell density. **(A)** Total phytoplankton, **(B)** Cyanobacteria, **(C)** *Microcystis*.

Koopman, 1993; Zhou et al., 2006), but has not been applied before to algal bloom forecasting. Again, our results show that it can fit to the purpose of reconstructing seasonal patterns of cell density, F_v/F_m and $\Delta F/F_m'$. The combination of results from the GLMMs and trigonometric regressions allowed in turn for the estimation of time lags between algal cell density and the fluorescence parameter using the ACF, and the random error was examined by Permutation test. Given light intensity play an important role in the dynamics of phytoplankton of Lake Erhai, the fluorescence parameters could capture the physiological characteristics of algae. The model created by fluorescence parameters had considerable predictive capacity of early bloom warning.

Our method should be applicable to algal bloom forecasting in other eutrophic lakes, but it might be not suitable for lakes where the diversity of phytoplankton is too high. Due to the complex pigment composition of chloroplast, each species of algae has its own excitation and emission wavelength, resulting in species-specific channel in different water environments through the fluorescence method (Schreiber, 2004). In the present study, cyanophyta was the clear dominant phylum and *Microcystis* the overwhelming dominant genus of cyanophyta. Thus, the blue channel value of F_v/F_m can reflect the PSII function of *Microcystis* and infer the possible cell density. The forecasting ability of a model for early warning of algal blooms depends also on the quantity of data and the frequency of sampling (Andersen and Bollerslev, 1998; Ghysels et al., 2006). Whether monthly or higher sampling frequencies (e.g., fortnightly, weekly, or daily) are most appropriate for early warning by time lag analysis deserves further research. At the same time, an *in situ* measurement might be more helpful for accurate prediction.

CONCLUSION

We have established a rapid, simple and convenient novel method to estimate the algal cell density in a plateau lake by measuring chlorophyll fluorescence F_v/F_m; a sensitive physiological parameter which directly reflects growth potentiality of algal and forecasts algal further growth rather than early warning of contamination. The traits of F_v/F_m make it more efficient for prediction of algal bloom than using physicochemical parameters. Our study implies that in addition to the parameters of chlorophyll fluorescence, other physiological parameters of algal might also can be applied to the prediction of algal bloom. These results suggest using critical thresholds between F_v/F_m value and bloom occurrence might give new insight into prediction of cyanobacteria blooms and provide a convenient and efficient way for establishment of early warning of cyanobacteria bloom in eutrophic aquatic ecosystems.

AUTHOR CONTRIBUTIONS

PX and HS designed the study. HW and RZ conducted the experiments. HW analyzed the data and led the manuscript writing. JZ and LN helped perform the analysis. HS revised the manuscript. All authors contributed to the final draft.

FUNDING

This research was jointly supported by the National Key Research and Development Program of China (2017YFA0605201), the Project of Qinghai Science & Technology Department (2016-ZJ-Y01), the Open Project of State Key Laboratory of Plateau Ecology and Agriculture, Qinghai University (2017-KF-07), and the Major Science and Technology Program for Water Pollution Control and Treatment of China (2012ZX07105-004).

ACKNOWLEDGMENTS

We thank the three reviewers for their valuable comments and suggestions, Prof. Jun Xu and Prof. Jorge Molinos Garcia for their constructive suggestions and professional editing and Ms. Dandan Zhao and Mr. Changbo Yuan for their help on sample collection.

REFERENCES

Andersen, T. G., and Bollerslev, T. (1998). Answering the skeptics: yes, standard volatility models do provide accurate forecasts. *Int. Econ. Rev.* 394, 885–905. doi: 10.2307/2527343

Association, A. P. H., Association, A. W. W., Federation, W. P. C., and Federation, W. E. (1915). *Standard Methods for the Examination of Water and Wastewater*. Washington, DC: American Public Health Association.

Barlow, R., Mantoura, R., Gough, M., and Fileman, T. (1993). Pigment signatures of the phytoplankton composition in the northeastern Atlantic during the 1990 spring bloom. Deep Sea Research Part II. *Top. Stud. Oceanogr.* 40, 459–477. doi: 10.1016/0967-0645(93)90027-K

Bates, D., Maechler, M., and Bolker, B. (2011). *lme4: Linear Mixed-Effects Models using S4 Classes*. Available at: http://lme4.r-forge.r-project.org/

Bilger, W., Schreiber, U., and Bock, M. (1995). Determination of the quantum efficiency of photosystem II and of non-photochemical quenching of chlorophyll fluorescence in the field. *Oecologia* 102, 425–432. doi: 10.1007/BF00341354

Bolker, B. M., Brooks, M. E., Clark, C. J., Geange, S. W., and Poulsen, J. R. (2009). Generalized linear mixed models: a practical guide for ecology and evolution. *Trends Ecol. Evol.* 24, 127–135. doi: 10.1016/j.tree.2008.10.008

Boyd, P., Laroche, J., Gall, M., Frew, R., and Mckay, R. M. L. (1999). Role of iron, light, and silicate in controlling algal biomass in subantarctic waters SE of New Zealand. *J. Geophys. Res.* 104, 13395–13408. doi: 10.1029/1999JC900009

Boyd, R. W., Watson, A. J., Law, C. S., and Abraham, E. R. (2000). A mesoscale phytoplankton bloom in the polar Southern Ocean stimulated by iron fertilization. *Nature* 407, 695–702. doi: 10.1038/35037500

Carlson, R. E. (1977). A trophic state index for lakes. *Limnol. Oceanogr.* 22, 361–369. doi: 10.4319/lo.1977.22.2.0361

Chattopadhayay, J., Sarkar, R., and Mandal, S. (2002). Toxin-producing plankton may act as a biological control for planktonic blooms—field study and mathematical modelling. *J. Theor. Biol.* 215, 333–344. doi: 10.1006/jtbi.2001.2510

Chen, Y., Fan, C., Teubner, K., and Dokulil, M. (2003). Changes of nutrients and phytoplankton chlorophyll-a in a large shallow lake, Taihu, China: an 8-year investigation. *Hydrobiologia* 506, 273–279. doi: 10.1023/B:HYDR.0000008604.09751.01

de Figueiredo, D. R., Azeiteiro, U. M., Esteves, S. M., Gonçalves, F. J., and Pereira, M. J. (2004). Microcystin-producing blooms—a serious global public health issue. *Ecotoxicol. Environ. Saf.* 59, 151–163. doi: 10.1016/j.ecoenv.2004.04.006

Dong, Y. (1999). Research on blue algae plakton bloom in Erhai lake. *Yunnan Environ. Sci.* 4:010. doi: 10.13623/j.cnki.hkdk.1999.04.010

Dorigo, U., and Leboulanger, C. (2001). A pulse-amplitude modulated fluorescence-based method for assessing the effects of photosystem II herbicides on freshwater periphyton. *J. Appl. Phycol.* 13, 509–515. doi: 10.1023/A:1012598816581

Duarte, C. M., Kalff, J., and Peters, R. H. (1986). Patterns in biomass and cover of aquatic macrophytes in lakes. *Can. J. Fish. Aquat. Sci.* 43, 1900–1908. doi: 10.1139/f86-235

Genty, B., Harbinson, J., Briantais, J.-M., and Baker, N. R. (1990). The relationship between non-photochemical quenching of chlorophyll fluorescence and the rate of photosystem 2 photochemistry in leaves. *Photosynth. Res.* 25, 249–257. doi: 10.1007/BF00033166

Ghysels, E., Santa-Clara, P., and Valkanov, R. (2006). Predicting volatility: getting the most out of return data sampled at different frequencies. *J. Economet.* 131, 59–95. doi: 10.1016/j.jeconom.2005.01.004

Gill, D., Ming, T., and Ouyang, W. (2017). *Improving the Lake Erie HAB Tracker: A Forecasting & Decision Support Tool for Harmful Algal Blooms*. Available at: http://hdl.handle.net/2027.42/136562

González, J. M., Simó, R., Massana, R., Covert, J. S., and Casamayor, E. O. (2000). Bacterial community structure associated with a dimethylsulfoniopropionate-producing North Atlantic algal bloom. *Appl. Environ. Microbiol.* 66, 4237–4246. doi: 10.1128/AEM.66.10.4237-4246.2000

Harvey, A., and Koopman, S. J. (1993). Forecasting hourly electricity demand using time-varying splines. *J. Am. Statist. Assoc.* 88, 1228–1236. doi: 10.2307/2291261

Hu, H. (2006). *The Freshwater Algae of China: Systematics, Taxonomy and Ecology*. Ottawa, ON: Science Press.

Huang, C., Wang, X., Yang, H., Li, Y., and Wang, Y. (2014). Satellite data regarding the eutrophication response to human activities in the plateau lake Dianchi in China from 1974 to 2009. *Sci. Total Environ.* 485, 1–11. doi: 10.1016/j.scitotenv.2014.03.031

Huang, X., Chen, W., and Cai, Q. (1999). *Survey, Observation and Analysis of Lake Ecology*. Beijing: Science Press.

Hurlbert, S. H. (1984). Pseudoreplication and the design of ecological field experiments. *Ecol. Monogr.* 54, 187–211. doi: 10.2307/1942661

Jin, X., Xu, Q., and Huang, C. (2005). Current status and future tendency of lake eutrophication in China. *Sci. China Ser. C* 48, 948–954. doi: 10.1360/062005-286

Kalaji, H. M., Schansker, G., Brestic, M., Bussotti, F., and Calatayud, A. (2017). Frequently asked questions about chlorophyll fluorescence, the sequel. *Photosynth. Res.* 132, 13–66. doi: 10.1007/s11120-016-0318-y

Kalaji, H. M., Schansker, G., Ladle, R. J., Goltsev, V., and Bosa, K. (2014). Frequently asked questions about in vivo chlorophyll fluorescence: practical issues. *Photosynth. Res.* 122, 121–158. doi: 10.1007/s11120-014-0024-6

Kühl, M., Glud, R. N., Borum, J., Roberts, R., and Rysgaard, S. (2001). Photosynthetic performance of surface-associated algae below sea ice as measured with a pulse amplitude-modulated (PAM) fluorometer and O2 microsensors. *Mar. Ecol. Prog. Ser.* 223, 1–14. doi: 10.3354/meps223001

Kutser, T. (2004). Quantitative detection of chlorophyll in cyanobacterial blooms by satellite remote sensing. *Limnol. Oceanogr.* 49, 2179–2189. doi: 10.4319/lo.2004.49.6.2179

Lamon, E. C., Reckhow, K. H., and Havens, K. E. (1996). Using generalized additive models for prediction of chlorophyll *a* in Lake Okeechobee, Florida. *Lakes Reservoirs Res. Manag.* 2, 37–46. doi: 10.1111/j.1440-1770.1996.tb00046.x

Lee, J. H., Huang, Y., Dickman, M., and Jayawardena, A. W. (2003). Neural network modelling of coastal algal blooms. *Ecol. Model.* 159, 179–201. doi: 10.1016/S0304-3800(02)00281-8

Lorenzen, C. J. (1967). Determination of chlorophyll and pheo-pigments: spectrophotometric equations. *Limnol. Oceanogr.* 12, 343–346. doi: 10.4319/lo.1967.12.2.0343

Michalak, A. M., Anderson, E. J., Beletsky, D., Boland, S., and Bosch, N. S. (2013). Record-setting algal bloom in Lake Erie caused by agricultural and meteorological trends consistent with expected future conditions. *Proc. Natl. Acad. Sci. U.S.A.* 110, 6448–6452. doi: 10.1073/pnas.1216006110

Miller, T. R., Beversdorf, L. J., Weirich, C. A., and Bartlett, S. L. (2017). Cyanobacterial toxins of the laurentian great lakes, their toxicological effects, and numerical limits in drinking water. *Mar. Drugs* 15:E160. doi: 10.3390/md15060160

Misra, A. N., Misra, M., and Singh, R. (2012). *Chlorophyll Fluorescence in Plant Biology*. Available at: http://www.intechopen.com/books/biophysics/chlorophyll-fluorescence-in-plant-biology

Muttil, N., and Chau, K.-W. (2006). Neural network and genetic programming for modelling coastal algal blooms. *Int. J. Environ. Pollut.* 28, 223–238. doi: 10.1504/IJEP.2006.011208

O'neil, J., Davis, T., Burford, M., and Gobler, C. (2012). The rise of harmful cyanobacteria blooms: the potential roles of eutrophication and climate change. *Harm. Algae* 14, 313–334. doi: 10.1016/j.hal.2011.10.027

Oxborough, K., and Baker, N. R. (1997). Resolving chlorophyll a fluorescence images of photosynthetic efficiency into photochemical and non-photochemical components–calculation of qP and Fv′/Fm′ without measuring Fo. *Photosynth. Res.* 54, 135–142. doi: 10.1023/A:1005936823310

Paerl, H. W., Fulton, R. S., Moisander, P. H., and Dyble, J. (2001). Harmful freshwater algal blooms, with an emphasis on cyanobacteria. *Sci. World J.* 1, 76–113. doi: 10.1100/tsw.2001.16

Paerl, H. W., and Paul, V. J. (2012). Climate change: links to global expansion of harmful cyanobacteria. *Water Res.* 46, 1349–1363. doi: 10.1016/j.watres.2011.08.002

Paerl, H. W., Xu, H., Mccarthy, M. J., Zhu, G., and Qin, B. (2011). Controlling harmful cyanobacterial blooms in a hyper-eutrophic lake (Lake Taihu, China): the need for a dual nutrient (N & P) management strategy. *Water Res.* 45, 1973–1983. doi: 10.1016/j.watres.2010.09.018

Pollock, D. (2000). Trend estimation and de-trending via rational square-wave filters. *J. Economet.* 99, 317–334. doi: 10.1016/S0304-4076(00)00028-2

Provasoli, L. (1958). Nutrition and ecology of protozoa and algae. *Annu. Rev. Microbiol.* 12, 279–308. doi: 10.1146/annurev.mi.12.100158.001431

Psenner, R. (2002). Alpine waters in the interplay of global change: complex links-simple effects. *Moun. Res. Dev.* 25, 376–385.

Psenner, R., and Schmidt, R. (1992). Climate-driven pH control of remote alpine lakes and effects of acid deposition. *Nature* 356:781. doi: 10.1038/356781a0

Qin, B., Zhu, G., Gao, G., Zhang, Y., and Li, W. (2010). A drinking water crisis in Lake Taihu, China: linkage to climatic variability and lake management. *Environ. Manag.* 45, 105–112. doi: 10.1007/s00267-009-9393-6

R Core Team (2014). *R: A Language and Environment for Statistical Computing*. Vienna: R Foundation for Statistical Computing.

Recknagel, F., French, M., Harkonen, P., and Yabunaka, K.-I. (1997). Artificial neural network approach for modelling and prediction of algal blooms. *Ecol. Model.* 96, 11–28. doi: 10.1016/S0304-3800(96)00049-X

Ruiz-de la Torre, M. C., Maske, H., Ochoa, J., and Almeda-Jauregui, C. O. (2013). Maintenance of coastal surface blooms by surface temperature stratification and wind drift. *PLoS One* 8:e58958. doi: 10.1371/journal.pone.0058958

Schlüter, L., Møhlenberg, F., Havskum, H., and Larsen, S. (2000). The use of phytoplankton pigments for identifying and quantifying phytoplankton groups in coastal areas: testing the influence of light and nutrients on pigment/chlorophyll a ratios. *Mar. Ecol. Prog. Ser.* 192, 49–63. doi: 10.3354/meps192049

Schmitt-Jansen, M., and Altenburger, R. (2008). Community-level microalgal toxicity assessment by multiwavelength-excitation PAM fluorometry. *Aquat. Toxicol.* 86, 49–58. doi: 10.1016/j.aquatox.2007.10.001

Schreiber, U. (2004). *Pulse-Amplitude-Modulation (PAM) Fluorometry and Saturation Pulse Method: An Overview*. Würzburg: University of Wuerzburg. doi: 10.1007/978-1-4020-3218-9_11

Schreiber, U., Bilger, W., and Neubauer, C. (1995a). "Chlorophyll fluorescence as a nonintrusive indicator for rapid assessment of in vivo photosynthesis," in *Ecophysiology of Photosynthesis*, ed. M. Martyn (Berlin: Springer), 49–70.

Schreiber, U., Hormann, H., Neubauer, C., and Klughammer, C. (1995b). Assessment of photosystem II photochemical quantum yield by chlorophyll fluorescence quenching analysis. *Aust. J. Plant Physiol.* 22, 209–220. doi: 10.1071/PP9950209

Shen, H., and Song, L. (2007). Comparative studies on physiological responses to phosphorus in two phenotypes of bloom-forming Microcystis. *Hydrobiologia* 592, 475–486. doi: 10.1007/s10750-007-0794-3

Shi, P., Shen, H., Wang, W., Yang, Q., and Xie, P. (2016). Habitat-specific differences in adaptation to light in freshwater diatoms. *J. Appl. Phycol.* 28, 227–239. doi: 10.1007/s10811-015-0531-7

Stumpf, R. P. (2001). Applications of satellite ocean color sensors for monitoring and predicting harmful algal blooms. *Hum. Ecol. Risk Assess.* 7, 1363–1368. doi: 10.1080/20018091095050

Tao, M., Xie, P., Chen, J., Qin, B., Zhang, D., Niu, Y., et al. (2012). Use of a generalized additive model to investigate key abiotic factors affecting microcystin cellular quotas in heavy bloom areas of Lake Taihu. *PLoS One* 7:e32020. doi: 10.1371/journal.pone.0032020

Tolotti, M., Manca, M., Angeli, N., Morabito, G., and Thaler, B. (2006). Phytoplankton and zooplankton associations in a set of Alpine high altitude lakes: geographic distribution and ecology. *Hydrobiologia* 562, 99–122. doi: 10.1007/s10750-005-1807-8

Trimbee, A. M., and Prepas, E. (1987). Evaluation of total phosphorus as a predictor of the relative biomass of blue-green algae with emphasis on Alberta lakes. *Can. J. Fish. Aquat. Sci.* 44, 1337–1342. doi: 10.1139/f87-158

Veen, G. F., Sundqvist, M. K., and Wardle, D. A. (2015). Environmental factors and traits that drive plant litter decomposition do not determine home-field advantage effects. *Funct. Ecol.* 29, 981–991. doi: 10.1111/1365-2435.12421

Venables, W. N., and Dichmont, C. M. (2004). GLMs, GAMs and GLMMs: an overview of theory for applications in fisheries research. *Fish. Res.* 70, 319–337. doi: 10.1016/j.fishres.2004.08.011

Watson, S. B., Zastepa, A., Boyer, G. L., and Matthews, E. (2017). Algal bloom response and risk management: on-site response tools. *Toxicon* 129, 144–152. doi: 10.1016/j.toxicon.2017.02.005

Wei, Z., Zhang, L., Yang, S., Lv, X., Zhu, J., Dou, J. et al. (2012). Community structure and seasonal succession of Phytoplankton in Erhai Lake. *J. Hydroecology* 1674–3075. doi: 10.15928/j.1674-3075.2012.04.002

Wen, H., and Ma, G. (2011). Study of water quality and algae in Erhai Lake during 2008–2010. *Environ. Sci. Manag.* 11, 44–48. doi: 10.3969/j.issn.1673-1212.2011.11.010

White, S., Anandraj, A., and Bux, F. (2011). PAM fluorometry as a tool to assess microalgal nutrient stress and monitor cellular neutral lipids. *Bioresour. Technol.* 102, 1675–1682. doi: 10.1016/j.biortech.2010.09.097

Wickham, H. (2007). Reshaping Data with the reshape Package. *J. Statist. Software* 21, 1–20. doi: 10.3978/j.issn.2305-5839.2016.01.33

Wickham, H. (2009). *ggplot2: Elegant Graphics for Data Analysis*. New York, NY: Springer. doi: 10.1007/978-0-387-98141-3

Winder, M., and Sommer, U. (2012). Phytoplankton response to a changing climate. *Hydrobiologia* 698, 5–16. doi: 10.1007/s10750-012-1149-2

Wong, K. T., Lee, J. H., and Hodgkiss, I. (2007). A simple model for forecast of coastal algal blooms. *Estuar. Coast. Shelf Sci.* 74, 175–196. doi: 10.1016/j.ecss.2007.04.012

Wu, Q., and Wang, Y. (1999). On the succession of aquatic communities in Erhai Lake. *J. Lake Sci.* 11, 273–281. doi: 10.18307/1999.0312

Wynne, T. T., Stumpf, R. P., Tomlinson, M. C., Fahnenstiel, G. L., and Dyble, J. (2013). Evolution of a cyanobacterial bloom forecast system in western Lake Erie: development and initial evaluation. *J. Great Lakes Res.* 39, 90–99. doi: 10.1016/j.jglr.2012.10.003

Xu, F. (1996). Ecosystem health assessment of Lake Chao, a shallow eutrophic Chinese lake. *Lakes Res.* 2, 101–109. doi: 10.1016/j.jglr.2012.10.003

Zhou, P., Ang, B., and Poh, K. (2006). A trigonometric grey prediction approach to forecasting electricity demand. *Energy* 31, 2839–2847. doi: 10.1016/j.energy.2005.12.002

Conflict of Interest Statement: The authors declare that the research was conducted in the absence of any commercial or financial relationships that could be construed as a potential conflict of interest.

frontiers in Plant Science

ORIGINAL RESEARCH
published: 28 June 2018
doi: 10.3389/fpls.2018.00741

Enhanced Lipid Production in *Chlamydomonas reinhardtii* by Co-culturing With *Azotobacter chroococcum*

*Lili Xu, Xianglong Cheng and Quanxi Wang**

Department of Biology, College of Life and Environmental Science, Shanghai Normal University, Shanghai, China

The green algae, *Chlamydomonas reinhardtii*, is one of the model species used to study lipid production, although research has focused on nitrogen-deficient cultures, that inhibit the development of biomass by *C. reinhardtii* and limit lipid production. In this study, *Azotobacter chroococcum* was added to the algal culture to improve lipid accumulation and productivity of *C. reinhardtii*. The maximum lipid content and production of *C. reinhardtii* in the co-culture were 65.85% and 387.76 mg/L, respectively, which were 2.3 and 5.9 times the control's levels of 29.11% and 65.99 mg/L, respectively. The maximum lipid productivity of *C. reinhardtii* in the co-culture was 141.86 mg/(L·day), which was 19.4 times the control's levels of 7.33 mg/(L·day). These increases were attributed to the enhanced growth and biomass and the change in the activity of enzymes related to lipid regulation (ACCase, DGAT, and PDAT). Compared to the conventional strategy of nitrogen deprivation, *A. chroococcum* added to the culture of *C. reinhardtii* resulted in higher lipid accumulation and activity, greater efficiency in the conversion of proteins to lipids, higher biomass, and increased growth of *C. reinhardtii*. Therefore, using *A. chroococcum* to improve the growth and biomass of *C. reinhardtii* is an efficient, rapid, and economically viable strategy for enhancing lipid production in *C. reinhardtii*.

Keywords: ***Chlamydomonas reinhardtii*, *Azotobacter chroococcum*, co-culture, lipid production, biomass**

OPEN ACCESS

Edited by:
Jianhua Fan,
East China University of Science and Technology, China

Reviewed by:
Jianhui Zhang,
North Carolina Central University, United States
Arshad Ali,
South China Normal University, China
Arumugam Muthu,
Council of Scientific and Industrial Research (CSIR), India

****Correspondence:***
Quanxi Wang
wangqx@shnu.edu.cn

Specialty section:
This article was submitted to Plant Biotechnology, a section of the journal Frontiers in Plant Science

Received: *07 December 2017*
Accepted: *15 May 2018*
Published: *28 June 2018*

Citation:
Xu L, Cheng X and Wang Q (2018) Enhanced Lipid Production in Chlamydomonas reinhardtii by Co-culturing With Azotobacter chroococcum. Front. Plant Sci. 9:741. doi: 10.3389/fpls.2018.00741

INTRODUCTION

The global supply of traditional fossil fuels is limited and the combustion of fossil fuels produces CO_2 and other greenhouse gases that cause climate change (Hui et al., 2016). There is an urgent need for new types of renewable, clean energy resources. Biodiesel is a renewable and biodegradable fuel that is considered environmentally friendly because it is produced from unprocessed or recycled vegetable oils and animal fats through various chemical reactions (Ho et al., 2014). The–supply and price of raw materials are the key limiting factors of biodiesel applications; thus, cheap and renewable raw materials for biodiesel production are required for the large-scale utilization of biodiesel.

Through photosynthesis, algae can convert CO_2 and water to O_2 and macromolecular organic matter in the form of carbohydrates and lipids (Hu et al., 2008; Scott et al., 2010). Under certain stress conditions, such as high light intensity or nutrient deficiency, some algae can accumulate large amounts of lipids, such as triacylglycerides. Because of their fast growth, high lipid content,

and optimized lipid composition, microalgae are ideal materials for biodiesel production (Hu et al., 2008; Wang et al., 2009; Siaut et al., 2011). *Chlamydomonas reinhardtii* (*C. reinhardtii*) is a unicellular green algae species, whose genome has been fully sequenced. It grows quickly, costs little to cultivate, and can produce lipids under nitrogen-deficient conditions; thus, it has been widely used for lipid production (Park et al., 2015). As with other microalgae, the growth of *C. reinhardtii* is repressed by nitrogen deficiency. Algal biomass and lipid accumulation showed a negative correlation with nitrogen deficiency (Park et al., 2013, 2015; Fan et al., 2014). This has resulted in lower lipid accumulation and productivity than its theoretical capacity. The ideal model involves increasing lipid accumulation using green algae by removing nitrogen from the medium without limiting the algal biomass. In order to improve the lipid accumulation by *C. reinhardtii*, we need to identify an effective way to increase the biomass of *C. reinhardtii* in the absence of nitrogen.

In natural environments, bacteria and algae share a complex ecological relationship. Some bacteria can promote the growth and biomass of algae by metabolic complementarity. Ietswaart et al. (1994) found that two obligate aerobic bacteria, *Pseudomonas diminuta* and *P. vesicularis*, could promote the growth of *Scnedesmus obliquus* and *Chlorella* sp. Bell et al. (1974) reported that *Skeletonema costatum* cultivated alongside *Pseudomonas* strain grew faster than in its absence and did not survive without *Pseudomonas*. Riquelm et al. (1988) suggested that the glycoprotein secreted by *Pseudomonas* promoted the growth of *A. glacialis.* Some marine microalgae and heterotrophic bacteria, when co-grown, can secrete extracellular enzymes or specific growth factors that promote each other's growth. These include *Bacillus halmapalus* and *Alexandrium tamarense* (Zheng et al., 2002). *Azotobacter chroococcum* (*A. chroococcum*) is a nitrogen-fixing aerobic bacteria species that can draw nitrogen from the air (Walker and Yater, 1978). It is widely used in the study of biochemical processes, electron transport, and iron storage (Krakow and Ochoa, 1963). Great progress has been made in understanding the biochemistry and genetics of hydrogen metabolism and nitrogen fixation by studying *A. chroococcum*. These studies determined the ability of *A. chroococcum* to stimulate plant growth through the production of plant growth substances and fixed nitrogen, and other factors (Rubenchik, 1963).

In this work, to increase the biomass and lipid accumulation of *C. reinhardtii*, we co-cultured *C. reinhardtii* cc849 with *A. chroococcum* under nitrogen-deficient conditions and investigated the underlying mechanism of the resulting increased lipid content. The lipid content and lipid productivity of *C. reinhardtii,* when mixed with *A. chroococcum* were monitored. The growth, biomass, cellular biochemical components and fatty acid of *C. reinhardtii* in the co-culture and pure algal culture were compared in this study. Finally, the transcription levels of the genes related to the lipid production of algae and its co-culture with *A. chroococcum* were analyzed. The special ecological relationship between green algae and bacteria was used to improve the biomass and lipid content of *C. reinhardtii*, which is a clean and sustainable way to produce biofuel. This research provides a novel and useful strategy to enhance the lipid accumulation and productivity of *C. reinhardtii* for treatment by the co-culture with bacteria.

MATERIALS AND METHODS

Algal and Bacterial Strains and Culture Conditions

Chlamydomonas reinhardtii cc849 was purchased from the *Chlamy* Center. It is a type of cell deficient strain. The algae grew in the Tris-acetate-phosphate (TAP) medium (pH = 7.0) under light conditions of 100 $\mu E \cdot m^{-2} \cdot s^{-1}$ at 25 ± 1°C (Harris, 2009). The cell density was determined by absorbance at 750 nm (OD_{750}). Chlorophyll of *C. reinhardtii* was extracted with alcohol. Cells (1 mL) were extracted and centrifuged at 12,000 g for 1 min at room temperature and the supernatant was removed. Then, 1 mL of 95% alcohol was added to the tube and the pellet was resuspended and centrifuged at 12,000 g for 1 min at room temperature (Harris, 2009). The supernatant was extracted and absorbance was measured at 665 nm and 649 nm (Wu et al., 2011).

$$\text{Chlorophyll content (mg/L)} = OD_{665} \times 6.01 + OD_{649} \times 20.04$$

Azotobacter chroococcum No 1.0233 was purchased from China General Microbiological Culture Collection Center (CGMCC) and cultured in a nitrogen fixation medium (pH = 7.0) at 28 ± 1°C. The cell density is expressed as the absorbance at 600 nm (OD_{600}) (Winogradski, 1935). The cell density of *A. chroococcum* in the co-culture was obtained by OD_{600} of the mixture minus the OD_{600} of pure algal culture.

$$OD_{600\ (\text{bacteria in co-culture})} = OD_{600\ (\text{co-culture})} - OD_{600\ (\text{pure algal culture})}.$$

Co-culture of Algae and Bacteria for Lipid Production

The algal cells in the culture flask were harvested by centrifugation at 4,500 g and 25°C for 5 min when they grew to saturation. The algal pellet was washed gently with the TAP-N medium three times to remove nitrogen thoroughly (Wan et al., 2013). The bacterial medium was also harvested by centrifugation at 5,000 g and 25°C for 5 min when it is grown to saturation then resuspended with the TAP-N medium three times. The bacterial pellet was resuspended with a suitable volume of the TAP-N medium so that OD_{600} = 1.0. Then, 10 mL of the resuspended bacterial sample was added to a 500 mL flask followed by the addition of 0.5 mg algae. Finally, the TAP-N medium was replenished in the flask. The sample in the flask was shaken gently so that bacteria and algae are mixed well. The flask was placed under 200 $\mu E \cdot m^{-2} \cdot s^{-1}$.

Samples were dried in an oven at 80°C for 24 h until the weight ceased to decrease (dry weight is designated as DW here). Ten microliter of the bacterial culture broth was mixed with 990 μl water and spreaded on a solid plate medium, then the number of colonies were counted after culturing in 28°C for 48 h. The cells number/mL of algae was obtain through the

microscope observation. The linear relationship between cells number/mL and biomass of *C. reinhardtii* and *A. chroococcum* were determined. The cells number/mL of algae and bacteria in the co-culture could obtain by microscopy and plate medium coating, respectively. The biomass of bacteria and algae in the co-culture medium were obtained by the following equation:

$$DW_{bacteria} = \text{Cell number/mL} \times 0.0557 + 0.032 \; R^2 = 0.9931;$$
$$DW_{algae} = \text{Cell number/mL} \times 0.8451 + 0.263 \; R^2 = 0.9923.$$

Observation of *C. reinhardtii* and *A. chroococcum* by Microscopy

In this experiment, 1 mL of the cells of the culture was stained with Nile Red (Sigma) by adding the dye to a final concentration of 1 mg/mL and running the reaction for 15 min. The bright-field images of *C. reinhardtii* cells grown in the TAP-N media were captured using a confocal laser scanning microscope (Nikon Eclipse 80i) equipped with a digital camera (Nikon DS-Ri1), respectively. Subsequently, the corresponding fluorescence images of the Nile Red signal were captured by the excitation line at 488 nm (Chen et al., 2009; Boyle et al., 2012).

Extraction and Detection of Lipid Content

Total lipids were extracted using a modified version of the protocol reported by Bligh and Dyer (1959). Here, 400 mL of algal cells were harvested by centrifuging at 7,500 g for 10 min and the sediment was washed with fresh TAP-N medium three times. Solid samples were placed in dry weighing bottles and dried in an oven at 80°C for 24 h until the weight ceased to decrease. Then, 0.2 g (weight is designated W_0) of dry cells were transferred into the centrifugal tube. Subsequently, 5 mL mixture of chloroform and methyl alcohol at a volume ratio of 1:1 were added to the centrifugal tube. The cells in the centrifugal tube were shaken for 30 min, placed in a centrifuge tube, and centrifuged at 8,000 g for 10 min. All the steps were repeated until the supernatant was colorless. The supernatant was collected (weight is designated W_1) and transferred, to a dry rotary evaporator, of known weight, and evaporated to dryness (weight was designated W_2).

Biomass (mg) = DW;
Unit biomass (mg/L) = DW/0.5;
Lipid content = $(W_2 - W_1)/ W_0 \times 100\%$;
Lipid production (mg/L) = W_2;
Lipid productivity (mg/(L·day)) = W_2/day.

Fatty Acid Analysis of Lipid of Algae and *A. chroococcum*

Fatty acids in algae were analyzed using a previously described method (Wang et al., 2013) with some modifications. First, 0.1 g dry sample was added to a 15 mL glass vial and then it was dissolved in a 2 mL methanolic HCl and 3 mL chloroform-methanol solution (volume ratio 1:1). Finally, 1 mL heptane containing 50 μg heptadecanoic acid methyl ester ($C_{18}H_{37}COOCH_3$) as the internal standard was added to the glass vial. The reaction proceeded at 85°C for 1 h, after which 1 mL hexane was added to the vial. The solution was left to stand for 1 h to obtain the supernatant, which was used for FAME analysis. Samples were detected by GC-MS (Thermo, Fisher, ISQ) equipped with a flame ionization detector (FID) and Agilent HP-5 GC Capillary Column (30 m × 0.25 mm × 0.25 μm). Nitrogen was used as a carrier gas. The injector temperature was set at 290°C with an injection volume of 2 μL under split mode (10:1). The detector temperature was set at 280°C. The individual FAMEs were identified by comparing their retention time with those of the authentic standards.

Determination of Protein Content and Carbohydrate Content

The protein content of *C. reinhardtii* was measured using the BCA method (Hu et al., 2008). Algal cells (5 mL) were harvested and centrifuged at 7,500 g for 10 min. The supernatant was discarded. Subsequently, 1 mL of 15 mM KH_2PO_4 (pH 4.5) and 2 mL of 20% NaOH were added to the tube and shaken for 30 s. The tube was put into boiling water for 10 min, and then centrifuged at 7,500 g for 10 min. The supernatant was collected and used to assay the protein content using Pierce BCA protein assay kit (Thermo). Bovine serum albumin was used as the standard sample to obtain a standard curve. Subsequently, the protein content was calculated from the absorbance measured using the microplate reader at 560 nm and the standard curve. Carbohydrate content of *C. reinhardtii* was detected by anthrone colorimetry (Dubois et al., 1956). First, 10 mg of algal powder was put into a tube and synchronously, 0.5 N H_2SO_4 was added. Then the tube was incubated in a bath at 80°C for 1 h. Finally, the reactant was centrifuged at 8,000 g for 5 min to collect the supernatant and the steps were repeated once. The supernatant was extracted and the absorbance was measured at 625 nm (Dubois et al., 1956).

RNA Extraction and Real-Time Quantitative PCR

Two milliliters of cells were collected from the samples on days 0, 1, 5, and 9 in the TAP-N medium and RNA was extracted using a QIAGEN Plant Mini Kit. The concentration and purity of the extracted RNA were measured using a UV spectrophotometer. Single stranded cDNA was synthesized from 2 μg of DNA-digested total RNA following the reverse transcription protocol provided by the manufacturer (Promega™). Transcriptional levels of genes related to lipid accumulation were detected using real-time quantitative PCR. Primers for quantitative real-time RT-PCR were designed using the Primer 5 software and are shown in **Table 1**. Real-time quantitative PCR was performed as stipulated by the manufacturer of the SYBR Green real-time PCR Master Mix Kit (TOYOBO™, Japan). The actin gene from *C. reinhardtii* was used as an internal control to normalize the differences between the loading amounts of the template (Makarova et al., 2007). Each PCR reaction contained 1 μL (8 ng) of cDNA, 10 μL of SYBR Green 2×Master Mix, and 1 μL of each gene-specific primer pair (10 mM) to a final volume of 20 μL. PCR was performed as follows: 95°C for 10 min followed by 40 cycles at 95°C for 10 s, 60°C for 1 min, and 72°C for 30 s. PCR products were analyzed using the Dissociation Curves

Software of ABI. The $2^{-\Delta\Delta ct}$ method was used to calculate the fold changes of differentially expressed genes.

Statistical Analysis

All experiments were repeated three times independently, and data were recorded as the mean with SD. Statistical analyses were conducted using SPSS 19.0. Spearman correlation coefficients were computed. The results with a P-value < 0.05 was considered statistically significant. "*" indicates a significant differences between the experimental and control groups.

RESULTS AND DISCUSSION

After *A. chroococcum* was added to the algal culture, the maximum lipid production of *C. reinhardtii* in the co-culture was 387.76 mg/L, which was 65.85% of the composition of the algal cell. The maximum lipid productivity of *C. reinhardtii in* the co-culture was 141.86 mg/(L·day), which was 19.4 times the control's value of 7.33 mg/(L·day). These were attributed to enhanced growth and biomass. Furthermore, compared with the controls, the activity of enzymes related to lipid regulation, ACCase, DGAT, and PDAT was changed.

TABLE 1 | Primers used for real-time quantitative PCR.

Gene Name	Accesion Number	Primer
ACTIN	XM_001699016	F′-ATGGGCCAGAAGGACTCGTA
		B′-GTCGTCCCAGTTGGTCACAA
ACC	XM_001703135	F′-CAAGACTCTGGTTAGCGATGC
		B′-CCCAAAGCGAGACAGGATAG
DGAT1	XM_001693137	F′-ACTGGTGGAATGCGGCTAC
		B′-TAGCAGCTCGTGGAACACAG
DGTT1	KC788199.1	F′-CGGCGGAGGGAACTTAT
		B′-GAAGAGGTGCGGGGACA
DGTT2	KC788200.1	F′-GTTCCCGCACGGTGTCTT
		B′-ACTTCGTTCCTTCGCACC
DGTT3	KC788201.1	F′-GTCAGAGCCAAGTGCTGGAC
		B′- TCCACCTCCTTGTCGAACTC
DGTT4	KC788202.1	F′-TGCCAGATGGAAGGTGGAGTG
		B′-GTAAGCATGTGCGGTGAAGGG
DGTT5	XM_001701615.1	F′-GCCGTCACAGGGCTTGGGAGAA
		B′-TCCGCCTGTGCCTCTGACGG
PDAT1	AFB 73928	F′-AGCACAAAGCCGTGTCGATG
		B′-TTGCCCAGGATGTCGATGTG
PEPC2	XM_001695765	F′-CGTGAACCCCCGTAGAAAAG
		B′-CGGAGACAGTCGTCAAGCAG

Growth and Biomass of Algae Co-cultured With *A. chroococcum*

Lipid production was directly related to algal biomass; thus, the growth and biomass of algae and the algae co-cultured with *A. chroococcum* were detected under nitrogen deprived conditions. The initial OD_{750} value of both pure algae and the algae co-cultured with *A. chroococcum* was 1.42. After nitrogen deprivation, OD_{750} of pure algae gradually decreased and reached a minimum value of 0.91, while OD_{750} of algae co-cultured with *A. chroococcum* increased sharply, especially after day 3. It peaked at 3.75, which was 4.1 times the control value, on day 9 (**Figure 1A**). Consistent with the change in OD_{750}, the initial chlorophyll content of both pure algae and algae co-cultured with *A. chroococcum* was 9.95 mg/mL. After nitrogen starvation chlorophyll content of pure algae decreased slightly and reached the minimum value of 4.85 mg/mL on day 9. Conversely, the chlorophyll content of algae co-cultured with *A. chroococcum* increased significantly after day 3. It peaked at 39.13 mg/mL, which was 8.1 times that of pure algae on day 9 (**Figure 1B**). A significant difference in the growth of algae co-cultured with *A. chroococcum* and pure algal culture was detected by *t-test* on days 3, 5, 7, and 9 ($p < 0.05$).

The growth of *A. chroococcum* co-cultured with algae in TAP-N was monitored and the results are shown in **Figure 2**. Pure algae cells in TAP and TAP-N media were used as controls. The results indicated that the initial OD_{600} value of both pure *A. chroococcum* and *A. chroococcum* co-cultured with algae was 0.006. The OD_{600} value of pure *A. chroococcum* in both media increased slightly from day 1 to day 9 and reached the maximum value of 0.15 and 0.07 on day 9, respectively. The OD_{600} value of

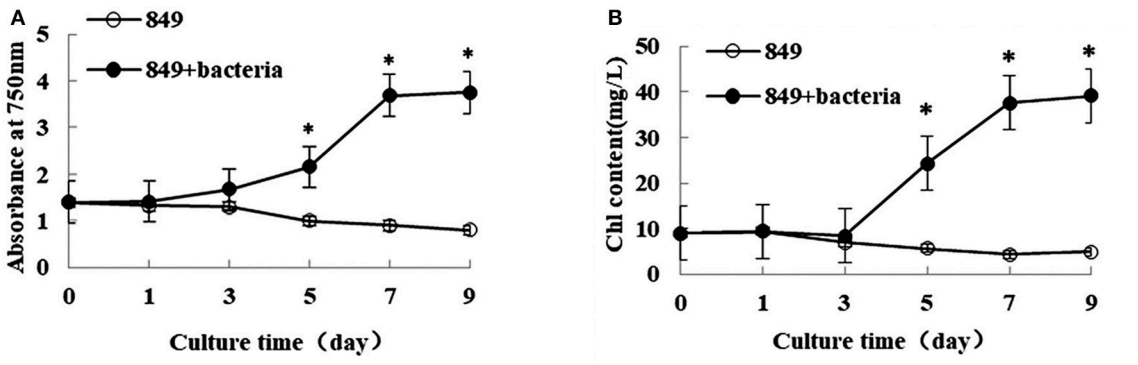

FIGURE 1 | OD_{750} **(A)** and chlorophyll content **(B)** of algae in the co-culture were measured on days 0, 1, 3, 5, 7, and 9 after incubation in a nitrogen-deprived medium. Pure algae culture was used as the control. Light intensity was 200 $\mu E \cdot m^{-2} \cdot s^{-1}$ and the volume ratio of bacteria ($OD_{600} = 1.0$) and ($OD_{750} = 1.0$) was 1:40. *significant difference between the experimental and control groups. The vertical bars indicate standard errors calculated from at least three independent experiments.

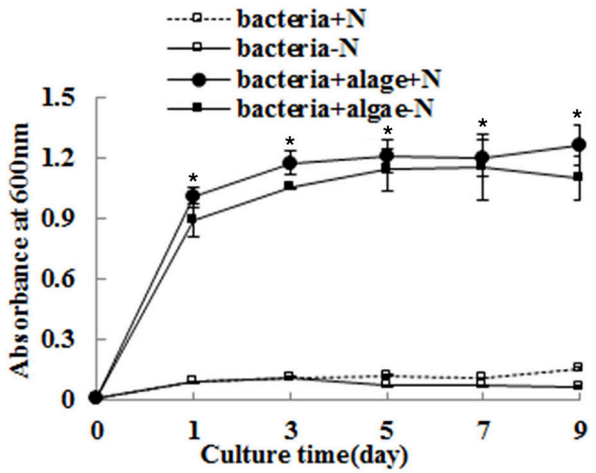

FIGURE 2 | The growth of *A. chroococcum* co-cultured with algae were measured in TAP and TAP-N media. Pure bacterial culture in both media was used as controls. Light intensity was 200 $\mu E \cdot m^{-2} \cdot s^{-1}$. The same condition as the algae in the co-culture produced lipids. The volume ratio of bacteria ($OD_{600} = 1.0$) and algae ($OD_{750} = 1.0$) was 1:40. *significant difference between the experimental and control groups. The vertical bars indicate standard errors calculated from at least three independent experiments.

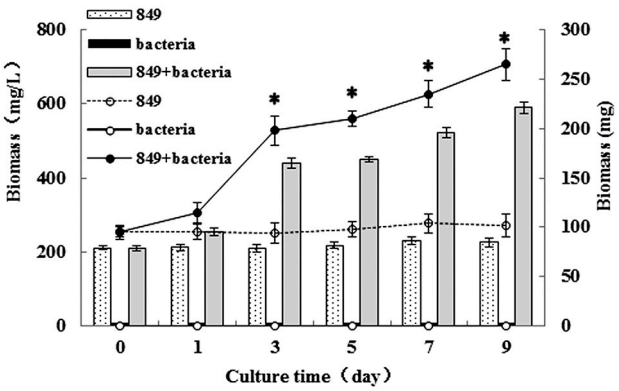

FIGURE 3 | Unit biomass (mg/L) and total biomass (mg) of algae in the co-culture were measured on days 0, 1, 3, 5, 7, and 9 after incubation in a nitrogen-deprived medium. Pure algae culture was used as the controls. Unit biomass is shown with bars and total biomass is shown with dashed and solid lines, respectively. *significant difference between the experimental and control groups. The vertical bars indicate standard errors calculated from at least three independent experiments.

A. chroococcum co-cultured with algae in both media increased significantly and reached the maximum value of 1.27 and 1.16 on day 9 and day 7, respectively. A significant difference between the growth of *A. chroococcum* co-cultured with algae and pure algae in the TAP and TAP-N media was detected by *t-test* on days 1, 3, 5, 7, and 9 ($p < 0.05$).

The biomass of algae co-cultured with *A. chroococcum* was also monitored and the results are shown in **Figure 3**. Pure algae and bacteria were used as controls. Biomass of pure algae and pure bacteria was labeled by the dry weight (DW) of algal and bacterial cells. Biomass of algae co-cultured with *A. chroococcum* was calculated by reducing the weight of the pure bacteria cells (**Figure 3**). The results indicated that nitrogen deprivation caused a decline in the biomass of pure algae. However, the biomass of algae co-cultured with *A. chroococcum* increased (**Figure 3**). The total biomass of the pure algae decreased from 95.00 mg to the minimum value of 90.01 mg on day 9 (**Figure 3**). Total biomass of the algae mixed with *A. chroococcum* dramatically increased and reached the maximum value of 265 mg, 2.9 times the control. As with the change in total biomass, the initial unit biomass of pure algae and samples mixed with *A. chroococcum* was 211 mg. The unit biomass of pure algae decreased slightly to the minimum value of 200.00 mg on day 9, while the total biomass of algae mixed with *A. chroococcum* increased to the maximum value of 588 mg, also 2.9 times the control. A significant difference between the biomass of algae co-cultured with *A. chroococcum* and pure algal culture was observed by *t-test* on 3, 5, 7, and 9 days ($p < 0.05$). The number of bacteria added to the algal culture was mostly small. Total biomass and unit biomass of pure *A. chroococcum* slightly increased from the initial value of 0.006 mg and 0.015 mg/L to the maximum value of 0.010 mg and 0.025 mg/L, respectively (**Figure 3**).

Nitrogen is essential to the growth of micro-algae; thus, the growth and biomass of micro-algae are commonly repressed (Fan et al., 2014). In this study, the growth and biomass of *C. reinhardtii* exhibited little inhibition after 3 days, while the growth and biomass of *C. reinhardtii* co-cultured with *A. chroococcum* increased sharply, this resulted in the nitrogen reservoir could sustain the cell growth for a few days. This suggests that the nitrogen reservoir could sustain cell growth for a few days; thus, there were no differences in the growth on the first 3 days of nitrogen deficiency (Fan et al., 2014). With the consumption of stored nitrogen, the growth and biomass of *C. reinhardtii* were repressed. Conversely, the growth and biomass of *C. reinhardtii* co-cultured with *A. chroococcum* increased significantly (**Figures 1**, **3**). *A. chroococcum* is a type of nitrogen-fixing aerobic bacteria that can draw nitrogen from the air (Walker and Yater, 1978); therefore, the nitrogen in the medium is not needed. In our research, the growth of pure *A. chroococcum* both in TAP and TAP-N media was similar, while the growth of *A. chroococcum* increased after it was co-cultured with algae in both media (**Figure 2**). This result indicated that nitrogen is not a limiting factor for the growth of *A. chroococcum*. Algae and bacteria exhibit mutually beneficial complex symbiotic relationships. Bacteria release a lot of extracellular metabolites, such as amino acids, enzymes, vitamins, carbohydrates, and lipids into the surrounding environment, which promote the growth of algae. Algal and bacterial growth is also promoted through metabolic regulations and materials exchange. The growth of *S. obliquus* and *Chlorella* increased by their exposure to *P. diminuta* and *P. vesicularis* (Ietswaart et al., 1994); the growth of *Pseudomonas* cultivated alongside *Skeletonema costatum* was more pronounced than that of *Pseudomonas* cultivated alone (Bell et al., 1974); *Pseudomonas* could secrete glycoprotein to *A. glacialis*, which led to their further growth (Riquelm et al., 1988). In our previous work, *Bradyrhizobium japonicum* improved

the biomass and hydrogen production of *C. reinhardtii* (Wu et al., 2012; Xu et al., 2016). Similarly, microalgae were always observed near the surface of one type of nitrogen-fixing bacteria by Gyurjan et al. (1984); during the process, algae and bacteria underwent exosymbiotic action by complementary metabolism. In our research, *A. chroococcum* gathered around *C. reinhardtii* and formed a specific "algae-bacteria aggregate" observable under a microscope (Figure S1). In this composite system, algae and bacteria could enhance the growth and biomass of each other through materials exchange; algae supplied carbohydrates and O_2 by photosynthesis, while *A. chroococcum* could supply nitrogen and CO_2 to algae by nitrogen fixation (Gyurjan et al., 1984) (**Figure 4**).

Total Lipid Content, Lipid Production, and Lipid Productivity of Algae Co-cultured With *A. chroococcum*

To analyze the effect of *A. chroococcum* on lipid production of *C. reinhardtii* in the nitrogen-deficient medium, the algal cells were pre-cultured to saturation and transferred into the nitrogen-deficient medium containing *A. chroococcum* (OD_{600} = 1.0). The pure algal culture served as the control. Samples were extracted at specific points in time to assess the lipid content, lipid production, and lipid productivity. Nitrogen starvation enhances lipid accumulation in microalgae. Consistent with the findings of previous studies, lipid content, lipid production, and lipid productivity of pure algae increased gradually after nitrogen starvation, and those of algae co-cultured with *A. chroococcum* increased profoundly (**Figure 5**). The lipid content of *A. chroococcum* was not monitored. The maximum lipid content of algae co-cultured with *A. chroococcum* increased from the initial 28.00% to a maximum of 65.85% on day 9, which was 2.3 times that of the pure algae, 29.11% (**Figure 5A**). Correspondingly, the maximum lipid production and productivity of algae co-cultured with *A. chroococcum* were 387.76 mg/L and 141.86 mg/(L·day), which were 5.9 and 19.4 times the control values, (65.99 mg/(L·day) and 7.33 mg/L, respectively) on day 9 (**Figure 5B**). A significant difference between lipid production of algae co-cultured with *A. chroococcum* and pure algal culture was observed by the *t-test* on days 3, 5, 7, and 9 ($p < 0.05$). Additionally, algal cells were examined by fluorescent microscopy after staining with the lipid fluorophore Nile Red (Chen et al., 2009). As indicated by Nile Red fluorescence, lipid granules of algae in the co-culture and the lipid body were larger and more numerous than those of pure algae in the nitrogen-rich medium on days 1, 3, 5, 7 and 9 (Figure S2).

C. reinhardtii can accumulate lipid even in the absence of certain nutrients, such as nitrogen (Hu et al., 2008; Yeesang and Cheirsilp, 2011; Fan et al., 2014; Park et al., 2015). Therefore, in this study, samples were transferred to a nitrogen-deficient medium when cultured to saturation to induce the lipid accumulation. However, nutrient limitation stimulates lipid accumulation but does so at the expense of growth (Rodolfi et al., 2009; Li et al., 2011). Biomass productivity and lipid content are inversely correlated (Hu et al., 2008; Rodolfi et al., 2009). Similarly, in our study, the biomass of pure *C. reinhardtii* was lower in the nitrogen-deficient medium, but it increased significantly after it was co-cultured with *A. chroococcum* (**Figure 3**). Consistent with the increased growth and biomass

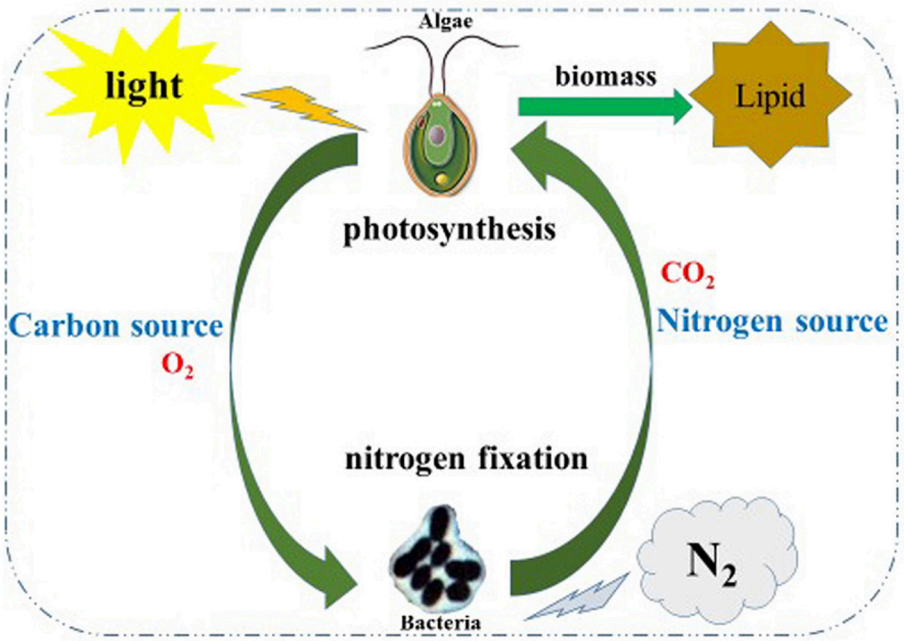

FIGURE 4 | Schematic illustration of the co-cultivation of the algae-bacterial system to improve biomass of and lipid production by algae. In this co-system, algae and bacteria could enhance the growth and biomass of each other through material exchange; algae supply carbohydrates and O_2 by photosynthesis meanwhile *A. chroococcum* supply the nitrogen source and CO_2 to algae by nitrogen fixation.

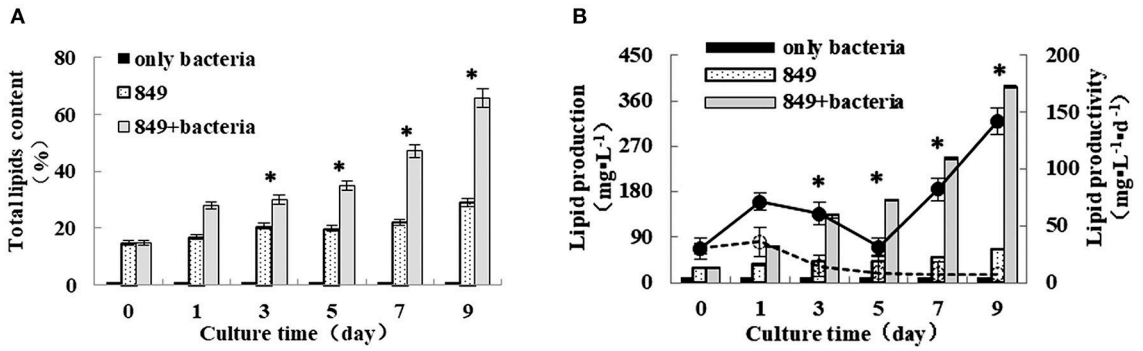

FIGURE 5 | (A) Lipid content **(B)** lipid production and lipid productivity of algae in the co-culture were measured on days 0, 1, 3, 5, 7, and 9 after incubation in a nitrogen-deprived medium. Pure algae culture was used as the controls. Lipid content and lipid production are shown with bars and lipid productivity of algae in the co-culture are shown with solid and dashed lines, respectively. *significant difference between the experimental and control groups. The vertical bars indicate standard errors calculated from at least three independent experiments.

of *C. reinhardtii*, the lipid content, lipid production, and lipid productivity of *C. reinhardtii* in the co-cultures also increased. The increased growth and biomass of *C. reinhardtii* co-cultured with *A. chroococcum* causes the increased lipid content, lipid production, and lipid productivity of *C. reinhardtii* in the co-culture. Because of the number of bacteria added to the algal culture was mostly small, total biomass of pure bacteria slightly increased from the initial value of 0.006 mg to the maximum value of 0.010 mg (**Figure 3**), the lipid content of *A. chroococcum* was not monitored.

Fatty Acid Analysis of Algae and *A. chroococcum*

To evaluate the quality and suppliers of lipids from the mixture, the fatty acid profile of lipids in the mixture was analyzed. Pure algae and pure bacteria were used as controls. The FAME composition of algae co-cultured with bacteria and the controls (pure algae and pure bacteria) were determined by GC-MS (**Table 2**). The fatty acid carbon chain composition of the samples ranged from C8 to C20. The saturated fatty acid in algae, bacteria, and the mixture were C16:0, C18:0, and C19:0. The contents of C16:0 in algae and the mixture were 12.79 and 12.89%, respectively, while C16:0 of bacteria was only 8.15%. The most abundant fatty acid in bacteria was C18:0 and its content was 47.16%, which was 2.39 and 21.05 times its content in algae and bacteria. The contents of C19:0 in algae and the mixture were similar, 3.67% and 4.57%, respectively. The C19:0 content in bacteria was higher than that of them, with a value of 10.97%. The unsaturated fatty acid in algae, bacteria, and the mixture were polyunsaturated fatty acids, mainly C18:2, C18:3. The C18:2 content in algae, bacteria, and the mixture was very low, only the polyunsaturated fatty acids C18:2 in algae and the mixture could be monitored; their values were 2.24% and 1.28%, the polyunsaturated fatty acids C18:2 were not detected in bacteria. Interestingly, C18:3 of algae was 49.53%, which was almost half the ratio of total fatty acids. Inversely, there was almost no C18:3 in bacteria (0.01%) and the amount of the C18:3 of the mixture was 17.43%.

The results of the fatty acid analysis indicated that the composition and content of fatty acids in algae, bacteria, and the mixture were different. The highest contents of fatty acids in the three types of samples were C18:3, C16:1, and C18:0, respectively. In our study, the minimum and maximum values of bacterial biomass in the co-culture were 0.002 mg and 0.010 mg (**Figure 3**); therefore, the proportion of bacteria in the mixture was low and the lipid yield in the mixture was mainly supported from *C. reinhardtii*. Nonetheless, the contents of C19:0 in the mixture was 4.57%. As we all know, algae do not produce any odd number fatty aicds in general, therefore, all the odd number fatty aicds in mixture may supported by the biomass of bacteria. The change in the fatty acid content of the mixture is not caused by the contribution of fatty acids in bacteria but by metabolic regulations and materials exchange between algae and bacteria (Gyurjan et al., 1984) (**Figure 4** and Figure S1).

Effect of *A. chroococcum* on Cellular Biochemical Components of *C. reinhardtii* Under Nitrogen-Deprived Conditions

The components of algal cells were analyzed after nitrogen depletion and the results are shown in **Figure 6**. Total cellular composition analysis indicated that the pure algal cells consisted of 15% lipids, 11% carbohydrate, and 59% protein in the TAP medium on day 0 (**Figure 6A**). Nitrogen depletion caused the lipid content of pure *C. reinhardtii* to increase from 15 to 24% (**Figure 6B**), while the lipid content of *C. reinhardtii* in the co-culture increased significantly, peaking at 57% on day 9 (**Figure 6C**), which was 2.2 times that of pure *C. reinhardtii*. Inversely, the protein content of pure *C. reinhardtii* decreased from an initial value of 59% to 40% (**Figure 6B**), and the protein content of *C. reinhardtii* in the co-culture decreased to 13% on day 9, a change of 4.5 folds (**Figure 6C**). The carbohydrate content in pure *C. reinhardtii* increased from the initial value of 11–22% (**Figure 6B**)and the lipid content of *C. reinhardtii* in the co-culture increased to 25% (**Figure 6C**), which was 1.1 times that in pure *C. reinhardtii*. In summary, the lipid and

TABLE 2 | Fatty acid analysis of algae co-cultured with bacteria, pure algae, and pure bacteria.

Fatty acid composition		Content (%)		
		C. reinhardtii	*A. chroococcum*	*C. reinhardtii* + *A. chroococcum*
Saturated fatty acids (SFA)	C8:0	0.01	0.01	0.07
	C10:0	0.02	0.14	0.23
	C11:0	0.00	0.00	0.01
	C12:0	0.09	7.88	1.57
	C13:0	0.01	0.01	0.01
	C14:0	2.00	12.43	4.00
	C15:0	0.42	0.11	0.23
	C16:0	12.79	8.15	12.89
	C17:0	1.22	0.26	0.97
	C18:0	19.72	2.24	47.16
	C19:0	3.67	10.97	4.57
	C20:0	0.57	0.01	2.35
	C21:0	0.01	0.01	0.02
	C22:0	0.08	0.00	0.56
	C23:0	0.00	0.00	0.01
	C24:0	0.09	0.00	0.30
Monounsaturated fatty acids (MUFA)	C14:1	0.02	0.11	0.06
	C15:1	0.18	0.00	0.09
	C16:1	1.40	38.20	3.94
	C17:1	0.18	0.49	0.10
	C20:1	0.19	0.01	0.14
Polyunsaturated fatty acids (PUFA)	C18:2	2.24	0.00	1.28
	C18:3	49.65	0.01	17.47
	C20:2	0.02	0.01	0.02
	C20:3	0.15	0.00	0.04
	C20:4	0.01	0.00	0.02

carbohydrate content of pure algae and algae in the co-culture gradually increased while the protein content decreased after the onset of nitrogen deficiency; thus, it is likely that nitrogen deficiency causes the protein in algae to transform into lipid or carbohydrates. After the addition of *A. chroococcum*, the lipid and carbohydrate content in algae became much higher than in pure algae, while the protein content was lower than that of in pure algae. These changes were pronounced on day 9. This indicated that *A. chroococcum* facilitated the transformation of proteins in algae to lipids or carbohydrates. Nitrogen deficiency can cause significant increase in the lipid content of microalgae and a drop in protein content. Ho et al. (2014) found that nitrogen deficiency could dramatically increase the lipid content in algae but has little effect on carbohydrate accumulation, similar to our results. Yen et al. (2013) and Siaut et al. (2011) also found that *C. reinhardtii* could transform protein or peptides to lipids or carbohydrates.

Expression of Lipid Biosynthesis Genes in *C. reinhardtii* Co-cultured With *A. chroococcum* Under Nitrogen-Deprived Conditions

To explore the reasons for the increased lipid production by *C. reinhardtii* upon addition of *A. chroococcum*, we compared the transcription levels of key genes that dominate the lipid metabolism on day 0 (in TAP medium), day 1 (starting point), day 5 (exponential growth phase), and day 9 (stationary phase) (**Figure 7**). The results were assessed using Spearman correlation analysis (using SPSS 19.0) to determine the quantitative relationship between the expression level of these genes and lipid content under nutrient-deficient conditions. The results provide an overall perspective for the mechanisms of improved lipid accumulation in response to nutrient stress. The *actin* gene from *C. reinhardtii* was used as an internal control and three biological repetitions were completed; the average CT value of *actin* was 20.3.

Acetyl-CoA carboxylase (ACCase) is a key rate-limiting enzyme that catalyzes the first step in the synthesis of fatty acids and plays an important role in fatty-acid biosynthetic synthesis and catabolism (Cronan and Waldrop, 2002). The levels of expression of the *ACC* gene in *C. reinhardtii* in the co-culture and in the control were analyzed. The results indicated that levels of expression of both *C. reinhardtii* in the co-culture and pure *C. reinhardtii* increased with the increased lipid production and the expression of *ACC* in *C. reinhardtii* in the co-culture was higher than that of the control. A significant difference between the levels of expression of the *ACC* gene in algae co-cultured with *A. chroococcum* and in pure algal culture was observed by the *t-test* on days 5 and 9 ($p < 0.05$). Adding *A. chroococcum* into the algal culture led to a significant increase in the nitrogen deprived medium relative to the control values and the peak level of expression of *C. reinhardtii* in the co-culture was 1.5 times control levels. The lipid content, lipid production, and lipid productivity peaked on day 9 (**Figure 5**). Carbon from fatty acids is made available from the pool of acetyl-Coenzyme A (CoA) present in the plastid and acts as a precursor for the fatty acid synthesis pathway. An ACCase can catalyze the first reaction of the fatty acid biosynthetic pathway and transform acetyl CoA and CO_2 into malonyl CoA (Hu et al., 2008). The pattern of ACCase in fatty acid biosynthesis has been thoroughly investigated and it has been proposed that increased ACCase activity is an effective method of stimulating the accumulation of lipids in *Chlorella* (Hsieh and Wu, 2009). Another study showed that lipid accumulation increased with the increased ACCase activity of *Chlorella sorokiniana* (Wan et al., 2011). Similarly, Fan et al. (Fan et al., 2014) reported that the ACCase activity of *Chlorella pyrenoidosa* exhibited a large increase when it was subjected to nitrogen starvation. The role of the ACCase gene expression in *Crypthecodinium cohnii* was studied by Liu et al. and the results indicated that the growth and lipid accumulation were higher in a *C. cohnii* mutant with high ACCase activity (Liu et al., 2017). In our study, the levels of expression in both *C. reinhardtii* in the co-culture and pure *C. reinhardtii*

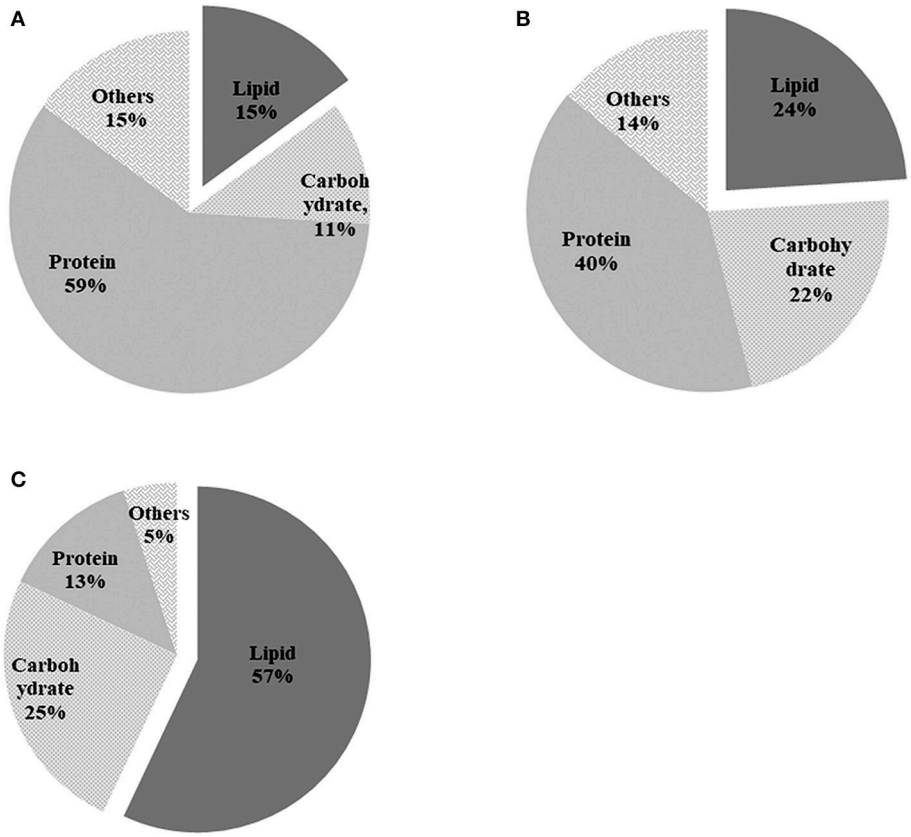

FIGURE 6 | Biochemical composition of pure algae in **(A)** TAP medium before incubation in the nitrogen-deprived medium; **(B)** pure algae; and **(C)** algae in the co-culture after 9 d of incubation in the TAP-N medium. Pure algae in the TAP medium and pure algae incubated for 9 d in the TAP-N medium were used as controls**.** Light intensity was 200 $\mu E \cdot m^{-2} \cdot s^{-1}$ and the volume ratio of bacteria (OD_{600} = 1.0) and (OD_{750} = 1.0) was 1:40. All the data are the means of three independent experiments with triplicates performed for each experiment.

were higher than those in pure *C. reinhardtii* cultured in a nutrient-rich medium. The levels of expression in *C. reinhardtii* co-cultured with *A. chroococcum* were higher than those in the controls. Our results were consistent with those of previous studies.

Diacylglycerol acyltransferase (DGAT) catalyzes the biosynthesis of triacylglycerol (TAG) by the reaction of diacylglycerol with acyl-CoA, and it is the only catalyzing enzyme in the Kennedy pathway that participates solely in the biosynthesis of TAG. The enzyme is an important regulator of lipid biosynthesis, involved in lipid metabolism and lipid deposition. There are two isoforms of DGAT, of which DGAT1 acts extensively on the metabolism of triglycerides and DGAT2 on the accumulation of TAG under nitrogen-limited conditions. In *C. reinhardtii*, the DGAT2 are encoded by five genes in *C. reinhardtii*, *DATT1*, *DATT2*, *DATT3*, *DATT4*, *DATT5* (Sugimoto et al., 1989; Miller et al., 2010). The levels of expression of each gene of *C. reinhardtii* in the co-culture and pure algae were assessed under nitrogen deficient conditions. The results showed large differences between the sample in the co-culture and the control. The results of the real-time quantitative PCR indicated that the level of expression of *DGAT1* in *C. reinhardtii* in the co-culture and pure algae decreased during day 1, then increased through day 5. Addition of *A. chroococcum* led to an increase of the expression level of *DGAT1* on day 9. The expression level of *DGTT1* increased dramatically on day 1, then gradually decreased from day 1 through day 9 and reached a minimum on day 9. The levels of expression levels of *DGTT2* and *DGTT4* in *C. reinhardtii* in the co-culture and pure algae decreased from day 1 to day 9 and reached a minimum on day 9, while those of *C. reinhardtii* in the co-culture were higher than those of the control, (1.5 and 1.3 times the control levels, respectively) on day 1. Inversely, the levels of expression of *DGTT3* and *DGTT5* in both co-cultured *C. reinhardtii* increased from day 1 to day 9, peaking on day 9. The levels of expression of all six DGAT genes in *C. reinhardtii* in the co-culture were higher than those of the controls. It is likely that adding *A. chroococcum* led to an increase in the level of expression of DGAT genes. A significant difference between the levels of expression of the *DGAT1* gene in algae co-cultured with *A. chroococcum* and pure algal culture was observed by *t-test* on days 1 and 9 ($p < 0.05$); the levels of expression of the *DGTT1*, *DGTT2,* and *DGTT5* genes showed significant differences on days 1, 5, and 9 ($p < 0.05$); the levels of expression

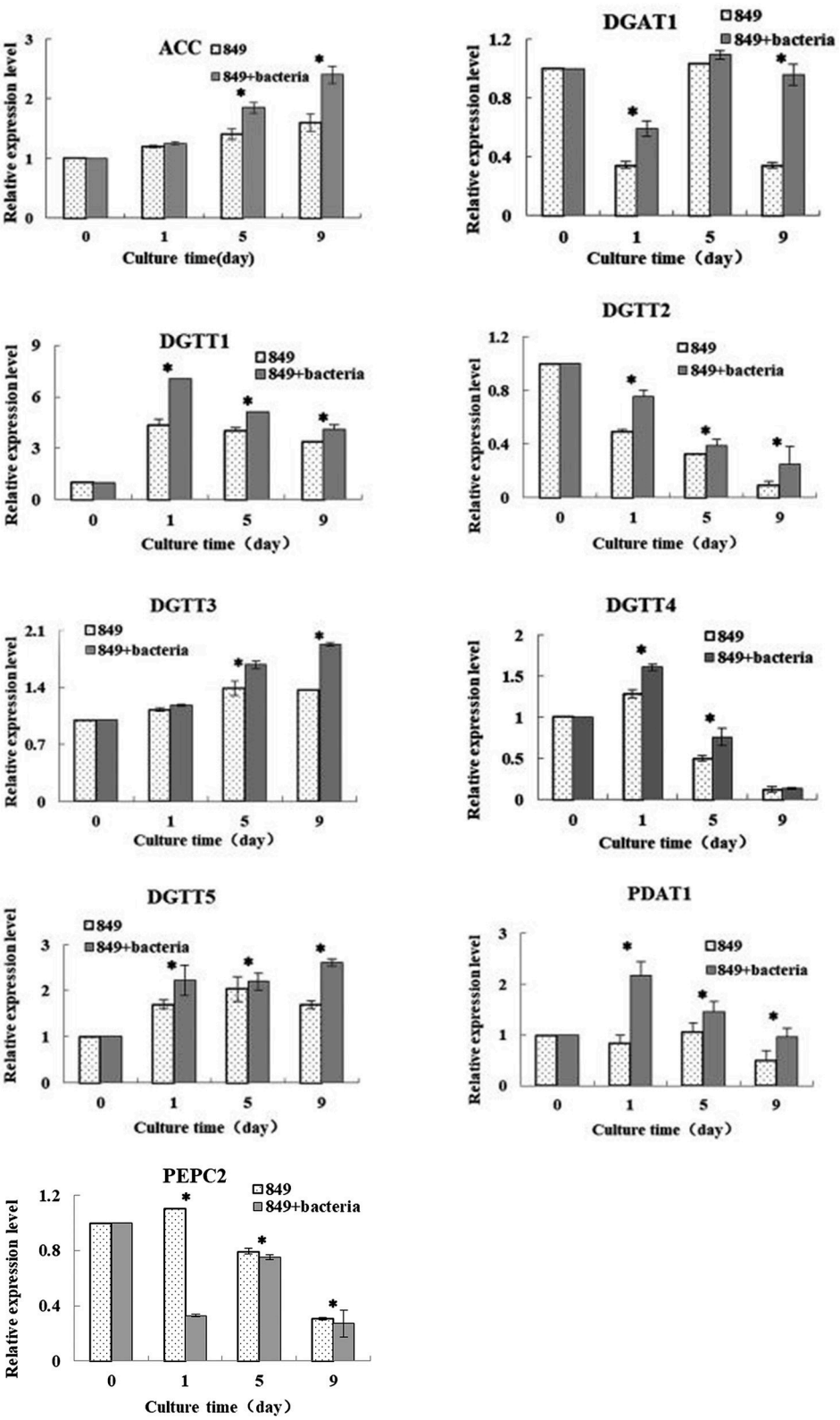

FIGURE 7 | Expression levels of lipid synthesis genes of C. *reinhardtii* in the co-culture on day 0 (in TAP medium), 1 (the initial stage of lipid production), 5 (logarithmic growth period of lipid production), and 9 (the stable growth period of lipid production) in the TAP-N medium. Examined genes included those encoding diacylglycerol: acetal-CoA carboxylase (ACCase); acyl-CoA aceyltransferases type 1 (DGAT1); and type 2 (DGTT1, DGTT2, DGTT3, and DGTT4); phosphoenolpyruvate carboxylase (PEPC); Phospholipid: diacylglycerol acyitransferase (PDAT). Algae cells were used as controls. The vertical bars indicate standard errors calculated from at least three independent experiments.

of the *DGTT3* gene showed significant difference on days 5 and 9 ($p < 0.05$); and the levels of expression of the *DGTT4* gene showed significant difference on days 1 and 5 ($p < 0.05$). Miller et al. (2010) investigated the transcriptomic analysis of photoheterotrophic *C. reinhardtii* under nitrogen-deprived conditions. In their research, *DGTT1* showed a significant increase and the expression of other *DGAT* genes changed little or not at all. In a study by Msanne et al. (Msanne et al., 2012), *DGTT1* and *DGTT3* displayed a large increase as a response to nitrogen starvation. Unlike in the current work, *DGTT4* was also expressed at a high level. Adding *A. chroococcum* to the algal culture resulted in a large increase in the expression levels of *DGAT1*, *DATT1*, *DATT2*, *DATT3*, *DATT4*, and *DATT5*, which suggests that the increased expression level of DGAT genes may contribute to lipid synthesis of *C. reinhardtii* co-cultured with *A. chroococcum* subjected to nitrogen starvation. This is another important reason for the increased lipid accumulation of *C. reinhardtii* after addition of *A. chroococcum* to the culture.

The enzyme phosphoenolpyruvate carboxylase (PEPC) is involved in the regulation of photosynthesis and photorespiration. It is also involved in the replenishment of amino acid metabolism. It catalyzes the formation of oxaloacetate into pyruvate and then enters the protein metabolism pathway. As shown in the results of *PEPC2* gene expression, we also detected gene encoding in *C. reinhardtii*, *PEPC2*. In our work, the levels of expression of *PEPC2* were determined under nutrient-deficient conditions. The results showed that the level of expression of *C. reinhardtii* co-cultured with *A. chroococcum* and pure algae decreased from day 1 to day 9 under nutrient-deficient conditions. The levels of the genes expression of *C. reinhardtii* co-cultured with *A. chroococcum* declined much faster than those of the pure algae. The levels of expression of the *PEPC* gene showed significant differences on days 1, 5, and 9 ($p < 0.05$). This demonstrated that nitrogen depletion leads to the inhibition of the expression of *PEPC2*. After the addition of *A. chroococcum*, the expression of *PEPC2* was more severely inhibited. In theory, when *PEPC* expression is inhibited, more pyruvate will become acetyl-CoA through a process catalyzed by pyruvate dehydrogenase, which facilitates lipid synthesis. Nitrogen as a signal molecule can be induced and regulated by the expression of genes. *PEPC* gene expression, protein content and *PEPC* gene activity were highly positive (Sugimoto et al., 1989; Chen et al., 1998). Therefore, *PEPC* plays a negative regulatory role in lipid production. Blocking the *PEPC* gene can increase lipid accumulation in many species (Sugimoto et al., 1989; Chen et al., 1998). Lipid content increases dramatically with decreased expression of the *PEPC2* gene in *C. reinhardtii* under nitrogen-deficient conditions (Deng et al., 2011). This is consistent with our results.

Phospholipid diacylglycerol acyltransferase (PDAT) is an acyl-CoA independent enzyme that transfers the acyl group from the sn-2 position of a phospholipid to the sn-3 position of a diacylglycerol (Boyle et al., 2012). Boyle et al. (2012) reported lipid accumulation by a *C. reinhardtii* mutant lacking the *PDAT1* gene at 25% of wild algae, indicating that *PDAT1* plays an important role in the lipid synthesis of *C. reinhardtii*. In our research, the levels of expression of both *C. reinhardtii* in the co-culture and pure *C. reinhardtii* increased with the increased lipid production. The expression levels of *C. reinhardtii* in the co-culture were higher than those of the control; i.e., adding *A. chroococcum* to the algal culture led to a significant increase in the expression level of the *PDAT1* gene in the depletion of the nitrogen medium. The levels of expression of the *PDAT1* gene showed significant differences on days 1, 5 and 9 ($p < 0.05$). Especially, the lowest level of expression of the *PDAT1* gene in *C. reinhardtii* in the co-culture was 1.5 times the control levels on day 9, which is when the lipid content, lipid production, and lipid productivity were the greatest (**Figure 3**).

CONCLUSIONS

In this study, we co-cultured *C. reinhardtii* with *A. chroococcum* to enhance lipid accumulation of *C. reinhardtii* by increasing the growth and biomass of *C. reinhardtii* under nitrogen-deprived conditions. After the addition of *A. chroococcum*, the growth and biomass of *C. reinhardtii* increased, as well as lipid accumulation, lipid content, and lipid productivity. In summary, *A. chroococcum* improved the lipid accumulation and the activity of *C. reinhardtii* by enhancing the growth, biomass, and levels of expression of genes that positively regulate lipid metabolism and by decreasing the expression levels of genes that negatively regulate lipid metabolism. This study provides an effective method for increasing the lipid production of *C. reinhardtii* by increasing its biomass and through its ecological relationship with *A. chroococcum*.

AUTHOR CONTRIBUTIONS

LX and QW proposed the idea and hypothesis. XC carried out the experiment. LX and XC analyzed data and drafted the manuscript. All authors read and approved the final manuscript for publication.

ACKNOWLEDGMENTS

This work was supported by the National Natural Science Foundation of China (NSFC No. 31600284) and Shanghai Engineering Research Center of Plant Germplasm Resources (No. 17DZ2252700).

SUPPLEMENTARY MATERIAL

The Supplementary Material for this article can be found online at: https://www.frontiersin.org/articles/10.3389/fpls.2018.00741/full#supplementary-material

REFERENCES

Bell, W. H., Lang, J. M., and Mitchell, R.,(1974). Selective stimulation of marine bacteria by algal extracellular products. *Linnol. Oceanogr*. 19, 833–839. doi: 10.4319/lo.1974.19.5.0833

Bligh, E. G., and Dyer, W. J. (1959). A rapid method of total lipid extraction and purification. *Can. J. Biochem. Physiol*. 37, 911–917. doi: 10.1139/y59-099

Boyle, N. R., Page, M. D., Liu, B., Blaby, I. K., Casero, D., Kropat, J., et al. (2012). Three acyltransferases and nitrogen-responsive regulator are implicated in nitrogen starvation-induced triacylglycerol accumulation in *Chlamydomonas*. *J. Biol. Chem*. 287, 15811–15825. doi: 10.1074/jbc.M111.334052

Chen, J., Lang, C., Hu, Z., Liu, Z., and Huang, R. (1998). Antisense PEP gene regulates to ratio of protein and lipid content in Brassica napus seeds. *J. Agric. Biotechnol*. 7, 316–320.

Chen, W., Zhang, C., Song, L., Sommerfeld, M., and Hu, Q. (2009). A high throughput Nile red method for quantitative measurement of neutral lipids in microalgae. *J. Microbiol. Methods* 77, 41–47. doi: 10.1016/j.mimet.2009.01.001

Cronan, J. E., and Waldrop, G. L. (2002). Multi-subunit acetyl-CoA carboxylases. *Prog. Lipid Res*. 41, 407–435. doi: 10.1016/S0163-7827(02)00007-3

Deng, X., Li, Y., and Fei, X. (2011). The mRNA abundance of pepc2 gene is negatively correlated with oil content in *Chlamydomonas reinhardtii*. *Biomass. Bioenerg*. 35, 1811–1817. doi: 10.1016/j.biombioe.2011.01.005

Dubois, M., Gilles, K. A., Hamilton, J. K., Rebers, P. A., and Smith, F. (1956). Colorimetric method for determination of sugars and related substances. *Anal. Chem*. 28, 350–356. doi: 10.1021/ac60111a017

Fan, J. H., Cui, Y. B., Wan, M. X., Wang, W., and Li, X. G. (2014). Lipid accumulation and biosynthesis genes response of the oleaginous *Chlorella pyrenoidosa* under three nutrition stressors. *Biotechnol. Biofuels* 7:17. doi: 10.1186/1754-6834-7-17

Gyurjan, I., Turtoczky, I., Toth, G., Paless, G., and Nghia N. H. (1984). Intercellular symbiosis of nitrogen-fixing bacteria and green alga. *Acta. Botanica. Hungarica*. 30, 249–256.

Harris, E. H. (2009). *The Chlamydomonas Sourcebook: Introduction to Chlamydomonas and Its Laboratory Use*. San Diego, CA: Academic Press.

Ho, S. H., Chan, M. C., Liu, C. C., Chen, C. Y., Lee, W. L., Lee, D. J., et al. (2014). Enhancing lutein productivity of an indigenous microalga *Scenedesmus obliquus* FSP-3 using light-related strategies. *Bioresour. Technol*. 152, 275–282. doi: 10.1016/j.biortech.2013.11.031

Hsieh, C. H., and Wu, W. T. (2009). Cultivation of microalgae for oil production with a cultivation strategy of urea limitation. *Bioresour. Technol*. 100, 3921–3926. doi: 10.1016/j.biortech.2009.03.019

Hu, Q., Sommerfeld, M., Jarvis, E.,Ghirardi, M., Posewitz, M., Seibert, M., et al., (2008). Microalgal triacylglycerols as feedstocks for biofuel production: perspectives and advances. *Plant J*. 54, 621–639. doi: 10.1111/j.1365-313X.2008.03492.x

Hui, W., Zhou, W. J., Chen, W. T., Gao, L. L., and Liu, T. Z. (2016). Strategy study on enhancing lipid productivity of filamentous oleaginous microalgae *Tribonema*. *Bioresour. Technol*. 218, 161–166. doi: 10.1016/j.biortech.2016.06.083

Ietswaart, I., Schneider, P. J., and Prinsra, R. A. (1994). Utilization of organic nitrogen sources by two phytoplankton species and a bacterial isolate in pure and mixed cultures. *Appl. Environ. Microbiol*. 60, 1554–1560.

Krakow, J. S., and Ochoa, S. (1963). Ribonucleic acid ribonucleic acid nucleotidyl transferase of *Azotobacter vinelandii*. IV. Purification and properties. *Biochem. Z*. 338, 796–808.

Li, Y., Han, D., Sommerfeld, M., and Hu, Q. (2011). Photosynthetic carbon partitioning and lipid production in the oleaginous microalga *Pseudochlorococcum* sp. (Chlorophyceae) under nitrogen-limited conditions. *Bioresour. Technol*. 102, 123–129. doi: 10.1016/j.biortech.2010.06.036

Liu, J., Pei, G., Diao, J., Chen, Z., Liu. L., Chen, L., Zhang, W., (2017). Screening and transcriptomic analysis of *Crypthecodinium cohnii* mutants with high growth and lipid content using the acetyl-CoA carboxylase inhibitor sethoxydim. *Appl. Microbiol. Biotechnol*. 101, 6179–6191. doi: 10.1007/s00253-017-8397-z

Makarova, V. V., Kosourov, S., Krendeleva, T. E., Semin, B. K., Kukarskikh, G. P., Rubin, A. B., et al. (2007). Photoproduction of hydrogen by sulfur-deprived *C. reinhardtii* mutants with impaired photosystem II photochemical activity. *Photosynth. Res*. 94, 79–89. doi: 10.1007/s11120-007-9219-4

Miller, R., Wu, G., Deshpande, R. R., Vieler, A., Gärtner, K., Li, X.,et al. (2010). Changes in transcript abundance in *Chlamydomonas reinhardtii* following nitrogen deprivation predict diversion of metabolism. *Plant Physiol*. 154, 1737–1752. doi: 10.1104/pp.110.165159

Msanne, J., Xu, D., Konda, A. R., Casas-Mollano, J. A., Awada, T., Cahoon, E. B., et al. (2012). Metabolic and gene expression changes triggered by nitrogen deprivation in the photoautotrophically grown microalgae *Chlamydomonas reinhardtii* and *Coccomyxa* sp. C-169. *Phytochemistry* 75, 50–59. doi: 10.1016/j.phytochem.2011.12.007

Park, J.-J., Wang, H. X., Gargouri, M., Deshpande, R. R., Skepper, J. N., Holguin, F. O., et al. (2015). The response of *Chlamydomonas reinhardtii* to nitrogen deprivation: a systems biology analysis. *Plant J*. 81, 611–624. doi: 10.1111/tpj.12747

Park, W.-K., Yoo, G., Moon, M., Kim, C. W., Choi, Y.-E., and Yang, J.-W. (2013). Phytohormone supplementation significantly increases growth of *Chlamydomonas reinhardtii* cultivated for biodiesel production. *Appl. Biochem. Biotechnol*. 171, 1128–1142. doi: 10.1007/s12010-013-0386-9

Riquelm, C. E., Fukami, K., and Ishida, Y. (1988). Effects of bacteria on the growth of a marine diatom, *Asterionella gracialis*. *Bull. Jap. Soc. Microb. Ecol*. 3, 29–34. doi: 10.1264/microbes1986.3.29

Rodolfi, L., Chini Zittelli, G., Bassi, N., Padovani, G., Biondi, N., Bonini, G., et al. (2009). Microalgae for oil: strain selection, induction of lipid synthesis and outdoor mass cultivation in a low-cost photobioreactor. *Biotechnol. Bioeng*. 102, 100–112. doi: 10.1002/bit.22033

Rubenchik, L. I. (1963). Azotobacter and its uses in agriculture. *Soil Sci*. 98, 6–8.

Scott, S. A., Davey, M. P., Dennis, J. S., Horst, I., Howe, C. J., Lea-Smith, D. J., et al. (2010). Biodiesel from algae: challenges and prospects. *Curr. Opin. Biotechnol*. 21, 277–286. doi: 10.1016/j.copbio.2010.03.005

Siaut, M., Cuiné, S., Cagnon, C., Fessler, B., Nguyen, M., Carrier, P., et al. (2011). Oil accumulation in the model green alga *Chlamydomonas reinhardtii*: characterization, variability between common laboratory strains and relationship with starch reserves. *BMC Biotechnol*. 11:7. doi: 10.1186/1472-6750-11-7

Sugimoto, T., Tanaka, K., Monma, M., Kawamura, Y., and Saio, K. (1989). Phosphoenolpyruvate carboxylase level in soybean seed highly correlates to its contents of protein and lipid. *Agric. Biol. Chem*. 53, 885–887. doi: 10.1080/00021369.1989.10869369

Walker, C. C., and Yater, M. G. (1978). The hydrogen cycle in nitrogen-fixing *Azotobacter chroococcum*. *Biochimie* 60, 225–231. doi: 10.1016/S0300-9084(78)80818-9

Wan, C., Bai, F.-W., and Zhao, X.-Q. (2013). Effects of nitrogen concentration and media replacement on cell growth and lipid production of oleaginous marine microalga *Nannochloropsis oceanica* DUT01. *Biochem. Eng. J*. 78, 32–38. doi: 10.1016/j.bej.2013.04.014

Wan, M., Liu, P., Xia, J., Rosenberg, J. N., Oyler, G. A., Betenbaugh, M. J., et al. (2011). The effect of mixotrophy on microalgal growth, lipid content, and expression levels of three pathway genes in Chlorella sorokiniana. *Appl. Microbiol. Biotechnol*. 91 , 835–844. doi: 10.1007/s00253-011-3399-8

Wang, H., Gao, L. L., Chen, L., Guo, F. J., and Liu, T. Z. (2013). Integration process of biodiesel production from filamentous oleaginous microalgae *Tribonema minus*. *Bioresour. Technol*.142, 39–44. doi: 10.1016/j.biortech.2013.05.058

Wang, Z. T., Ullrich, N., Joo, S., Waffenschmidt, S., and Goodenough, U. (2009). Algal lipid bodies: stress induction, purification, and biochemical characterization in wildtype and starchless *Chlamydomonas reinhardtii*. *Eukaryot Cell*. 8, 1856–1868. doi: 10.1128/EC.00272-09

Winogradski, S. (1935). The method in soil microbiology as illustrated by studies on *Azotobacter* and the nitrifying organisms. *Soil Sci*. 40, 59–76. doi: 10.1097/00010694-193507000-00009

Wu, S. X., Li, X. X., Yu, J., and Wang, Q. X. (2012). Increased hydrogen production in co-culture of *Chlamydomonas reinhardtii* and *Bradyrhizobium japonicum*. *Bioresour. Technol*. 123, 184–188. doi: 10.1016/j.biortech.2012.07.055

Wu, S. X., Xu, L. L., Wang, R. R., Liu, X. L., and Wang, Q. X. (2011). A high yield mutant of *Chlamydomonas reinhardtii* for photoproduction of hydrogen. *Int. J. Hydrogen Energy* 36, 14134–14140. doi: 10.1016/j.ijhydene.2011.05.001

Xu, L. L., Li, D. Z., Wang, Q. X., and Wu, S. X. (2016). Improved hydrogen production and biomass through the co-cultivation of *Chlamydomonas reinhardtii* and *Bradyrhizobium japonicum*. *Int. J. Hydrogen. Energ*. 41, 9276–9283. doi: 10.1016/j.ijhydene.2016.04.009

Yeesang, C., and Cheirsilp, B. (2011). Effect of nitrogen, salt, and iron content in the growth medium and light intensity on lipid production by microalgae isolated from freshwater sources in Thailand. *Bioresour. Technol.* 102, 3034–3040. doi: 10.1016/j.biortech.2010.10.013

Yen, H.-W., Hu, I. C., Chen, C.-Y., Ho, S.-H., Lee, D.-J., and Chang, J.-S. (2013). Microalgae-based Biorefinery-from biofuels to natural products. *Bioresour. Technol.* 135, 166–174. doi: 10.1016/j.biortech.2012.10.099

Zheng, T. L., Xu, M. Z., Yu, Z. M., and Song, X. X. (2002). The variation of bacterial extracellular enzymatic activity under the interaction between bacteria and algae. *Mari Sci.* 26 , 41–44.

Conflict of Interest Statement: The authors declare that the research was conducted in the absence of any commercial or financial relationships that could be construed as a potential conflict of interest.

frontiers in Plant Science

ORIGINAL RESEARCH
published: 19 June 2018
doi: 10.3389/fpls.2018.00826

The Role of Malic Enzyme on Promoting Total Lipid and Fatty Acid Production in *Phaeodactylum tricornutum*

Bao-Hua Zhu[1], Rui-Hao Zhang[1], Na-Na Lv[1], Guan-Pin Yang[2], Yi-Sheng Wang[1] and Ke-Hou Pan[1,3]**

[1] Key Laboratory of Mariculture, Ministry of Education, Ocean University of China, Qingdao, China, [2] College of Marine Life Sciences, Ocean University of China, Qingdao, China, [3] Qingdao National Laboratory for Marine Science and Technology, Qingdao, China

OPEN ACCESS

Edited by:
Jianhua Fan,
East China University of Science and Technology, China

Reviewed by:
Jianhui Zhang,
North Carolina Central University, United States
Guo Fu Chen,
Harbin Institute of Technology, Weihai, China
Zhengquan Gao,
Shandong University of Technology, China

***Correspondence:**
Bao-Hua Zhu
zhubaohua@ouc.edu.cn
Ke-Hou Pan
qdkhpan@126.com

Specialty section:
This article was submitted to Plant Biotechnology, a section of the journal Frontiers in Plant Science

Received: 10 February 2018
Accepted: 28 May 2018
Published: 19 June 2018

Citation:
Zhu B-H, Zhang R-H, Lv N-N, Yang G-P, Wang Y-S and Pan K-H (2018) The Role of Malic Enzyme on Promoting Total Lipid and Fatty Acid Production in Phaeodactylum tricornutum. Front. Plant Sci. 9:826. doi: 10.3389/fpls.2018.00826

To verify the function of malic enzyme (ME1), the ME1 gene was endogenously overexpressed in *Phaeodactylum tricornutum*. Overexpression of *ME1* increased neutral and total lipid content and significantly increased saturated fatty acids (SFAs) and polyunsaturated fatty acids (PUFAs) in transformants, which varied between 23.19 and 25.32% in SFAs and between 49.02 and 54.04% in PUFAs, respectively. Additionally, increased ME1 activity was accompanied by elevated NADPH content in all three transformants, indicating that increased ME1 activity produced additional NADPH comparing with that of WT. These results indicated that ME1 activity is NADP-dependent and plays an important role in the NADPH levels required for lipid synthesis and fatty acid desaturation in *P. tricornutum*. Furthermore, our findings suggested that overexpression of endogenous *ME1* represents a valid method for boosting neutral-lipid yield in diatom.

Keywords: malic enzyme, lipid, fatty acid, NADPH, *Phaeodactylum tricornutum*

INTRODUCTION

Malic enzyme (ME) is widespread in all kinds of organisms and catalyzes the reversible oxidative decarboxylation of malate to pyruvate, CO_2, and NAD(P)H in the presence of a divalent metal ion (Drincovich et al., 2001). Malic enzymes are divided into three categories on the basis of the substrate specificity and coenzyme preference: NAD^+(EC 1.1.1.38-39), $NADP^+$-dependent (EC1.1.1.40), or dependent upon both cofactors. These enzymes localize to the cytoplasm, mitochondria or chloroplasts in eukaryotes (Tang et al., 2010); however, little is known about the molecular basis for cofactor selectivity of these enzymes (Chang and Tong, 2003).

In spite of decades of research, the physiological function of ME remains poorly understood, and its role might vary from organism to organism (Kendrick and Ratledge, 1992). ME plays a crucial part in the provision of NADPH to promote desaturation and elongation reactions leading to the formation of polyunsaturated fatty acids (PUFAs) in some oleaginous organisms (Kendrick and Ratledge, 1992; Ren et al., 2013; Ratledge, 2014; Lv et al., 2016). Previous studies also reported novel physiological functions associated with this enzyme, including renovating UV-induced damage in maize seedlings (Drincovich et al., 1998; Casati et al., 1998), affecting the development of chloroplasts by generating excessive reducing power in transgenic C3 plants (Takeuchi et al., 2000),

lengthening the lifespan of *Drosophila* during the larval stage (Kim et al., 2015), keeping stable levels of TCA-cycle intermediates in the bacterium *Sinorhizobium meliloti* (Zhang et al., 2016), and acting as a potential target of cancer chemotherapy (Chang and Tong, 2003) and as an anaplerotic enzyme in *Saccharomyces cerevisiae* (Zelle et al., 2011) and *Streptomyces coelicolor* (Rodriguez et al., 2012).

Few studies have centered on the role of MEs in lipid accumulation, with those undertaken focusing mainly in plants and mammals; however, little is known about the role of these enzymes in microalgae. An NADP-dependent ME was proposed for diatoms, with possible function as a decarboxylase of releasing CO_2 in chloroplasts of diatoms, similar to that in C4 plants (Granum et al., 2005). The gene encoding ME in *Dunaliella parva* was cloned and characterized, but further research on the function of this gene was not conducted (Shang et al., 2012). Kroth et al. (2008) reported that *Phaeodactylum tricornutum* appears to contain two mitochondrial ME that are either NAD- or NADP-dependent. One of the ME-encoding genes was overexpressed endogenously in *P. tricornutum* (PtME), revealing its predominant localization to the mitochondria, as well as its significant impact on promoting lipid accumulation; however no further studies were performed on the role of ME in increasing lipid content (Xue et al., 2015).

The marine diatom *P. tricornutum* represents a potential producer of biodiesel because of its rapid growth, lipid-accumulation capability, and the availability of genetic tools (Zaslavskaia et al., 2000). Therefore, it is possible to genetically manipulate the key genes involved in fatty acid synthesis in this alga to enhance characters to gain both high lipid and high biomass levels necessary for industrial production.

To verify ME function, the ME1 gene from *P. tricornutum* (different from that studied by Xue et al., 2015), which possesses a mitochondria presequence and might have a dinucleotide-binding site given for NADP (Kroth et al., 2008), was overexpressed in *Escherichia coli* (Lv et al., 2016) and in *P. tricornutum* (this study). The results of this study, as well as those previously published (Lv et al., 2016), indicated that ME1 from *P. tricornutum* is NADP-dependent and can supply enough NADPH for both fatty acid biosynthesis and desaturation in *E. coli* (Lv et al., 2016) and *P. tricornutum* (this study).

MATERIALS AND METHODS

Strains and the Growth Conditions

Wild-type (WT) *P. tricornutum* Bohlin (LAMB118), provided by Institute of Hydrobiology, Chinese Academy of Sciences, and zeocin-resistant colonies (named as PtME1-1, PtME1-2, and PtME1-3) were cultured in f/2 medium (Guillard, 1975) prepared with sterile seawater at 20 ± 1°C and under 37.50 μmol photons m^{-2} s^{-1}, following a 12:12 photoperiod. Three cultures for every transformant and the WT strain (300-mL each) were cultivated axenically to monitor their growth. To set up growth curves, the optical density (OD) was measured at 750 nm every 2 days using a UV-3310 spectrophotometer (Hitachi, Tokyo, Japan) (Griffiths et al., 2011).

Construction of the Plasmid Containing the ME1 Gene and Particle Bombardment Transformation

The *ME1* gene was amplified by polymerase chain reaction (PCR) using cDNA from *P. tricornutum* (GenBank accession: XP_002177890.1) as the template and the primers PtME1-F (GGGGTACCATGATATCATCGGCGTGTCG) and PtME1-R (GCTCTAGACTAGTGGTGGTGGTGGTGGTGGATTGATATTTCTCGTTTTTCC). To generate the pPha-T1-ME1 recombinant plasmid, the amplified gene was inserted into the pPha-T1 (Zaslavskaia et al., 2000) plasmid using an *fcp*A promoter driving the *ME1* gene, and the resistant strains were selected with Zeocin™ (Invitrogen, Carlsbad, CA, United States).

The recombinant plasmid (pPha-T1-ME1) was introduced into *P. tricornutum* by a Bio-Rad Biolistic PDS-1000/He particle-delivery system (Bio-Rad, Hercules, CA, United States), according to the methods described by Zaslavskaia et al. (2000) and Zhu et al. (2016). It should be pointed out that seawater f/2 medium was used for culturing in this study.

Genomic DNA Extraction and Molecular Identification

Total genomic DNA was isolated in the light of the method described by Watanabe et al. (1998). Transformants were screened by PCR using the gene-specific *Sh-ble* and *PtME1-ble* primers (**Table 1**), respectively. To prepare a digoxigenin-labeled probe for Southern blot analysis (Falciatore et al., 1999), the *ble* fragment was used as the template and genomic DNA was digested with *EcoR* I and *Kpn*I, respectively. For western blot (Poulsen and Kröger, 2005), an anti-His-tag antibody (Bioss, Woburn, MA, United States) was used to detect the ME1 protein, and actin was served as the internal control. Cells were harvested by centrifugation at late exponential stage for assays.

TABLE 1 | Primers used in this study.

Primer name	Primer sequence (5′-3′)
PtME1-F	GGGGTACCATGATATCATCGGCGTGTCG
PtME1-R	GCTCTAGACTAGTGGTGGTGGTGGTGGTGGATTGATATTTCTCGCTTTTTCC
Sh ble-F	CCAACAGCATCACCCAGAT
Sh ble-R	GGTAGAACTCGTCGCTCAGG
ME1- ble-F	GGGGCTGGGAGCATCAGTTTG
ME1-ble-R	ACCCAGGCCAGGGTGTTGTC
RT-PtME1-F	GTGTCGTGGCAGCCTGAAATC
RT-PtME1-R	CGGACCGAAATCCTTATTGGTATCA
RT-H4-F	GTGGTAAAGGAGGCAAGGGTC
RT-H4-R	CACGGGTCTCTTCGTAAATC

Underlined bases and double underlines indicate the nucleotide sequences recognized by and digested by restriction endonucleases and encoding the His tags, respectively.

RNA Extraction and Quantitative Real-Time (qPCR)

RNA extraction and qPCR were performed as previously described (Zhu et al., 2016) using primers shown in **Table 1**. The histone H4 gene was served as the internal reference (Siaut et al., 2007). The $2^{-\Delta\Delta Ct}$ method (Livak and Schmittgen, 2001) was used to analyze the *ME1* expression and calculate relative *ME1*-transcript abundance.

Analytical Methods for Measuring Total and Neutral-Lipid Contents

Total lipids were extracted according to the method as described previously (Zhu et al., 2016). To detect cellular neutral-lipid content in *P. tricornutum*, BODIPY505/515 (Invitrogen) staining was carried out according to the protocol described by Cooper et al. (2010). Algal cells (10^6 cells/mL) were first treated with 2% dimethyl sulfoxide (DMSO) for 10 min at room temperature. A stock solution of 100 μg/mL BODIPY505/515 was prepared using anhydrous DMSO and added directly to algal solution to obtain a final BODIPY 505/515-labeling concentration of 0.87 μg/mL, followed by incubation in darkness for 10 min at room temperature. Stained cells were detected by their fluorescence intensity with flow cytometry (BD FACSVantage SE; BD Biosciences, Franklin Lakes, NJ, United States). Excitation and emission wavelengths were 485 nm and 535 nm, respectively. Quantitative comparison of neutral-lipid content between samples was obtained according to relative fluorescence-intensity values.

Determination of Fatty Acid Composition

Fatty acid methyl esters were analyzed using gas chromatography (Agilent 6890 Series GC System; US10251016; Agilent, Santa Clara, CA, United States) as previously described (Zhu et al., 2014) after transmethylation according to a method described by Lepage and Roy (1984). Mixed external standards of fatty acids (Supelco 37, United States) were used to detect and determine the Fatty acid composition.

Measurement of ME Enzyme Activity

Malic enzyme activity in *P. tricornutum* was measured using an NADPH-ME kit (Solarbio, Beijing, China) according to manufacturer instructions. The optimum reaction system was prepared as followed: 50 mM, pH 7.5 Tris–HCl, 1 mM $MgCl_2$, 0.5 mM $NADP^+$, 10 mM L-malate. Soluble protein concentration was quantified using a Bradford assay kit (Genmed Scientifics, Shanghai, China). ME activity was determined by monitoring the change in absorbance at 1-min intervals continuously at 340 nm using a UV-3310 spectrophotometer (Hitachi). One unit of ME activity was defined as 1 μM NADPH generated by 1 mg protein per minute in the reaction system:

$$\text{ME (U/mg protein)} = [(A2 - A1)/6.22] \times (1/t) \times (V1/V2)/C$$

where A1 is the initial absorbance, A2 is the absorbance after the reaction, 6.22 represents the extinction coefficient per mM NADPH, t is the reaction time (1 min), l is the path length of the cuvette (1 cm), V1 is the total reaction volume (900 μL), V2 is the volume of ME solution (30 μL), and C is the concentration of protein (mg/mL).

NADPH-Content Analysis

NADPH content in *P. tricornutum* was analyzed with the Amplite Fluorimetric NADP/NADPH ratio assay kit (AAT Bioquest, Sunnyvale, CA, United States) according to manufacturer instructions. After lysis and ultrasonication extraction, microalgal samples were centrifuged at 8000 × *g* for 10 min at 4°C, and the supernatant was prepared for testing. Traditional NADPH assays are performed by monitoring the changes in NADPH absorption at 340 nm using a Synergy microplate reader (BioTek, Winooski, VT, United States). The excitation and emission wavelengths used were 540 nm and 590 nm, respectively. The concentration of NADPH was determined from the standard curve of NADPH.

Statistical Analysis

One-way analysis of variance was used at a level of significance of $P < 0.05$ to calculate significant differences between treatments using SPSS 17.0 software (IBM, Armonk, NY, United States), and all data are reported as the mean ± standard deviation (three replicates were used, $n = 3$).

RESULTS AND DISCUSSION

Effect of the Transgene on *P. tricornutum* Growth

Similar growth curves were shown in **Figure 1** for both the WT strain and transformants although all the resistant strains showed a slightly increased growth rate and did not differ significantly from that of the WT strain, which suggested that the transgene exerted a temperate influence on the growth of the transformants. In contrast to this study, Jiang et al. (2013) reported that depletion of *ME1* or *ME2* strongly impaired tumor-cell growth, and overexpression of these genes enhanced tumor-cell growth. By contrast, growth reductions in transgenic strains were reported by other studies (Li et al., 2010; Radakovits et al., 2011). Therefore, further research is needed to understand the underlying mechanism.

Transgene Detection via Molecular Approaches

Resistant clones were first selected by growth on f/2 solid medium (1% agar) with 100 μg/mL Zeocin. Further screening was conducted by PCR using the gene-specific *Sh-ble* and *ME1-ble* primers (**Table 1**). As shown in **Figures 2A,B**, all resistant clones presented the expected fragment sizes, but no DNA band was seen in the WT strain. To further verify gene integration, Southern blot analysis was performed in all three resistant strains and the WT strain. As shown in **Figure 2C**, all three resistant strains showed two or more hybridized bands detected with the *ble* probe digested using different restriction enzymes, indicating that exogenous *sh-ble* and endogenous *ME1* had been integrated into the *P. tricornutum* genome, and that

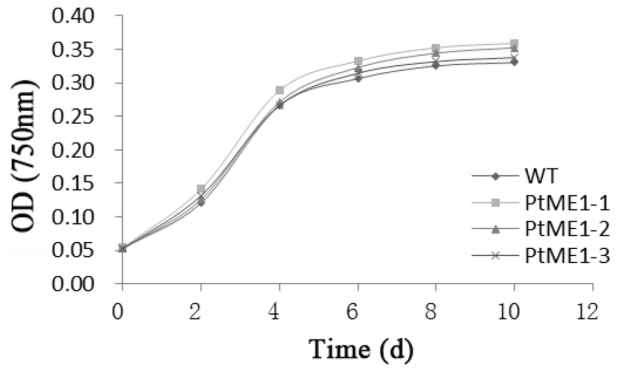

FIGURE 1 | Growth curves of transgenic clones and the WT strain. Values represent averages of three replicates (n = 3).

these clones were undoubted transformants. To detect target protein levels translated from the introduced *ME1* gene in all the resistant strains, western blot was conducted with an anti-His-tag antibody. A cross-reacting band, the same size as expected, was shown in all the resistant strains, whereas this was not observed in the WT strain (**Figure 2D**).

The impact of *ME1* overexpression on *ME1* mRNA levels was investigated by qPCR analysis in three resistant clones and the WT strain. As shown in **Figure 3A**, all transformants displayed elevated *ME1*-transcript abundance as compared with the WT strain. Additionally, the relative *ME1*-transcript abundance of the transformants was 6.09–11.87 time higher than that of the WT strain. Furthermore, the increase in *ME1*-transcript abundance was accompanied by enhanced ME1 activity (**Figure 3B**), which increased 1.52–1.81 fold relative to that observed in the WT strain. These results validated these resistant colonies as the expected transformants.

ME1 Overexpression Increases Neutral and Total Lipid Contents

As shown in **Figure 4A**, the neutral-lipid content of all three transformants (PtME1-1, PtME1-2, and PtME1-3) increased significantly ($P < 0.05$; 33.33, 20.25, and 29.63%, respectively) as compared with that in the WT strain. Additionally, total lipid content of the three resistant clones was enhanced significantly, and that of the PtME1-1 transformant increased by 48.42% as compared with that of the WT strain (**Figure 4B**). These findings suggested that *PtME1* overexpression induced the accumulation of neutral- and total lipids in *P. tricornutum*. Similarly, overexpression of two exogenous *ME* genes in *M. circinelloides* led to a 2.5-fold increase in lipid accumulation (Zhang et al., 2007). Moreover, *PtME* expressed in the green microalga *Chlorella pyrenoidosa* resulted in a 3.2-fold increase in neutral-lipid content relative to that observed in the WT strain, with total lipid content reaching 40.9% (dry cell weight) (Xue et al., 2016).

A previous study reported that overexpressing *ME* in *E. coli* led to a 4-fold increase in intracellular lipids by providing a high level of NADPH (Meng et al., 2011). In a previous study with different methods (the recombinant plasmid pHY-PtME instead of pPha-T1-ME1, transformation by electroporation rather than Biolistic PDS-1000/He particle-delivery system) to the present study, *PtME* overexpressed endogenously in *P. tricornutum*,

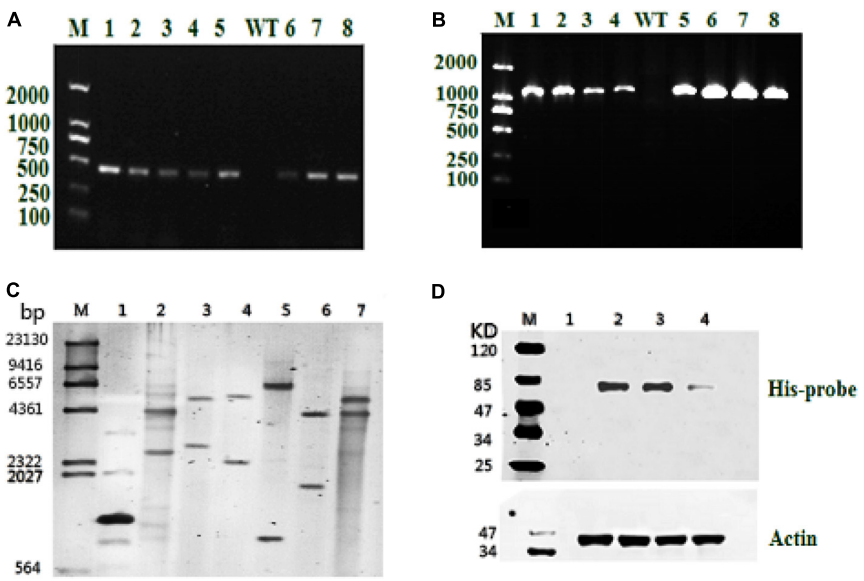

FIGURE 2 | Molecular analysis of resistant clones. **(A)** PCR of the resistant gene *Sh-ble* in selected clones and the WT strain. M: DNA-size marker. **(B)** PCR performed using primers designed from tandem *ME1* and *ble* sequences in the recombinant plasmid pPha-T1-ME1. The reference band is 1126 bp. M: DNA-size marker. **(C)** Southern blot analysis of *EcoR* I-digested products (lane 1: positive control represents the plasmid, pPha-T1; lanes 2–4: PtME1-1, PtME1-2, and PtME1-3) and *Kpn* I-digested products (lanes 5–7: PtME1-1, PtME1-2, and PtME1-3) from genomic DNA with a *ble* fragment used as a digoxigenin-labeled probe. **(D)** Western blot analysis using an anti-His-tag antibody. Actin was used as an internal control (lanes 2–4: PtME1-1, PtME1-2, and PtME1-3).

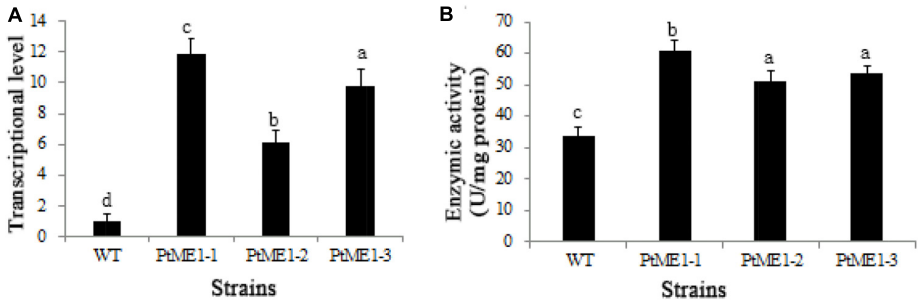

FIGURE 3 | Molecular characterization of resistant clones. **(A)** Relative quantification of *ME1* transcripts in the WT strain and the three *Phaeodactylum tricornutum* resistant clones. *ME1*-transcript abundance in the resistant clones was quantified with WT cells as the standard and normalized to endogenous histone *H4* expression ($n = 6$). **(B)** NADP-ME activity (U/10^6 cells) in the WT strain and the three *P. tricornutum* transformants. Activity assays were performed on samples from the same experiments. Values represent averages of at least three replicates. Error bars indicate standard deviations. Values with different letters (a,b,c,d) indicate a significant difference between them ($p < 0.05$).

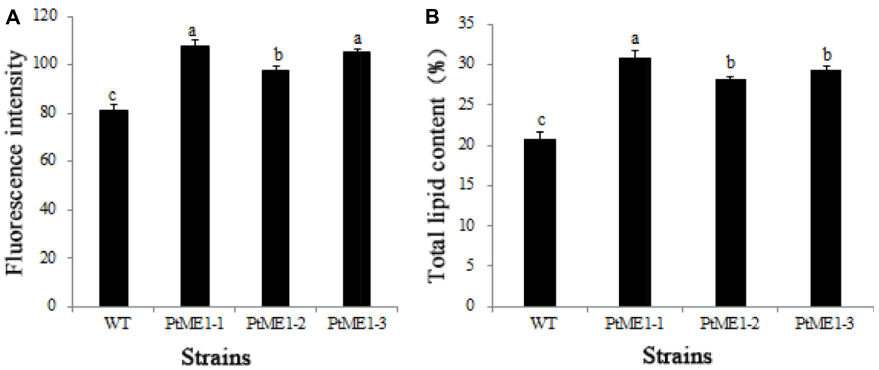

FIGURE 4 | Neutral-lipid accumulation and total lipid contents. **(A)** Neutral-lipid and **(B)** total lipid contents in the WT strain and the three *Phaeodactylum tricornutum* transformants. Values represent averages of three replicates ($n = 3$). Values with different letters (a,b,c) indicate a significant difference between them ($p < 0.05$).

resulting in a marked increase (2.5-fold) in total lipid content in transgenic strains, reaching a 57.8% dry cell weight and a similar growth rate to that observed in the WT strain (Xue et al., 2015). However, in that study, the authors did not confirm the $NADP^+$-dependence of the ME-encoding gene, suggesting that it would not necessarily have produced NADPH. Therefore, the mechanisms associated with the increases in lipids remains unclear.

The Effects of ME1 Overexpression on Fatty Acid Composition

As shown in **Table 2**, Significant decreases in monounsaturated fatty acids (MUFAs) from 24.61 to 19.96% were detected in transgenic microalgae. With regard to saturated fatty acids (SFAs) and PUFAs, marked increases in the transgenic lines, from 23.19 to 25.32% and from 49.02 to 54.04%, respectively, were observed, revealing that overexpression of endogenous *ME1* facilitated SFA and PUFA biosynthesis. In contrast to the present study, other *PtME*s different from those in this study were overexpressed endogenously in *P. tricornutum*, resulting in an increase in MUFAs and a slight decrease in PUFAs in transgenic microalgae (Xue et al., 2015). Wynn and Ratledge (1997) reported that enhanced ME activity leads increases in the cytosolic NADPH pool, and that ME plays a vital role in the provision of NADPH for storage lipids synthesis by *Aspergillus nidulans*. These findings indicated that the function of ME in lipid biosynthesis involves supplying NADPH for fatty acid desaturation (Liang and Jiang, 2013).

It is likely that the elevated ME activity generated NADPH for fatty acid desaturases and also increased fatty acid desaturase activity. (Zhang et al., 2007). The present study showed a 1.52- to 1.81-fold increase in ME1 activity (**Figure 3B**) as compared with that in the WT strain, which led to an increase in fatty acid desaturase activity and induced further accumulation of PUFAs in transgenic microalgae. A previous study showed that docosahexaenoic acid content increased significantly by adding ME based on the resulting elevation in ME activity and NADPH supply during a specific fermentation stage in *Schizochytrium* sp. HX-308 (Ren et al., 2009). Exogenously overexpressing *ME* in the green microalga *C. pyrenoidosa* results in a 34% increase in PUFAs in the transformed line, with the content of C16:3 and C18:3 lipids in the transgenic lines also elevated by 68.5 and 42.9%, respectively (Xue et al., 2016). Overexpressing *ME1* in *E. coli* showed that C14:0, C16:0, C18:1, and total fatty acid contents were increased by 34.8, 69.9, 54.2, and 50.2%, respectively, and that the content of C16:1 lipids was elevated

TABLE 2 | Fatty acid composition of the WT strain and the three transformants (% of total fatty acids).

	Strains				
Fatty acid	**WT**	**PtMEl-1**	**RME1-2**	**PtMEl-3**	**Mean value**
C14:0	8.31 ± 0.09^{a}	8.62 ± 0.35^{a}	9.26 ± 0.30^{b}	8.60 ± 0.13^{a}	8.83 ± 0.37^{ab}
C16:0	12.10 ± 0.39^{a}	13.13 ± 0.66^{b}	13.04 ± 0.41^{b}	12.91 ± 0.35^{b}	13.03 ± 0.11^{b}
C16:l	23.66 ± 0.52^{c}	18.11 ± 0.70^{ab}	17.72 ± 0.61^{a}	19.16 ± 0.11^{b}	18.33 ± 0.74^{ab}
C16:2	1.62 ± 0.03^{c}	1.52 ± 0.06^{b}	1.50 ± 0.05^{ab}	1.43 ± 0.03^{a}	1.48 ± 0.05^{ab}
C16:3	13.63 ± 0.60^{a}	17.13 ± 0.91^{c}	14.87 ± 0.41^{ab}	15.09 ± 0.13^{ab}	15.70 ± 1.25^{b}
C18:0	2.77 ± 0.29^{a}	3.02 ± 0.06^{a}	2.89 ± 0.17^{a}	3.71 ± 0.10^{b}	3.21 ± 0.44^{a}
C18:l	1.29 ± 0.05^{a}	1.41 ± 0.06^{a}	1.60 ± 0.35^{ab}	1.86 ± 0.12^{b}	1.62 ± 0.23^{ab}
C18:2	3.09 ± 0.06^{a}	3.24 ± 0.21^{a}	3.16 ± 0.09^{a}	3.20 ± 0.35^{a}	3.20 ± 0.04^{a}
C20:5	29.53 ± 0.46^{a}	29.93 ± 0.20^{ab}	30.48 ± 0.22^{b}	29.73 ± 0.36^{a}	30.05 ± 0.39^{ab}
C22:6	1.15 ± 0.09^{a}	2.22 ± 0.14^{b}	2.66 ± 0.13^{c}	2.76 ± 0.19^{c}	2.54 ± 0.29^{bc}
SFA	23.19 ± 0.15^{a}	24.78 ± 0.87^{b}	25.19 ± 0.45^{b}	25.23 ± 0.49^{b}	25.07 ± 0.25^{b}
MUFA	24.61 ± 0.19^{c}	19.52 ± 0.76^{a}	19.33 ± 0.29^{a}	21.02 ± 0.23^{b}	19.96 ± 0.92^{a}
PUFA	49.02 ± 0.80^{a}	54.04 ± 0.70^{c}	52.67 ± 0.29^{b}	52.21 ± 0.59^{b}	52.98 ± 0.95^{bc}

The values in the same row with different superscripts represent statistically significant differences ($P < 0.05$). Values represent averages of three replicates ($n = 3$).

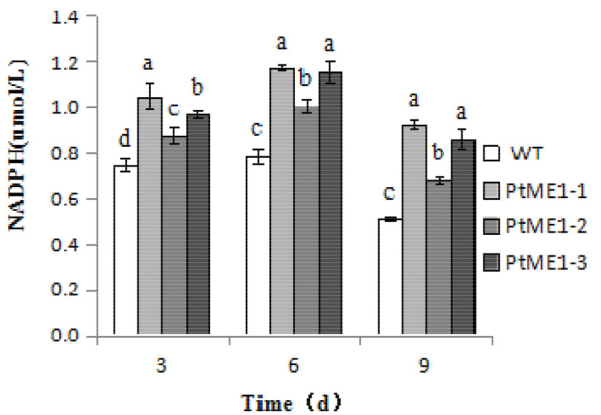

FIGURE 5 | NADPH content in the WT strain and the three *Phaeodactylum tricornutum* transformants. Values represent averages of three replicates ($n = 3$). Values with different letters (a,b,c,d) indicate a significant difference between them ($p < 0.05$).

5.6-fold as compared with that of controls (Lv et al., 2016). These findings suggested that *PtME* influenced fatty acid composition by regulating lipogenesis (Xue et al., 2016).

The Role of ME1 in NADPH Generation in *P. tricornutum*

To verify whether *ME1* overexpression can promote NADPH production, NADPH content was measured in the three transformants and the WT strain during cultivation on days 3, 6, and 9. As shown in **Figure 5**, the NADPH content of all algal strains increased markedly on day 6 and decreased significantly on day 9, indicating that NADPH could be used to produce other compounds, such as lipids, and expended during the late exponential-growth phase. However, the NADPH content of three transformants was clearly enhanced relative to that observed in the WT strain during the cultivation stage, increasing by 40.6, 17.8, and 30.0% on day 3, 49.3, 28.4, and 46.7% on day 6, and 80.3, 33.2, and 68.2% on day 9 for PtME1-1, PtME1-2, and PtME1-3, respectively, suggesting that *ME1* overexpressing significantly improved NADPH biosynthesis in *P. tricornutum*. Furthermore, the increase in ME1 activity was accompanied by elevated NADPH content, indicating that increased ME1 activity produced additional NADPH.

NADPH plays a crucial part in fatty acid accumulation in oleaginous organisms, with these organisms exhibiting a unique mechanism involving NADPH supply. Wynn et al. (1999) reported that ME was important for providing sufficient NADPH for lipid biosynthesis in the fungi, hypothesizing that lipid production was controlled by ME-mediated NADPH generation to fatty acid synthase activity, given that no other enzyme activity has displayed such a strong link with the content of lipid accumulation. A previous report indicated that ME represents the only NADPH source for fatty acid biosynthesis in the yeast *Rhodosporidium toruloides* (Evans and Ratledge, 1985). Furthermore, *ME* overexpression in *E. coli* resulted in increased lipid accumulation in engineered strains relative to controls due to two potentially linked results: increased NADPH and pyruvate levels (Meng et al., 2011).

Until now, no study reported whether ME was capable of providing NADPH in eukaryotic microalgae. Xue et al. (2015) reported that *PtME* overexpression significantly impacted the promotion of lipid accumulation, attaining a 57.8% increase in dry cell weight, along with a similar growth rate to that of the WT strain in *P. tricornutum*. That study also showed that *PtME* was predominantly localized to the mitochondria, although no further studies were performed on the role of ME in accumulating lipid content. The data obtained from this study along with our previously published work (Lv et al., 2016) suggested that ME1 plays an important role in NADPH supply for lipid synthesis and fatty acid desaturation in *P. tricornutum* (Wynn et al., 1999).

However, the role of ME in the provision of NADPH for lipid biosynthesis remains incompletely understood

(Ratledge, 2014; Liang and Jiang, 2015). Ren et al. (2013) reported that the main source of NADPH might be from glucose-6-phosphate dehydrogenase at the early stage of fermentation, whereas ME was the main provider during the late stage in the oleaginous fungi *Schizochytrium* sp. HX-308.

Malic enzyme can promote NADPH production in oleaginous organisms; however, other some studies indicated that the enzyme cannot provide all of the NADPH required. In animal cells, although ME is important for generating NADPH for fatty acid biosynthesis (Ceddia et al., 2000), it is not the sole supplier, as 50% of the NADPH is from both glucose-6-phosphate dehydrogenase and 6-phosphogluconate dehydrogenase (Shimomura et al., 1998; Zhang et al., 2007). Pentose phosphate pathway related reactions seem to be the most likely way, in spite of a possibility that a cytosolic isocitrate dehydrogenase (ICDH) reaction with a mitochondrial ICDH function might also produce some NADPH in the reverse reaction (Ratledge, 2014).

NADPH production was not affected in the strain *Saccharomyces cerevisiae* overexpressing ME gene (lacking the mitochondria-target sequence) and exhibiting ME localization to the mitochondria due to transfer of NADPH across the mitochondrial membrane (Moreira dos Santos et al., 2004). The ME shunt proved to be diversified in this respect because of the possibility of outputting additional NADPH to the cytosol (Moreira dos Santos et al., 2004). Therefore, it is difficult to identify the correct *ME* gene involved in producing NADPH particularly for fatty acid biosynthesis (Zhang et al., 2007).

Two additional decarboxylating enzymes, which belong to the ME family, have been identified (27477 and 56501 represent NCBI predicted ME protein sequences), with both possessing mitochondria presequences in *P. tricornutum* (Kroth et al., 2008), suggesting that ME likely localizes to the mitochondria (Valenzuela et al., 2012). One of these enzymes (56501) has a dinucleotide-binding site given for NAD rather than NADP. Therefore, *P. tricornutum* appears to have two mitochondrial MEs that are either NAD- or NADP-dependent (Kroth et al., 2008). Further research is needed to determine ME1 localization.

These results along with those from other studies (Kroth et al., 2008; Xue et al., 2015) indicated that *P. tricornutum* possesses two MEs, one being an NAD cofactor (Xue et al., 2015) and the other NADP-dependent (this study).

CONCLUSION

In this study, endogenous *ME1* was succeed in overexpressing in *P. tricornutum,* resulting in a significant increase in total lipid and PUFA content, and producing additional NADPH, thereby demonstrating that ME1 is NADP-dependent and plays a vital role in the supply of NADPH for lipid biosynthesis and desaturation of fatty acids in *P. tricornutum*. These findings suggested that overexpression of endogenous *ME1* represents a valid method for boosting neutral-lipid yield in diatom.

AUTHOR CONTRIBUTIONS

B-HZ, R-HZ, and N-NL designed the experiments, analyzed and interpreted the data, and wrote the article. Y-SW participated in algal cultivation and analyzed the data. G-PY and K-HP supervised specific experiments and gave critical revisions of the article. All authors agreed on the manuscript.

FUNDING

This work was supported by The National Key Research and Development Program-China (2016YFB0601001).

ACKNOWLEDGMENTS

The authors thank Prof. Matsuda (Kwansei-Gakuin University, Nishinomiya, Japan) for kindly offering the pPha-T1 plasmid and the three reviewers for their valuable suggestions.

REFERENCES

Casati, P., Drincovich, M. F., Andreo, C. S., Donahue, R., and Edwards, G. E. (1998). UV-B, red and far-red light regulate induction of the C4 isoform of NADP-malic enzyme in etiolated maize seedlings. *Aust. J. Plant Physiol.* 25, 701–708. doi: 10.1071/PP98004

Ceddia, R. B., William, W. N., Lima, F. B., Flandin, P., Curi, R., and Giacobino, J. P. (2000). Leptin stimulates uncoupling protein-2 mRNA expression and Krebs cycle activity and inhibits lipid synthesis in isolated rat white adipocytes. *Eur. J. Biochem.* 267, 5952–5958. doi: 10.1046/j.1432-1327.2000.01664.x

Chang, G. G., and Tong, L. (2003). Structure and function of malic enzymes, a new class of oxidative decarboxylases. *Biochemistry* 42, 12721–12733. doi: 10.1021/bi035251+

Cooper, M. S., Hardin, W. R., Petersen, T. W., and Cattolico, R. A. (2010). Visualizing "green oil" in live algal cells. *J. Biosci. Bioeng.* 109, 198–201. doi: 10.1016/j.jbiosc.2009.08.004

Drincovich, M. F., Casati, P., and Andreo, C. S. (2001). NADP-malic enzyme from plants: a ubiquitous enzyme involved in different metabolic pathways. *FEBS Lett.* 490, 1–6. doi: 10.1016/S0014-5793(00)02331-0

Drincovich, M. F., Casati, P., Andreo, C. S., Donahue, R., and Edwards, G. E. (1998). UV-B induction of NADP-malic enzyme in etiolated and green maize seedlings. *Plant Cell Environ.* 21, 63–70. doi: 10.1046/j.1365-3040.1998.00240.x

Evans, C. T., and Ratledge, C. (1985). Possible regulatory roles of ATP: citrate lyase, malic enzyme, and AMPdeaminase in lipid accumulation by *Rhodosporidium toruloides* CBS 14. *Can. J. Microbiol.* 31, 1000–1005. doi: 10.1139/m85-189

Falciatore, A., Casotti, R., Leblanc, C., Abrescia, C., and Bowler, C. (1999). Transformation of nonselectable reporter genes in marine diatoms. *Mar. Biotechnol.* 1, 239–251. doi: 10.1007/PL00011773

Granum, E., Raven, J. A., and Leegood, R. C. (2005). How do marine diatoms fix 10 billion tonnes of anorganic carbon per year. *Can. J. Bot.* 83, 898–908. doi: 10.1139/b05-077

Griffiths, M. J., Garcin, C., VanHille, R. P., and Harrison, S. T. (2011). Interference by pigment in the estimation of microalgal biomass concentration by optical density. *J. Microbiol. Met.* 85, 119–123. doi: 10.1016/j.mimet.2011.02.005

Guillard, R. R. L. (1975). "Culture of phytoplankton for feeding marine invertebrates," in *Culture of Marine Invertebrate Animals*, eds W. L. Smith and M. H. Chanley (New York, NY: Plenum Press), 29–60.

Jiang, P., Du, W. J., Mancuso, A., Wellen, K. E., and Yang, X. L. (2013). Reciprocal regulation of p53 and malic enzymes modulates metabolism and senescence. *Nature* 493, 689–693. doi: 10.1038/nature11776

Kendrick, A., and Ratledge, C. (1992). Desaturation of polyunsaturated fatty acids in *Mucor circinelloides* and the involvement of a novel membrane-bound malic enzyme. *Eur. J. Biochem.* 209, 667–673. doi: 10.1111/j.1432-1033.1992.tb17334.x

Kim, G. H., Lee, Y. E., Lee, G. H., Cho, Y. H., Lee, Y. N., Jang, Y., et al. (2015). Overexpression of malic enzyme in the larval stage extends *Drosophila* lifespan. *Biochem. Biophys. Res. Commun.* 456, 676–682. doi: 10.1016/j.bbrc.2014.12.020

Kroth, P. G., Chiovitti, A., Gruber, A., Martin-Jezequel, V., Mock, T., Parker, M. S., et al. (2008). A model for carbohydrate metabolism in the diatom *Phaeodactylum tricornutum* deduced from comparative whole genome analysis. *PLoS One* 3:1426. doi: 10.1371/journal.pone.0001426

Lepage, G., and Roy, C. C. (1984). Improved recovery of fatty acid through direct transesterification without prior extraction or purification. *J. Lipid Res.* 25, 1391–1396.

Li, Y., Han, D., Hu, G., Dauvillee, D., Sommerfeld, M., and Ball, S. (2010). *Chlamydomonas* starchless mutant defective in ADP-glucose pyrophosphorylase hyper-accumulates triacylglycerol. *Metab. Eng.* 12, 387–391. doi: 10.1016/j.ymben.2010.02.002

Liang, M. H., and Jiang, J. G. (2013). Advancing oleaginous microorganisms to produce lipid via metabolic engineering technology. *Prog. Lipid Res.* 52, 395–408. doi: 10.1016/j.plipres.2013.05.002

Liang, Y. J., and Jiang, J. G. (2015). Characterization of malic enzyme and the regulation of its activity and metabolic engineering on lipid production. *RSC Adv.* 5, 45558–45570. doi: 10.1039/C5RA04635A

Livak, K. J., and Schmittgen, T. D. (2001). Analysis of relative gene expression data using real-time quantitative PCR and the $2^{-\Delta\Delta C_T}$ method. *Methods* 25, 402–408. doi: 10.1006/meth.2001.1262

Lv, N. N., Zhu, B. H., Lu, L., Yang, G. P., and Pan, K. H. (2016). Overexpression of malic enzyme gene from *Phaeodactylum tricornutum* promotes fatty acids production in *Escherichia coli*. *Period. Ocean Univ. China* 46, 65–69.

Meng, X., Yang, J., Cao, Y., Li, L., Jiang, X., and Xu, X. (2011). Increasing fatty acid production in *E. coli* by simulating the lipid accumulation of oleaginous microorganisms. *J. Ind. Microbiol. Biotechnol.* 38, 919–925. doi: 10.1007/s10295-010-0861-z

Moreira dos Santos, M., Raghevendran, V., Kötter, P., Olssona, L., and Nielsen, J. (2004). Manipulation of malic enzyme in Saccharomyces cerevisiae for increasing NADPH production capacity aerobically in different cellular compartments. *Metab. Eng.* 6, 352–363. doi: 10.1016/j.ymben.2004.06.002

Poulsen, N., and Kröger, N. (2005). A new molecular tool for transgenic diatoms: control of mRNA and protein biosynthesis by an inducible promoter–terminator cassette. *FEBS J.* 272, 3413–3423. doi: 10.1111/j.1742-4658.2005.04760.x

Radakovits, R., Eduafo, P. M., and Posewitz, M. C. (2011). Genetic engineering of fatty acid chain length in *Phaeodactylum tricornutum*. *Metab. Eng.* 13, 89–95. doi: 10.1016/j.ymben.2010.10.003

Ratledge, C. (2014). The role of malic enzyme as the provider of NADPH in oleaginous microorganisms: a reappraisal and unsolved problems. *Biotechnol. Lett.* 36, 1557–1568. doi: 10.1007/s10529-014-1532-3

Ren, L. J., Feng, Y., Li, J., Qu, L., and Huang, H. (2013). Impact of phosphate concentration on docosahexaenoic acid production and related enzyme activities in fermentation of *Schizochytrium* sp. *Bioprocess Biosyst. Eng.* 36, 1177–1183. doi: 10.1007/s00449-012-0844-8

Ren, L. J., Huang, H., Xiao, A. H., Lian, M., Jin, L. J., and Ji, X. J. (2009). Enhanced docosahexaenoic acid production by reinforcing acetyl-CoA and NADPH supply in *Schizochytrium* sp. HX-308. *Bioprocess Biosyst. Eng.* 32, 837–843. doi: 10.1007/s00449-009-0310-4

Rodriguez, E., Navone, L., Casati, P., and Gramajo, H. (2012). Impact of malic enzymes on antibiotic and triacylglycerol production in *Streptomyces coelicolor*. *Appl. Environ. Microbiol.* 78, 4571–4579. doi: 10.1128/AEM.00838-12

Shang, C. H., Zhu, S. N., Yuan, Z. H., and Wang, Z. M. (2012). Molecular cloning and characterization analysis of malic enzyme gene from *Dunaliella parva*. *Adv. Mater. Res.* 347, 2536–2540.

Shimomura, I., Shimano, H., Korn, B. S., Bashmakov, Y., and Horton, J. D. (1998). Nuclear sterol regulatory element-binding proteins activate genes responsible for the entire program of unsaturated fatty acid biosynthesis in transgenic mouse liver. *J. Biol. Chem.* 273, 35299–35306. doi: 10.1074/jbc.273.52.35299

Siaut, M., Heijde, M., Mangogna, M., Montsant, A., Coesel, S., and Allen, A. (2007). Molecular toolbox for studying diatom biology in *Phaeodactylum tricornutum*. *Gene* 406, 23–35. doi: 10.1016/j.gene.2007.05.022

Takeuchi, Y., Akagi, H., Kamasawa, N., Osumi, M., and Honda, H. (2000). Aberrant chloroplasts in transgenic rice plants expressing a high level of maize NADP-dependent malic enzyme. *Planta* 211, 265–274. doi: 10.1007/s004250000282

Tang, W., Zhang, S. F., Tan, H. D., and Zhao, Z. K. (2010). Molecular cloning and characterization of a malic enzyme genefrom the oleaginous yeast *Lipomyces starkeyi*. *Mol. Biotechnol.* 45, 121–128. doi: 10.1007/s12033-010-9255-8

Valenzuela, J., Mazurie, A., Carlson, R. P., Gerlach, R., Cooksey, K. E., Peyton, B. M., et al. (2012). Potential role of multiple carbon fixation pathways during lipid accumulation in *Phaeodactylum tricornutum*. *Biotechnol. Biofuels* 5:40. doi: 10.1186/1754-6834-5-40

Watanabe, K. I., Ehara, M., Inagaki, Y., and Ohama, T. (1998). Distinctive origins of group I introns found in the COXI genes of three green algae. *Gene* 213, 1–7. doi: 10.1016/S0378-1119(98)00235-2

Wynn, J. P., Bin Abdul Hamid, A., and Ratledge, C. (1999). The role of malic enzyme in the regulation of lipid accumulation infilamentous fungi. *Microbiology* 145, 1911–1917. doi: 10.1099/13500872-145-8-1911

Wynn, J. P., and Ratledge, C. (1997). Malic enzyme is a major source of NADPH for lipid accumulation by *Aspergillus nidulans*. *Microbiology* 143, 253–257. doi: 10.1099/00221287-143-1-253

Xue, J., Niu, Y. F., Huang, T., Yang, W. D., Liu, J. S., and Li, H. Y. (2015). Genetic improvement of the microalga *Phaeodactylum tricornutum* for boosting neutral lipid accumulation. *Metab. Eng.* 27, 1–9. doi: 10.1016/j.ymben.2014.10.002

Xue, J., Wang, L., Zhang, L., Balamurugan, S., Li, D. W., Zeng, H., et al. (2016). The pivotal role of malicenzyme in enhancing oil accumulation in green microalga *Chlorella pyrenoidosa*. *Microb. Cell Fact* 15, 120–129. doi: 10.1186/s12934-016-0519-2

Zaslavskaia, L. A., Lippmeier, J. C., Kroth, P. G., Grossman, A. R., and Apt, K. E. (2000). Transformation of the diatom *Phaeodactylum tricornutum* (Bacillariophyceae) with a variety of selectable marker and reporter genes. *J. Phycol.* 36, 379–386. doi: 10.1046/j.1529-8817.2000.99164.x

Zelle, R. M., Harrison, J. C., Pronk, J. T., and van Maris, A. J. (2011). Anaplerotic role for cytosolic malic enzyme in engineered *Saccharomyces cerevisiae* strains. *Appl. Environ. Microbiol.* 7, 732–738. doi: 10.1128/AEM.02132-10

Zhang, Y., Adams, I. P., and Ratledge, C. (2007). Malic enzyme: the controlling activity for lipid production? Overexpression of malic enzyme in *Mucor circinelloides* leads to a 2.5-fold increase in lipid accumulation. *Microbiology* 153, 2013–2025. doi: 10.1099/mic.0.2006/002683-0

Zhang, Y., Smallbone, L. A., diCenzo, G. C., Morton, R., and Finan, T. M. (2016). Loss of malic enzymes leads to metabolic imbalance and altered levels of trehalose and putrescine in the bacterium *Sinorhizobium meliloti*. *BMC Microbiol.* 16:163. doi: 10.1186/s12866-016-0780-x

Zhu, B. H., Shi, H. P., Yang, G. P., Lv, N. N., Yang, M., and Pan, K. H. (2016). Silencing UDP-glucose pyrophosphorylase gene in *Phaeodactylum tricornutum* affects carbon allocation. *New Biotechnol.* 33, 237–244. doi: 10.1016/j.nbt.2015.06.003

Zhu, B. H., Sun, F. Q., Yang, M., Lu, L., Yang, G. P., and Pan, K. H. (2014). Large-scale biodiesel production using flue gas from coal-fired powerplants with *Nannochloropsis* microalgal biomass in open raceway ponds. *Bioresour. Technol.* 174, 53–59. doi: 10.1016/j.biortech.2014.09.116

Conflict of Interest Statement: The authors declare that the research was conducted in the absence of any commercial or financial relationships that could be construed as a potential conflict of interest.

frontiers in Plant Science

ORIGINAL RESEARCH
published: 17 April 2018
doi: 10.3389/fpls.2018.00491

Enhancing EPA Content in an Arctic Diatom: A Factorial Design Study to Evaluate Interactive Effects of Growth Factors

Pia Steinrücken[1]*, *Svein A. Mjøs*[2], *Siv K. Prestegard*[3] and *Svein R. Erga*[1]

[1] Department of Biological Sciences, University of Bergen, Bergen, Norway, [2] Department of Chemistry, University of Bergen, Bergen, Norway, [3] Applied Biotechnology, Uni Research Environment, Bergen, Norway

Microalgae with a high content of the omega-3 polyunsaturated fatty acids (PUFAs), eicosapentaenoic acid (EPA), and docosahexaenoic acid (DHA) are of great demand for microalgae-based technologies. An Arctic strain of the diatom *Attheya septentrionalis* was shown in previous experiments to increase its EPA content from 3.0 to 4.6% of dry weight (DW) in the nutrient-replete exponential phase and nutrient-depleted stationary phase, respectively. In the present study, a factorial-design experiment was used, to investigate this effect in more detail and in combination with varying salinities and irradiances. A mathematical model revealed that both growth phase and salinity, alone and in combination, influenced the EPA content significantly. Maximum EPA values of 7.1% DW were obtained at a salinity of 22 and after 5 days in stationary phase, and might be related to a decreased silica content, an accumulation of storage lipids containing EPA, or both. However, growth rates were lower for low salinity (0.54 and 0.57 d^{-1}) than high salinity (0.77 and 0.98 d^{-1}) cultures.

Keywords: eicosapentaenoic acid (EPA), arctic diatom, factorial design, salinity, growth phase, interactive effects, microalgal biotechnology

OPEN ACCESS

Edited by:
Jianhua Fan,
East China University of Science and Technology, China

Reviewed by:
Adolfo Rivero-Muller,
Turku Centre for Biotechnology, Finland
Zhi-Gang Zhou,
Shanghai Ocean University, China

***Correspondence:**
Pia Steinrücken
pia.steinrucken@uib.no

Specialty section:
This article was submitted to Plant Biotechnology, a section of the journal Frontiers in Plant Science

Received: *24 January 2018*
Accepted: *03 April 2018*
Published: *17 April 2018*

Citation:
Steinrücken P, Mjøs SA, Prestegard SK and Erga SR (2018) Enhancing EPA Content in an Arctic Diatom: A Factorial Design Study to Evaluate Interactive Effects of Growth Factors. Front. Plant Sci. 9:491. doi: 10.3389/fpls.2018.00491

INTRODUCTION

The omega-3 polyunsaturated fatty acids (PUFAs), eicosapentaenoic acid (EPA), and docosahexaenoic acid (DHA) are known to contribute significantly to human health (Martins et al., 2013). The current major source for the two fatty acids (FA) is fish oil from marine wild fish. The fish obtain and accumulate these PUFAs themselves predominantly via the marine food chain from EPA- and DHA-synthesizing microalgae (Spolaore et al., 2006). As EPA and DHA are also essential for farmed fish (Khozin-Goldberg et al., 2016), fish oil is an important additive in aquaculture feed. The increasing demand for EPA and DHA, particularly from the growing aquaculture industries, but also increasingly from the health and food sectors, necessitates other sustainable production sources. Many marine microalgae naturally produce EPA and DHA, and are therefore considered a promising alternative (Patil et al., 2005; Chauton et al., 2015). Although there has been intensive research in this field, the costs associated with microalgae large-scale cultivation and processing for FAs are still greater than in fish oil production. Improvements at the different parts of the production chain are therefore essential in order to reduce production costs. The selection of suitable species that are superior to existing cultures in terms of growth and EPA and DHA content, and the optimization of cultivation conditions are important contributions to the ongoing improvement of microalgae-based technologies (Adarme-Vega et al., 2012).

In previous research, we searched for new and fast growing microalgal strains from North Atlantic habitats with high growth rates and high EPA and DHA contents (Steinrücken et al., 2017). A strain of the diatom *Attheya septentrionalis*, isolated from Arctic Waters, demonstrated rapid growth at temperatures of 10°C (0.7 d^{-1}) and a high EPA content, which increased from 3.0 to 4.6% of the dry weight (DW) from exponential phase to Day 3 of the stationary phase. This EPA content under nutrient-depleted conditions was higher than typically found in industrially applied microalgae and this strain was therefore suggested to be a potential candidate for future large-scale cultivation and EPA production. A high growth rate and EPA content in stationary phase in *A. septentrionalis* were also found by Knuckey et al. (2002) who suggested this diatom to be a promising feed source for oyster hatcheries. However, only few studies on *Attheya* species exist (Aizdaicher and Markina, 2011; Stonik et al., 2017), and more explicit investigations are needed in order to assess the potential of this diatom for microalgae-based technologies.

It is well-known that microalgae modify their biochemical composition and FA content in response to environmental factors, including nutrient availability, irradiance, temperature, and salinity (Dunstan et al., 1993; Renaud and Parry, 1994; Tatsuzawa and Takizawa, 1995; Xu and Beardall, 1997; Van Wagenen et al., 2012; Boelen et al., 2013; Cepák et al., 2013). To investigate the impact of the different factors, traditional methods vary one condition at a time, while keeping all other factors constant. However, FA composition and content in microalgae are dependent on synergistic and antagonistic interactions of cultivation conditions. Factorial designs are based on a multivariate approach, in which the variation in different factors are tested simultaneously (Duarte et al., 2001). These yield a predictive model which provides information on the magnitude of the effects of both individual factors and combinations of factors, and on their statistical significance (Chen et al., 2012).

In this study, we aimed to elucidate additional information on the dynamics of the EPA content and relative FA composition in *A. septentrionalis*, and to determine the experimental conditions that might lead to a further increase in the EPA content. A factorial-design experiment was used to investigate the impact of nutrient starvation in greater detail, together with the effects of salinity and irradiance, and their respective interactions. Both salinity and irradiance are known to affect the FA composition in microalgae (Xu and Beardall, 1997; Lu et al., 2001; Chen et al., 2008), and are highly variable in Arctic environments due to melting and freezing sea ice, and strong variations in photoperiod. Hence, microalgae from these environments are expected to be promising in this context, and possess the necessary adaptations to cope with these changing conditions.

METHODS

Stock Cultures and Inoculum

Attheya septentrionalis is a single celled diatom with four long setae, and is broadly distributed in Arctic and Temperate Waters (Rampen et al., 2009; Stonik et al., 2017). The strain used in this experiment was isolated from Arctic Waters north-west of Spitzbergen (N 79° 25.14′ E 08° 18.84′) in May 2014 (3.5°C water temperature, salinity of 35, and 24 h daylight). For strain characterization, a region of the 28S ribosomal RNA (rRNA) gene was sequenced and compared with previously published sequences from diatoms at GenBank (Steinrücken et al., 2017). Partial sequence of the 28S rRNA gene have been deposited in GenBank (http://www.ncbi.nlm.nih.gov/) with accession number MH020639. Stock cultures were maintained in 50 mL Erlenmeyer flasks at 10°C and 50 μmol photons m^{-2} s^{-1}, in nutrient-enriched (Walne, 1970) 80% seawater (SW) by monthly dilution. Eighty percent SW was obtained by dilution of filtered and autoclaved fjord-SW (from 90 m depth, salinity of 35) with distilled water (80:20, v:v), giving a salinity of 29. For the inoculum, biomass was harvested from exponential phase stock cultures by centrifugation (2,264 × g, 5 min), washed twice with fresh medium and re-inoculated into 10 mL fresh medium.

Experimental Design

Factorial design was used to investigate the effects of salinity, irradiance, and growth phase and their interactions on the EPA and total fatty acid (TFA) content, and the FA composition in the diatom *A. septentrionalis,* by growth of batch cultures at different conditions. The effects of salinity and irradiance were assessed at two levels (22 and 35, and 50 and 200 μmol photons m^{-2} s^{-1}, respectively), and the growth phase at three levels; exponential phase (e), Day 3 of stationary phase (first stationary phase, s1), and Day 5 of stationary phase (second stationary phase, s2), resulting in 12 treatment groups. Salinity and irradiance levels were selected as being representative of those occurring under natural conditions in the Arctic and additionally, so as to induce different responses but not to impair the cultures. Before the start of the batch experiment, pre-cultures (one biological replicate for each condition) were grown semi-continuously for 14 d at either low or high salinity and low or high irradiance (LSLI, HSLI, LSHI, and HSHI), to acclimate the cultures to their respective conditions. Two sterile and nutrient enriched media (Walne, 1970) were prepared with aged SW (salinity of 35) and respective dilutions with distilled water (salinity of 22). Pre-cultures were prepared in glass tubes (300 mL, 3.5 cm inner diameter), by adding 1 mL inoculum to 60 mL fresh medium of the respective salinity, and placed into temperature-controlled water tanks (10°C). Continuous illumination with 50 or 200 μmol photons m^{-2} s^{-1} (measured with 4π quantum scalar irradiance sensor [QSL-100, Biospherical Instruments, San Diego, CA, USA], inside the empty glass cylinder) was provided by banks of six white fluorescent tubes (Philips MASTER, TL-D 90 Graphica, 58W/95) in the back of the water tanks, running perpendicular to the glass tubes. To ensure adequate mixing and carbon supply, 0.2 μm-filtered and 1% CO_2-enriched air was bubbled through glass capillaries into the bottom of each glass tube. Pre-cultures were kept in exponential phase by maintaining an optical density (OD_{750}) between 0.15 and 0.50, by the addition of fresh medium, successively added until volumes reached 260 mL. Thereafter, half of the culture volume was replaced with fresh medium daily or every other day. After the 2-week acclimation period, the batch experiment was started. Biomass from each pre-culture was distributed into two sterile glass tubes to obtain two biological

replicates, and each diluted with fresh medium to yield a starting OD and volume of ∼0.15 and 260 mL, respectively. Cultures were then grown until Day 5 of the stationary phase, and all cultures were sampled daily for OD and maximum quantum yield (QY), and on Day 1 in exponential phase (e) and Days 3 and 5 in stationary phase (s1 and s2, respectively) for DW and FA analysis. Additionally, cultures were sampled for nutrient analysis of the media at the start of the experiment, and on the DW and FA sampling days.

Analytical Procedures

Relative growth rates between repeated dilutions during pre-cultivation were calculated according to the changes in attenuation with Equation (1). N_{x0} and N_x are OD_{750} after dilution (t_{x0}) and before the subsequent dilution (t_x), respectively.

$$\mu\ \left(d^{-1}\right) = \frac{\ln\left(N_x\right) - \ln(N_{x0})}{\left(t_x - t_{x0}\right)} \quad (1)$$

Optical density measurements were performed using a spectrophotometer (UV1800, Shimadzu Corporation, Kyoto, Japan) at 750 nm and if required, samples were diluted to give an attenuation between 0.2 and 0.8. The QY was measured with AquaPen (AquaPen-C, AP-C 100, Photon System Instruments, Brno, Czech Republic) after initial dark incubation between 10 and 60 min. DWs (expressed as weight of the dried biomass [g] per volume [L]) were determined in triplicates as described by Zhu and Lee (1997), with 0.5 M ammonium formate as a washing buffer.

For FA analysis, triplicate 10 mL microalgal cultures were harvested by centrifugation (6 min at 2,264 × g) into glass tubes (PYREX), the supernatant discarded, and the pellet covered in nitrogen atmosphere and stored at −20°C until analysis. FAs were extracted and derivatized to fatty acid methyl esters (FAME) by direct esterification (Meier et al., 2006). The pellet was dried in the 10 mL tube by evaporating the remaining water under a nitrogen stream, and 18 or 34 μg internal standard (23:0 FAME dissolved in isooctane) was added to exponential or stationary phase samples, respectively. The solvent was evaporated under nitrogen stream and 0.5 mL methylation reagent (2M HCl in methanol) was added. Samples were covered with nitrogen gas, sealed and incubated at 90°C for 2 h. After cooling to room temperature, half of the methylation reagent was evaporated, 0.5 mL water was added, and the samples were extracted twice with 1 mL isooctane. The combined extracts of stationary phase samples were diluted with isooctane (1:1, v:v) to yield a final internal standard concentration of approximately 18 μg mL^{-1} (Steinrücken et al., 2017). FAMEs were analyzed by GC (7890 gas chromatograph, Agilent, Santa Clara, CA, USA) equipped with an autosampler, split-splitless injector, flame ionization detector (FID), and a 60 m BPX70 capillary column (SGE, Ringwood, Australia) with internal diameter of 0.25 mm and film thickness of 0.25 μm. One microliters of sample volumes were injected splitless at 60°C. This temperature was maintained for 3 min before raised by 40°C min^{-1} to 150°C and by 1.5°C min^{-1} to 230°C. Helium, with an estimated average velocity of 30 cm s^{-1} was used as carrier gas in constant flow mode. Injector and detector temperatures were 250 and 300°C, respectively (Prestegard et al., 2015). The FAMEs were identified by analysis on gas chromatography coupled to mass spectrometry (GC-MS) as described in Wasta and Mjøs (2013), and by using libraries of mass spectra and retention indices available at www.chrombox.org/data.

For nutrient measurements of the media, 20 mL GF/F filtrates were collected in white plastic vials, 100 μl chloroform added and stored at 4°C before analysis. Dissolved inorganic nitrate, nitrite, orthophosphate, and silicate were analyzed at the Institute of Marine Research, Bergen, which offers accredited and standardized service for nutrient analyses, using colorimetric absorption measurements on an Alpkem-Lab analyzer (Alpkem Corporation, Oregon USA) according to Parsons et al. (1992).

Regression Models

The model for growth rate as a function of salinity, irradiance and their interactions, and models for TFA and EPA content as functions of salinity, irradiance, growth phase, and their interactions were calculated by multiple least squares regression. The models reported in the paper are based on the coded factor levels, where the low values are assigned −1 and the high values are assigned +1. For the growth phase, there are three levels; exponential phase, and first and second stationary phase. Exponential and second stationary phase were assigned the levels −1 and +1, respectively. The level for first stationary phase was set to 0.74. This level was found by iteratively testing values from −1 to 1 with increments of 0.01, and selecting the value that minimized the sum of squared residuals of the model. Models and model statistics were calculated by the fitlm function in the Statistics and Machine Learning Toolbox running under Matlab R2017a (Mathworks, Natick, MA, USA).

Statistics

The batch experiment was performed with two individual cultures (biological replicates) for each treatment, which is sufficient for solid statistics when using regression analysis and factorial design. One measurement replicate was taken for OD and QY measurements, whereas *FA* and *DW* were analyzed in triplicates for each biological replicate. The *FA* content and the *DW* were analyzed from individual subsamples, and the standard deviation (*SD*) for FA content relative to the *DW* was calculated using Equation (2).

$$SD_{FA/DW} = \frac{\sqrt{\%SD_{FA}{}^2 + \%SD_{DW}{}^2}}{100} \times \frac{FA}{DW} \quad (2)$$

Euclidean dendrograms and Principal Component Analysis (PCA) of treatment groups and their FA composition were calculated using Sirius 10.0 (Pattern Recognition Systems AS, Bergen, Norway) and edited in GraphPad Prism 6.

RESULTS

Pre-cultivation—Growth Rates

Pre-cultures were grown for 2 weeks to allow for cells to acclimate to the respective salinities and irradiances. After three dilutions, growth rates for each condition became more constant although they still varied slightly between the repeated dilutions. Only growth rates from the final seven dilutions prior to the batch experiment were used for analyses (Table S1). Average values, together with the estimates provided by the mathematical model, are shown in **Figure 1A**. Lower growth rates (0.54 d^{-1} for low irradiance [LI] and 0.57 d^{-1} for high irradiance [HI]) were observed for low salinity (LS) cultures, compared to high salinity (HS) cultures (0.77 d^{-1} for LI and 0.98 d^{-1} for HI), together with increased values for HI cultures. High irradiance had a stronger positive effect on the growth rate at HS. The mathematical model representing the growth rate as a function of salinity (*X1*), irradiance (*X2*), and their combination (*X1X2*) in the experimental setup is expressed by Equation (3). Positive coefficients in the equations indicate that increasing values increase the growth rate and bold numbers indicate a high statistical significance (black: $p < 0.05$ and red: $p < 0.01$). According to the model, salinity had the strongest positive influence on the growth rate, with high significance (0.163, *p*-value $1.4{*}10^{-09}$), while irradiance (0.062, $p = 0.001$) and the combination of salinity and irradiance (0.043, $p = 0.016$) had lower, but still significant, impacts. A strong and significant correlation ($R^2 = 0.8484$) between the estimated values of the model and the measured values indicates a good fit between the model and the experimental data (**Figure 1B**). Details on the measured and estimated growth rates can be found in the Supplementary Material (Table S1).

$$\mu\ (d^{-1})_{est} = 0.715 + \mathbf{0.163}{*}X1 + \mathbf{0.062}{*}X2 + \mathbf{0.043}{*}X1X2 \quad (3)$$

Batch Experiment—Growth and Maximum Quantum Yield (QY)

Growth curves and QY during the batch experiment were very similar for the biological replicates, but there were differences between the cultivation conditions, especially between low and high salinities (**Figures 2A,B**). Cultures grown at LS, revealed a declined slope of the growth curves and reached stationary phase 1 day later (Day 4) than cultures grown at HS (Day 3). During exponential growth, the QY was slightly lower for the LS cultures (replicate averages of 0.64 at Day 1, both for low and high irradiances) than for the HS cultures (replicate averages of 0.69 and 0.68 at Day 1, for low and high irradiance, respectively). During stationary phase, the QY decreased in all cultures. In HS cultures, QY dropped by 10% (LI) and 30% (HI) after entering stationary phase, and by 23 and 32%, respectively, at the end of cultivation period. A lower reduction was observed for the LS cultures, where QY was reduced by 6 and 8% (low and high irradiance, respectively) after entering stationary phase, and by 14 and 17% at the end of cultivation.

The nitrate, silicate, and phosphate concentrations of the media decreased from the start of the experiment to the first day of exponential phase by 14, 39, and 27% for low salinity cultures and by 23, 45, and 38% for high salinity cultures, respectively (**Figures 2C,D**). At the first stationary phase (Day 3), all nutrients had been consumed in all cultures (nitrate 99%, silicate 99%, and phosphate 97%).

Batch Experiment—Dry Weights (DW), Total Fatty Acids (TFA), and EPA

DW together with TFA and EPA contents (% DW) for the 12 different treatment groups, each with two biological replicates are shown in **Figure 3**. The DW (average of the biological replicates) increased from the exponential phase to the first stationary phase by 0.13, 0.12, 0.13, and 0.11 g L^{-1} and further by 0.04, 0.03, 0.01, 0.02 g L^{-1} to the second stationary phase, giving a total increase of 0.17, 0.15, 0.14, and 0.13, g L^{-1} for low salinity-low irradiance (LSLI), high salinity-low irradiance (HSLI), low salinity-high irradiance (LSHI), and high salinity-high irradiance (HSHI) conditions, respectively (**Figure 3A**).

The TFA and EPA contents (**Figures 3B,C** respectively) increased from the exponential to the stationary phase at all growth conditions, but to different extents. In exponential phase, EPA contents (average of replicates) were 2.8, 3.2, 2.4, and 3.1% DW for LSLI, HSLI, LSHI, and HSHI conditions, respectively, and increased to 6.8, 5.7, 5.8, and 5.5% DW, respectively, in the first stationary phase. For LSLI, LSHI, and HSHI cultures, EPA content increased further to 7.2, 7.1, and 5.8% DW, respectively, in the second stationary phase, while it decreased in the HSLI conditions to 5.2% DW. A similar pattern with increase from the exponential phase to the first stationary phase in all cultures and further increase to the second stationary phase in LSLI, LSHI and HSHI cultures, and decrease from the first to the second stationary phase in HSLI cultures was found for the TFA content. Corresponding values with standard deviation can be found in the Supplementary Material (Table S2). In exponential phase, TFA and EPA contents were higher in HS cultures, while after 5 days of stationary phase, levels were higher for LS cultures. EPA and TFA contents (% DW), estimated by the model, are shown in Figure S1 in the Supplementary Material.

The mathematical models, representing the EPA and the TFA content as a function of salinity (X1), irradiance (X2), growth phase (X3), and their combinations (X1X2, X1X3, X2X3) are expressed by Equations (4, 5), respectively. A positive term for the combinations in the equations indicates a synergistic effect (increasing values increase the content), whereas negative terms indicate an antagonistic effect (increasing values decrease the content; Chen et al., 2012). Coefficients in bold indicate statistical significance for the corresponding coefficients (black: $p < 0.05$ and red $p < 0.01$). For the EPA content, coefficients for growth phase, salinity, and the combination of salinity and growth phase were statistically significant whilst the other factors were not. The most significant variable with highest impact on EPA content was the growth phase with a positive estimated effect of 1.74 ($p = 2.0{*}10^{-13}$). The combined effect of salinity and growth phase was lower (−0.48, $p = 0.00003$) and negative, while salinity had a less negative effect on EPA content (−0.19, $p = 0.0241$). The TFA content was also significantly influenced by growth phase (8.34, $p = 1.1{*}10^{-15}$), salinity (−0.77, $p = 0.0116$),

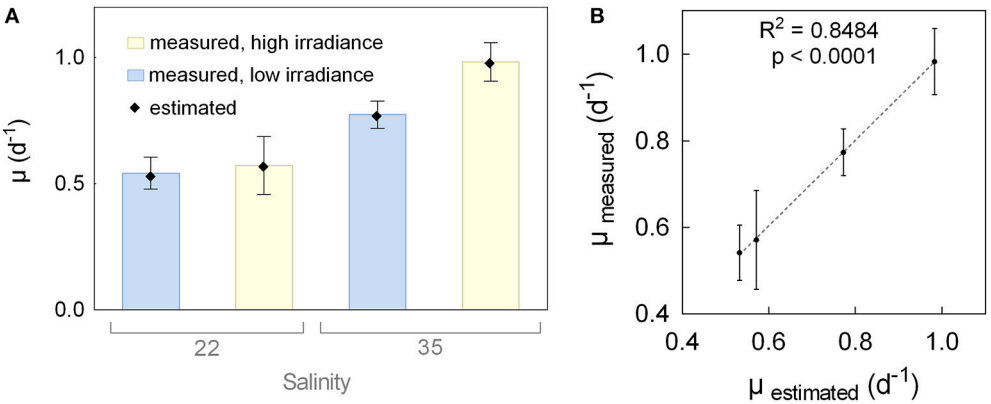

FIGURE 1 | Growth rates (μ) during pre-cultivation. **(A)** Average growth rates of repeated dilutions (bars, $n = 7$) and estimated growth rates by the model (dots) of the diatom *Attheya septentrionalis* grown at four different cultivation conditions (combinations of low or high salinity [22 and 35] and irradiance [50 and 200 μmol photons m^{-2} s^{-1}]. **(B)** Average and standard deviation ($n = 7$) of measured growth rates, plotted against the estimated growth rates by the model, with linear regression.

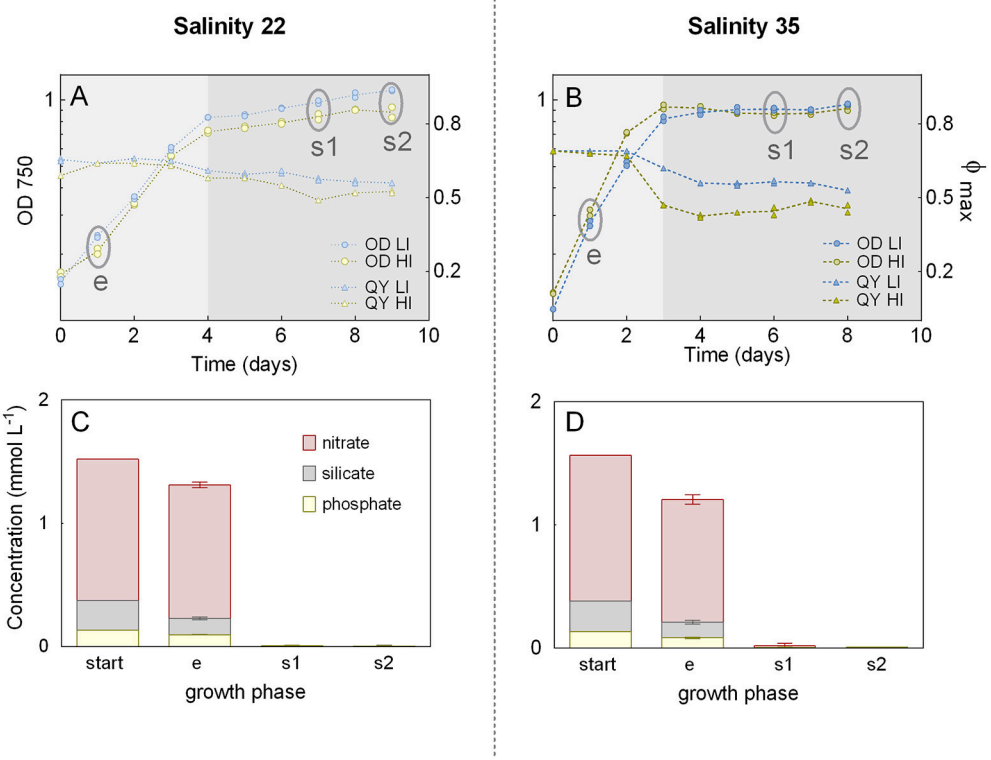

FIGURE 2 | Growth during batch experiment. Batch cultures of the diatom *Attheya septentrionalis* grown at four conditions (combinations of low and high salinity [22 and 35] and irradiance [50 and 200 μmol photons m^{-2} s^{-1}] with two biological replicates for each condition). **(A,B)** Optical density (OD_{750}) based growth curves and maximum quantum yields (QY, Φmax) for low and high salinities, respectively. Circles indicate sampling time points (e, exponential phase; s1, first stationary phase; s2, second stationary phase). LI, low irradiance; HI, high irradiance. **(C,D)** Superimposed nutrient concentration in the media at the start of the experiment and during exponential (e) and stationary (s1 and s2) sampling time points for low and high salinities, respectively. Values are the averages and standard deviations from samples of the respective salinity.

and the combination of salinity and growth phase (−1.43, $p = 0.0002$), and additionally, by the combination of salinity and irradiance (0.73, $p = 0.0126$). A high correlation ($R^2 = 0.9651$ and 0.9802 for EPA and TFA content, respectively) of estimated values by the model and measured values indicates a good fit between the model and the experimental data (Figure S2). More

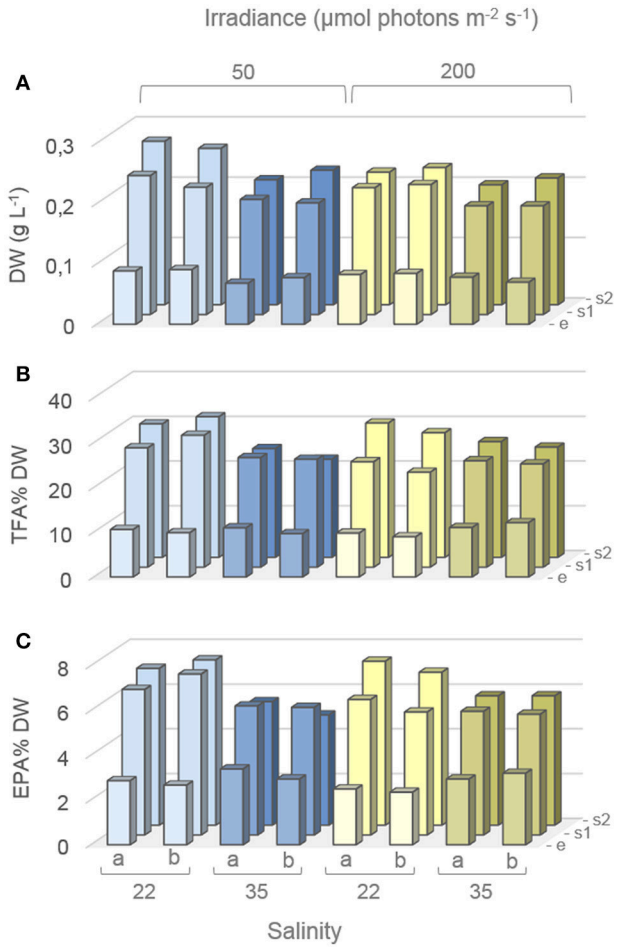

FIGURE 3 | Dry weights (DW) and fatty acid content during factorial-design batch experiment. Average DW **(A)**, and total fatty acid (TFA) and EPA contents (**B,C** respectively) of *Attheya septentrionalis* cultures at 12 different treatments (two biological replicates per treatment, a and b). Values are average of three measurement replicates. Detailed values with standard deviations can be found in Table S2. e, exponential phase; s1, first stationary phase (Day3); s2, second stationary phase (Day 5).

details on measured and estimated values can be found in the Supplementary Material (Table S2).

$$\text{EPA\% DW}_{\text{est}} = 4.61 - \mathbf{0.19{*}X1} - 0.12{*}\text{X2} + \mathbf{1.74{*}X3} + 0.14{*}\text{X1X2} - \mathbf{0.48{*}X1X3} + 0.02{*}\text{X2X3} \quad (4)$$

$$\text{TFA\% DW}_{\text{est}} = 18.74 - \mathbf{0.77{*}X1} - 0.25{*}\text{X2} + \mathbf{8.34{*}X3} + \mathbf{0.73{*}X1X2} - \mathbf{1.43{*}X1X3} - 0.26{*}\text{X2X3} \quad (5)$$

Batch Experiment—Relative Fatty Acid (FA) Composition

In total 36 FAs were detected in the GC for *A. septentrionalis*, from which 11 (14:0, 16:0, 16:1 n−7, 16:2 n−4, 16:3 n−4, 16:4 n−1, 18:1 n−7, 18:4 n−3, 20:4 n−3, 20:5 n−3, and 22:6 n−3) constituted more than 1% TFA (**Figure 4**). C16-FA were the most abundant, whereas C18-FA were present in only low amounts. In all treatments, palmitoleic acid (16:1 n−7), and EPA (20:5 n−3) were the two major FA, together accounting for between 45 and 52% TFA, followed by myristic acid (14:0) with 10–18% TFA, palmitic acid (16:0) with 6–16% TFA, and DHA (22:6 n−3) with 3–6% TFA. However, small variations in the relative FA content between the different treatment groups were apparent. These differences became more distinct by means of a principal component analysis (PCA, **Figure 5A**). The distribution of the 12 different treatment groups (objects) represents their similarities and differences in the relative FA composition (% TFA), and the distribution of the FAs (vectors) indicate their contribution to the grouping of the objects.

Objects were arranged along component 1 and component 2 according to the growth phases and salinities, respectively. The exponential phase objects, grouping on the left side of component 1, were clearly separated from the stationary phase objects, which clustered on the right side, and objects were shifted further to the right along component 1 with increasing nutrient starvation (stationary phases). Palmitic and palmitoleic acids were correlated positively with stationary phase samples while the PUFAs were correlated with exponential phase samples. Except for the treatment HSLI_e (high-salinity, low-irradiance, and exponential phase), treatments of the same salinity were grouped together, with LS samples on the upper region along component 2, and HS samples arranged on the lower part of component 2. Myristic acid, and to a lesser extent hexadecatetraenoic acid (16:4 n-1) were correlated positively with HS treatments, while hexadecadienoic acid (16:2 n-4) was correlated positively with LS samples. Irradiance had only small effect on the FA composition.

The Euclidean Dendrogram illustrates the distinct grouping of the treatments (**Figure 5B**). Exponential phase samples were separated from stationary phase samples and both groups were then further divided according to the salinity treatment. For stationary phase samples, all LS samples grouped separately from the HS samples, followed by grouping according to their growth phase (s1 and s2) and finally by irradiance. Within exponential phase samples, HSHI samples grouped between HSLI and the LS samples, and separation was followed by irradiance, where replicates of LI were separated from the HI replicates. The two biological replicates of each treatment group were very similar.

DISCUSSION

Impact of Culture Conditions on Growth

Growth rates during the pre-cultivation were strongly dependent on the salinity, followed by irradiance and the interaction of both factors. Growth rates were 43% (LI) and 72% higher (HI) at HS compared to LS, and 5% (LS) and 27% (HS) higher when grown at HI compared to LI. The negligible effect of HI on the growth rate at LS, and the much stronger effect it caused at HS conditions, reveals the combined effect of salinity and irradiance and emphasizes the importance of investigating combinatory effects of different growth factors.

These growth characteristics during the pre-cultivation also became evident when considering the growth curves during the batch experiment. The transition from exponential to stationary

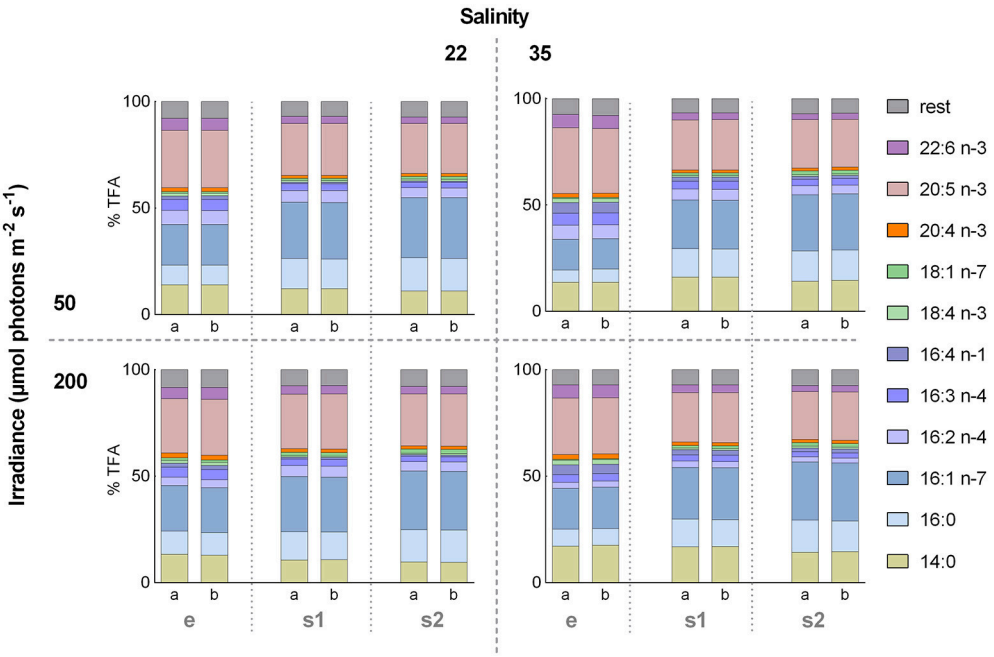

FIGURE 4 | Relative fatty acid (FA) composition during factorial-design batch experiment**.** Effect of the 12 different treatments on the relative FA composition (% of total fatty acids [TFA]) of the diatom *Attheya septentrionalis* (each with two biological replicates, a and b). Treatments were altering combinations of the three factors salinity (22 and 35), irradiance (50 and 200 µmol photons m^{-2} s^{-1}) and growth phase (exponential [e], 3 days stationary phase [s1], and 5 days stationary phase [s2]). Values are average of three measurement replicates.

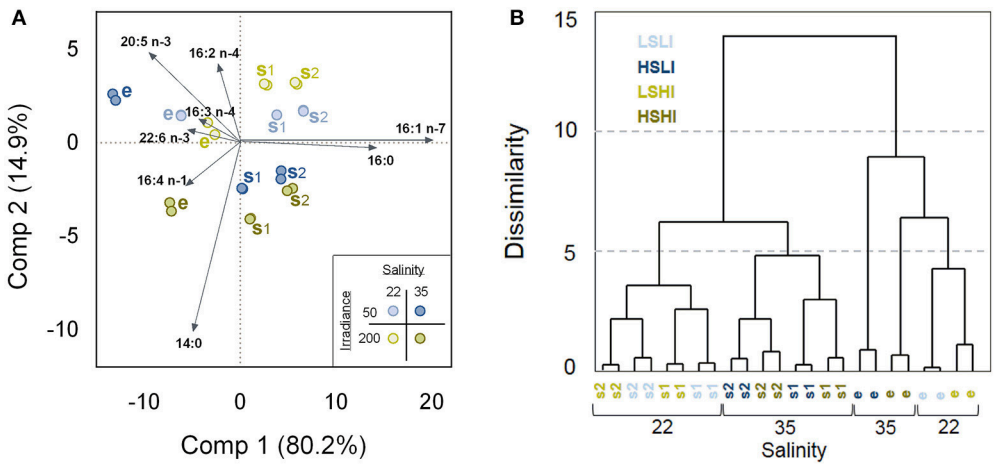

FIGURE 5 | Similarities and differences in relative fatty acids (FA) composition (% of total fatty acids [TFA]) of *Attheya septentrionalis* cultures at 12 treatments during the factorial-design batch experiment (each with two biological replicates). Treatments were altering combinations of the three factors salinity (22 and 35), irradiance (50 and 200 µmol photons m^{-2} s^{-1}) and growth phase (e, s1, s2). **(A)** Principal component analysis (PCA). Twenty-four objects representing the 12 treatment groups, and eight variables, representing the FAs with highest impact on the distributions. Values are average of three measurement replicates. e, exponential phase; s1, first stationary phase (Day 3); s2, second stationary phase (Day 5). **(B)** Euclidean Dendrogram showing dissimilarities between the treatment groups. LSLI, low salinity and low irradiance; HSLI, high salinity and low irradiance; LSHI, low salinity and high irradiance; HSHI, high salinity and high irradiance.

phase was defined by the decline of the growth curve with a concomitant decrease in the QY and was one day earlier for HS than for LS cultures. The QY reflects the photosynthetic performance of photosystem II and is used as a vitality indicator for cultures, as decreasing values are associated with stressful growth conditions (Maxwell and Johnson, 2000; Kräbs and Büchel, 2011). During exponential growth, QYs were slightly lower for LS cultures, but decreased to a lesser extent in stationary phase than they did for HS cultures. The strongest decrease in QY was observed for cultures grown at HS and HI. Hence, while

the combination HSHI appeared most advantageous during nutrient replete conditions as it caused the highest growth rates in exponential phase, it was also most stressful for the cultures during nutrient starvation.

After the transition from exponential to stationary phase, cell division was assumed to have stopped due to nutrient depletion. Although all nutrients had been consumed on Day 3 in stationary phase, silicate most likely became the major limiting nutrient, as almost half of the silicate was consumed after one day in exponential phase, whereas nitrate and phosphate were both consumed to a lesser extent. When one element becomes limiting, other elements, that are more abundant, may be accumulated in the cell (Reynolds, 2006). Therefore, nitrate and phosphate, whilst not necessarily limiting, might have been taken up by the microalgae cells after silicate was depleted. In contrast to other elements that are essential for survival, diatoms rarely take up more silicon than is required for cell division (Reynolds, 2006). When silicon becomes scarce, its uptake depends on special silicic transport proteins (SITs); however, when silicon is abundant, its uptake is by diffusion (Shrestha and Hildebrand, 2015).

EPA Content During Batch Experiment

Within the range of experimental variables considered, three factors were identified by the model as having affected the EPA content in the present *A. septentrionalis* strain significantly; the growth phase, salinity, and the interaction of both. Growth phase had the greatest impact, with increasing nutrient starvation leading to a higher EPA content relative to DW. The effect of salinity and the combined effects of both salinity and growth phase were lower and negative. Irradiances used in this experimental set-up did not affect the EPA content significantly. The mathematical model reflected the measured EPA values very accurately, with one exception: during the experiment, the EPA content decreased slightly from first to second stationary phase under HSLI conditions, while the model predicted a further increase, similar to under the other conditions. Both the measured data and the model emphasized, that combining LS with 5 days' nutrient starvation yielded a maximum EPA content of 7.1% DW on average. This DW-based EPA content is, to our knowledge, higher than previously reported for microalgae (Sukenik et al., 1991; Lu et al., 2001; Jiang and Gao, 2004; Hu and Gao, 2006; Patil et al., 2006).

The EPA dynamics revealed the same pattern as for the TFA, suggesting that they were triggered by the same processes. Following exponential growth, the DW continued to increase between 5 and 20% from the first to the second stationary phase, although nutrients were depleted, and accordingly cell division inhibited. When cell division is hampered due to an insufficient nutrient supply, microalgae often produce carbonaceous storage compounds like carbohydrates and lipids. Many diatoms accumulate neutral storage lipids in the form of triacylglycerol (TAG), causing the lipid content to increase up to 50% of DW (Hu et al., 2008). Total FA content increased in all cultures from on average 10% in exponential phase, to 25 and 27% DW in the two stationary phases. Storage lipids consist predominantly of saturated and monounsaturated FAs, while PUFAs are generally present in polar membrane lipids (Olofsson et al., 2012). Therefore, TAG accumulation is typically accompanied by a noticeable increase of both palmitic (16:0) and palmitoleic acids (16:1 n-7), which often constitute the predominant FA in the TAG. Yet, PUFAs have also been reported to accumulate in TAG in different microalgae species (Tonon et al., 2002; Sharma et al., 2012). The relative FA compositions (% TFA) observed during the experiment revealed a slight increase of the palmitic and palmitoleic acid fractions, together with a weak decrease of PUFAs after cultures progressed from exponential to stationary phase in all conditions. However, these shifts toward palmitic and palmitoleic acids were lower than typically observed during TAG accumulation, and revealed a concurrent increase of all major FA. This might indicate that TAG accumulated in the cells during stationary phase, containing PUFAs such as EPA, alongside palmitic, and palmitoleic acids.

Another reason for the increase of the FA fraction in stationary phase might be a decrease of silica in the cells. As a result of the silicified cell walls of diatoms, silicate availability in the medium is a key factor regulating their growth, as cells can only divide when new valves can be synthesized (Martin-Jézéquel et al., 2000). Studies have shown that in silicate-limited diatom cultures, uptake is restricted to the SITs (Shrestha and Hildebrand, 2015), and silicification is reduced, resulting in thinner cell walls and a decreased silica content per cell (Martin-Jézéquel et al., 2000; Javaheri et al., 2015). Knuckey et al. (2002) found comparable results to our findings in an *A. septentrionalis* isolate from coastal waters in Tasmania, with an EPA content increasing from 1.3 to 4.2% DW from exponential to stationary phase. Concomitantly, the ash content fell sharply from 26.1 to 8.8% DW resulting in a corresponding increase of the other major organic fractions; proteins, carbohydrates, and lipids. The decreased ash content was most likely related to a diminished silica content of the DW, due to silicate limitation in the stationary phase. The same effect might have contributed to the observed increase in TFA and EPA contents relative to DW in the stationary phase in our study. The typical ash content of microalgae contributes between 5 and 12% DW, but these values are higher in silicified diatoms, between 20 and 55% DW (Nalewajko, 1966; Renaud and Parry, 1994), where much of it is attributable to the extent of silicon in the cell walls. Hildebrand et al. (2012) stated that expressing the FA content as percentage of DW might underestimate the actual amount of FA in diatoms in terms of a per cell carbon basis, when compared with other microalgae, due to their high silica content. Expressing the FA content relative to the ash-free DW might preclude such an underestimation and furthermore might give a better understanding of the FA content and dynamics during silicate-replete and silicate-depleted conditions.

Salinity also affected the TFA and EPA content, especially in combination with the growth phase. Interestingly, TFA and EPA contents were higher for HS cultures in exponential phase, but in contrast were higher for LS cultures in stationary phase. Hence, a greater increase in TFA and EPA from exponential to stationary phase occurred in the LS cultures. These observations

might also be linked to differences in the FA accumulation and silica content of cells grown at different salinities, but might also be related to the changing FA composition of membrane lipids, as an adaptation to variable salt concentrations and the resultant osmotic stress, as has been reported in several studies (Chen et al., 2008; Kumari et al., 2013). Microalgae grown at higher salinities might also reveal an increased ash content, due to an increased ion concentration (Renaud and Parry, 1994).

Determining the ash and silicon contents of the cells and differentiating between polar (membrane) and neutral (storage) lipids, and their FA compositions in future experiments, might contribute to a better understanding of the reasons we observe different EPA and TFA contents relative to DW under different salinities and growth phases, and furthermore, might reveal in which lipid fraction the increased EPA levels are located.

Relative Fatty Acid (FA) Composition During Batch Experiment

Interestingly, irradiance did not significantly affect the EPA content relative to DW, although irradiances have been shown to affect photosynthetic membranes. Generally, photosynthetic membranes increase at low irradiance and are reduced at high irradiances and hence, increasing irradiance has been reported to result in a decrease in EPA and other PUFAs in different microalgae species (Adlerstein et al., 1997; Fábregas et al., 2004). However, irradiance did affect the FA profile in this study, although only to a minor degree. The relative amounts of the main FAs (% TFA) were for the most part affected by nutrient availability primarily, followed by salinity, time of nutrient starvation (days in stationary phase) and irradiance. The differences between the growth phases were mainly due to palmitic and palmitoleic acids and therefore might be related to an accumulation of TAG in stationary phase. The effects of the growth conditions (salinity and irradiance) were less distinct and are more difficult to explain, but might be related to reconstructions of cellular membranes as an adaptation to the cultivation conditions.

Potential for Microalgae-Based Technologies

The low salinity of 22 was more effective in increasing EPA content in the stationary phase in the prevalent *A. septentrionalis* strain, but at the same time, it considerably decreased growth rates compared to a HS of 35. In future large-scale cultivations, EPA productivity would be dependent on both the growth rates and the EPA content in the cells. Calculating the EPA productivities from exponential phase until Day 5 of the stationary phase revealed 0.97 mg L^{-1} d^{-1} for LS cultures and 0.72 mg L^{-1} d^{-1} for HS cultures. Thus, under the prevailing conditions, higher productivities were obtained for the LS cultures, although these productivities are much lower than those seen in commercial production due to the much lower biomass concentrations used in this experimental setup. Whether our results can be successfully repeated in up-scaled systems needs to be evaluated further. Higher nutrient concentrations would be necessary in order to achieve higher cell densities and productivities before cultures reach the stationary phase. Furthermore, other growth conditions such as irradiance, temperature and pH might change considerably when moving from small-scale to large-scale systems, and can thereby affect the EPA content of the cells. The strain used in the current study was isolated from an Arctic habitat and adapted to low temperatures, and therefore temperatures in the experiment were maintained at 10°C. Several studies have shown that low temperatures can increase the PUFA content to maintain membrane fluidity (Boelen et al., 2013). EPA values in the present experiments were higher than values recorded for the *A. septentrionalis* strain by Knuckey et al. (2002) grown at 20°C. However, at the same time, growth rates of their strain were twice as high as the ones observed in this study. Hence, changing temperatures could additionally affect both the EPA content and growth rates. This should also be evaluated with further work.

Knuckey et al. (2002) suggested *A. septentrionalis* to be an excellent feed species for juvenile bivalve molluscs and other filter feeders. Its cell size is within the range that is suitable for ingestion by filter feeders and its protein level (32% DW) remained stable from exponential to stationary phase, while carbohydrate and lipid fractions increased. As shown in our study, EPA contents can be further increased in stationary phase, by changing growth conditions. This could make this diatom strain a promising EPA source for the North Atlantic fish aquaculture industry or for other application areas, such as the health and food sectors.

CONCLUSION

The effect of growth phase, salinity and irradiance, and their interactions on the EPA content in an Arctic *A. septentrionalis* strain was investigated by means of a factorial design experiment. The highest EPA values of 7.1% DW were achieved at a salinity of 22 and Day 5 of the stationary phase. However, at the same time, growth rates during exponential phase were reduced considerably at low salinities. Mathematical models revealed interactive effects of salinity and irradiance on growth and of salinity and growth phase on the EPA content, emphasizing the importance of investigating the additive effects of different growth factors.

AUTHOR CONTRIBUTIONS

PS, SP, SM, and SE: designed research; PS: performed research; PS and SM: analyzed data; PS: wrote the paper; SE and SM: revised the paper. All authors read and approved the final manuscript.

FUNDING

This work was supported by EU MIRACLES project and has received funding from the European Union's Seventh Framework Programme for research, technological development, and demonstration under grant agreement No 613588.

ACKNOWLEDGMENTS

Big thanks to Dorinde Kleinegris for the helpful input, and to Bryan Wilson for valiantly giving up 1 week of lunch hours to read about algae and proofread the English!!

SUPPLEMENTARY MATERIAL

The Supplementary Material for this article can be found online at: https://www.frontiersin.org/articles/10.3389/fpls.2018.00491/full#supplementary-material

REFERENCES

Adarme-Vega, T. C., Lim, D. K. Y., Timmins, M., Vernen, F., Li, Y., and Schenk, P. M. (2012). Microalgal biofactories: a promising approach towards sustainable omega-3 fatty acid production. *Microb. Cell Fact.* 11:96. doi: 10.1186/1475-2859-11-96

Adlerstein, D., Bigogno, C., Khozin, I., and Cohen, Z. (1997). The effect of growth temperature and culture density on the molecular species composition of the galactolipids in the red microalga *Porpyridium cruentum* (Rhodophyta). *J. Phycol.* 33, 975–979. doi: 10.1111/j.0022-3646.1997.00975.x

Aizdaicher, N. A., and Markina, Z. V. (2011). Influence of changes in sea water salinity on the growth, photosynthetic pigment content, and cell size of the benthic alga *Attheya ussurensis* Stonik, Orlova et Crawford, 2006 (Bacillariophyta). *Russ. J. Mar. Biol.* 37, 472–477. doi: 10.1134/S1063074011060034

Boelen, P., van Dijk, R., Sinninghe Damsté, J. S., Rijpstra, W. I. C., and Buma, A. G. J. (2013). On the potential application of polar and temperate marine microalgae for EPA and DHA production. *AMB Express* 3:26. doi: 10.1186/2191-0855-3-26

Cepák, V., Pribyl, P., Kohoutková, J., and Kaštánek, P. (2013). Optimization of cultivation conditions for fatty acid composition and EPA production in the eustigmatophycean microalga *Trachydiscus minutus*. *J. Appl. Phycol.* 26, 181–190. doi: 10.1007/s10811-013-0119-z

Chauton, M. S., Reitan, K. I., Norsker, N. H., Tveterås, R., and Kleivdal, H. T. (2015). A techno-economic analysis of industrial production of marine microalgae as a source of EPA and DHA-rich raw material for aquafeed: research challenges and possibilities. *Aquaculture* 436, 95–103. doi: 10.1016/j.aquaculture.2014.10.038

Chen, G. Q., Jiang, Y., and Chen, F. (2008). Salt-induced alterations in lipid composition of diatom *Nitzschia laevis* (Bacillariophyceae) under heterotrophic culture condition. *J. Phycol.* 44, 1309–1314. doi: 10.1111/j.1529-8817.2008.00565.x

Chen, J., Li, Y., Xie, M., Chiu, C., Liao, S., and Lai, W. (2012). Factorial design of experiment for biofuel production by *Isochrysis galbana*. *Int. Conf. Environ. Energy Biotechnol.* 33, 91–95.

Duarte, M. M. M. B., Da Silva, J. E., Passavante, J. Z. D. O., Fernanda Pimentel, M., De Barros Neto, B., and Da Silva, V. L. (2001). Macroalgae as lead trapping agents in industrial effluents - a factorial design analysis. *J. Braz. Chem. Soc.* 12, 499–506. doi: 10.1590/S0103-50532001000400010

Dunstan, G. A., Volkman, J. K., Barrett, S. M., and Garland, C. D. (1993). Changes in the lipid composition and maximisation of the polyunsaturated fatty acid content of three microalgae grown in mass culture. *J. Appl. Phycol.* 5, 71–83. doi: 10.1007/BF02182424

Fábregas, J., Maseda, A., Domínguez, A., and Otero, A. (2004). The cell composition of *Nannochloropsis* sp. changes under different irradiances in semicontinuous culture. *World J. Microbiol. Biotechnol.* 20, 31–35. doi: 10.1023/B:WIBI.0000013288.67536.ed

Hildebrand, M., Davis, A. K., Smith, S. R., Traller, J. C., and Abbriano, R. (2012). The place of diatoms in the biofuels industry. *Biofuels* 3, 221–240. doi: 10.4155/bfs.11.157

Hu, H., and Gao, K. (2006). Response of growth and fatty acid compositions of *Nannochloropsis* sp. to environmental factors under elevated CO_2 concentration. *Biotechnol. Lett.* 28, 987–992. doi: 10.1007/s10529-006-9026-6

Hu, Q., Sommerfeld, M., Jarvis, E., Ghirardi, M., Posewitz, M., Seibert, M., et al. (2008). Microalgal triacylglycerols as feedstocks for biofuel production: perspectives and advances. *Plant J.* 54, 621–639. doi: 10.1111/j.1365-313X.2008.03492.x

Javaheri, N., Dries, R., Burson, A., Stal, L. J., Sloot, P. M. A., and Kaandorp, J. A. (2015). Temperature affects the silicate morphology in a diatom. *Sci. Rep.* 5:11652. doi: 10.1038/srep11652

Jiang, H., and Gao, K. (2004). Effects of lowering temperature during culture on the production of polyunsaturated fatty acids in the marine diatom *Phaeodactylum tricornutum* (Bacillariophyceae). *J. Phycol.* 40, 651–654. doi: 10.1111/j.1529-8817.2004.03112.x

Khozin-Goldberg, I., Leu, S., and Boussiba, S. (2016). "Microalgae as a source for VLC-PUFA production," in *Lipids in Plant and Algae Development*, eds Y. Nakamura and Y. Li-Beisson (Berlin: Springer), 471–509.

Knuckey, R. M., Brown, M. R., Barrett, S. M., and Hallegraeff, G. M. (2002). Isolation of new nanoplanktonic diatom strains and their evaluation as diets for juvenile Pacific oysters (*Crassostrea gigas*). *Aquaculture* 211, 253–274. doi: 10.1016/S0044-8486(02)00010-8

Kräbs, G., and Büchel, C. (2011). Temperature and salinity tolerances of geographically separated *Phaeodactylum tricornutum* Böhlin strains: maximum quantum yield of primary photochemistry, pigmentation, proline content and growth. *Bot. Mar.* 54, 231–241. doi: 10.1515/bot.2011.037

Kumari, P., Kumar, M., Reddy, C. R., and Jha, B. (2013). "Algal lipids, fatty acids and sterols," in *Functional Ingredients From Algae for Foods and Nutraceuticals*, ed H. Domínguez (Cambridge: Woodhead Publishing Limited), 87–134.

Lu, C., Rao, K., Hall, D., and Vonshak, A. (2001). Production of eicosapentaenoic acid (EPA) in *Monodus subterraneus* grown in a helical tubular photobioreactor as affected by cell density and light intensity. *J. Appl. Phycol.* 13, 517–522. doi: 10.1023/A:1012515500651

Martin-Jézéquel, V., Hildebrand, M., and Brzezinski, M. A. (2000). Silicon metabolism in diatoms: Implications for growth. *J. Phycol.* 36, 821–840. doi: 10.1046/j.1529-8817.2000.00019.x

Martins, D. A., Custódio, L., Barreira, L., Pereira, H., Ben-Hamadou, R., Varela, J., et al. (2013). Alternative sources of n-3 long-chain polyunsaturated fatty acids in marine microalgae. *Mar. Drugs* 11, 2259–2281. doi: 10.3390/md11072259

Maxwell, K., and Johnson, G. N. (2000). Chlorophyll fluorescence - a practical guide. *J. Exp. Bot.* 51, 659–668. doi: 10.1093/jexbot/51.345.659

Meier, S., Mjøs, S. A., Joensen, H., and Grahl-Nielsen, O. (2006). Validation of a one-step extraction/methylation method for determination of fatty acids and cholesterol in marine tissues. *J. Chromatogr. A* 1104, 291–298. doi: 10.1016/j.chroma.2005.11.045

Nalewajko, C. (1966). Dry weight, ash, and volume data for some freshwater planktonic algae. *J. Fish. Res. Board Canada* 23, 1285–1288. doi: 10.1139/f66-119

Olofsson, M., Lamela, T., Nilsson, E., Bergé, J. P., del Pino, V., Uronen, P., et al. (2012). Seasonal variation of lipids and fatty acids of the microalgae *Nannochloropsis oculata* grown in outdoor large-scale photobioreactors. *Energies* 5, 1577–1592. doi: 10.3390/en5051577

Parsons, T. R., Maita, Y., and Lalli, C. M. (1992). *A Manual of Chemical and Biological Methods for Seawater Analysis*. Oxford: Pergamon Press.

Patil, V., Källqvist, T., Olsen, E., Vogt, G., and Gislerød, H. R. (2006). Fatty acid composition of 12 microalgae for possible use in aquaculture feed. *Aquac. Int.* 15, 1–9. doi: 10.1007/s10499-006-9060-3

Patil, V., Reitan, K. I., Knutsen, G., Mortensen, L. M., Källqvist, T., Olsen, E., et al. (2005). Microalgae as source of polyunsaturated fatty acids for aquaculture. *Curr. Top. Plant Biol.* 6, 57–65.

Prestegard, S. K., Erga, S. R., Steinrücken, P., Mjøs, S. A., Knutsen, G., and Rohloff, J. (2015). Specific metabolites in a *Phaeodactylum tricornutum* strain isolated from western Norwegian fjord water. *Mar. Drugs* 14:9. doi: 10.3390/md14010009

Rampen, S. W., Schouten, S., Elda Panoto, F., Brink, M., Andersen, R. A., Muyzer, G., et al. (2009). Phylogenetic position of *Attheya longicornis* and *Attheya septentrionalis* (bacillariophyta). *J. Phycol.* 45, 444–453. doi: 10.1111/j.1529-8817.2009.00657.x

Renaud, S. M., and Parry, D. L. (1994). Microalgae for use in tropical aquaculture II: Effect of salinity on growth, gross chemical composition and fatty acid composition of three species of marine microalgae. *J. Appl. Phycol.* 6, 347–356. doi: 10.1007/BF02181949

Reynolds, C. S. (2006). *Ecology of Phytoplankton*. Cambridge: Cambridge University Press.

Sharma, K. K., Schuhmann, H., and Schenk, P. M. (2012). High lipid induction in microalgae for biodiesel production. *Energies* 5, 1532–1553. doi: 10.3390/en5051532

Shrestha, R. P., and Hildebrand, M. (2015). Evidence for a regulatory role of diatom silicon transporters in cellular silicon responses. *Eukaryot. Cell* 14, 29-40. doi: 10.1128/EC.00209-14

Spolaore, P., Joannis-Cassan, C., Duran, E., and Isambert, A. (2006). Commercial applications of microalgae. *J. Biosci. Bioeng.* 101, 87–96. doi: 10.1263/jbb.101.87

Steinrücken, P., Erga, S. R., Mjøs, S. A., Kleivdal, H., and Prestegard, S. K. (2017). Bioprospecting North Atlantic microalgae with fast growth and high polyunsaturated fatty acid (PUFA) content for microalgae-based technologies. *Algal Res.* 26, 392–401. doi: 10.1016/j.algal.2017.07.030

Stonik, I. V., Kapustina, I. I., Aizdaicher, N. A., and Svetashev, V. I. (2017). Sterols and fatty acids from *Attheya* planktonic diatoms. *Chem. Nat. Compd.* 53, 422–425. doi: 10.1007/s10600-017-2013-4

Sukenik, A., Zmora, O., and Carmeli, Y. (1991). Biochemical quality of marine unicellular algae with special emphasis on lipid composition. II. *Nannochloropsis* sp. *Aquaculture* 117, 313–326. doi: 10.1016/0044-8486(93)90328-V

Tatsuzawa, H., and Takizawa, E. (1995). Changes in lipid and fatty acid composition of *Pavlova lutheri*. *Phytochemistry* 40, 397–400. doi: 10.1016/0031-9422(95)00327-4

Tonon, T., Harvey, D., Larson, T. R., and Graham, I. A. (2002). Long chain polyunsaturated fatty acid production and partitioning to triacylglycerols in four microalgae. *Phytochemistry* 61, 15–24. doi: 10.1016/S0031-9422(02)00201-7

Van Wagenen, J., Miller, T. W., Hobbs, S., Hook, P., Crowe, B., and Huesemann, M. (2012). Effects of light and temperature on fatty acid production in *Nannochloropsis salina*. *Energies* 5, 731–740. doi: 10.3390/en5030731

Walne, P. R. (1970). Studies on the food value of nineteen genera of algae to juvenile bivalves of the genera *Ostrea*, *Crassostrea*, *Mercenaria* and *Mytilus*. *Fish. Invest. Ser.* 2, 1–62.

Wasta, Z., and Mjøs, S. A. (2013). A database of chromatographic properties and mass spectra of fatty acid methyl esters from omega-3 products. *J. Chromatogr. A* 1299, 94–102. doi: 10.1016/j.chroma.2013.05.056

Xu, X. Q., and Beardall, J. (1997). Effect of salinity on fatty acid composition of a green microalga from an antarctic hypersaline lake. *Phytochemistry* 45, 655–658. doi: 10.1016/S0031-9422(96)00868-0

Zhu, C. J., and Lee, Y. K. (1997). Determination of biomass dry weight of marine microalgae. *J. Appl. Phycol.* 9, 189–194. doi: 10.1023/A:1007914806640

Conflict of Interest Statement: The authors declare that the research was conducted in the absence of any commercial or financial relationships that could be construed as a potential conflict of interest.

frontiers in Plant Science

ORIGINAL RESEARCH
published: 17 April 2018
doi: 10.3389/fpls.2018.00506

Naphthylacetic Acid and Tea Polyphenol Application Promote Biomass and Lipid Production of Nervonic Acid-Producing Microalgae

Feng Xu[1,2†], Yong Fan[2†], Fuhong Miao[1†], Guang-Rong Hu[2], Juan Sun[1], Guofeng Yang[1] and Fu-Li Li[2]*

[1] *Forage Research and Development Center for Arable Region, Qingdao Agricultural University, Qingdao, China,* [2] *Shandong Provincial Key Laboratory of Synthetic Biology, Qingdao Institute of Bioenergy and Bioprocess Technology, Chinese Academy of Sciences, Qingdao, China*

Mychonastes afer HSO-3-1 is a potential producer of nervonic acid, which could be accumulated to 2–3% of dry cell weight. Improving the productivity of nervonic acid is critical to promote the commercialization of this product. In this study, 1-naphthylacetic acid (NAA) and tea polyphenol (TP) were selected as bioactive additives to stimulate the growth of *M. afer*. Supplementing NAA in the early growth stage and TP in the middle and late growth stage led to improved lipid accumulation in *M. afer*. The cultures supplemented with TP at the late growth stage maintained higher photosynthetic efficiency than the control groups without TP. Furthermore, the intracellular reactive oxygen species (ROS) accumulations in *M. afer* supplemented with 500 mg/L of TP was 63% lower than the control group. A linear relationship (R^2 = 0.899) between the values of Fv/Fm and ROS accumulation was established. We hypothesize supplement of bioactive additives at different growth stage could promote the cell growth rate and nervonic acid productivity of *M. afer* by retrieving intracellular ROS level. Further analysis of photosynthetic system II (PSII) protein in *M. afer* cultured in presence of NAA and TP indicated the levels of D1 and D2 proteins, the core skeleton proteins of PSII, showed 33.3 and 25.6% higher than the control group. CP43 protein, a critical module in PSII repair cycle, decreased significantly. These implied that TP possesses the function of slowing down the damage of PSII by scavenging excess intracellular ROS.

Keywords: ***Mychonastes afer*, photosynthetic efficiency, reactive oxygen species, photosynthetic system II, CP43, bioactive additive**

OPEN ACCESS

Edited by:
Yandu Lu,
Hainan University, China

Reviewed by:
Taras P. Pasternak,
Albert Ludwigs University of Freiburg, Germany
Abdulsamie Hanano,
Atomic Energy Commission of Syria, Syria

****Correspondence:***
Guofeng Yang
yanggf@qau.edu.cn

† These authors have contributed equally to this work.

Specialty section:
This article was submitted to Plant Biotechnology, a section of the journal Frontiers in Plant Science

Received: *15 February 2018*
Accepted: *03 April 2018*
Published: *17 April 2018*

Citation:
Xu F, Fan Y, Miao F, Hu G-R, Sun J, Yang G and Li F-L (2018) Naphthylacetic Acid and Tea Polyphenol Application Promote Biomass and Lipid Production of Nervonic Acid-Producing Microalgae. Front. Plant Sci. 9:506. doi: 10.3389/fpls.2018.00506

INTRODUCTION

As a promising feed-stock of biodiesel or jet fuel, microalgae have received extensive attention in recent years due to its ability of producing substantial amounts of triacylglycerols (TAGs) under stress conditions (Hu et al., 2008). The concept of using microalgae as an alternative and renewable source of lipid-rich biomass feed-stock for biodiesel has been explored over the past few decades, while technical and economic barriers still limit the development of the whole industry chain (Williams and Laurens, 2010). Outstanding strains with high lipid yield and effective culture technology are main challenges for commercialization of microalgal biodiesel (Chisti, 2007).

Mychonastes afer HSO-3-1 is a promising candidate for biodiesel production, because of its high lipid content (50% dry cell weight) and fast growth rate. Furthermore, nervonic acid (NA, C24:1 Δ15, *cis*-tetracos-15-enoic acid, ω-9) could account for more than 5% of the neutral fatty acids in *M. afer*. NA, a very long chain monounsaturated fatty acid (VLMFA), is essential for brain development (Sandhir et al., 1998; Yuan et al., 2011; Fan et al., 2018b). It could be used to treat genetic disorders of the lipid metabolism, such as Zellweger syndrome or adrenoleukodystrophy (Coupland and Langley, 1993; Fan et al., 2018a). An impairment in the provision of NA in demyelinating diseases (like multiple sclerosis) suggests that a diet rich with NA could improve the treatment (Sargent et al., 1994).

In order to increase the productivity of NA in *M. afer,* optimization of the culture conditions should be developed firstly. Phytohormones are found not only in higher plants but also in algae, and the biological activities of hormones in algae are similar to the functions of hormones in higher plant (Lu and Xu, 2015). Exogenous IAA (0.1–10 μM) increased *Chlamydomonas reinhardtii* biomass production by 54–69% (Park et al., 2013). The supplement of IAA (0.1 μM) or 1-naphthylacetic acid (NAA) (1 μM) induced a significant increase in cell number by 53 and 24% in *Chlorella vulgaris,* and it would increase the amount of monosaccharides, photosynthetic pigments, and soluble enzymes in *C. vulgaris* (Piotrowska-Niczyporuk and Bajguz, 2014).

Compound additives will be a trend in the cultivation process, and the combination of additives needs to be analyzed and tried unceasingly. According to our previous research, intracellular reactive oxygen species (ROS) level is another key factor that influences the growth of microalgae. Plants maintain complex systems of overlapping antioxidants to balance the oxidative state *in vivo* (Munne-Bosch, 2005), while microalgal antioxidant system may not deal with the over-oxidation stress efficiently due to its simple cell structure (Cavas and Yurdakoc, 2005). Reactive oxygen species can function as signaling molecules that control the cellular basal metabolism such as induced cell re-programming toward programmed cell death or many other developmental processes. Unbalanced oxidative state will cause abiotic stress responses in plants, and excess ROS accumulation is toxic to cells (Mittler, 2002). Antioxidants can prevent cells from ROS accumulation by scavenging the excessive ROS (Wolf, 2005). In addition, algal antioxidant system plays crucial roles in stress tolerance, like heavy metal, salinity and heat stress (Geider et al., 1993; Pinto et al., 2003; Liu and Pang, 2010). In our previous work, varieties of potential candidate additives were selected from phytohormones and antioxidants, like NAA, indole-3-acetic acid, gibberellic acid, kinetin, abscisic acid, tocopherol, epigallocatechin-3-gallate (EGCG), and tea polyphenol (TP) (Frei and Higdon, 2003). In consideration of solubility, stability, and photo-sensitivity, one phytohormone (NAA) and two antioxidants (EGCG and TP) were finally selected for further investigation of the effects on the growth and lipid accumulation of *M. afer*. We hypothesize that the supplement of bioactive additives at different growth stages could promote the cell growth rate and nervonic acid productivity of *M. afer*. Orthogonal experiments were used to analyze the additive doses, and it was further confirmed by single factor experiment analysis. We found that the supplement of these additives at different growth stages led to different effects on microalgal growth. Interestingly, supplement of TP increases the tolerance to ROS in *M. afer* at later growth stage. Photosynthetic efficiency of the cells cultured in presence of NAA and TP was analyzed.

MATERIALS AND METHODS

Strains and Culture Conditions

Mychonastes afer was stored in the China General Microbiological Culture Collection Center with the identifying code CGMCC No. 4654. It was cultured in a column photobioreactor (20 cm high, 4 cm diameter, 100 mL culture volume) under continuous illumination at light intensity of 120 μmol photons $m^{-2}{\cdot}s^{-1}$. Culture mixing and aerating was provided by aeration with filter-sterilized air containing 2% CO_2 (Yuan et al., 2017). The initial OD_{750} of algal culture was 1.0. All strains were cultured at room temperature (25 ± 2°C) for 12 days. The cells were grown in a modified BG-11 medium with 0.374 g/L $NaNO_3$ (Li et al., 2011). The other compositions of the BG-11 medium are as follows: 0.03 g/L K_2HPO_4, 0.075 g/L $MgSO_4{\cdot}7H_2O$, 0.036 g/L $CaCl_2{\cdot}2H_2O$, 0.006 g/L citric acid, 0.006 g/L ferric ammonium citrate, 0.001 g/L EDTA, 0.02 g/L Na_2CO_3. And 1 ml of trace metal solution per liter medium, which content: 2.86 g/L H_3BO_3, 1.81 g/L $MnCl_2{\cdot}4H_2O$, 0.222 g/L $ZnSO_4{\cdot}7H_2O$, 0.39 g/L $NaMoO_4{\cdot}5H_2O$, 0.079 g/L $CuSO_4{\cdot}5H_2O$, 0.0494 g/L $Co(NO_3)_2{\cdot}6H_2O$. The culture medium was sterilized in an autoclave at 121°C for 20 min. TP (Food grade, Xitang Biological Technology, Co., Ltd., China), EGCG and NAA (TCI Development, Co., Ltd., Shanghai, China) were sterilized by filtration.

In the first step, orthogonal experiments were carried out with four levels as follows: 0 mg/L (A_1), 0.5 mg/L (A_2), 1.5 mg/L (A_3), and 5 mg/L (A_4) for NAA dosage, 0 mg/L (B_1), 0.5 mg/L EGCG (B_2), 2 mg/L TP (B_3), and 20 mg/L TP (B_4) for antioxidants dosage. And 120 μmol photons $m^{-2}{\cdot}s^{-1}$ of light intensity was used as low-light level (LL, C_1/C_2), 400 μmol photons $m^{-2}{\cdot}s^{-1}$ was used as high-light level (HL, C_3/C_4). Three-factors-four-levels experiments were conducted by the orthogonal list L_{16} (4^5). NAA was added at the early growth stage when the OD_{750} of algal culture was about 3.0 at day 2. EGCG and TP were added at the middle growth stage when the OD_{750} of algal culture was about 6.0 at day 6. Experimental scheme and results were shown in Supplementary Table 1. All data were analyzed by SPSS Statistics (Version 19, IBM, Armonk, NY, United States).

To confirm the effects of the candidate factors selected by orthogonal experiments, single factor experimental scheme was conducted with a wider gradient of the additive concentration. A new range of NAA concentrations (0, 0.1, and 10 mg/L) and TP concentrations (0, 50, and 500 mg/L) were chosen. Nine experimental groups were as follows: CT, 0.1 NAA, 10 NAA, 50 TP, 500 TP, 0.1 NAA+50 TP, 0.1 NAA+500 TP, 10 NAA+50 TP, and 10 NAA+500 TP. An additive combination of NAA (0.1 mg/L) and TP (500 mg/L) in the medium was expressed as 0.1 NAA+500 TP. CT was the control group without additives.

Algal Biomass and Chlorophyll Fluorescence Measurements

Algal samples (10 mL) were filtered through the pre-weighed filter paper (0.22 mm, Whatman International, Ltd., Maidstone, United Kingdom) and dried at 105°C for 8 h. The difference between the final weight and initial weight of the filter paper was the dry weight of the samples.

Algal cells suspension was transferred to the 96-well plates and analyzed by Imaging-PAM Chlorophyll Fluorometer (Walz, Effeltrich, Germany). The chlorophyll fluorescence was measured and calculated, the data of photosynthetic efficiency were determined, including the data of Fv/Fm, non-photochemical quenching (NPQ) and quantum yield of photochemical energy conversion in PSII (YII) (Klughammer and Schreiber, 2008; Hu et al., 2013).

Lipid Extraction, Quantification, and Composition Analysis

Nile red staining was carried out for measurement of neutral lipids in microalgae (Chen et al., 2009). Freeze-dried biomass was further used for total lipid extraction (Bigogno et al., 2002). Following procedures: 30 mg dry algae powder was resuspended with the chloroform-methanol (4 vs. 2 ml) to extract the lipid by shaking with a speed of 200 rpm at 37°C for 2 h. After centrifuging at 3200 *g* for 10 min, the supernatant was transferred to a new tube and mixed with 2 ml methanol and 3.6 ml 5% NaCl. The remaining lipid was dissolved in chloroform phase by centrifuging at 3200 *g* for 5 min, then the chloroform phase was transferred into pre-weight vials. The residuals were weighed after removing chloroform by nitrogen evaporator.

Total lipid composition was analyzed after methyl esterification processing by reacting with 2% H_2SO_4 in methanol at 85°C for 3 h. Gas chromatography analysis was carried out with a GC system (7890A, Agilent Technologies, Inc., Santa Clara, CA, United States). HP-5 (30 m × 320 μm × 0.25 μm, Agilent, United States) was selected as the chromatographic column. Gas heating process was as follows: rise the column temperature to 190°C with a heat rate of 10°C/min, and maintain 1 min. Then rise the temperature to 207°C with a heat rate of 0.8°C/min, and maintain 1 min. N_2 was used as carrying gas with a speed (28.5 mL/min) and split ratio (10:1, *v/v*). Heptadecanoic acid (C17:0, 3 mg/mL) was used as an internal standard.

Intracellular ROS Level, Lipid Peroxidation, and ROS Scavenging Enzyme (Catalase) Activity Analysis

Intracellular ROS analysis was performed by using a Reactive Oxygen Species Assay Kit (Beijing Solarbio Science & Technology, Co., Ltd., China; code: CA1410-100T) according to the manufacturer's instructions. This kit used 2,7-Dichlorodi-hydrofluorescein diacetate (DCFH-DA) as probe. This non-fluorescence probe could be oxidized by intracellular ROS, including hydrogen peroxide (H_2O_2) and hydroxyl radicals (OH•), to the fluorescence probe of DCF. This fluorescence was most sensitive to the level of H_2O_2 and could be used to compare the levels of this ROS in different conditions of the cells. Culture samples of *M. afer* were collected and adjusted to a final cell concentration of 1×10^7 cells per milliliter with culture medium which collected from the culture system. Then cells were incubated with 1 μM DCFH-DA for 20 min under culture condition (same light intensity and temperature). DCF fluorescence was measured with 488 nm excitation wavelength and 525 nm emission wavelength by a multi-mode microplate reader (SynergyTM HT, BioTek, Winooski, VT, United States).

Malondialdehyde (MDA, the by product of lipid peroxidation) content and Catalase (CAT) activities were measured according to Shi et al. (2009). MDA and CAT kits were purchased from Nanjing Bioengineering Institute, China.

Thylakoid Membrane Preparation and Protein Level Analysis

Microalgae cells were harvested by centrifugation at 4000 *g* for 10 min and resuspended in 10 ml of Hepes-OH buffer (20 mM, pH 7.5). After centrifuged at 3200 *g* for 5 min, the pellets were suspended with 5 ml of extraction buffer (300 mM sorbitol; 50 mM Hepes-OH, pH 7.5; 2 mM Na_2EDTA, pH 8.0; 1 mM $MgCl_2 \cdot 6H_2O$ and 1% BSA). The microalgae cells were homogenized by grinding in liquid nitrogen and the extraction were performed in triplicates. All subsequent steps were carried out on ice. The supernatant was collected in centrifuge tube by centrifugation at 4000 *g* for 10 min. Following centrifugation at 13000 *g* for 30 min with the collected supernatant, the precipitated thylakoid membranes were resuspended in extraction buffer.

For the qualification of chlorophyll and protein content in thylakoid, thylakoid membrane was soaked with 80% acetone at 60°C for 2 h, then separate the chlorophyll and protein by centrifugation at 13000 *g* for 15 min. Chlorophyll content in thylakoid was determined by the method published (Wellburn, 1994). And the total protein content was determined by BCA Protein Assay Kit (by protein reduction chromogenic reaction) following the manufacturer's instructions (Beijing Solarbio Science & Technology, Co., Ltd., China).

Sodium dodecyl sulfate polyacrylamide gel electrophoresis (SDS-PAGE) was performed according to the protocol (Ikeuchi and Inoue, 1988), and thylakoid membrane proteins were used as testing samples. For semi-quantification analysis, the gray scale of each band was measured by Image J software. Target bands which had significant differences were excised and decolorized using decolor-buffer (100 mM NH_4CO_3/30% acetonitrile) at 4°C for 2 h. This step was repeated two times until the spot gels were totally clean. After centrifugation at 13800 *g* for 5 min, the pellets of gels were lyophilized and then transferred in 5 μl Trypsin solution (12.5 ng/μl in 50 mM NH_4HCO_3) at 4°C for 60 min, followed by adding 20 μl 50 mM NH_4HCO_3 at 37°C for 20 h. The enzymatic hydrolysate was transferred to another tube, and the supernatant was used for LC–MS/MS analysis.

Samples were analyzed on a Surveyer plus a LC-LTQ XL (Thermo Fisher Scientific, Inc., Waltham, MA, United States). The electrospray voltage of 2.2 kV was carried out with the ion transfer tube temperature at 220°C. Digested peptides were

analyzed by using data-dependent acquisition of a MS scan (600–2000 m/z), and then MS/MS scans were performed for the three most abundant ions in each MS scan. Normalized collision energy for MS/MS was set to 35% with an isolation width of 1.5 amu. From raw files, MS/MS spectra were exported to individual files in data format according to the following setup: peptide mass range, 350–5000 Da; minimal total ion intensity threshold, 1000; minimal number of fragment ions, 15; precursor mass tolerance, 1.4 amu; group scan, 1; minimum group count, 1.

Extracted MS/MS spectra were converted to a Mascot genetic format file (mgf) and searched against a *C. reinhardtii* database [from the National Center for Biotechnology Information (NCBI), updated November 17, 2017, containing 33,220 entries] or Swiss_Prot (updated November 17, 2017, containing 560,836 entries) by Mascot (Version 2.4, Matrix Science, Ltd., London, United Kingdom).

For western-blot analysis, thylakoid membrane proteins of *M. afer* were used as total protein samples. Primary antibodies [D1 protein of photosynthetic system II (PSII), C-terminal, rabbit antibody, code: AS05_084] were purchased from Agrisera, Co., Ltd., Sweden. Western-blotting was performed by probing with specific antibodies after electroblotting onto nitrocellulose membranes (GE Healthcare, Co., Ltd., Chicago, IL, United States) (Liu et al., 2012b). Primary antibody was diluted 10000-fold (antibody against D1), and signals from horseradish peroxidase-conjugated goat anti-rabbit IgG (H+L) were visualized using Clarity Western ECL substrate (MDBio, Inc., Qingdao, China) and the blotting-spots were analyzed using ImageJ software (National Institutes of Health, United States) (Liu et al., 2012a).

Statistical Analysis

All the experiments were repeated three times. Unless otherwise stated, all data were expressed as mean standard deviation (SD). Statistical significance and determination coefficients of the values obtained from each experiment was evaluated by variance (ANOVA) using the software SPSS (version 19.0, IBM, Chicago, IL, United States). Significant differences were considered when $p < 0.05$.

RESULTS

Growth and Lipid Content of *M. afer* After NAA and Antioxidants Supplement

Experimental scheme and results of the orthogonal experiments were shown in Supplementary Table 1. Light intensity, NAA and antioxidants all had significant ($p < 0.05$) influence on *M. afer* photosynthetic efficiency (Supplementary Table 3), while the growth was only significantly ($p = 0.001$) affected by light intensity (Supplementary Table 2). No significant effect on lipid content was observed from all of these factors (Supplementary Table 4). Microalgal photosynthetic efficiencies were significantly influenced by NAA ($p = 0.046$) and antioxidants ($p = 0.033$), while these effects were not reflected by the growth of *M. afer* (**Figure 1**).

Based on the relationship between photosynthetic efficiency of *M. afer* and additives, new experimental scheme was conducted with a wider gradient of the additive concentration to further verify the orthogonal experiment results. The algal growth rate increased with an addition of 0.1 mg/L NAA on the 2nd day of cultivation, and this promotion was amplified when TP was added on the 6th day of cultivation. After the supplement of NAA (0.1 mg/L) and TP (500 mg/L) in the medium, the maximum algal biomass was 3.69 g/L, which was 18.76% higher ($p = 0.002$) than control (**Figure 2A**).

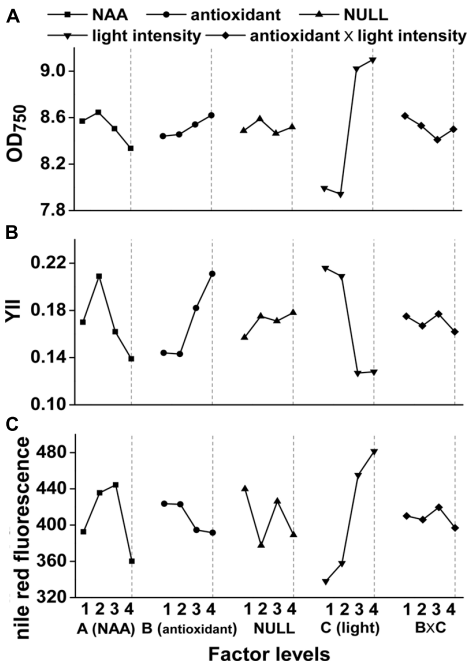

FIGURE 1 | Orthogonal effect curves of NAA, antioxidants, and light intensity on growth (OD_{750}), photosynthetic efficiency (YII), and lipid accumulation of *Mychonastes afer*. NAA **(A)**, antioxidant **(B)**, light intensity **(C)** and the interactions between the light intensity and antioxidants (B × C) were the factors investigated here with four levels, and NULL is for the error assessment. The four levels of these factors were as follows: 0 mg/L (A_1), 0.5 mg/L (A_2), 1.5 mg/L (A_3), and 5 mg/L (A_4) for NAA dosage, 0 mg/L (B_1), 0.5 mg/L EGCG (B_2), 2 mg/L TP (B_3), and 20 mg/L TP (B_4) for antioxidants dosage. And 120 μmol photons $m^{-2}·s^{-1}$ of light intensity was used as low-light level (LL, C_1/C_2), 400 μmol photons $m^{-2}·s^{-1}$ was used as high-light level (HL, C_3/C_4).

Total lipid content of *M. afer* was increased with the supplementary of 0.1 mg/L NAA and TP. The maximum algal total lipid content and lipid yield was 17.6 and 39.6% higher than control without additives, respectively. It appeared in the experimental group with the supplement of NAA (0.1 mg/L) and TP (500 mg/L) in the medium (**Figure 2B**). However, no significant difference of fatty acids composition was observed under different culture conditions, according to the GC analysis data (Supplementary Table 5).

Effects of NAA and TP on Photosynthetic Efficiency of *M. afer*

Microalgae utilize light energy to maintain the energy requirements for life activities and growth. In order to elucidate

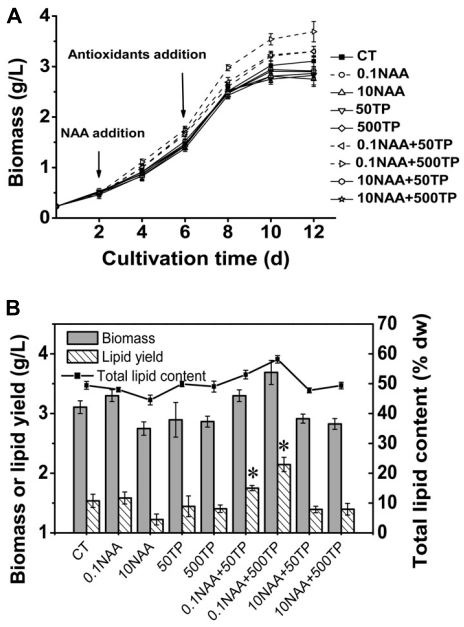

FIGURE 2 | Growth and lipid content of *M. afer* supplemented with NAA and TP. **(A)** Growth curves of *M. afer* that grew under different treatment of additive combinations. CT is the control group without additives. NAA and TP were added at day 2 and day 6, respectively. **(B)** Final algal biomass (dry weight), lipid content (% dry weight), and lipid yield of *M. afer* under different culture conditions. Values are means ± SE (n = 3). Asterisks indicate statistically significant differences compared with the control group (*$p < 0.05$; ANOVA).

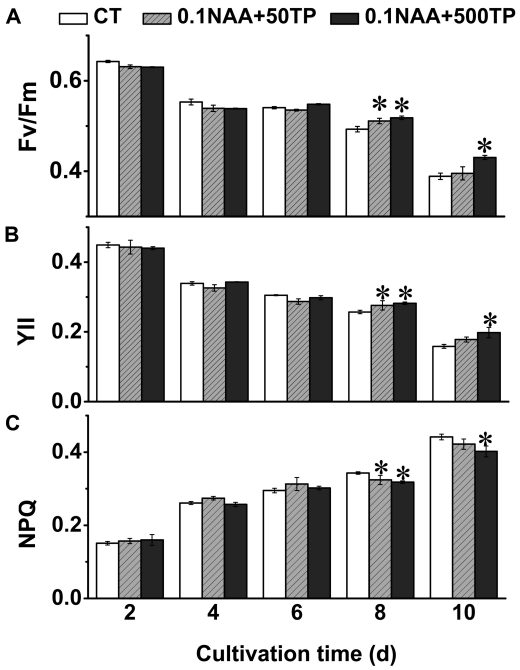

FIGURE 3 | Effects of NAA and TP on photosynthetic efficiency of *M. afer.* Photosynthetic parameters Fv/Fm **(A)**, YII **(B)**, and NPQ **(C)** were detected. NAA and TP were added at day 2 and day 6, respectively. Values are means ± SE (n = 3). Asterisks indicate statistically significant differences compared with the control group (*$p < 0.05$; ANOVA).

the mechanism for the higher growth rate and lipid content of *M. afer* after adding NAA and TP, the photosynthetic efficiency of *M. afer* under different culture conditions were measured. Fv/Fm was the potential maximum photosynthetic activity of the photosynthetic organisms. Fv/Fm could also reflect the activity of the PSII complex. YII stands for the actual quantum yield (actual photosynthetic efficiency) of PSII in any light state and can reflect the activity of linear electron transport (Klughammer and Schreiber, 2008). NPQ reflects the ability of photosynthetic organisms to dissipate excess light to heat. The Fv/Fm and YII of *M. afer* decreased in the later stage of culture, while some groups which added TP at day 6 showed higher Fv/Fm than control group (p = 0.002). Consequently, the NPQ of *M. afer* increased in the later stage of culture, while the groups added with TP would lead a lower NPQ, indicating a lesser light energy dissipation in the cells with TP supplement (**Figure 3**). These results suggested that TP could maintain higher photosynthesis efficiency of *M. afer* at later growth stage compared with the control group.

Intracellular Reactive Oxygen Species (ROS), Lipid Peroxidation, and ROS Scavenging Enzyme (CAT) Activity Analysis

At the late growth stage, algae grew under stress conditions due to deplete of nutrition in medium, which in general led to decreased energy converting efficiency (Kolber et al., 1988). Excess light energy would lead to sustained increases in intracellular ROS level, which would have detrimental effects on algal growth (Choo et al., 2004). The observation that cells of *M. afer* could maintain high photosynthetic efficiency at later growth stage after TP supplement, implying that TP might regulate the photosynthesis efficiency of *M. afer* by alleviating its intracellular ROS. We selected day 8 as the time point to analyze the relationship between photosynthetic efficiency of *M. afer* and its intracellular ROS level, because the photosynthetic efficiency of *M. afer* showed the most significant difference between the control group and the cells cultured with 0.1 mg/L NAA and 500 mg/L TP at this time point (p = 0.0004). A linear relationship was observed between Fv/Fm values and intracellular ROS levels, which suggested that TP could promote the photosynthesis efficiency of *M. afer* by alleviating its intracellular ROS at later growth stage (**Figures 4A,B**). Base on the method, the species of these reactive oxygen were mainly H_2O_2. The cells of two experimental groups (0.1 NAA+50 TP and 0.1 NAA+500 TP) which had the highest lipid yield were harvested for further MDA content and CAT activities analysis. MDA is the by product of lipid peroxidation. MDA content was analyzed as the indicator for lipid peroxidation, and the excess ROS accumulation in cells can be represented by their lipid peroxidation (Zhang et al., 2013). CAT is a key enzyme which is located in peroxisomes and mitochondria in ROS scavenging system (Kato et al., 1997). CAT became more abundant in the later stage of the

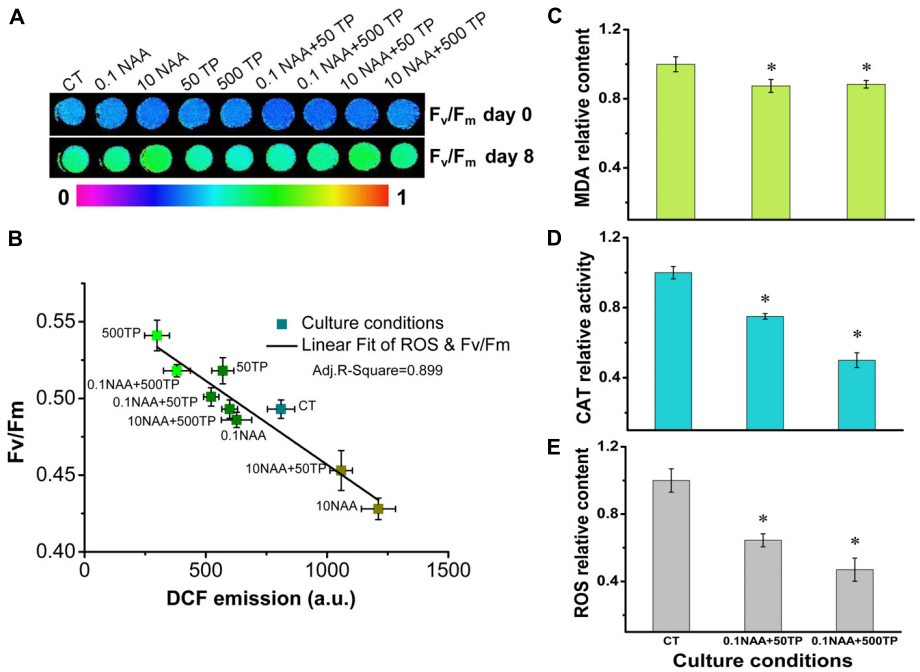

FIGURE 4 | Intracellular ROS analysis of *M. afer* and their relationship with the Fv/Fm values under different culture conditions. **(A)** False-color images showed Fv/Fm variations of *M. afer* under different culture conditions. Algal cells suspension was added to the 96-well plates. After 10 min of dark adaptation, Fv/Fm was determined following a saturating pulse of light, and chlorophyll fluorescence images of algal cells suspension were obtained at this time point. **(B)** Linear fit of ROS and Fv/Fm. DCF fluorescence was used to semi-quantitative analyze the accumulation of H_2O_2 in *M. afer*. Quantification analysis of intracellular ROS level **(C)**, MDA content **(D)**, and CAT activity **(E)** of *M. afer* under different culture conditions. *M. afer* cells were harvested and analyzed immediately at day 8. Values are means ± SE ($n = 3$). Asterisks indicate statistically significant differences compared with the control group (*$p < 0.05$; ANOVA).

cell culture, and higher CAT activity reflected a later stage of the cell culture. Over-expression of CAT in cytosolic or mitochondrial compartment protects cells against oxidant injury (Bai et al., 1999). Intracellular ROS level (DCF fluorescence) of *M. afer* cultured with NAA (0.1 mg/L) and TP (500 mg/L) were significantly lower than the control group, which decreased 53% (**Figure 4C**). Correspondingly, MDA content and CAT activity of *M. afer* cultured with NAA (0.1 mg/L) and TP (500 mg/L) were about 88.4 and 50% compared with control group, respectively (**Figures 4D,E**). The lower intracellular ROS level and MDA content indicated that the cells of *M. afer* cultured with TP supplement were under lower oxidant stress than the control group. Meanwhile, a lower CAT activity was enough for excessive ROS neutralization in TP supplemented cultures.

Western-Blot Analysis of Photosynthetic Proteins

The cells of two experimental groups (0.1 NAA+50 TP and 0.1 NAA+500 TP) which had the highest lipid yield were harvested for further quantification analysis of photosynthetic proteins. As the core photosynthetic apparatus of PSII, the abundance of chloroplast photosynthetic protein D1 could represent the amount of functional PSII in algal cells (Schnettger et al., 1994). According to the western-blot result, D1 content in the cells that cultured with 0.1 mg/L NAA and 500 mg/L TP supplement was 33.3% higher than control (**Figures 5A,B**). Dilutions of control group were used to proving the accuracy of western-blotting process. Combined with the ROS level results, it is speculated that the cells with higher TP supplement were suffered less oxidant damage on the PSII.

In order to get more clues about how TP induced the high robust of PSII to response to high ROS stress, thylakoid membrane proteins were analyzed by SDS-PAGE. Four bands at 24, 25, 27, and 50 kDa were chosen for further composition and semi-quantification analysis (Supplementary Figure 1). Based on our western-blotting experience of D1 protein (two bands with close dimensions at 25 kDa), bands at 24 and 25 kDa are D1 and pD1 proteins (precursor D1 protein), respectively. Two bands at 50 and 27 kDa exhibit significant differences between the treatment samples and control by the gray scale analysis of blue Coomassie-stained gel (**Figure 5D**). Further LC–MS/MS analysis predicted these are the protein bands of CP43 (PSBC_CHLEU) and D2 (PSBD_BIGNA), respectively (**Figure 5D** and Supplementary Table 6). With TP supplement, the amount of D2 protein was 25.6% higher than control, while the amount of CP43 was 84.2% lower than control (**Figures 5C,D**).

DISCUSSION AND CONCLUSION

Auxins play a particular role in higher plant development by affecting several physiological processes

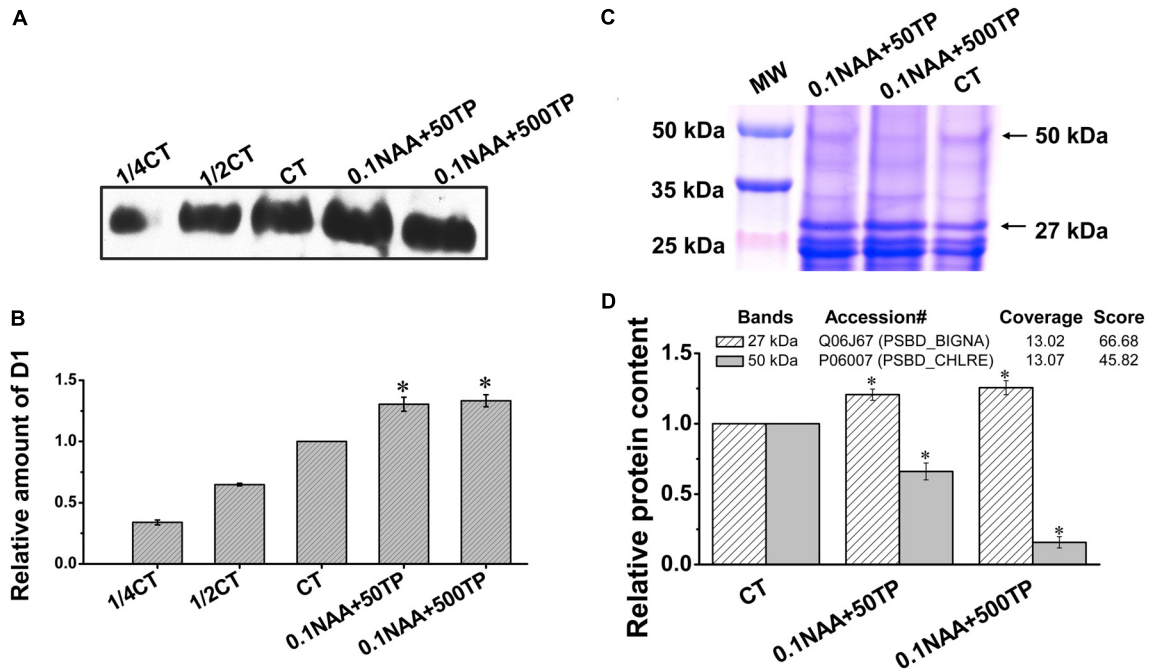

FIGURE 5 | Quantification analysis of photosynthetic proteins of *M. afer* under different culture conditions. **(A)** Western-blot analyses of D1 protein under different culture conditions. Thylakoid membrane proteins were separated by 12% SDS-PAGE and subsequently probed with D1 antibody. Thylakoid samples were loaded on the basis of equivalent total protein content (15 μg) in each lane. 1/4 CT and 1/2 CT: a fourfold and twofold dilution of extract of control group. **(B)** The amounts of D1 in *M. afer* harvested from different culture conditions were calculated based on the gray analysis of western-blot by Image J software. **(C)** Isolated thylakoid membrane proteins under different culture conditions on SDS-PAGE. Thylakoid samples were loaded on the basis of equivalent total protein content (15 μg) in each lane. **(D)** Semi-quantification analysis of two target bands (27 and 50 kDa) according to their gray scale. Values are means ± SE (n = 3). The insert table showed the protein predicted by LC–MS/MS. Asterisks indicate statistically significant differences compared with the control group (*$p < 0.05$; ANOVA).

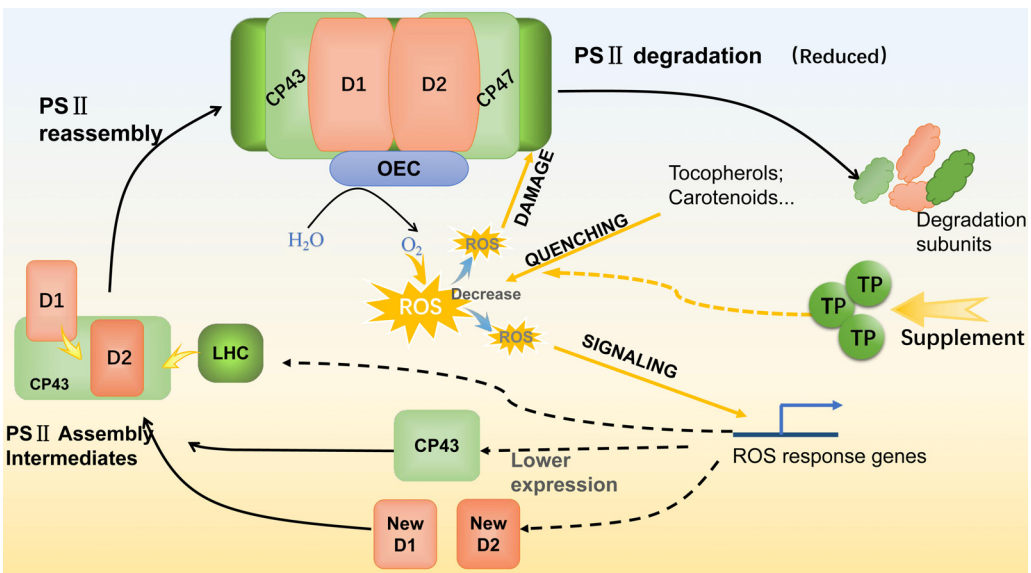

FIGURE 6 | Schematic diagram of the PSII repair cycle under the supplement of TP. With TP supplement, ROS quenching was enhanced and lead to the decrease of ROS for damage and signaling processes. As the result of less ROS damaging, PSII degradation was reduced and performed as the increasing of D1 and D2 content. For ROS signaling, a less amount of CP43 gives the hint that PSII re-assembly process was decelerated. Colored squares are core protein components (D1, D2, CP43, CP47, LHC, and OEC) of PSII. LHC, light harvesting complex; OEC, oxygen evolving complex.

(Perrot-Rechenmann, 2010). Nowadays, the presence of auxins in algal lineages were also demonstrated, and parts of their effects on cell growth and development were uncovered (Lu and Xu, 2015). Microalgae might have similar auxin signal and response system of plants (Lau et al., 2009). Auxin signaling, like transport inhibitor response1-auxin signaling F-box protein (TIR1-AFB), auxin response factor (ARF) and auxin-indole-3-acetic acid proteins (AUX-IAA), has been studied (Gray et al., 2001; Tiwari et al., 2003; Parry et al., 2009). Evidence for phytohormone function in microalgae is rare but beginning to accumulate. For instance, auxin was demonstrated to induce cell division in the unicellular *desmid Micrasterias thomasiana* (*Charophyta*) and *Chlorella pyrenoidosa* (*Chlorophyta*) (Wood and Berliner, 1979; Vance, 1987). Two AUX-IAAs were presented in *C. reinhardtii* (Palenik et al., 2007). As exogenous synthetic auxin, effects of NAA on the growth and lipid accumulation of *M. afer* were investigated in this study. According to the orthogonal experiments, the cell growth of *M. afer* would be promoted by NAA at the concentration below 1 mg/L, further it was confirmed by the single factor analysis with 0.1 mg/L NAA treatment. This concentration brought the most significant effect to the growth of *M. afer* at the 2nd day after supplement, which may be due to the regulatory effect of NAA in cell division (Palenik et al., 2007). Furthermore, NAA was stable in the culture system, and had a better growth promoting effect when combined with TP supplement in the later growth stage of *M. afer*.

The growth and lipid accumulation of *M. afer* were promoted with antioxidant supplement in our study. TP includes catechins, theaflavins, tannins, and flavonoids. Catechins are the main component of TP (60–80%), and are mainly composed of EGCG (50%), epicatechin-3-gallate (ECG, 20%), epigallocatechin (EGC, 20%), epicatechin (EC), catechin, and gallocatechin (GC) (Lin et al., 1996; Frei and Higdon, 2003). TP and EGCG were investigated as antioxidant additives in this study, and showed similar effects on *M. afer* growth. Due to the consideration of large-scale production application, TP would be more economical and it was selected for further investigation in this work. With the addition of 0.1 mg/L NAA and 500 mg/L TP, the final lipid yield of *M. afer* was 2.15 g/L, which was 39.6% higher than control. The extra fee for additives addition mainly comes from TP, whose price is 60–80 CNY per kilogram for large-scale food grade raw material procurement. It only additional accounted for 15–20 CNY to harvest 1 kg of algae oil with high NA content (5%).

With the supplement of NAA and TP, the variation of intracellular ROS level was observed, the changes of photosynthetic efficiency were also significant. As a photosynthetic organism, algae converted light energy into chemical energy for life activities or stored in the form of biochemical compounds. However, the excess light energy could lead to excess ROS accumulation and photo-oxidative damage to the photosynthetic apparatus (Mullineaux and Karpinski, 2002). Photosynthetic organisms need to alleviate the detrimental effects of high ROS stress, especially under stressful conditions (Kolber et al., 1988). In this work, there was an obvious linear relationship between the photosynthetic efficiency and intracellular ROS level. As expected, *M. afer* cultured with TP was detected a lower ROS level, MDA content, and CAT activity than the control. These indicated that the cells of *M. afer* cultured with TP supplement were under lower oxidant stress (Zhang et al., 2013). The variation of CAT activity was due to the ROS quenching effort of TP, lower activity of CAT is enough for the ROS neutralization. Further analysis of thylakoid membrane proteins by SDS-PAGE and western-blot analysis, the amounts of D1 and D2 proteins in cells cultured with TP were higher than the control, while the amounts of CP43 protein decreased 84.2% compared with the control. We speculated that TP possesses the function of slowing down the damage of PSII by scavenging excess intracellular ROS and resulting the higher amount of D1 and D2 in the cells. Photo-oxidative damages of PS II are frequently generated by breaking its reaction center and damaging the thylakoid membranes. Organisms maintain the photosynthetic ability through an intricate repair mechanism involving degradation of the damaged D1 reaction center protein and re-assembly by fresh core skeleton proteins into the photosynthetic system (Andersson and Aro, 2001). Under stress conditions, the rate of photo-oxidative damage exceeds the capacity of self-repair, which leads to a decrease of D1 and D2 abundance in photosynthetic system (Krieger-Liszkay et al., 2008). The higher amounts of D1 and D2 proteins might indicated a less degradation of PSII (Erickson et al., 2015). Moreover, instead of the previously known function of CP43, which acted as one of the core PSII antenna proteins. It was also demonstrated the Loop E of CP43 played a crucial role in the assembly of the water oxidizing center during PSII biosynthesis. The structural dynamics of the luminal domain of CP43 determined its role in the assembly of functional PSII centers (Liu et al., 2013). The reduction of CP43 could be associated with the retard of PSII assembly. Based on these, we hypothesis that the ROS level could play a role on the expression of CP43. This was confirmed by our results of ROS analysis. When cells were supplemented with TP, they had a lower ROS level, which lead to a less PSII degradation. Furthermore, the lower ROS level would cause the down-regulation of CP43 protein and less re-assembly of PSII. The regulation pathway from ROS to CP43 is interesting and will be analyzed by future research. In summary, supplement of TP enhanced ROS quenching, therefore the amount of ROS targeted to PSII damage and PSII repair signaling was decreased, which leaded to a less PSII damage (**Figure 6**). As a result, TP could reduce the damage of PSII by scavenging intracellular excess ROS at later growth stage. The cells supplied with NAA and TP could get higher growth rate, the energy and reducing power could accumulated in the form of fatty acids.

AUTHOR CONTRIBUTIONS

YF: conceived and designed the experiments. FX, YF, and G-RH: performed the experiments. YF, FM, and JS: analyzed

the data and discussed the results. YF, FX, F-LL, and GY: wrote the paper.

FUNDING

This work was supported by China Agriculture Research System (CARS-34), the Forage Industrial Innovation Team, Shandong Modern Agricultural Industrial and Technical System (SDAIT-23-01), and a grant from the National Natural Science Foundation of China (31602154).

ACKNOWLEDGMENTS

We thank Eike Krautter for proof reading the manuscript and discussion.

SUPPLEMENTARY MATERIAL

The Supplementary Material for this article can be found online at: https://www.frontiersin.org/articles/10.3389/fpls.2018.00506/full#supplementary-material

REFERENCES

Andersson, B., and Aro, E.-M. (2001). "Photodamage and D1 protein turnover in photosystem II," in *Regulation of Photosynthesis*, eds E.-M. Aro and B. Andersson (Berlin: Springer), 377–393. doi: 10.1007/0-306-48148-0_22

Bai, J., Rodriguez, A. M., Melendez, J. A., and Cederbaum, A. I. (1999). Overexpression of catalase in cytosolic or mitochondrial compartment protects HepG2 cells against oxidative injury. *J. Biol. Chem.* 274, 26217–26224. doi: 10.1074/jbc.274.37.26217

Bigogno, C., Khozin-Goldberg, I., Boussiba, S., Vonshak, A., and Cohen, Z. (2002). Lipid and fatty acid composition of the green oleaginous alga *Parietochloris incisa*, the richest plant source of arachidonic acid. *Phytochemistry* 60, 497–503. doi: 10.1016/S0031-9422(02)00100-0

Cavas, L., and Yurdakoc, K. (2005). A comparative study: assessment of the antioxidant system in the invasive green alga *Caulerpa racemosa* and some macrophytes from the Mediterranean. *J. Exp. Mar. Biol. Ecol.* 321, 35–41. doi: 10.1016/j.jembe.2004.12.035

Chen, W., Zhang, C., Song, L., Sommerfeld, M., and Hu, Q. (2009). A high throughput Nile red method for quantitative measurement of neutral lipids in microalgae. *J. Microbiol. Methods* 77, 41–47. doi: 10.1016/j.mimet.2009.01.001

Chisti, Y. (2007). Biodiesel from microalgae. *Biotechnol. Adv.* 25, 294–306. doi: 10.1016/j.biotechadv.2007.02.001

Choo, K. S., Snoeijs, P., and Pedersén, M. (2004). Oxidative stress tolerance in the filamentous green algae *Cladophora glomerata* and *Enteromorpha ahlneriana*. *J. Exp. Mar. Biol. Ecol.* 298, 111–123. doi: 10.1016/j.jembe.2003.08.007

Coupland, K., and Langley, N. A. (1993). Use of nervonic acid and long chain fatty acids for the treatment of demyelinating disorders. U.S. Patent No. 5,194,448. Washington, DC: U.S. Patent and Trademark Office.

Erickson, E., Wakao, S., and Niyogi, K. K. (2015). Light stress and photoprotection in *Chlamydomonas reinhardtii*. *Plant J.* 82, 449–465. doi: 10.1111/tpj.12825

Fan, Y., Meng, H. M., Hu, G. R., and Li, F. L. (2018a). Biosynthesis of nervonic acid and perspectives for its production by microalgae and other microorganisms. *Appl. Microbiol. Biotechnol.* 102, 3027–3035. doi: 10.1007/s00253-018-8859-y

Fan, Y., Yuan, C., Jin, Y., Hu, G. R., and Li, F. L. (2018b). Characterization of 3-ketoacyl-coA synthase in a nervonic acid producing oleaginous microalgae *Mychonastes afer*. *Algal Res.* 31, 225–231. doi: 10.1016/j.algal.2018.02.017

Frei, B., and Higdon, J. V. (2003). Antioxidant activity of tea polyphenols in vivo: evidence from animal studies. *J. Nutr.* 133, 3275S–3284S. doi: 10.1093/jn/133.10.3275S

Geider, R. J., Roche, J., Greene, R. M., and Olaizola, M. (1993). Response of the photosynthetic apparatus of *Phaeodactylum tricornutum* (Bacillariophyceae) to nitrate, phosphate, or iron starvation. *J. Phycol.* 29, 755–766. doi: 10.1111/j.0022-3646.1993.00755.x

Gray, W. M., Kepinski, S., Rouse, D., Leyser, O., and Estelle, M. (2001). Auxin regulates SCFTIR1-dependent degradation of AUX/IAA proteins. *Nature* 414, 271–276. doi: 10.1038/35104500

Hu, G., Fan, Y., Zhang, L., Yuan, C., Wang, J., Li, W., et al. (2013). Enhanced lipid productivity and photosynthesis efficiency in a *Desmodesmus* sp. mutant induced by heavy carbon ions. *PLoS One* 8:e60700. doi: 10.137/journal.pone.0060700

Hu, Q., Sommerfeld, M., Jarvis, E., Ghirardi, M., Posewitz, M., Seibert, M., et al. (2008). Microalgal triacylglycerols as feedstocks for biofuel production: perspectives and advances. *Plant J.* 54, 621–639. doi: 10.1111/j.1365-313X.2008.03492.x

Ikeuchi, M., and Inoue, Y. (1988). A new 4.8-kDa polypeptide intrinsic to the PS II reaction center, as revealed by modified SDS-PAGE with improved resolution of low-molecular-weight proteins. *Plant Cell Physiol.* 29, 1233–1239. doi: 10.1093/oxfordjournals.pcp.a077628

Kato, J., Yamahara, T., Tanaka, K., Takio, S., and Satoh, T. (1997). Characterization of catalase from green algae *Chlamydomonas reinhardtii*. *J. Plant Physiol.* 151, 262–268. doi: 10.1016/S0176-1617(97)80251-9

Klughammer, C., and Schreiber, U. (2008). Complementary PS II quantum yields calculated from simple fluorescence parameters measured by PAM fluorometry and the Saturation Pulse method. *PAM Appl. Notes* 1, 201–247.

Kolber, Z., Zehr, J., and Falkowski, P. (1988). Effects of growth irradiance and nitrogen limitation on photosynthetic energy conversion in photosystem II. *Plant Physiol.* 88, 923–929. doi: 10.1104/pp.88.3.923

Krieger-Liszkay, A., Fufezan, C., and Trebst, A. (2008). Singlet oxygen production in photosystem II and related protection mechanism. *Photosynth. Res.* 98, 551–564. doi: 10.1007/s11120-008-9349-3

Lau, S., Shao, N., Bock, R., Jürgens, G., and De Smet, I. (2009). Auxin signaling in algal lineages: fact or myth? *Trends Plant Sci.* 14, 182–188. doi: 10.1016/j.tplants.2009.01.004

Li, Y., Han, D., Sommerfeld, M., and Hu, Q. (2011). Photosynthetic carbon partitioning and lipid production in the oleaginous microalga *Pseudochlorococcum* sp. (Chlorophyceae) under nitrogen-limited conditions. *Bioresour. Technol.* 102, 123–129. doi: 10.1016/j.biortech.2010.06.036

Lin, Y.-L., Juan, I.-M., Chen, Y.-L., Liang, Y.-C., and Lin, J.-K. (1996). Composition of polyphenols in fresh tea leaves and associations of their oxygen-radical-absorbing capacity with antiproliferative actions in fibroblast cells. *J. Agric. Food Chem.* 44, 1387–1394. doi: 10.1021/jf950652k

Liu, F., and Pang, S. J. (2010). Stress tolerance and antioxidant enzymatic activities in the metabolisms of the reactive oxygen species in two intertidal red algae *Grateloupia turuturu* and *Palmaria palmata*. *J. Exp. Mar. Biol. Ecol.* 382, 82–87. doi: 10.1016/j.jembe.2009.11.005

Liu, H., Chen, J., Huang, R. Y.-C., Weisz, D., Gross, M. L., and Pakrasi, H. B. (2013). Mass spectrometry-based footprinting reveals structural dynamics of loop E of the chlorophyll-binding protein CP43 during photosystem II assembly in the cyanobacterium *Synechocystis* 6803. *J. Biol. Chem.* 288, 14212–14220. doi: 10.1074/jbc.M113.467613

Liu, J., Dietz, K., DeLoyht, J. M., Pedre, X., Kelkar, D., Kaur, J., et al. (2012a). Impaired adult myelination in the prefrontal cortex of socially isolated mice. *Nat. Neurosci.* 15, 1621–1623. doi: 10.1038/nn.3263

Liu, J., Yang, H., Lu, Q., Wen, X., Chen, F., Peng, L., et al. (2012b). PSBP-DOMAIN PROTEIN1, a nuclear-encoded thylakoid lumenal protein, is essential for photosystem I assembly in *Arabidopsis*. *Plant Cell* 24, 4992–5006. doi: 10.1105/tpc.112.106542

Lu, Y., and Xu, J. (2015). Phytohormones in microalgae: a new opportunity for microalgal biotechnology? *Trends Plant Sci.* 20, 273–282. doi: 10.1016/j.tplants.2015.01.006

Mittler, R. (2002). Oxidative stress, antioxidants and stress tolerance. *Trends Plant Sci.* 7, 405–410. doi: 10.1016/S1360-1385(02)02312-9

Mullineaux, P., and Karpinski, S. (2002). Signal transduction in response to excess light: getting out of the chloroplast. *Curr. Opin. Plant Biol.* 5, 43–48. doi: 10.1016/S1369-5266(01)00226-6

Munne-Bosch, S. (2005). The role of α-tocopherol in plant stress tolerance. *J. Plant Physiol.* 162, 743–748. doi: 10.1016/j.jplph.2005.04.022

Palenik, B., Grimwood, J., Aerts, A., Rouzé, P., Salamov, A., Putnam, N., et al. (2007). The tiny eukaryote *Ostreococcus* provides genomic insights into the paradox of plankton speciation. *Proc. Natl. Acad. Sci. U.S.A.* 104, 7705–7710. doi: 10.1073/pnas.0611046104

Park, W.-K., Yoo, G., Moon, M., Kim, C. W., Choi, Y.-E., and Yang, J.-W. (2013). Phytohormone supplementation significantly increases growth of *Chlamydomonas reinhardtii* cultivated for biodiesel production. *Appl. Biochem. Biotechnol.* 171, 1128–1142. doi: 10.1007/s12010-013-0386-9

Parry, G., Calderon-Villalobos, L., Prigge, M., Peret, B., Dharmasiri, S., Itoh, H., et al. (2009). Complex regulation of the TIR1/AFB family of auxin receptors. *Proc. Natl. Acad. Sci. U.S.A.* 106, 22540–22545. doi: 10.1073/pnas.0911967106

Perrot-Rechenmann, C. (2010). Cellular responses to auxin: division versus expansion. *Cold Spring Harb. Perspect. Biol.* 2:a001446. doi: 10.1101/cshperspect.a001446

Pinto, E., Sigaud-kutner, T., Leitao, M. A., Okamoto, O. K., Morse, D., and Colepicolo, P. (2003). Heavy metal-induced oxidative stress in algae. *J. Phycol.* 39, 1008–1018. doi: 10.1111/j.0022-3646.2003.02-193.x

Piotrowska-Niczyporuk, A., and Bajguz, A. (2014). The effect of natural and synthetic auxins on the growth, metabolite content and antioxidant response of green alga *Chlorella vulgaris* (Trebouxiophyceae). *Plant Growth Regul.* 73, 57–66. doi: 10.1007/s10725-013-9867-7

Sandhir, R., Khan, M., Chahal, A., and Singh, I. (1998). Localization of nervonic acid β-oxidation in human and rodent peroxisomes: impaired oxidation in Zellweger syndrome and X-linked adrenoleukodystrophy. *J. Lipid Res.* 39, 2161–2171.

Sargent, J., Coupland, K., and Wilson, R. (1994). Nervonic acid and demyelinating disease. *Med. Hypotheses* 42, 237–242. doi: 10.1016/0306-9877(94)90122-8

Schnettger, B., Critchley, C., Santore, U., Graf, M., and Krause, G. (1994). Relationship between photoinhibition of photosynthesis, D1 protein turnover and chloroplast structure: effects of protein synthesis inhibitors. *Plant Cell Environ.* 17, 55–64. doi: 10.1111/j.1365-3040.1994.tb00265.x

Shi, S., Tang, D., and Liu, Y. (2009). Effects of an algicidal bacterium *Pseudomonas mendocina* on the growth and antioxidant system of *Aphanizomenon flos-aquae*. *Curr. Microbiol.* 59, 107–112. doi: 10.1007/s00284-009-9404-0

Tiwari, S. B., Hagen, G., and Guilfoyle, T. (2003). The roles of auxin response factor domains in auxin-responsive transcription. *Plant Cell* 15, 533–543. doi: 10.1105/tpc.008417

Vance, B. D. (1987). Phytohormone effects on cell division in *Chlorella pyrenoidosa* chick (TX-7-11-05) (Chlorellaceae). *J. Plant Growth Regul.* 5, 169–173. doi: 10.1007/BF02087185

Wellburn, A. R. (1994). The spectral determination of chlorophylls a and b, as well as total carotenoids, using various solvents with spectrophotometers of different resolution. *J. Plant Physiol.* 144, 307–313. doi: 10.1016/S0176-1617(11)81192-2

Williams, P. J. L., and Laurens, L. M. L. (2010). Microalgae as biodiesel & biomass feedstocks: review & analysis of the biochemistry, energetics & economics. *Energy Environ. Sci.* 3, 554–590. doi: 10.1039/B924978H

Wolf, G. (2005). The discovery of the antioxidant function of vitamin E: the contribution of Henry A. Mattill. *J. Nutr.* 135, 363–366. doi: 10.1093/jn/135.3.363

Wood, N. L., and Berliner, M. D. (1979). Effects of indoleacetic acid on the desmid *Micrasterias thomasiana*. *Plant Sci. Lett.* 16, 285–289. doi: 10.1016/0304-4211(79)90040-3

Yuan, C., Liu, J., Fan, Y., Ren, X., Hu, G., and Li, F. (2011). *Mychonastes afer* HSO-3-1 as a potential new source of biodiesel. *Biotechnol. Biofuels* 4:47. doi: 10.1186/1754-6834-4-47

Yuan, C., Xu, K., Sun, J., Hu, G. R., and Li, F. L. (2017). Ammonium, nitrate, and urea play different roles for lipid accumulation in the nervonic acid - producing microalgae *Mychonastes afer* HSO-3-1. *J. Appl. Phycol.* 1–9. doi: 10.1007/s10811-017-1308-y

Zhang, Y.-M., Chen, H., He, C.-L., and Wang, Q. (2013). Nitrogen starvation induced oxidative stress in an oil-producing green alga *Chlorella sorokiniana* C3. *PLoS One* 8:e69225. doi: 10.1371/journal.pone.0069225

Conflict of Interest Statement: The authors declare that the research was conducted in the absence of any commercial or financial relationships that could be construed as a potential conflict of interest.

frontiers in Plant Science

METHODS
published: 11 April 2018
doi: 10.3389/fpls.2018.00439

Engineering the Chloroplast Genome of Oleaginous Marine Microalga *Nannochloropsis oceanica*

Qinhua Gan[1], *Jiaoyun Jiang*[1], *Xiao Han*[1], *Shifan Wang*[1,2] *and Yandu Lu*[1,2]*

[1] State Key Laboratory of Marine Resource Utilization in South China Sea, College of Oceanology, Hainan University, Haikou, China, [2] Key Laboratory of Tropical Biological Resources, Ministry of Education, Hainan University, Haikou, China

Plastid engineering offers an important tool to fill the gap between the technical and the enormous potential of microalgal photosynthetic cell factory. However, to date, few reports on plastid engineering in industrial microalgae have been documented. This is largely due to the small cell sizes and complex cell-wall structures which make these species intractable to current plastid transformation methods (i.e., biolistic transformation and polyethylene glycol-mediated transformation). Here, employing the industrial oleaginous microalga *Nannochloropsis oceanica* as a model, an electroporation-mediated chloroplast transformation approach was established. Fluorescent microscopy and laser confocal scanning microscopy confirmed the expression of the green fluorescence protein, driven by the endogenous plastid promoter and terminator. Zeocin-resistance selection led to an acquisition of homoplasmic strains of which a stable and site-specific recombination within the chloroplast genome was revealed by sequencing and DNA gel blotting. This demonstration of electroporation-mediated chloroplast transformation opens many doors for plastid genome editing in industrial microalgae, particularly species of which the chloroplasts are recalcitrant to chemical and microparticle bombardment transformation.

Keywords: *Nannochloropsis*, plastid transformation, oleaginous microalga, green fluorescent protein, photosynthetic cell factory

OPEN ACCESS

Edited by:
Junhua Peng,
Center for Life Sci&Tech of China National Seed Group Co. Ltd., China

Reviewed by:
Liang Chen,
University of Chinese Academy of Sciences (UCAS), China
Man Zhou,
University of Minnesota, United States

***Correspondence:**
Yandu Lu
ydlu@hainu.edu.cn

Specialty section:
This article was submitted to Plant Biotechnology, a section of the journal Frontiers in Plant Science

Received: *07 September 2017*
Accepted: *21 March 2018*
Published: *11 April 2018*

Citation:
Gan Q, Jiang J, Han X, Wang S and Lu Y (2018) Engineering the Chloroplast Genome of Oleaginous Marine Microalga Nannochloropsis oceanica. Front. Plant Sci. 9:439. doi: 10.3389/fpls.2018.00439

INTRODUCTION

Microalga-based biochemical factory is regarded as an ideal strategy for sequestering greenhouse gas and producing valuable molecules ranging from therapeutic proteins to biofuels (Tran et al., 2013; Moody et al., 2014). However, few natural strains exhibit the demanding traits as feedstock for biofuel production which have led to a quest for more specific genomic and biological models (Scott et al., 2010; Ge et al., 2014). *Nannochloropsis* spp. have attracted sustained interest from algal biofuels researchers owing to their rapid growth, high amounts of triacylglycerol (TAG) and high-value polyunsaturated fatty acid (FA) and their successful cultivation at large scale using natural sunlight by multiple institutes and companies (Radakovits et al., 2012; Vieler et al., 2012; Wang et al., 2012, 2014; Corteggiani Carpinelli et al., 2014; Lu et al., 2014a,b; Moody et al., 2014; Lu and Xu, 2015; Ajjawi et al., 2017; Wei H. et al., 2017; Zienkiewicz et al., 2017).

Genetic engineering of industrial microalgae provides a viable way to optimize crucial traits for commercial feedstock development (Gimpel et al., 2013; Zhang and Hu, 2014; Wang et al., 2016; Cui et al., 2018). A nuclear transformation method has been developed for *Nannochloropsis* sp.

(Kilian et al., 2011; Vieler et al., 2012; Li et al., 2014; Iwai et al., 2015; Kang et al., 2015; Poliner et al., 2017; Xin et al., 2017), which facilitates the manipulation of crucial nodes in oil biosynthesis and the development of the RNA interference (RNAi) (Wei L. et al., 2017) and CRISPR/Cas9 methods (Wang et al., 2016). However, the plastome genetic engineering tools are not yet avaiable for *Nannochloropsis* spp. There are considerable attractions associated with placing transgenes into the plastid genome rather than the nuclear genome (Bock, 2014; Doron et al., 2016), particularly where plastid genomes are engineered to express valuable proteins (e.g., therapeutics proteins) (Tran et al., 2013): (i) high transgene expression levels; (ii) capacity for expressing multigene in artificial operons; (iii) devoid of gene silencing and other epigenetic mechanisms; (iv) higher precise insertion site than nuclear expression (which normally integrate foreign DNA into their nuclear genomes by non-homologous recombination).

Besides the manipulation of plastid genes (with a number of ∼100) (Wei et al., 2013), transplastomic technology may utilized to express heterologous genes or gene clusters with economic values (e.g., pharmaceutical proteins) (Mayfield et al., 2007; Rasala et al., 2010). Moreover, ∼10% of the nuclear gene products (mainly FA biosynthetic enzymes and photosynthesis related proteins which determine the key features of oleaginous microalgae for biofuel production) are targeted to plastids (Leister, 2003). This further expands the plastome engineering gene repertoire. Thus, transplastomic technology provided fundamental opportunities for rational trait-improvement of microalgae (Bock, 2014).

Although progresses have been made for several reference plants, plastid transformation is still restricted to a relatively small number of species (Bock, 2014). This is mainly due to the fastidious requirements in cell handling to match the methods currently available for plastid transformation (Maliga, 2004). For instance, although microparticle bombardment is a rountine pratice to delivery exogenous DNA into plant or microalgal plastids, it has a rigid requirement to cell diameters of target species (Cui et al., 2014). Genetic manipulation of chloroplasts of small-size microalgal species is intractable due to the limitation of availablity of golden particles (of which the smallest diameter is 0.6 μm). Therefore, biolistic plastid transformation have only been developed for a few micoalgal species (exclusively for species with relatively large cell sizes and huge chloroplasts), e.g., *Chlamydomonas reinhardtii* (with a diameter of ∼10 μm) (Boynton et al., 1988), red alga *Porphyridium* sp. (with a diameter of ∼15 μm) (Lapidot et al., 2002) and green alga *Platymonas subcordiformis* (with a diameter of ∼15 μm) (Cui et al., 2014). However, as for most industrial microalgal species of which the diameters are approximately a few microns (e.g., *Nannochloropsis* sp. and *Chlorella* sp., both with a diameter of ∼2 μm), plastome genetic engineering tools have not yet been developed. Polyethylene glycol (PEG) treatment of protoplasts provides an alternative way for chloroplast transformation (Golds et al., 1993). However, as all protoplast-based methods, PEG-mediated protoplast transformation requires removal of the cell wall prior to transformation (or, alternatively, use of cell wall-deficient mutant strains), which makes the procedures technically demanding, labor intensive, and time consuming (Bock, 2015). Even worse, protoplast preparation is always intractable to most microalgal species of which the cell wall is complex (Maliga and Bock, 2011). Therefore, research and development of plastid biotechnology remain challenge for most industrial microalgae.

During the creation of nuclear mutagenesis library for industrial oleaginous microalga *Nannochloropsis oceanica*, we found that antibiotic constructs were inserted into the plastid genome by electroporation. A similar phenomenon has also been documented in *C. reinhardtii* (Zhang et al., 2014; Li et al., 2016). Therefore, to probe the potential of applying electroporation in chloroplast transformation, employing *N. oceanica* as a model, a simple and rapid approach for chloroplast transformation was developed for *N. oceanica*.

MATERIALS AND METHODS

Gene Cloning and Vector Construction

Genomic DNA was extracted using Plant Genomic DNA Extraction Kit (Omega, China) following a described procedure (Lu et al., 2009, 2010). *N. oceanica* endogenous *chlL* gene fragments, *rbcL* promoter and *psbA* terminator were amplified using sequence specific primers (Supplementary Table 1). The upstream and downstream fragments of *chlL* gene were subcloned into pBluescript SK vector (Stratagene, USA) using *Kpn*I, *Xho*I and *Sac*I, *Bam*HI sites, respectively. The *rbcL* promoter and *psbA* terminator were subsequently ligated into the resulting vector between the *Xho*I, *Hind*III and *Eco*RV, *Eco*RI sites, respectively. The codon optimized *gfp* gene was synthesized by Sangon Biotech (Shanghai, China) and was ligated into the above vector with a *Hind*III restriction site at the 5′ end and an *Eco*RV site at the 3′ end of the coding region. All enzymes were commercially available from New England BioLabs (NEB, UK). The obtained vector was nominated as pMEMc1. The zeosin resistance (BLE) gene was amplified from vector pSP124 using primers BLE-F and BLE-R (Supplementary Table 1). The *gfp* gene of pMEMc1 was substituted by the *BLE* gene and generated vector pMEMc2.

Strains, Transformation, and Growth Conditions

N. oceanica was inoculated into modified f/2 liquid medium, which was prepared as early description (Gan et al., 2017). The cells were grown in liquid cultures under continuous light (∼50 μmol photons m^{-2} s^{-1}) at 25°C. Transformation was conducted as description with minor modification (Wang et al., 2016; Xin et al., 2017). Vectors were linearized by restriction digestion, and purified and concentrated by ethanol precipitation. Microalgal cells at early log phase were harvested by centrifugation at 5,000 g for 5 min at 4°C. Cells were washed with sorbitol at 4°C. For each transformation reaction, 4×10^8 cells were mixed with 1 μg transforming cassette DNA. The mixture was added into a cuvette (Bio-Rad, 2 mm) and pulsed using GenePulse Xcell™ (BioRad) apparatus with 12 kV cm^{-1} field strength, 50 μF capacitance, and 600 Ohm shunt resistance. The cells were immediately transferred into fresh f/2 medium and recovered under dim light for 48 h. For pMEMc1 transformants,

GFP fluorescence was observed at indicated intervals while for pMEMc2 transformants, cells were plated on solid f/2 with 2.5 μg ml^{-1} zeosin (Solarbio, China) and colonies appeared after ~4 weeks.

GFP Expression Detection of pMEMc1 Transformants

An Olympus BX51 microscope (Olympus, Japan), fitted with epifluorescence and differential interference contrast (DIC) optics, was used to visualize pMEMc1 transformants grown in liquid. Images were generated by either DIC or epifluorescence (excitation, 488 nm; emission, 520 nm) optics. An Olympus FluoView^{TM} FV1000 system was used to obtain laser confocal scanning microscope (LSCM) images of pMEMc1 transformants. Excitation at 488 and 559 nm were used for GFP and chlorophyll autofluorescence, respectively.

Genotyping of pMEMc2 Transformants

Approximately 10 mL cultures of wild-type and pMEMc2-transformed cells were harvested by centrifugation (7,000 rpm, 3 min at 4°C). The cell pellet was washed twice, and then genomic DNA was extracted. Genomic PCR was used to confirm the homoplasmic integration of the vector into the plastid genome of transgenic lines. With the primers crossing *chlL* gene regions (c2-F and c2-R; Supplementary Table 1 and **Figure 1**), 0.6 and 1.9 kb PCR products were expected to be detected for wild type and homoplasmic transformed cells (all copies of the chloroplast genome contained the *ble* gene), respectively. By contrast, for cells harboring heterogeneous chloroplast genomes, PCR amplification should generate both of the two bands (i.e., 0.6 and 1.9 kb DNA bands). All PCR fragments were purified (Cycle-Pure Kit, Omega, China) and sequenced (Sangon, China). Integration events were further analyzed by DNA gel blotting using non-radioactive DIG-containing ble gene probes (PCR DIG probe synthesis kit; Roche Diagnostics). The *ble* gene probes were labeled with DIG-dUTP using a pair of primer (BLE-F and BLE-R; Supplementary Table 1). Genomic DNA was digested with restriction enzyme *Hind*III or *Pst*I, separated on 0.8% agarose gels, blotted, hybridized, and visualized.

RESULTS

Design and Construction of Destination Vectors

To facilitate visualization of protein expression, the green florescence protein gene (*gfp*) was used as a reporter (**Figure 1**) and codon-optimized based on the featured codon bias and a high AT content (66.4%) of the *N. oceanica* chloroplast genome (Wei et al., 2013). The GFP gene was driven by an endogenous promoter (large subunit of RuBisCO, *rbcL*) and terminated by an endogenous terminator (3′ flanking sequence of gene encoding the D1 protein of Photosystem II, *psbA*) (**Figure 1** and Supplementary Dataset 1). This expression cassette contains homology to the chlorophyll synthetic gene light-independent protochlorophyllide reductase subunit (*chlL*) region of the *N. oceanica* chloroplast genome. Transforming cassette

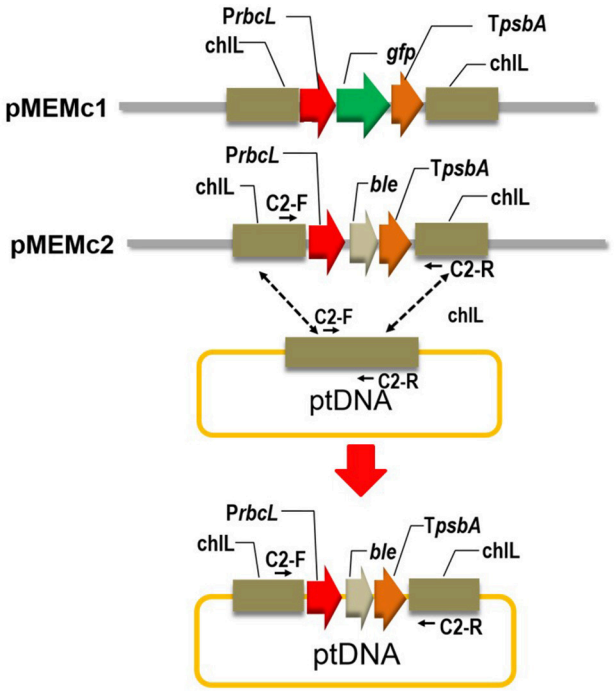

FIGURE 1 | Construct map of homologous recombinant vector in *N. oceanica* chloroplast. P*rbcL*, promoter of large subunit of RuBisCO gene (*rbcL*); T*psbA*, 3′ flanking sequence of gene encoding the D1 protein of Photosystem II (*psbA*); *gfp*, green florescence protein gene; chlL, light-independent protochlorophyllide reductase subunit; *ble*, zeosin resistance gene. Primers designed to examine the homoplasmic integration of the transforming cassette is indicated (c2-F and c2-R; Supplementary Table 1).

will insert into the *chl*L locus by homologous recombination in expected transformants (**Figure 1**). Transformation construct harboring *gfp* gene (*chlL-rbcL-gfp-psbA-chlL*) were cloned into the plasmid pBluescript SK(-) and nominated as pMEMc1. The coding sequence of GFP in the vector was substituted with that of BLE gene and the resulting vector was designated as pMEMc2 (*chlL-rbcL-ble-psbA-chlL*; **Figure 1** and Supplementary Dataset 2).

Introduction of Reporter Genes Into the Chloroplast Genome

To probe the proper *in vivo* functioning of selected plastid promoters and terminators in *N. oceanica*, we started by transforming pMEMc1 cassette into *N. oceanica* wild-type strain by electroporation. Fluorescence microscopy of representative cells revealed that GFP protein was delivered into and expressed in *N. oceanica* (excitation: 488 nm, emission: 500–545 nm; **Figure 2A** and Supplementary Video 1). The number of transformants expressing GFP increased, and reached the highest levels 3 days after pulse. Laser confocal microscopy further confirmed the *in vivo* GFP expression in *N. oceanica* (**Figure 2B**). Despite of a low possibility of functioning in nuclear expression of these utilized plastid promoter and terminator, we cannot exclude the possibility that GFP expressed in nuclear instead of chloroplast.

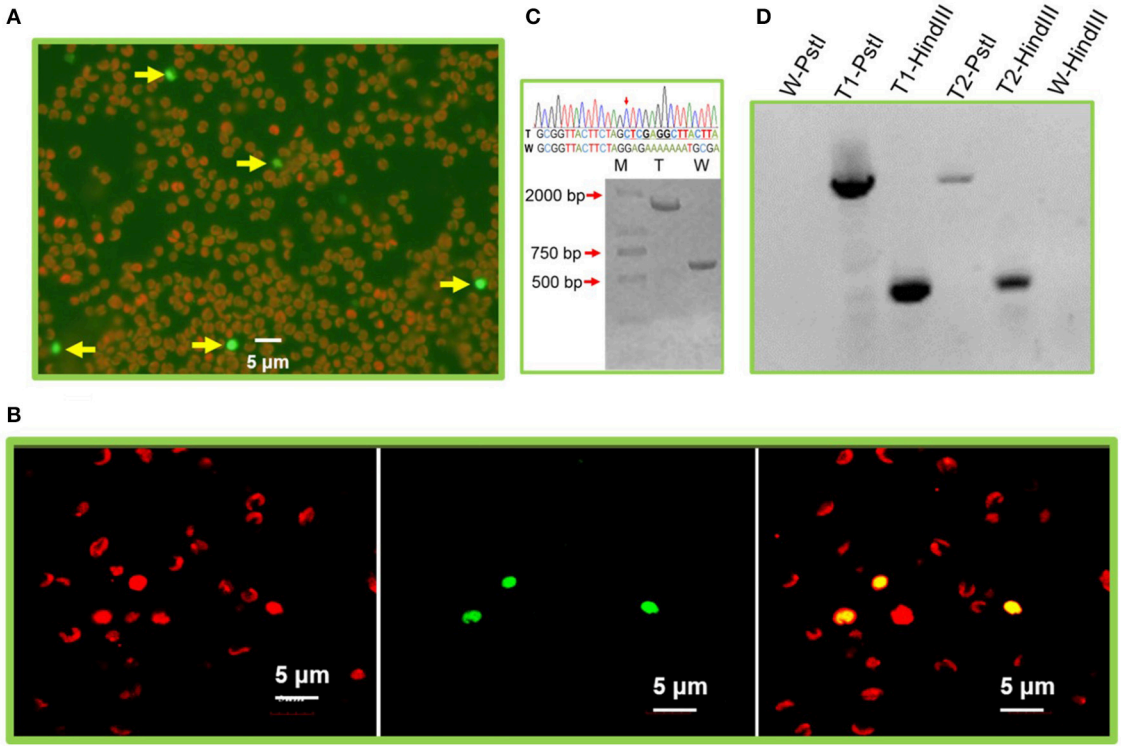

FIGURE 2 | Exogenous gene expression in the *N. oceanica* chloroplast. **(A)** Microscopy images of GFP signals from representative microalgal cells transformed by pMEMc1. The fluorescent micrographs show the GFP expressing cells with green color (excitation: 488 nm, emission: 500–545 nm) and wild type cells with auto red fluorescence of chlorophyll (excitation: 559 nm, emission: 570–650 nm). **(B)** Laser confocal microscopic observation of *N. oceanica* pMEMc1 transformants. Left, chlorophyll fluorescence; middle, GFP fluorescence; right, merged image. **(C)** PCR amplification of wild-type cells and pMEMc2 transformants genomic DNA using c2-F and c2-R primers. PCR product of wild type cells generates a single 0.6 kb DNA band. Homoplasmic cells harbors a 1.3 kb transforming constructs (*rbcL-ble-psbA*) and was expected to generate a single 1.9 kb DNA band. **(D)** DNA gel blot of pMEMc2 transformants. Wild-type cells was used as a control. Genomic DNA was digested with restriction enzyme *Hind*III or *Pst*I and blotted with DIG-dUTP labeled *ble* gene probes. W, Wild-type cells; T, pMEMc2 transformants; -PstI, genomic DNA digested *Pst*I; -HindIII, genomic DNA digested *Hind*III.

Site-Specific Integration of Transgenes Into the Chloroplast Genomes

To validate the homologous recombination of the exogenous constructs into chloroplast genomes, pMEMc2 was transformed into the wild-type *N. oceanica*. Appropriately 4×10^8 *N. oceanica* cells were used for each pulse with 1 μg transforming cassette DNA. The cells were recovered under dim light for 48 h before being plated on f/2 plates containing zeocin (2.5 μg/ml). Approximately eight transformed colonies appeared on the selective plates which translated to a transformation frequency of about 2×10^{-8} μg^{-1} DNA. Two transformants were selected and analyzed for integration and homoplasmicity after multiple rounds of streaking of single colonies under zeocin-resistance selection (no less than four rounds each of which took approximately a month). Genomic PCR and sequencing confirmed that homoplasmic strains (all copies of the chloroplast genome contained the *ble* gene) were obtained and the *rbcL-ble-psbA* constructs (∼1.3 kb) were integrated into all chloroplast genomes through homologous recombination of *chlL* regions (**Figure 2C** and Supplementary Dataset 3). Control reactions using genomic DNA from wild type as templates yield PCR products with a length of ∼0.6 kb because they did not contain the vector sequences (**Figure 2C** and Supplementary Dataset 4). It is not clear whether a single insertion occurred in transformed cells (or whether random insertions happened in transformant genome). Further analysis of integration events was performed by DNA gel blot where a single band was observed by using *ble* probe in either *Hind*III or *Pst*I digested genomic DNA of transformants (**Figure 2D**). Altogether, a stable and targeted transgene integration within the plastid genome was mediated by electroporation.

DISCUSSION AND CONCLUSION

Chloroplast transformation was generally achieved by the biolistic process and ocassionally by PEG-mediated method (Maliga, 2004). However, neither of them is competent for most industrial microalgae. The major bottleneck is the inaccessibility of competent methods for DNA delivery into various microalgae with myriad cell size, complex, and largely unknown cell wall components. Thus, microalgae amenable to plastid transformation have been confined to limited species (Doron et al., 2016). Electroporation, which is normally used for nuclear transformation, was found to be capable of

delivering exogenous DNA into plastid genome of *N. oceanica* (Supplementary Dataset 5) and *C. reinhardtii* (Zhang et al., 2014; Li et al., 2016).

Therefore, the aim of this study is to demonstrate the capacity of electroporation-mediated method in the development of transplastomic technology for species with small cell size and unknown cell-wall components. Using a plastid gene encoding chlorophyll biosynthetic enzyme CHLL as knock-in sites, the *gfp* gene was delivered into and expressed properly in *N. oceanica* by electroporation. Moreover, the antibiotic construct harboring the *ble* gene was utilized to validate the chloroplast integration of transformants. Genotyping of the homoplasmic cells showed a site-specific recombination of the transforming cassette into chloroplast genomes.

Restrictively, herein presented proof-of principle represents a starting point of plastome engineering for *N. oceanica* where the transformation frequency remains to be improved. To ensure the frequency, a standard practice should be developed and more recombination sites and more selectable marker genes should be tested. With a streamlined practice, electroporation should facilitate plastid engineering of relevant species with relative small cell sizes or unknown cell structure of which the chlroroplast manipultion is intractable by using microparticle bombardment or PEG-mediated transformation methods. Given that FA biosynthesis and photosynthesis processes predominantly take place in chloroplasts, transplastomic technology can be utilized to created engineered microalgal strains with optimized oil production and robust photosynthetic efficiency. Moreover, the incorporation of transgenes into the plastid genome for containment and high-level expression of recombinant proteins holds great promise for pharmaceutical and industrial applications.

AUTHOR CONTRIBUTIONS

YL: Design the research; QG, JJ, and XH: Conducted the experiments; YL and SW: Wrote the first version of the manuscript; YL: Contributed to the final writing and presentation of the data.

FUNDING

This work was supported by the Natural Science Foundation of Hainan Province (317010), Project of State Key Laboratory of Marine Resource Utilization in South China Sea (2018004 and 2016005), Foundation of Hainan University (KYQD1561), Project of Innovation & Development of Marine Economy (2017-285), and National Natural Science Foundation of China (31401705, 31660744, and 41466002).

ACKNOWLEDGMENTS

We would like to acknowledge with apologies many excellent studies could not be cited due to space limitations. We are grateful to the reviewers for their valuable improvement to this manuscript.

SUPPLEMENTARY MATERIAL

The Supplementary Material for this article can be found online at: https://www.frontiersin.org/articles/10.3389/fpls.2018.00439/full#supplementary-material

REFERENCES

Ajjawi, I., Verruto, J., Aqui, M., Soriaga, L. B., Coppersmith, J., Kwok, K., et al. (2017). Lipid production in *Nannochloropsis gaditana* is doubled by decreasing expression of a single transcriptional regulator. *Nat. Biotechnol.* 35, 647–652. doi: 10.1038/nbt.3865

Bock, R. (2014). Genetic engineering of the chloroplast: novel tools and new applications. *Curr. Opin. Biotechnol.* 26, 7–13. doi: 10.1016/j.copbio.2013.06.004

Bock, R. (2015). Engineering plastid genomes: methods, tools, and applications in basic research and biotechnology. *Annu. Rev. Plant Biol.* 66, 211–241. doi: 10.1146/annurev-arplant-050213-040212

Boynton, J., Gillham, N., Harris, E., Hosler, J., Johnson, A., Jones, A., et al. (1988). Chloroplast transformation in *Chlamydomonas* with high velocity microprojectiles. *Science* 240, 1534–1538. doi: 10.1126/science.2897716

Corteggiani Carpinelli, E., Telatin, A., Vitulo, N., Forcato, C., D'angelo, M., Schiavon, R., et al. (2014). Chromosome scale genome assembly and transcriptome profiling of *Nannochloropsis gaditana* in nitrogen depletion. *Mol. Plant* 7, 323–335. doi: 10.1093/mp/sst120

Cui, Y., Qin, S., and Jiang, P. (2014). Chloroplast transformation of *Platymonas* (*Tetraselmis*) subcordiformis with the bar gene as selectable marker. *PLoS ONE* 9:e98607. doi: 10.1371/journal.pone.0098607

Cui, Y., Zhao, J., Wang, Y., Qin, S., and Lu, Y. (2018). Characterization and engineering of a dual-function diacylglycerol acyltransferase in the oleaginous marine diatom *Phaeodactylum tricornutum*. *Biotechnol. Biofuels* 11:32. doi: 10.1186/s13068-018-1029-8

Doron, L., Segal, N., and Shapira, M. (2016). Transgene expression in microalgae-from tools to applications. *Front. Plant Sci.* 7:505. doi: 10.3389/fpls.2016.00505

Gan, Q., Zhou, W., Wang, S., Li, X., Xie, Z., Wang, J., et al. (2017). A customized contamination controlling approach for culturing oleaginous *Nannochloropsis oceanica*. *Algal Res.* 27, 376–382. doi: 10.1016/j.algal.2017.07.013

Ge, F., Huang, W., Chen, Z., Zhang, C., Xiong, Q., Bowler, C., et al. (2014). Methylcrotonyl-CoA carboxylase regulates triacylglycerol accumulation in the model diatom *Phaeodactylum tricornutum*. *Plant Cell* 26, 1681–1697. doi: 10.1105/tpc.114.124982

Gimpel, J. A., Specht, E. A., Georgianna, D. R., and Mayfield, S. P. (2013). Advances in microalgae engineering and synthetic biology applications for biofuel production. *Curr. Opin. Chem. Biol.* 17, 489–495. doi: 10.1016/j.cbpa.2013.03.038

Golds, T. J., Maliga, P., and Koop, H. (1993). Stable plastid transformation in PEG-treated protoplasts of *Nicotiana tabacum*. *Nat. Biotechnol.* 11, 95–97. doi: 10.1038/nbt0193-95

Iwai, M., Hori, K., Sasakisekimoto, Y., Shimojima, M., and Ohta, H. (2015). Manipulation of oil synthesis in *Nannochloropsis* strain NIES-2145 with a phosphorus starvation-inducible promoter from *Chlamydomonas reinhardtii*. *Front. Microbiol.* 6, 912–912. doi: 10.3389/fmicb.2015.00912

Kang, N. K., Jeon, S., Kwon, S., Koh, H. G., Shin, S., Lee, B., et al. (2015). Effects of overexpression of a bHLH transcription factor on biomass and lipid production in *Nannochloropsis salina*. *Biotechnol. Biofuels* 8, 200–200. doi: 10.1186/s13068-015-0386-9

Kilian, O., Benemann, C. S., Niyogi, K. K., and Vick, B. (2011). High-efficiency homologous recombination in the oil-producing alga *Nannochloropsis* sp. *Proc. Natl. Acad. Sci. U.S.A.* 108, 21265–21269. doi: 10.1073/pnas.1105861108

Lapidot, M., Raveh, D., Sivan, A., Arad, S. M., and Shapira, M. (2002). Stable chloroplast transformation of the unicellular red alga *Porphyridium* species. *Plant Physiol.* 129, 7–12. doi: 10.1104/pp.011023

Leister, D. (2003). Chloroplast research in the genomic age. *Trends Genet.* 19, 47–56. doi: 10.1016/S0168-9525(02)00003-3

Li, F., Gao, D., and Hu, H. (2014). High-efficiency nuclear transformation of the oleaginous marine *Nannochloropsis* species using PCR product. *Biosci. Biotechnol. Biochem.* 78, 812–817. doi: 10.1080/09168451.2014.905184

Li, X., Zhang, R., Patena, W., Gang, S. S., Blum, S. R., Ivanova, N., et al. (2016). An indexed, mapped mutant library enables reverse genetics studies of biological processes in *Chlamydomonas reinhardtii*. *Plant Cell* 28, 367–387. doi: 10.1105/tpc.15.00465

Lu, Y., Chi, X., Li, Z., Yang, Q., Li, F., Liu, S., et al. (2010). Isolation and characterization of a stress-dependent plastidial Δ12 fatty acid desaturase from the Antarctic microalga *Chlorella vulgaris* NJ-7. *Lipids* 45, 179–187. doi: 10.1007/s11745-009-3381-8

Lu, Y., Chi, X., Yang, Q., Li, Z., Liu, S., Gan, Q., et al. (2009). Molecular cloning and stress-dependent expression of a gene encoding Delta(12)-fatty acid desaturase in the Antarctic microalga *Chlorella vulgaris* NJ-7. *Extremophiles* 13, 875–884. doi: 10.1007/s00792-009-0275-x

Lu, Y., Tarkowská, D., Turecková, V., Luo, T., Xin, Y., Li, J., et al. (2014a). Antagonistic roles of abscisic acid and cytokinin during response to nitrogen depletion in oleaginous microalga *Nannochloropsis oceanica* expand the evolutionary breadth of phytohormone function. *Plant J.* 80, 52–68. doi: 10.1111/tpj.12615.

Lu, Y., and Xu, J. (2015). Phytohormones in microalgae: a new opportunity for microalgal biotechnology. *Trends Plant Sci.* 20, 273–282. doi: 10.1016/j.tplants.2015.01.006

Lu, Y., Zhou, W., Wei, L., Li, J., Jia, J., Li, F., et al. (2014b). Regulation of the cholesterol biosynthetic pathway and its integration with fatty acid biosynthesis in the oleaginous microalga *Nannochloropsis oceanica*. *Biotechnol. Biofuels* 7:81. doi: 10.1186/1754-6834-7-81

Maliga, P. (2004). Plastid transformation in higher plants. *Annu. Rev. Plant Biol.* 55, 289–313. doi: 10.1146/annurev.arplant.55.031903.141633

Maliga, P., and Bock, R. (2011). Plastid biotechnology: food, fuel, and medicine for the 21st Century. *Plant Physiol.* 155, 1501–1510. doi: 10.1104/pp.110.170969

Mayfield, S. P., Manuell, A. L., Chen, S., Wu, J., Tran, M., Siefker, D., et al. (2007). *Chlamydomonas reinhardtii* chloroplasts as protein factories. *Curr. Opin. Biotechnol.* 18, 126–133. doi: 10.1016/j.copbio.2007.02.001

Moody, J. W., McGinty, C, M., and Quinn, J. C. (2014). Global evaluation of biofuel potential from microalgae. *Proc. Natl. Acad. Sci. U.S.A.* 26, 7–13. doi: 10.1073/pnas.1321652111

Poliner, E., Pulman, J. A., Zienkiewicz, K., Childs, K., Benning, C., and Farré, E. M. (2017). A toolkit for *Nannochloropsis oceanica* CCMP1779 enables gene stacking and genetic engineering of the eicosapentaenoic acid pathway for enhanced long-chain polyunsaturated fatty acid production. *Plant Biotechnol. J.* 16, 298–309. doi: 10.1111/pbi.12772

Radakovits, R., Jinkerson, R. E., Fuerstenberg, S. I., Tae, H., Settlage, R. E., Boore, J. L., et al. (2012). Draft genome sequence and genetic transformation of the oleaginous alga *Nannochloropis gaditana*. *Nat. Commun.* 3:686. doi: 10.1038/ncomms1688

Rasala, B. A., Muto, M., Lee, P. A., Jager, M., Cardoso, R. M., Behnke, C. A., et al. (2010). Production of therapeutic proteins in algae, analysis of expression of seven human proteins in the chloroplast of *Chlamydomonas reinhardtii*. *Plant Biotechnol. J.* 8, 719–733. doi: 10.1111/j.1467-7652.2010.00503.x

Scott, S. A., Davey, M. P., Dennis, J. S., Horst, I., Howe, C. J., Lea-Smith, D. J., et al. (2010). Biodiesel from algae: challenges and prospects. *Curr. Opin. Biotech.* 21, 277–286. doi: 10.1016/j.copbio.2010.03.005

Tran, M., Van, C., Barrera, D. J., Pettersson, P. L., Peinado, C. D., Bui, J., et al. (2013). Production of unique immunotoxin cancer therapeutics in algal chloroplasts. *Proc. Natl. Acad. Sci. U.S.A.* 110, 14–14. doi: 10.1073/pnas.1214638110

Vieler, A., Wu, G., Tsai, C.-H., Bullard, B., Cornish, A. J., Harvey, C., et al. (2012). Genome, functional gene annotation, and nuclear transformation of the heterokont oleaginous alga *Nannochloropsis oceanica* CCMP1779. *PLoS Genet.* 8:e1003064. doi: 10.1371/journal.pgen.1003064

Wang, D., Lu, Y., Huang, H., and Xu, J. (2012). Establishing oleaginous microalgae research models for consolidated bioprocessing of solar energy. *Adv. Biochem. Eng. Biotechnol.* 128, 69–84. doi: 10.1007/10_2011_122

Wang, D., Ning, K., Li, J., Hu, Q., and Xu, J. (2014). *Nannochloropsis* genomes reveal evolution of microalgal oleaginous traits. *PLoS Genet.* 10:e1004094. doi: 10.1371/journal.pgen.1004094.

Wang, Q., Lu, Y., Xin, Y., Wei, L., Huang, S., and Xu, J. (2016). Genome editing of model oleaginous microalgae *Nannochloropsis* spp. by CRISPR/Cas9. *Plant J.* 88, 1071–1081. doi: 10.1111/tpj.13307

Wei, H., Shi, Y., Ma, X., Pan, Y., Hu, H., Li, Y., et al. (2017). A type-I diacylglycerol acyltransferase modulates triacylglycerol biosynthesis and fatty acid composition in the oleaginous microalga, *Nannochloropsis oceanica*. *Biotechnol. Biofuels* 10:174. doi: 10.1186/s13068-017-0858-1

Wei, L., Xin, Y., Wang, D., Jing, X., Zhou, Q., Su, X., et al. (2013). *Nannochloropsis* plastid and mitochondrial phylogenomes reveal organelle diversification mechanism and intragenus phylotyping strategy in microalgae. *BMC Genomics* 14:534. doi: 10.1186/1471-2164-14-534

Wei, L., Xin, Y., Wang, Q., Yang, J., Hu, H., and Xu, J. (2017). RNAi-based targeted gene knockdown in the model oleaginous microalgae *Nannochloropsis oceanica*. *Plant J.* 89, 1236–1250. doi: 10.1111/tpj.13411

Xin, Y., Lu, Y., Lee, Y.-Y., Wei, L., Jia, J., Wang, Q., et al. (2017). Producing designer oils in industrial microalgae by rational modulation of co-evolving type-2 diacylglycerol acyltransferases. *Mol. Plant* 10, 1523–1539. doi: 10.1016/j.molp.2017.10.011

Zhang, C., and Hu, H. (2014). High-efficiency nuclear transformation of the diatom *Phaeodactylum tricornutum* by electroporation. *Mar. Genomics* 16, 63–66. doi: 10.1016/j.margen.2013.10.003

Zhang, R., Patena, W., Armbruster, U., Gang, S. S., Blum, S. R., and Jonikas, M. C. (2014). High-throughput genotyping of green algal mutants reveals random distribution of mutagenic insertion sites and endonucleolytic cleavage of transforming DNA. *Plant Cell* 26, 1398–1409. doi: 10.1105/tpc.114.124099

Zienkiewicz, K., Zienkiewicz, A., Poliner, E., Du, Z.-Y., Vollheyde, K., Herrfurth, C., et al. (2017). *Nannochloropsis*, a rich source of diacylglycerol acyltransferases for engineering of triacylglycerol content in different hosts. *Biotechnol. Biofuels* 10:8. doi: 10.1186/s13068-016-0686-8

Conflict of Interest Statement: The authors declare that the research was conducted in the absence of any commercial or financial relationships that could be construed as a potential conflict of interest.

frontiers in Plant Science

ORIGINAL RESEARCH
published: 20 November 2017
doi: 10.3389/fpls.2017.01997

Flocculation of *Chlamydomonas reinhardtii* with Different Phenotypic Traits by Metal Cations and High pH

Jianhua Fan[1,2,3], Lvhong Zheng[1], Yunpeng Bai[1], Shai Saroussi[3] and Arthur R. Grossman[3]*

[1] State Key Laboratory of Bioreactor Engineering, East China University of Science and Technology, Shanghai, China, [2] Department of Applied Biology, East China University of Science and Technology, Shanghai, China, [3] Department of Plant Biology, Carnegie Institution for Science, Stanford, CA, United States

Concentrating algal cells by flocculation as a prelude to centrifugation could significantly reduce the energy and cost of harvesting the algae. However, how variation in phenotypic traits such as cell surface features, cell size and motility alter the efficiency of metal cation and pH-induced flocculation is not well understood. Our results demonstrate that both wild-type and cell wall-deficient strains of the green unicellular alga *Chlamydomonas reinhardtii* efficiently flocculate (>90%) at an elevated pH of the medium (pH 11) upon the addition of divalent cations such as calcium and magnesium (>5 mM). The trivalent ferric cation (at 10 mM) proved to be essential for promoting flocculation under weak alkaline conditions (pH ~8.5), with a maximum efficiency that exceeded 95 and 85% for wild-type CC1690 and the cell wall-deficient *sta6* mutant, respectively. Near complete flocculation could be achieved using a combination of 5 mM calcium and a pH >11, while the medium recovered following cell removal could be re-cycled without affecting algal growth rates. Moreover, the absence of starch in the cell had little overall impact on flocculation efficiency. These findings contribute to our understanding of flocculation in different Chlamydomonas strains and have implications with respect to inexpensive methods for harvesting algae with different phenotypic traits. Additional research on the conditions (e.g., pH and metal ions) used for efficient flocculation of diverse algal groups with diverse characteristics, at both small and large scale, will help establish inexpensive procedures for harvesting cell biomass.

Keywords: flocculation, cell wall deficient, Chlamydomonas, multivalent metal ions, microalgae, pH, algal biotechnology

OPEN ACCESS

Edited by:
Agnieszka Ludwików, Adam Mickiewicz University in Poznań, Poland

Reviewed by:
Jon Pittman, University of Manchester, United Kingdom
Jean-David Rochaix, Université de Genève, Switzerland

****Correspondence:***
Jianhua Fan
jhfan@ecust.edu.cn;
jhfanster@gmail.com

Specialty section:
This article was submitted to Plant Biotechnology, a section of the journal Frontiers in Plant Science

Received: *08 September 2017*
Accepted: *08 November 2017*
Published: *20 November 2017*

Citation:
Fan J, Zheng L, Bai Y, Saroussi S and Grossman AR (2017) Flocculation of Chlamydomonas reinhardtii with Different Phenotypic Traits by Metal Cations and High pH. Front. Plant Sci. 8:1997. doi: 10.3389/fpls.2017.01997

INTRODUCTION

Over the past decade there has been an increasing interest in microalgae as a promising feedstock for sustainable, large-scale production of commodities such as food, feed, chemicals, materials and fuels (Abomohra et al., 2016; Waghmare et al., 2016). For all of the products that could potentially be developed, overcoming technical issues and reducing production costs will be the primary determinants of feasibility for achieving sustainable algal biomass production (Laurens et al., 2017). Among key technical issues, a major challenge for commercial-scale applications is the ability to inexpensively harvest large quantities of microalgal biomass from dilute cultures.

Conventional methods like centrifugation are fast and effective, but also costly and energy intensive, making it only suitable for the production of high-value biomass or metabolites (Demirbas, 2017). The various other techniques that have been used to harvest microalgae include membrane filtration (Lorente et al., 2017), foam fractionation (Ndikubwimana et al., 2016a), chemical/biological flocculation (Chatsungnoen and Chisti, 2016; Ndikubwimana et al., 2016b), electrolytic coagulation (Fayad et al., 2017), ultrasonic aggregation (Wang et al., 2015), magnetic separation (Safarik et al., 2017) and gravity sedimentation (Griffiths et al., 2012). Each of these methods has been reported, with some promising results under specific production conditions.

To generate algal biomass in an economically feasible, environmentally friendly way requires selection of appropriate harvesting technologies. Several factors must be considered when selecting the harvesting strategy, including strain phenotype, ionic strength and pH conditions of the culture medium, recycling of spent medium, and the final quality of harvested biomass. Chemical flocculation with polyvalent metal ions or polymeric flocculants is widely used in water treatment and has been shown to efficiently separate microalgal cells from its growth medium (Chatsungnoen and Chisti, 2016). For some species, flocculation can also be stimulated by changing the pH of the medium. However, increasing the pH can lead to precipitation of magnesium, calcium, phosphate and carbonate salts along with the algal cells (Vandamme et al., 2012; Wu et al., 2012). In contrast, decreasing the pH neutralizes negative charges on the cell surface, which decreases dispersal forces among the cells thereby promoting flocculation; the flocculated material can then be collected in a much smaller total culture volume (Liu et al., 2013) and be further concentrated by centrifugation. It was recently shown that the power consumption during the harvesting of microalgae by coagulation flocculation was much lower relative to the power consumption of conventional centrifugation [only 2.1 kWh/kg for *Chlorella vulgaris* and 0.2 kWh/kg for *Phaeodactylum tricornutum* (Vandamme et al., 2011) compared to ∼16 kWh/kg when assuming a microalga biomass concentration of 0.5 kg/m^3 in open ponds (Danquah et al., 2009)]. In sum, algal cell flocculation prior to harvesting by centrifugation could significantly reduce the energy 'cost' of the collection procedure (Xu et al., 2011).

Although it appears from previous studies that flocculation is an efficient technique to pre-harvest microalgal cells, there is still uncertainty about how general the procedure is for different species and for diverse strains of a single species that are phenotypically distinct, which would include differences in cell size, surface charge properties and motility. It would also be valuable to explore how cation and pH triggered flocculation is impacted when the production strains are lacking or deficient in a cell wall; such strains may be more amenable to molecular and genetic engineering as well as cell disruption.

To further develop simple, inexpensive methods to facilitate algal cell harvesting by flocculation, we evaluated flocculation of the green unicellular algae *Chlamydomonas reinhardtii* (hereafter Chlamydomonas) using a combination of metal cations in addition to medium of different pHs. Different strains with different physical and biological properties (cell wall, size, motility, etc.) were examined in these studies to determine if specific physical characteristics impact the extent or efficiency of flocculation. We therefore analyzed several Chlamydomonas strains with different properties including two wild-type strains, CC124 and CC1690 (also known as 21gr$^+$), that are widely used in the laboratory, and the cell wall deficient (*cw*$^-$) strain *cw15 sta6* (BAFJ5, lack flagella), which was derived from strain CC330 by random insertional mutagenesis with the *ARG7*-containing plasmid (Zabawinski et al., 2001); *cw15 sta6* is unable to synthesize starch as a consequence of the *STA6* gene deletion and lacks motility as it does not have a flagellum (Wang et al., 2009). Since the *sta6* mutant displays normal growth rates (relative to wild-type cells) in acetate-supplemented medium but does not synthesize starch, many studies over the last two decades have explored carbon partitioning in this strain and its potential to synthesize high levels of lipids for the production of sustainable, renewable liquid fuels (Siaut et al., 2011; Blaby et al., 2013; Goodenough et al., 2014). In addition, we examined CC400, which is a *cw*$^-$ strain that synthesizes starch, and a *sta6* strain (CC4567) genetically rescued for the starchless phenotype by transformation with a wild-type copy of the *STA6* gene [*sta6*::*STA6*, hereafter designated C6 (Li et al., 2010)]; these latter strains help distinguish the impact of starch accumulation and cell wall synthesis on flocculation. Overall, our findings challenge the idea that immobile strains that lack flagella and/or cell walls more readily flocculate, while at the same time furthering our understanding of flocculation in distinct Chlamydomonas strains. Similar experiments can now be performed with a range of microalgae that show promise for industrial applications.

MATERIALS AND METHODS

Microalgae Cultivation

Chlamydomonas reinhardtii cells were cultured in sterile Tris-Acetate-Phosphate (TAP) (Chlamydomonas Resource Center[1]) and high salt (HS) medium (Sueoka, 1960) adjusted to pH 7.2. For all experiments the cells were grown in triplicate in Erlenmeyer Flasks at 25°C with shaking. The *C. reinhardtii* strains (Supplementary Table S1) used in these experiments were standard parental strains CC124 (137c *mt*$^-$ *nit1 nit2*) and CC1690 (*mt*$^+$ *NIT1 NIT2*), the cell wall deficient strain CC400 (*cw15*), the cell wall-deficient mutant with a lesion at the *STA6* locus CC4348 (*cw15 arg7-7 nit1 nit2 sta6-1*::*ARG7*) that is generally denoted *sta6*, and the *sta6* rescued strain CC4567, generally denoted *sta6*-C6, which was generated by transformating *sta6* with the plasmid pSL-*STA6*; this plasmid carries a genomic copy of the wild-type *STA6* gene (*cw15 arg7-7 nit1 nit2 sta6-1*::*ARG7 STA6*). These strains were obtained from the Chlamydomonas

[1]https://www.chlamycollection.org/methods/media-recipes/tap-and-tris-minimal/

Resource Center. Before use in flocculation experiments, 5 mL of cells grown photoautotrophically in HS medium were inoculated into 100 mL of TAP medium in a 250-mL Erlenmeyer flask that was exposed to continuous light (100 μmol photons $m^{-2}s^{-1}$) with agitation (150 rpm) at 25°C for 8 days.

Flocculation Experiments

Flocculation experiments were performed at an algal density of ∼0.7 g dry weight per liter. The effects of pH were examined for algal suspensions by either increasing or decreasing the pH with the addition of sodium hydroxide (NaOH) and hydrochloric acid (HCl) from 2 M stock solutions. Experiments were performed in 100-mL beakers that were magnetically stirred and mixed vigorously for 2 min during and immediately after pH adjustments. For metal cation treatments, 5 M stock solutions of ferric chloride ($FeCl_3$), calcium chloride ($CaCl_2$), and magnesium chloride ($MgCl_2$) were prepared and each was added to the medium to generate final concentrations of 0, 1, 2.5, 5, 10, and 30 mM.

To evaluate flocculation, 20 mL aliquots of the cultures were collected from the beakers, transferred to disposable test tubes and incubated without agitation for 15 min. Following this potential 'flocculation period,' an aliquot of culture was withdrawn (from the middle of the 'clarified zone') and used to determine both OD_{750} and the absolute number of cells per mL. The flocculation efficiency was calculated according to the equation: flocculation efficiency (%) = (1−A/B) × 100 (where *A* represents cell number in the clarified zone and *B* the cell number of the reference, untreated control).

Measuring Methods

Cell numbers were determined by counting intact cells using Countess II FL (Life Technology, United States). Microscopic snapshots were taken on a Leica optical microscope (LEITZ DMRB, Germany) which also enabled determination of cell diameter. A Malvern Zetasizer 2000HSA (Malvern, United Kingdom) was used to measure the zeta potential of the algal cultures in deionized water (cells were collected from the growth medium by centrifugation and resuspended in deionized water) (Liu et al., 2013), which relates to the surface charge of individual cells. For dry cell weight, the algal cells were collected by centrifugation at 12,000 *g* for 5 min, washed twice with distilled water, dried at 105°C for 24 h, and weighed to obtain total dry biomass. The dried cell powder was extracted with a solvent mixture of chloroform and methanol (2:1, v/v) to calculate the lipid content (Fan et al., 2014). The starch content was analyzed using a commercial enzymatic Starch Assay Kit (SA-20, Sigma–Aldrich). The concentrations of the metal cations in the spent medium were measured using inductively coupled-atomic emission spectrometry (ICP-AES). The operating conditions for ICP-AES instrument were as previously described (Matsuura et al., 2001). The measuring wavelength and atomic/ionic lines were as follows, Fe (259.9 nm, II), Ca (317.9 nm, II) and Mg (279.0 nm, II).

Reuse of the Liquid Phase as Growth Medium

Following 30 min of coagulation-flocculation, spent supernatants were tested for their ability to support algal growth (media recyclability). The pH value of the spent medium was adjusted to approximately neutral by adding HCl, while macronutrients and micronutrients were added according to the TAP medium recipe, except that we did not include acetate and added $CaCl_2$ to 50% of the level present in TAP medium. The adjusted supernatants were tested for their ability to sustain photoautotrophic growth of Chlamydomonas (25°C, 100 μmol photons $m^{-2}s^{-1}$, bubbled with 1% CO_2).

Statistical Analysis

All experiments were performed in triplicate (biological) and the data, presented as a mean ± standard deviation (*SD*), were further analyzed by Student's *t*-test ($n = 3$). Asterisks indicate a significant difference from the control.

RESULTS AND DISCUSSION

The Role of pH in Self-Flocculation for Different Chlamydomonas Strains

We first examined three different Chlamydomonas strains to determine whether different phenotypic characteristics [difference in cell wall, flagella and size (Zabawinski et al., 2001; Siaut et al., 2011); **Table 1**] impact the tendency of the cells to flocculate in response to various pHs and metal cations. The strains used were the 'wild-type' strains CC124 and CC1690, which contain a cell wall and flagella, but significantly differ in their genetic background (Gallaher et al., 2015), the starchless mutant, *sta6*, which has neither a cell wall nor a flagella (Zabawinski et al., 2001; Wang et al., 2009; Siaut et al., 2011) and its complemented strain, C6, as well as CC400 (**Table 1**). Eight days following inoculation, the cell densities of all of the cultures increased from 5×10^5 to between 4×10^7 and 9×10^7 cell mL^{-1} (**Supplementary Figure S1**). All strains were spherical, although the average diameter of the *sta6* mutant was much smaller than those of the other strains; 6.29 ± 0.37 μm (CC124), 6.88 ± 0.43 μm (CC1690), and 2.29 ± 0.20 μm (*sta6*) (**Table 1** and **Supplementary Figure S2**). The maximal dry cell weight ranged from 0.63 g/L (for *sta6*, which attained a density of 8.81×10^7) to 0.78 g/L (for CC1690, which attained a density of 4.53×10^7); similar biomass yields of 0.5–1 g/L are considered typical for photoautotrophic cultivation of oleaginous algae in open raceway ponds (Rawat et al., 2013).

The efficiency of cell flocculation in culture was first investigated as a function of pH (**Figure 1A**). Since an increase in metal precipitates would occur at the higher pH values and impact the OD measurements, the flocculation efficiency was calculated according to the absolute cell number. Less than 10% of flocculation effect on cell were observed when the pH of the cultures was varied between 5 and 9 for all measured strains. In this pH range, the flocculation efficiency

TABLE 1 | Cell properties and flocculation characteristics using calcium ions at pH ~11.5.

Strains	Cell wall and flagellar motility	Cell density (g/L)	Size (μm)	Starch content (%)	Lipid contents (%)	Optimized dosage (mM, $CaCl_2$)	Flocculation efficiency (%)	Zeta potential (mV)	
								Before flocculation	After flocculation
CC1690	+	0.78 ± 0.07	6.89 ± 0.25	32.5 ± 2.3	11.2 ± 1.9	5	94.8 ± 2.3	−22.15 ± 1.69	−5.67 ± 0.38
CC124	+	0.74 ± 0.09	5.96 ± 0.37	39.2 ± 3.4	14.7 ± 2.3	5	92.9 ± 2.6	−20.48 ± 2.31	−6.43 ± 0.57
sta6	−	0.63 ± 0.09	2.33 ± 0.18	ND	45.3 ± 2.6	10	93.7 ± 1.9	−26.63 ± 2.04	−4.92 ± 0.27
CC400	−	0.68 ± 0.06	4.27 ± 0.24	29.4 ± 2.9	13.4 ± 2.7	10	94.4 ± 2.2	−22.49 ± 2.18	−3.73 ± 0.44
sta6-C6	−	0.66 ± 0.07	3.57 ± 0.21	33.5 ± 1.9	16.2 ± 3.3	10	94.1 ± 1.7	−25.43 ± 1.95	−4.67 ± 0.51

+: intact cell wall and flagella-dependent motility; −: cell wall deficient and lacking flagella-dependent motility; ND, not detectable.

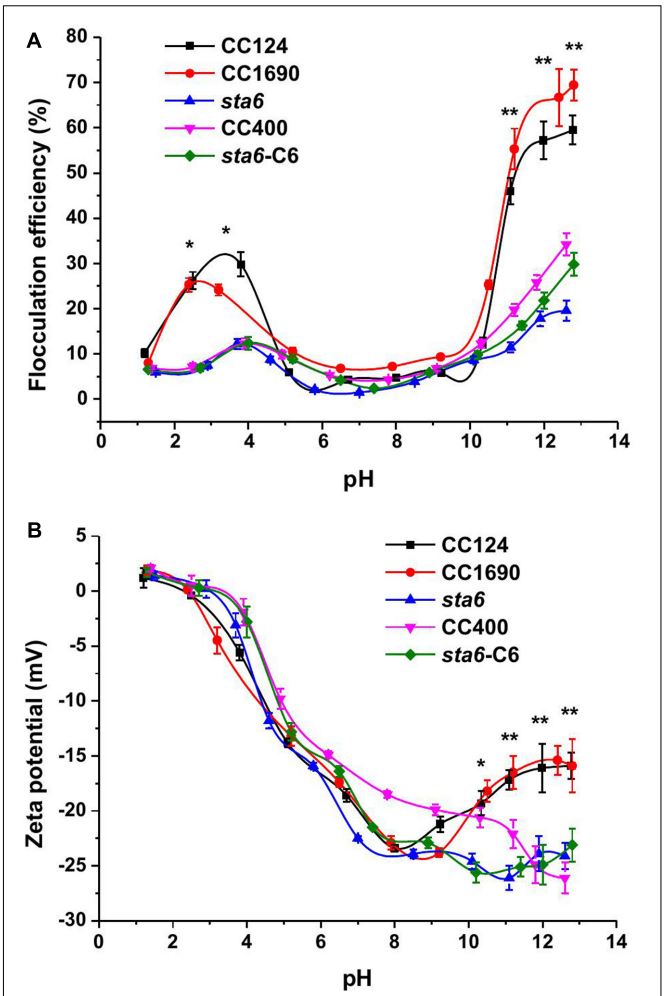

FIGURE 1 | Flocculation efficiency and charge characteristics (Zeta potential) as a function of pH in three *Chlamydomonas reinhardtii* strains. **(A)** flocculation efficiency; **(B)** zeta potential. Sometimes the data points are not aligned, as it is quite difficult to adjust the same pH values in the solution for each strain. The data was analyzed for significant differences using the Student's *t*-test ($n = 3$) (all mutants in comparison with the two wild-types). Asterisks indicate a significant difference from the control ($^*p < 0.05$, $^{**}p < 0.01$).

was less than 10% for all five of the Chlamydomonas strains. However, the flocculating efficiency increased for CC124 and CC1690 in both the acidic and alkaline pH range. In the pH range of 11–13, the flocculation efficiency was highest for the cell wall-containing strains (45–70% for CC1690 and CC124) but relatively low (~15–30%) with significant difference for the cell wall-deficient strains (CC400, *sta6* and *sta6*-C6). In the acidic range the flocculation efficiency was maximal at pH 4.0 for CC124 (32%) and pH 2.5 for CC1690 (26%). Overall, these results demonstrate that the highest flocculation efficiencies are obtained at high pH, although the efficiency values can be markedly different for the strains, probably a consequence differences in phenotypic characteristics, including the presence/absence of the cell wall (**Table 1** and **Figure 1A**).

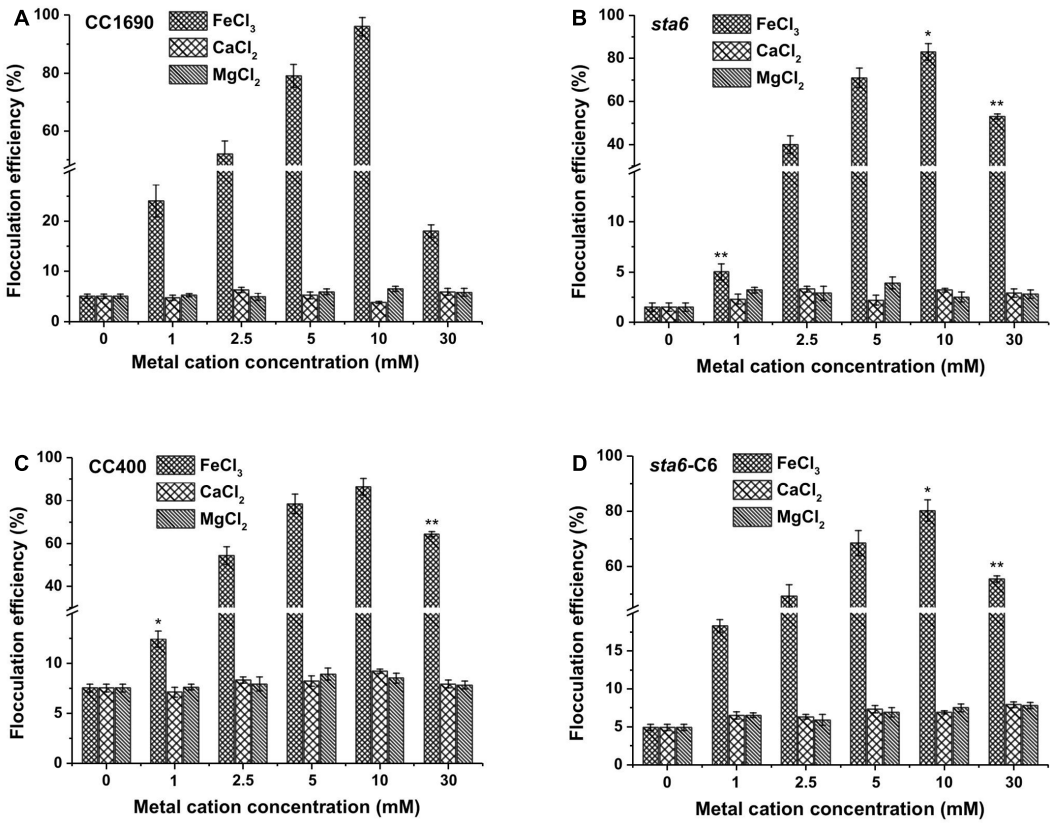

FIGURE 2 | Flocculation efficiency as a function of different metal cations and their concentrations in wild-type and cell wall-deficient *Chlamydomonas reinhardtii* strain at near neutral pH conditions. **(A)** Wild-type CC1690; **(B)** cell wall deficient mutant *sta6*; **(C)** CC400; **(D)** *sta6*-C6. Cells were grown to stationary phase and the pH of the medium was ∼8.5. The data was analyzed for significant differences using the Student's *t*-test ($n = 3$) (each mutant in comparison with wild-type). Asterisks indicate a significant difference from the control (wild-type) (*$p < 0.05$, **$p < 0.01$).

Similar to the flocculation efficiencies, the zeta potential, which is widely used for quantification of the cell surface charge, was also pH dependent (**Figure 1B**). Over an 8.5-1.5 pH interval, the zeta potential showed a sharp increase from −24 to ∼0 mV. The profile of the zeta potential may have some link to flocculation efficiency; at pH 3–4, when the flocculation efficiency peaked, the cells were electrically near neutral. The zeta potential in the acidic region appeared unaffected by the presence/absence of a cell wall or by differences in cell size among the strains. However, at pH 10–13, the zeta potentials of both of wild-type strains moderately rose from ∼−25 to ∼−15 mV. In the three cell wall deficient mutants the zeta potential remained approximately the same (**Figure 1B**).

Several self-flocculation studies of microalgae involving pH adjustment of the growth medium have been performed (Wu et al., 2012; Liu et al., 2013). Increasing or decreasing the pH of the medium can increase the flocculation efficiency by up to 90% for green microalgae, suggesting an effective strategy for harvesting the cells. In our studies the cells were also subjected to a range of pH conditions, however, self-flocculation for wild-type cells was only relatively efficient at elevated pH (more than 10), and was never very high for cell wall deficient and starchless mutant cells (**Figure 1A**).

Cation-Induced Flocculation

Tris-Acetate-Phosphate medium has high ionic strength with initial metal concentrations of Fe (∼1.0 mg/L), Ca (∼18.2 mg/L), and Mg (∼9.7 mg/L); after growth and pH adjustment, most of the metal salts were taken up and utilized by the algal cells. The background concentrations after flocculation were about 0.11, 1.83, and 0.94 mg/L for Fe, Ca, and Mg, respectively. Hence, it is likely that some of the flocculation elicited at high pH in the absence of additional metals (**Figure 1A**) is due to the presence of low concentrations of metal ions still present in the TAP media.

We selected the divalent (Ca^{2+} and Mg^{2+}) and trivalent (Fe^{3+}) cation metals for further investigating the potential for harvesting Chlamydomonas cells by flocculation. We first used cells cultured in TAP medium and grown to stationary phase, with the pH of the medium for all of the cultures reaching ∼8.5. As shown in **Figure 2**, divalent cations (Ca^{2+}, Mg^{2+}) alone did not appear to impact flocculation efficiency beyond what was observed in the absence of supplementing cations (less than 10% after 10 min for the wild-type CC1690 (**Figure 2A**)

TABLE 2 | Metal cation concentrations (5 mM of chlorides addition to the medium) before (C_1) and after (C_2) flocculation for wild-type and cell wall deficient *Chlamydomonas reinhardtii* strains at different pH level.

Strains	Elemental types	Fe^{3+}			Ca^{2+}			Mg^{2+}		
	pH level	4.0	8.5	12.0	4.0	8.5	12.0	4.0	8.5	12.0
CC124	C_1 (mg/L)	244.2 ± 3.4			203.4 ± 4.9			125.1 ± 4.4		
	C_2 (mg/L)	245.3 ± 3.8	66.5 ± 5.4 (27.2%)	25.2 ± 1.8 (10.3%)	202.6 ± 3.4	153.2 ± 2.6 (75.3%)	3.5 ± 0.9 (1.7%)	124.1 ± 4.7	91.6 ± 4.3 (73.2%)	29.5 ± 2.1 (23.6%)
CC1690	C_1 (mg/L)	249.5 ± 4.6			201.1 ± 5.4			121.7 ± 3.2		
	C_2 (mg/L)	244.8 ± 2.7	58.4 ± 4.9 (23.4%)	23.9 ± 2.7 (9.6%)	203.1 ± 4.2	143.5 ± 3.9 (71.4%)	3.1 ± 0.4 (1.5%)	130.5 ± 2.1	88.2 ± 6.3 (72.5%)	22.1 ± 3.2 (18.2%)
sta6	C_1 (mg/L)	245.8 ± 2.9			211.3 ± 3.6			133.8 ± 3.5		
	C_2 (mg/L)	246.4 ± 3.7	65.3 ± 3.6 (26.6 %)	27.6 ± 4.4 (11.2%)	205.3 ± 4.7	177.8 ± 4.6 (84.1%)	4.9 ± 0.7 (2.3%)	127.4 ± 3.9	105.4 ± 5.8 (78.8%)	39.2 ± 4.9 (29.3%)
CC400	C_1 (mg/L)	250.1 ± 3.3			209.3 ± 2.9			129.7 ± 3.9		
	C_2 (mg/L)	252.2 ± 4.3	62.3 ± 3.9 (24.9%)	26.4 ± 4.2 (10.6%)	207.1 ± 5.2	172.3 ± 4.1 (82.3%)	4.8 ± 0.5 (2.3%)	130.5 ± 4.4	99.3 ± 5.4 (76.6%)	34.5 ± 3.9 (26.6%)
sta6-C6	C_1 (mg/L)	248.4 ± 3.9			207.4 ± 3.2			131.4 ± 4.7		
	C_2 (mg/L)	249.9 ± 4.2	65.9 ± 3.6 (26.5%)	29.3 ± 4.1 (11.8%)	204.3 ± 4.8	180.2 ± 2.7 (86.9%)	5.8 ± 0.6 (2.8%)	134.3 ± 4.1	106.3 ± 5.1 (80.9%)	37.4 ± 3.7 (28.5%)

Numbers in brackets represent the percentage of remaining cation in the medium.

and the various mutants (**Figures 2B–D**). The monovalent cation (K^+) showed similar flocculation efficiencies as that of the divalent cations, although the resulting flocculants appeared more susceptible to disaggregation (data not shown). Although flocculation efficiencies following treatment with divalent cations were relatively low, the flocculation yields were somewhat higher in wild-type cells than in the mutant (5–6% for CC1690 compared to 2–3% for *sta6*; compare panel a to panel b in **Figure 2**); this could be explained by phenotypic differences such as cell size and/or motility (**Table 1**). In contrast, the trivalent ferric ion elicited strong flocculation, with efficiencies at 10 mM Fe^{3+} exceeding 95 and 85% for CC1690 and *sta6*, respectively. A further increase in the Fe^{3+} concentration to 30 mM caused a marked drop in flocculation efficiency to ∼18 and 50% for CC1690 and *sta6*, respectively (**Figures 2A,B**).

Since the pH adjustment and some cations were effective in eliciting self-flocculation for wild-type cells (**Figures 1A**, **2**), we further explored flocculation using different metal cations at a range of pH conditions and quantified the levels of cations in the medium before and after flocculation at three different pHs (**Table 2**). The concentrations of Fe^{3+}, Ca^{2+}, and Mg^{2+} in the medium remained almost unchanged before and after cell flocculation at pH 4.0. However, following flocculation at pH 8.5, ∼25% of the Fe^{3+} and 72–84% of the Ca^{2+} and Mg^{2+} remained in the medium. Finally, cell flocculation at pH 12.0 resulted in precipitation of the majority of the metal ions from the medium, i.e., only 9.6–11.2%, 1.5–2.3%, and 18.2–29.3% of Fe^{3+}, Ca^{2+}, and Mg^{2+} remained in the medium, respectively. These results suggest that precipitation of the metal ions during flocculation occurred when the conditions were alkaline and possibly explain the relatively high flocculation efficiencies when such conditions are applied. Moreover, while precipitation of multivalent metal cations may co-occur with cells during flocculation at high pH, flocculation at low pH does not appear to be accompanied by metal ion precipitation and as a consequence, the low pH medium after flocculation still contains high cation levels and could not be used for the initiation of new cultures (Liu et al., 2013). Furthermore, metal cation precipitation during flocculation of three cell wall deficient mutants (*sta6*, CC400, and *sta6*-C6), all of which are also lacking flagella (**Table 1**), was generally no significant difference (Student's *t*-test, $p > 0.05$) with what was observed for CC1690 and CC124, under any of the conditions examined (**Table 2**).

Using Coagulation-Flocculation Induced by High pH for Harvesting

Since the flocculation efficiencies and charge characteristics as a function of pH were similar between CC1690 and CC124 (both are CW^+), we analyzed CC1690 as a 'wild-type' representative for additional experiments. Since the highest flocculation efficiencies were observed at a high pH (**Figure 1A**), we evaluated the impact of metal cation concentrations at pH 11.5 on the flocculation efficiencies of both CC1690 and *sta6*. The flocculation efficiencies of CC1690 and *sta6* peaked at 5–10 mM Ca^{2+} and Mg^{2+} (**Figures 3A,B**), with the highest flocculating activities resulting in aggregation of 90–95% of

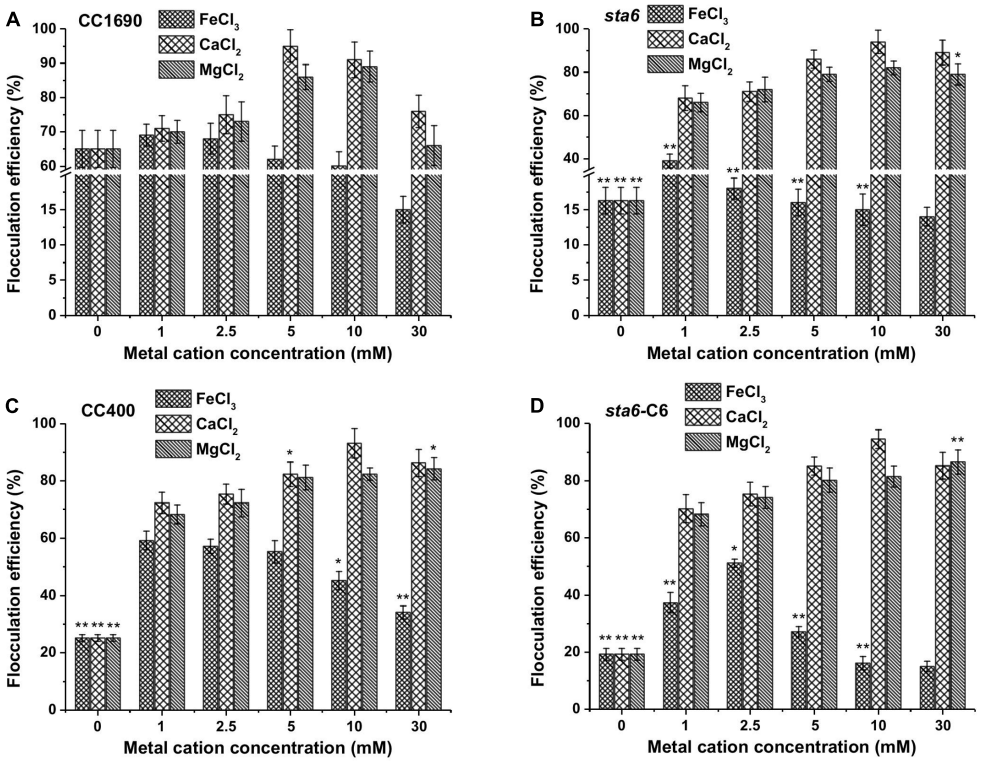

FIGURE 3 | Flocculation efficiency as a function of different metal cations and their concentrations in wild-type and cell wall deficient *Chlamydomonas reinhardtii* strains at pH 11.5. **(A)** Wild-type CC1690; **(B)** cell wall deficient mutant *sta6*; **(C)** CC400; **(D)** *sta6*-C6. Cells were grown to stationary phase and the pH of the medium was ∼11.5. The data was analyzed for significant differences using the Student's *t*-test ($n = 3$) (each mutant in comparison with wild-type). Asterisks indicate a significant difference from the control (wild-type) (*$p < 0.05$, **$p < 0.01$).

the cells (**Table 1**). For all divalent cations used in our study, the flocculation efficiencies either declined to some extent or remained the same when the ion concentration was elevated to 30 mM. Furthermore, Mg^{2+} was slightly less effective at eliciting aggregation than Ca^{2+} (**Figure 3** and **Supplementary Figure S2**), and the highest flocculation efficiencies, when using Mg^{2+}, were 89.1 and 81.9% for CC1690 and *sta6*, respectively. In contrast, at pH 11.5 the ferric ions generally caused some increase in flocculation at 1–5 mM, with a negative impact at higher concentrations (10 and 30 mM); at 1 mM Fe^{3+}, the maximal flocculation efficiencies were 69.2 and 39.3%, for CC1690 and *sta6*, respectively. Additionally, as a consequence of flocculation with Fe^{3+}, both the cells and supernatant turned sandy beige, while for the cultures that were subjected to Ca^{2+}- and Mg^{2+}-stimulated flocculation, a change in medium color did not occur (**Supplementary Figure S3**).

Previous studies have demonstrated that flocculation elicited by lowering the pH is likely the result of neutralizing of the negative surface charges of the cells by protonation of carboxyl and/or sulfate groups (Wyatt et al., 2012; Liu et al., 2013). However, in this work we demonstrated that cell flocculation occurs at high pH using Ca^{2+} and Mg^{2+} ions, and therefore the flocculation reaction is likely to result from a chemical precipitation of the calcium and/or magnesium salts (Vandamme et al., 2012; Beuckels et al., 2013). Indeed, self-flocculation greatly reduced the level of metal cations in the medium (**Table 2**). Hence, our results confirm that coagulation-flocculation could be induced by the addition of metal salts (**Figure 3** and **Supplementary Figure S2**), and that high pH (greater than 10) is required for this process to occur (**Table 1**).

A recent study showed that 83% of the cell wall deficient Chlamydomonas *cw15* cells that were nitrogen deprived flocculated when supplemented with Ca^{2+} under slightly alkaline conditions (Scholz et al., 2011). Moreover, Scholz et al. (2011) demonstrated that fresh TAP medium was less active in eliciting cell flocculation than nitrogen-free TAP medium. These results suggest that a flocculation inhibitory component of the medium was consumed during growth and/or that a metabolic byproduct released into the medium by nitrogen starved cells promotes flocculation (Scholz et al., 2011).

The Impact of Starch Accumulation on Flocculation

Since we compared the 'wild-type' cw^+ (CC1690) with the *sta6* cw^- starchless mutant, we sought to clarify whether or not cellular starch impacts flocculation efficiency. To address this issue we compared *sta6* to two cw^- strains,

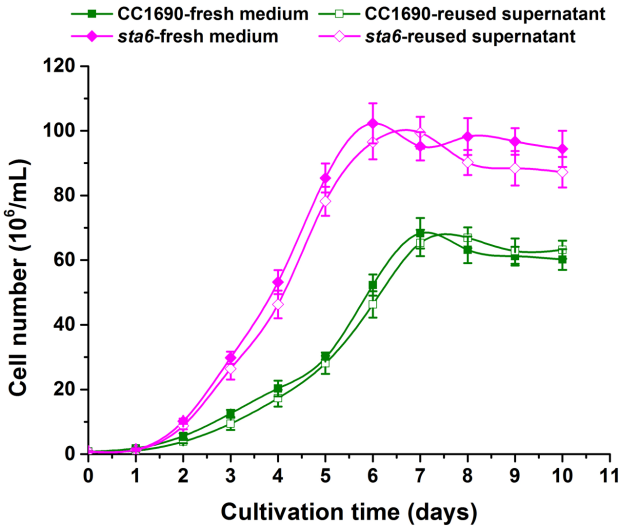

FIGURE 4 | Comparison of cell growth as a function of fresh and recycled medium.

CC400 (widely used wall-deficient mutant) and CC4567 (*sta6*-C6) (complemented *sta6* created by transformation of BAFJ5 with the plasmid pSL-STA6 harboring a genomic copy of the wild-type *STA6* gene) that are not impaired in starch production (Li et al., 2010). Importantly, the average size of *sta6* was smaller than CC400 and *sta6*-C6 (**Supplementary Figure S2**) and the cellular components, such as total lipids and starch contents among the strains varied from 11–45% to 0–39%, respectively (**Table 1**), with the highest lipid and no detectible starch in *sta6*. Despite differences in cells size and content of organic polymers, no substantial difference of Zeta potential was observed among the different strains (**Table 1**). Cation content in the medium derived from flocculated cells from each strain at a given pH exhibited similar levels (**Table 2**), although the level of cation in the medium was highly dependent on the pH value.

Flocculation efficiency at different divalent cation concentrations (pH 11.5) showed no significant difference between CC1690, CC400, *sta6*-C6, and *sta6*; all peaked at 5–10 mM Ca^{2+} and Mg^{2+} (with highest flocculating efficiencies of around 94 and 80%, respectively) (**Figures 3C,D**). These results suggest that cellular starch content has little overall impact on Chlamydomonas flocculation.

In this study, differences in flocculation efficiencies observed for wild-type and mutant cells are probably explained by the absence/presence of a cell wall and/or flagella. Intuitively, cells such as *sta6*, which lack flagella, might be thought to be more amenable to aggregation than motile cells since they might be more susceptible to the metal salt coagulants formed under strong alkali conditions. In addition, the loss of starch synthesis in *sta6* does not cause re-direction of fixed carbon to the synthesis of more protein or lipid; the *sta6* culture appears to accumulate ∼20% less biomass (because the cells are smaller) when grown in nutrient-replete medium (Krishnan et al., 2015), even though the cell density is higher. However, it was also shown that following growth under some stress conditions, *sta6* cells could accumulate more lipids, which makes them float to the surface of the culture (Goodenough et al., 2014). Based on the flocculation features of *sta6* reported here, we suggest that this strain can be effectively used for future biofuel research and production.

Reuse of Growth Medium

A highly important consideration in a large scale industrial application is the capacity to reuse the spent growth medium. The metal cation concentrations that remain in the medium following cell flocculation can have a marked and direct impact on media re-cycling capabilities. We therefore assessed the recyclability of the spent medium following photoautotrophic cultivation. Using 5–10 mM calcium with cultures of CC1690 and *sta6* we achieved efficient flocculation (>90%; **Figure 3**) and then determined whether the used medium affected the growth of new cultures. To address this, we compared the CC1690 and *sta6* growth rates over a period of 10 days in fresh and recycled medium. At any given time point the growth rate (for both CC1690 and *sta6*) was similar regardless of whether the cells were cultured in fresh or recycled medium (**Figure 4**). Moreover, both strains maintained their ability to flocculate with the addition of Ca^{2+} to the medium as long as there was a near neutral or alkaline environment during cultivation. Thus, residual Ca^{2+} or coagulant does not appear to be an obstacle to medium reuse. We also observed that cells grown in the spent supernatant, which contained a small quantity of residual Ca^{2+}, required less Ca^{2+} to flocculate. However, the amount of Ca^{2+} salts that precipitate was likely higher in the flocculated biomass; further analysis is required to evaluate whether the Ca^{2+} that precipitates with the flocculated cells interferes with specific microalgal biomass applications, e.g., biofuels production or bio-refinery.

CONCLUSION

Our experiments demonstrated that self-flocculation by direct pH adjustment does not work well for Chlamydomonas and that it depends on the presence of sufficiently high metal salts (>5 mM). The highest flocculation efficiency was achieved using a combination of added Ca^{2+} with elevated pH (>10). Slightly more metal cation appears to be needed to flocculate *sta6* (cell wall deficient, starchless mutant) potentially owing to the lack of motility, the different surface structure or the smaller cell size (Sathe and Durand, 2016). We also confirmed that cellular starch content has little overall impact on flocculation of Chlamydomonas, and importantly, the flocculated medium could be re-reused. Further examination of the flocculation mechanism would entail examining additional differences in flocculation characteristics among cells with different phenotypes, the impact of metal salts on flocculation when the culture is scaled up and whether or not the findings apply to other algal groups.

Additional research on the conditions (e.g., pH and metal ions) used for efficient flocculation of diverse algal groups with diverse characteristics, at both small and large scale, would help establish inexpensive procedures for harvesting cell biomass.

AUTHOR CONTRIBUTIONS

Conceived and designed the experiments: JF. Performed the experiments: JF and LZ. Analyzed the data: JF, SS, YB, and AG. Wrote the paper: JF, SS, YB, and AG.

ACKNOWLEDGMENTS

This work was sponsored by Natural Science Foundation of Shanghai 17ZR1406700, National Natural Science Foundation of China 21505044, and the "Chenguang Program" supported by Shanghai Education Development Foundation and Shanghai Municipal Education Commission 14CG27. The authors gratefully acknowledge financial support from China Scholarship Council 201606745004.

SUPPLEMENTARY MATERIAL

The Supplementary Material for this article can be found online at: https://www.frontiersin.org/articles/10.3389/fpls.2017.01997/full#supplementary-material

FIGURE S1 | Cell growth of different Chlamydomonas strains.

FIGURE S2 | Light Microscopy of Chlamydomonas cells. **(a)** CC1690; **(b)** CC124; **(c)** *sta6*; **(d)** CC400; **(e)** *sta6*-C6. Scale bars: 10 μm.

FIGURE S3 | Microscopic images of Chlamydomonas cells flocculated by metal cations and elevated pH (11.5). **(a)** Wild-type CC1690 before treatment; **(b)** wild-type CC1690 after treated with 5 mM $FeCl_3$; **(c)** wild-type CC1690 after treated with 5 mM $CaCl_2$; **(d)** wild-type CC1690 after treated with 5 mM $MgCl_2$; **(e)** cell wall deficient *sta6* mutant before treatment; **(f)** *sta6* mutant after treatment with 5 mM $FeCl_3$; **(g)** *sta6* mutant after treated with 5 mM $CaCl_2$; **(h)** *sta6* mutant after treated with 5 mM $MgCl_2$. Scale bars: 10 μm.

REFERENCES

Abomohra, A. E.-F., Jin, W., Tu, R., Han, S.-F., Eid, M., and Eladel, H. (2016). Microalgal biomass production as a sustainable feedstock for biodiesel: current status and perspectives. *Renew. Sustain. Energy Rev.* 64, 596–606. doi: 10.1016/j.rser.2016.06.056

Beuckels, A., Depraetere, O., Vandamme, D., Foubert, I., Smolders, E., and Muylaert, K. (2013). Influence of organic matter on flocculation of *Chlorella vulgaris* by calcium phosphate precipitation. *Biomass Bioenergy* 54, 107–114. doi: 10.1016/j.biombioe.2013.03.027

Blaby, I. K., Glaesener, A. G., Mettler, T., Fitz-Gibbon, S. T., Gallaher, S. D., Liu, B., et al. (2013). Systems-level analysis of nitrogen starvation–induced modifications of carbon metabolism in a *Chlamydomonas reinhardtii* starchless mutant. *Plant Cell* 25, 4305–4323. doi: 10.1105/tpc.113.117580

Chatsungnoen, T., and Chisti, Y. (2016). Harvesting microalgae by flocculation–sedimentation. *Algal Res.* 13, 271–283. doi: 10.1016/j.algal.2015.12.009

Danquah, M. K., Ang, L., Uduman, N., Moheimani, N., and Forde, G. M. (2009). Dewatering of microalgal culture for biodiesel production: exploring polymer flocculation and tangential flow filtration. *J. Chem. Technol. Biotechnol.* 84, 1078–1083. doi: 10.1002/jctb.2137

Demirbas, A. (2017). Production economics of high-quality microalgae. *Energy Sour. B Econ. Plan. Policy* 12, 395–401. doi: 10.1080/15567249.2015.1057655

Fan, J., Cui, Y., Wan, M., Wang, W., and Li, Y. (2014). Lipid accumulation and biosynthesis genes response of the oleaginous *Chlorella pyrenoidosa* under three nutrition stressors. *Biotechnol. Biofuels* 7:17. doi: 10.1186/1754-6834-7-17

Fayad, N., Yehya, T., Audonnet, F., and Vial, C. (2017). Harvesting of microalgae *Chlorella vulgaris* using electro-coagulation-flocculation in the batch mode. *Algal Res.* 25, 1–11. doi: 10.1016/j.algal.2017.03.015

Gallaher, S. D., Fitz-Gibbon, S. T., Glaesener, A. G., Pellegrini, M., and Merchant, S. S. (2015). *Chlamydomonas* genome resource for laboratory strains reveals a mosaic of sequence variation, identifies true strain histories, and enables strain-specific studies. *Plant Cell* 27, 2335–2352. doi: 10.1105/tpc.15.00508

Goodenough, U., Blaby, I., Casero, D., Gallaher, S. D., Goodson, C., Johnson, S., et al. (2014). The path to triacylglyceride obesity in the sta6 strain of *Chlamydomonas reinhardtii*. *Eukaryot. Cell* 13, 591–613. doi: 10.1128/EC.00013-14

Griffiths, M. J., van Hille, R. P., and Harrison, S. T. (2012). Lipid productivity, settling potential and fatty acid profile of 11 microalgal species grown under nitrogen replete and limited conditions. *J. Appl. Phycol.* 24, 989–1001. doi: 10.1007/s10811-011-9723-y

Krishnan, A., Kumaraswamy, G. K., Vinyard, D. J., Gu, H., Ananyev, G., Posewitz, M. C., et al. (2015). Metabolic and photosynthetic consequences of blocking starch biosynthesis in the green alga *Chlamydomonas reinhardtii* sta6 mutant. *Plant J.* 81, 947–960. doi: 10.1111/tpj.12783

Laurens, L. M., Chen-Glasser, M., and McMillan, J. D. (2017). A perspective on renewable bioenergy from photosynthetic algae as feedstock for biofuels and bioproducts. *Algal Res.* 24, 261–264. doi: 10.1016/j.algal.2017.04.002

Li, Y., Han, D., Hu, G., Dauvillee, D., Sommerfeld, M., Ball, S., et al. (2010). Chlamydomonas starchless mutant defective in ADP-glucose pyrophosphorylase hyper-accumulates triacylglycerol. *Metab. Eng.* 12, 387–391. doi: 10.1016/j.ymben.2010.02.002

Liu, J., Zhu, Y., Tao, Y., Zhang, Y., Li, A., Li, T., et al. (2013). Freshwater microalgae harvested via flocculation induced by pH decrease. *Biotechnol. Biofuels* 6:98. doi: 10.1186/1754-6834-6-98

Lorente, E., Hapońska, M., Clavero, E., Torras, C., and Salvadó, J. (2017). Microalgae fractionation using steam explosion, dynamic and tangential cross-flow membrane filtration. *Bioresour. Technol.* 237, 3–10. doi: 10.1016/j.biortech.2017.03.129

Matsuura, H., Hokura, A., Katsuki, F., Itoh, A., and Haraguchi, H. (2001). Multielement determination and speciation of major-to-trace elements in black tea leaves by ICP-AES and ICP-MS with the aid of size exclusion chromatography. *Anal. Sci.* 17, 391–398. doi: 10.2116/analsci.17.391

Ndikubwimana, T., Chang, J., Xiao, Z., Shao, W., Zeng, X., Ng, I. S., et al. (2016a). Flotation: a promising microalgae harvesting and dewatering technology for biofuels production. *Biotechnol. J.* 11, 315–326. doi: 10.1002/biot.201500175

Ndikubwimana, T., Zeng, X., Murwanashyaka, T., Manirafasha, E., He, N., Shao, W., et al. (2016b). Harvesting of freshwater microalgae with microbial bioflocculant: a pilot-scale study. *Biotechnol. Biofuels* 9:47. doi: 10.1186/s13068-016-0458-5

Rawat, I., Kumar, R. R., Mutanda, T., and Bux, F. (2013). Biodiesel from microalgae: a critical evaluation from laboratory to large scale production. *Appl. Energy* 103, 444–467. doi: 10.1016/j.apenergy.2012.10.004

Safarik, I., Pospiskova, K., Baldikova, E., and Safarikova, M. (2017). "Magnetic particles for microalgae separation and biotechnology," in *Food Bioactives*, ed. M. Puri (Berlin: Springer), 153–169.

Sathe, S., and Durand, P. M. (2016). Cellular aggregation in *Chlamydomonas* (Chlorophyceae) is chimaeric and depends on traits like cell size and motility. *Eur. J. Phycol.* 51, 129–138. doi: 10.1080/09670262.2015.1107759

Scholz, M., Hoshino, T., Johnson, D., Riley, M. R., and Cuello, J. (2011). Flocculation of wall-deficient cells of *Chlamydomonas reinhardtii* mutant cw15 by calcium and methanol. *Biomass Bioenergy* 35, 4835–4840. doi: 10.1016/j.biombioe.2011.08.020

Siaut, M., Cuiné, S., Cagnon, C., Fessler, B., Nguyen, M., Carrier, P., et al. (2011). Oil accumulation in the model green alga *Chlamydomonas reinhardtii*: characterization, variability between common laboratory strains

and relationship with starch reserves. *BMC Biotechnol.* 11:7. doi: 10.1186/1472-6750-11-7

Sueoka, N. (1960). Mitotic replication of deoxyribonucleic acid in *Chlamydomonas reinhardi*. *Proc. Natl. Acad. Sci. U.S.A.* 46, 83–91. doi: 10.1073/pnas.46.1.83

Vandamme, D., Foubert, I., Fraeye, I., Meesschaert, B., and Muylaert, K. (2012). Flocculation of *Chlorella vulgaris* induced by high pH: role of magnesium and calcium and practical implications. *Bioresour. Technol.* 105, 114–119. doi: 10.1016/j.biortech.2011.11.105

Vandamme, D., Pontes, S. C. V., Goiris, K., Foubert, I., Pinoy, L. J. J., and Muylaert, K. (2011). Evaluation of electro-coagulation–flocculation for harvesting marine and freshwater microalgae. *Biotechnol. Bioeng.* 108, 2320–2329. doi: 10.1002/bit.23199

Waghmare, A. G., Salve, M. K., LeBlanc, J. G., and Arya, S. S. (2016). Concentration and characterization of microalgae proteins from *Chlorella pyrenoidosa*. *Bioresour. Bioprocess.* 3:16. doi: 10.1186/s40643-016-0094-8

Wang, W., Lee, D.-J., and Lai, J.-Y. (2015). Aggregate formation affects ultrasonic disruption of microalgal cells. *Bioresour. Technol.* 198, 907–912. doi: 10.1016/j.biortech.2015.09.099

Wang, Z. T., Ullrich, N., Joo, S., Waffenschmidt, S., and Goodenough, U. (2009). Algal lipid bodies: stress induction, purification, and biochemical characterization in wild-type and starchless *Chlamydomonas reinhardtii*. *Eukaryot. Cell* 8, 1856–1868. doi: 10.1128/EC.00272-09

Wu, Z., Zhu, Y., Huang, W., Zhang, C., Li, T., Zhang, Y., et al. (2012). Evaluation of flocculation induced by pH increase for harvesting microalgae and reuse of flocculated medium. *Bioresour. Technol.* 110, 496–502. doi: 10.1016/j.biortech.2012.01.101

Wyatt, N. B., Gloe, L. M., Brady, P. V., Hewson, J. C., Grillet, A. M., Hankins, M. G., et al. (2012). Critical conditions for ferric chloride-induced flocculation of freshwater algae. *Biotechnol. Bioeng.* 109, 493–501. doi: 10.1002/bit.23319

Xu, L., Brilman, D. W. W., Withag, J. A., Brem, G., and Kersten, S. (2011). Assessment of a dry and a wet route for the production of biofuels from microalgae: energy balance analysis. *Bioresour. Technol.* 102, 5113–5122. doi: 10.1016/j.biortech.2011.01.066

Zabawinski, C., Van Den Koornhuyse, N., D'Hulst, C., Schlichting, R., Giersch, C., Delrue, B., et al. (2001). Starchless mutants of *Chlamydomonas reinhardtii* lack the small subunit of a heterotetrameric ADP-glucose pyrophosphorylase. *J. Bacteriol.* 183, 1069–1077. doi: 10.1128/JB.183.3.1069-1077.2001

Conflict of Interest Statement: The authors declare that the research was conducted in the absence of any commercial or financial relationships that could be construed as a potential conflict of interest.

frontiers in Plant Science

METHODS
published: 13 November 2017
doi: 10.3389/fpls.2017.01949

An Extended Approach to Quantify Triacylglycerol in Microalgae by Characteristic Fatty Acids

Miao Yang[1,2,3], Yan Fan[2,3], Pei-Chun Wu[2], Ya-Dong Chu[2], Pei-Li Shen[2,4], Song Xue[2] and Zhan-You Chi[1]*

[1] School of Life Sciences and Biotechnology, Dalian University of Technology, Dalian, China, [2] Marine Bioengineering Group, Dalian Institute of Chemical Physics, Chinese Academy of Sciences, Dalian, China, [3] University of Chinese Academy of Sciences, Beijing, China, [4] State Key Laboratory of Bioactive Seaweed Substances, Qingdao Bright Moon Seaweed Group Co., Ltd., Qingdao, China

Microalgae represent a third generation biofuel feedstock due to their high triacylglycerol (TAG) content under adverse environmental conditions. Microalgal TAG resides in a single cell and serves as a lipid class mixed with complicated compositions. We previously showed that TAG possessed characteristic fatty acids (CFAs) for quantification and was linearly correlated with the relative abundance of CFA within certain limits in microalgae. Here, we defined the application range of the linear correlation between TAG and CFA in the oleaginous microalgae *Chlamydomonas reinhardtii* and *Phaeodactylum tricornutum*. In addition, TAG quantification was further expanded to a wide range of levels and the absolute amounts of saturated or monounsaturated CFAs, 16:0 and 18:1n9 of *C. reinhardtii* and 16:0 and 16:1n7 of *P. tricornutum*, instead of polyunsaturated CFAs, were verified to be linearly correlated to TAG levels throughout the entire period of nitrogen stress. This approach utilizes a single fatty acid to quantify TAG mixtures, and is rapid, simple and precise, which provides a useful tool for monitoring TAG accumulation of distinct microalgal species and facilitating high-throughput mutant screening for microalgae.

Keywords: microalgae, triacylglycerol, quantification, characteristic fatty acid, linear correlation

OPEN ACCESS

Edited by:
Jianhua Fan,
Carnegie Institution for Science (CIS), United States

Reviewed by:
Kun Wang,
Michigan State University, United States
Nishikant Wase,
University of Nebraska–Lincoln, United States

****Correspondence:***
Song Xue
xuesong@dicp.ac.cn

Specialty section:
This article was submitted to Plant Biotechnology, a section of the journal Frontiers in Plant Science

Received: *20 September 2017*
Accepted: *30 October 2017*
Published: *13 November 2017*

Citation:
Yang M, Fan Y, Wu P-C, Chu Y-D, Shen P-L, Xue S and Chi Z-Y (2017) An Extended Approach to Quantify Triacylglycerol in Microalgae by Characteristic Fatty Acids. Front. Plant Sci. 8:1949. doi: 10.3389/fpls.2017.01949

INTRODUCTION

Microalgae have emerged as a promising renewable resource for producing triacylglycerols (TAGs), which can be used as biofuel feedstocks (Wijffels and Barbosa, 2010). Nitrogen starvation is the most effective manner to induce microalgal TAG biosynthesis (Zienkiewicz et al., 2016). It is necessary to investigate performance of TAG accumulation under distinct levels of nitrogen stress in microalgae to screen potential candidates for oleaginous species. However, microalgae are different from other oleaginous feedstocks, such as plant seeds, of which the lipids are dominated by TAG. In particular, microalgae exist in form of a single cell and contain various lipids with different polarities. In most microalgal cells, the chloroplast serves as the largest organelle and contains many complicated and hydrophobic components, which makes TAG quantification more intricate. Therefore, it is desirable to develop an approach to efficiently quantify TAG content of microalgal biomass under various growth conditions.

There are several methods to determine the TAG content of microalgal biomass. The gravimetric method of Bligh and Dyer (1959) is widely used to evaluate the lipid content in microalgae. Using

this method, many other liposoluble components, including pigments and other hydrophobic compounds, can be co-extracted. With the aid of solid phase extraction (SPE) column, neutral lipids that are mainly composed of TAG can be separated from polar lipids (Li et al., 2010; Danielewicz et al., 2011). However, the two extraction methods are both dependent on the similarity-intermiscibility theory and lead to overestimation of microalgal TAG levels (Na et al., 2011). Another commonly used approach is based on thin layer chromatography (TLC) separation followed by gas chromatography-flame ionization detection (GC-FID) or a TLC scanner in terms of densitometry quantification (Siaut et al., 2011), which is time and labor consuming or requires specialized expensive equipment, as well as not applicable for assessing TAG phenotypes in real-time. TAG can also be quantified by high performance liquid chromatography (HPLC) (Kobayashi et al., 2013), direct mass spectrometry (MS) (Danielewicz et al., 2011) and liquid chromatography-mass spectrometry (LC-MS) (Goold et al., 2016), but these methods are complicated due to the requirement of a lipid extraction pre-treatment and their complex molecule compositions accompanied with intricate data treatment. A specific quantification method (Allen et al., 2014) is also developed for algal TAG using LC-MS/MS in multiple reaction monitor mode and the incorporation of catalytic hydrogenation reduces complexity of targeted TAG pool; however, the relevant pre-treatment together with relatively complex data analysis are still of multiple steps, to a certain extent. Raman microspectroscopy (Wang T. et al., 2014), spontaneous Raman spectroscopy and coherent anti-Stokes Raman scattering (CARS) microscopy (He et al., 2012), Fourier transform infrared (FT-IR) spectroscopy (Miglio et al., 2013) and thermogravimetric analyses (Na et al., 2011) have also been used to monitor TAG production. Although there is no need to extract lipids from microalgal biomass using these methods, non-TAG molecules with similar biochemical bonds or thermal features can easily cause interference, which leads to inaccurate quantification.

To date, it has been reported that microalgal oils can be determined by direct transesterification of fresh or dry algal samples (Patil et al., 2013; Liu et al., 2015), which is rapid and precise, and has minor sample demands. Based on this technique, the specific fatty acids, 18:1 and 18:4, were identified as potential biomarkers of neutral lipids in *Isochrysis zhangjiangensis* and linear fits existed between the relative abundances of the specific fatty acids and the neutral lipid content as reported by our previous study (Wang H. et al., 2014). As the major components of neutral lipids, TAGs are mainly comprised of saturated or monounsaturated fatty acyl groups (Siaut et al., 2011), which are considered as the potential feedstocks for biodiesel production. Thus, quantifying TAG is indispensable for microalgal studies in terms of their use as renewable resources. Our recent study further showed that TAG could be quantified using the relative abundance of characteristic fatty acids (CFA) and an excellent linear correlation existed between them, which has been verified in three microalgal strains, including *Phaeodactylum tricornutum*, *Nannochloropsis oceanica* and *Chlorella pyrenoidosa* (Shen et al., 2016). Additionally, Liu et al. (2013) reported that, in *Chlamydomonas reinhardtii*, the 16:0-to-16:4 ratio in fatty acid methyl esters (FAMEs) was strongly correlated with the TAG-to-total acyl group ratio, which serves as an internal standard for TAG estimation. However, TAG quantification using fatty acids in these studies are only available within certain limits, usually when TAG accumulation is at a moderate or relatively low level, and the application range still remains unknown.

Based on these studies, the TAG has been validated to possess CFAs for quantification in microalgae. Many algal strains, including oleaginous and non-oleaginous species, present significant alterations in the fatty acyl profile in response to nitrogen deprivation along with an increase of TAG level (Breuer et al., 2012). This stage for TAG assembly is named Stage I. However, after that, the fatty acid profile is unaltered and TAG continues to accumulate (Breuer et al., 2012). At this point, the quantitative approach for TAG based on the relative abundance of CFA in our previous work (Shen et al., 2016) is no more available, and this period for TAG synthesis is named Stage II. Thus, it is crucial to evaluate TAG accumulation performance using CFAs in an expanding coverage, so that the TAG levels of microagal cells during distinct stages (Stage I and II) of TAG accumulation can be rapidly and accurately quantified.

Currently, *C. reinhardtii* has emerged as the leading organism to investigate algae-based biofuel production due to its most available and multiple genetic tools and techniques (Merchant et al., 2007; Scranton et al., 2015). Moreover, starchless mutants deficient in ADP-glucose pyrophosphorylase harbor a unique feature of hyper-accumulating TAG (Li et al., 2010). The model marine diatom *P. tricornutum* serves as a potential producer for biodiesel due to its high TAG accumulation capability and robust environmental adaptation (Breuer et al., 2012). The available genetic tools and genome engineering techniques have empowered this oleaginous microalgal strain for industrial biofuel production (Daboussi et al., 2014).

In this study, the two model microalgal strains *C. reinhardtii* and *P. tricornutum* were used to correlate the TAG content with the fatty acyl composition under distinct levels of nitrogen stress. During the entire period of nitrogen starvation, different relationships between the TAG levels and fatty acid components were explored, and the respective CFAs were confirmed to rapidly quantify the TAG amounts in these two algae. This extended approach to quantify distinct levels of TAG using CFAs was successfully applied to these two reference species and could serve as a useful tool for monitoring TAG accumulation of multiple microalgal species and facilitating high-throughput mutant screening for microalgae.

MATERIALS AND METHODS

Microalgal Cultivation

The *C. reinhardtii* cell wall-less strain, starchless mutant BAFJ5 (cw15 sta6, CC4348) was obtained from the Chlamydomonas Resource Center[1]. The *P. tricornutum* strain CCAP1055/1 was

[1]http://www.chlamycollection.org/

provided by the Culture Collection of Algae and Protozoa[2]. These two strains were maintained in a 500-mL Erlenmeyer flask with 200 mL of Tris-acetate-phosphate (TAP) medium (Harris, 2009) under orbital shaking (80 rpm) and in a 1000-mL Erlenmeyer flask with 400 mL of f/2 medium containing 1 M sodium silicate (Guillard, 1975), respectively. They were both sub-cultured under a 12 h light /12 h dark cycle at 25°C with an illumination of 50 μmol photons m^{-2} s^{-1}, and the illumination intensity was determined by a photosynthetically active radiation (PAR) detector (Optometer P9710, Gigahertz Optik Corporation, Germany).

Two-stage cultivations, including the first nitrogen repletion phase and the subsequent nitrogen-deprived phase, were used to induce TAG accumulation. Illumination was set as 50 μmol photons m^{-2} s^{-1} during N-replete cultivation. *C. reinhardtii* was cultured in TAP medium for 48 h under continuous illumination and *P. tricornutum* was cultured in 3 × f/2 medium containing 3 M sodium silicate (Feng et al., 2011) for 48 h under a 12 h light/12 h dark cycle. The batch culture mode was performed in a glass air bubble column photobioreactor (50 mm diameter, 450 mm height, 600 mL for a culture volume) with air (120 mL min^{-1}) containing 2% CO_2. When two algal cell populations grew to 1–2 × 10^7 cells mL^{-1} under N-replete conditions, *C. reinhardtii* and *P. tricornutum* were washed once with TAP-N and 3 × f/2-N medium, respectively, and inoculated at 1 × 10^7 cells mL^{-1} in the corresponding medium. During N-deprived cultivation for *C. reinhardtii* and *P. tricornutum*, the illuminations provided from one side rose to 100 and 500 μmol photons m^{-2} s^{-1} to enhance TAG accumulation, respectively, and the light cycles were the same as that used under the N-replete conditions.

One independent batch culture that included two biological replicates for *C. reinhardtii* and *P. tricornutum* was conducted. *C. reinhardtii* was sampled at a total of 30 time points over 120 h of N-deficiency. *P. tricornutum* was sampled at 21 time points during the light period over 336 h of N-starvation. The samples were first centrifuged at 4000 rpm for 5 min, and the pellets were immediately frozen at −80°C, followed by lyophilization for 4 h. In particular, pellets of *P. tricornutum* were rinsed with ammonium bicarbonate (0.5 M) to remove extracellular salt before lyophilization. After grinding cells into powder, the algal biomass was stored at −80°C for subsequent lipid and element analysis.

Lipid Analysis

The lyophilized algal powders were used to detect the fatty acid profiles or contents, and TAG contents. For the fatty acid profiles, algal biomass was converted to FAMEs through direct transesterification, followed by GC determination as previously reported (Liu et al., 2015). Briefly, approximately 5 mg of lyophilized cells were weighed using an analytical balance (MSE125P-1CE-DI, Sartorius, Germany). Five milliliters of 2% H_2SO_4 in methanol were added, and the mixture was heated at 70°C for 1 h. FAMEs were extracted by hexane and quantified using an Agilent GC 7890A fitted with FID and a DB-23 column (Agilent Technologies, United States). Glycerol triheptadecanoate (TAG 51:0, 17:0/17:0/17:0, Sigma–Aldrich, United States) was used as an internal standard to determine fatty acid recovery for quantification.

Unlike detection of fatty acid profiles or contents, TAG quantification required additional two steps beyond transesterification, including total lipid extraction from biomass (Bligh and Dyer, 1959) and lipid separation by TLC. Methanol:chloroform:water (1:1:0.9) was used as the extraction solvent. A 950 μL extraction solvent composed of methanol:chloroform:water (1:2:0.8) was first added to pre-weighed lyophilized cells with a pre-addition of the lipid standard TAG 51:0 followed by a 15-min sonication. After a complete mixing, an additional addition of 250 μL chloroform was mixed into the solvent, followed by a subsequent addition of 250 μL H_2O. The samples were vortexed and centrifuged for 2 min at 12,000 rpm. The organic phase of the lower layer was then transferred to a 2 mL glass vial. The lipid extraction process was repeated two more times and the extracted lipids were pooled and dried under a gentle stream of N_2. Next, 100 μL chloroform were added to redissolve the total lipids, and the lipid extracts were deposited onto a TLC plate (10 cm × 10 cm, TLC silica gel 60 F254, Merck KGA, Germany). The TLC plate was developed with hexane/diethyl ether/acetic acid (85:15:1, v/v/v), and the lipids were revealed by spraying with 0.05% (m/v) primuline (Sigma–Aldrich, United States) in acetone/water (80/20, v/v). The silica-containing TAG was scrapped off, followed by transesterification and GC detection.

The individual fatty acid percentage of the cellular total acyl groups and, the individual fatty acid and TAG contents based on the cellular dry weight (DW) were calculated as follows:

$$P_i = A_i / \Sigma A_i \times 100\% \quad (1)$$

$$M_i = (A_i / A_s \times M_s) / M_a \times 100\% \quad (2)$$

$$M_{TAG} = (\Sigma A_i / A_s \times M_s) / M_a \times 100\% \quad (3)$$

where P_i, M_i and M_{TAG} were the individual fatty acid percentage of total fatty acids, fatty acid content and TAG content, respectively. A_i and ΣA_i in Equation 1 were the peak area of the individual fatty acid and that of cellular total fatty acids, respectively. ΣA_i in Equation 3 was the peak area of total fatty acyls of TAG. A_s, M_s and M_a in Equations 2 and 3 were the peak area of the internal standard TAG 51:0, the addition amount of TAG 51:0 and the accurate algal biomass, respectively.

Elemental Analysis

Quantification of carbon and nitrogen of the algal biomass was performed using a vario EL cube elemental analyzer (Elementar, Germany). Two to four milligrams of lyophilized algal cells were accurately weighed using an automatic analytical balance (Mettler Toledo XP6, Switzerland).

Statistical Analysis

Correlation coefficients between CFAs and TAG contents were calculated using SPSS 19.0. Statistical significance of the result of

[2]https://www.ccap.ac.uk/

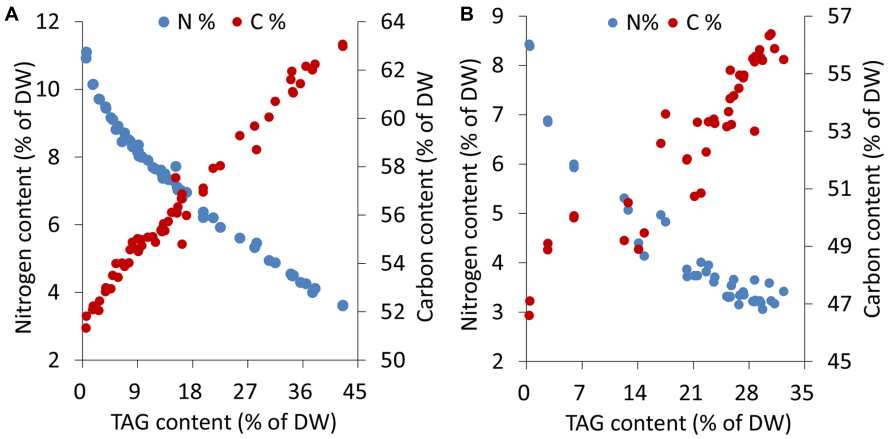

FIGURE 1 | Elemental analyses and TAG contents in *C. reinhardtii* **(A)** and *P. tricornutum* **(B)** under nitrogen deprivation. The sampling time points were 30 for *C. reinhardtii* **(A)** and 21 for *P. tricornutum* **(B)**. Each time point was derived from two biological replicates of a single cultivation, and each data point was drawn from an individual result rather than the mean of the two biological replicates (n = 60, **A**; n = 42, **B**).

each time point was evaluated by the Two-tailed t-test using SPSS 19.0, where the significance $P < 0.05$.

RESULTS

Variation of Fatty Acid Profiles and TAG Contents of *C. reinhardtii* and *P. tricornutum* under Distinct Levels of Nitrogen Stress

Microalgal cells underwent different levels of stress during an extended period of nitrogen deprivation. Elemental analyses indicated that the cellular nitrogen contents decreased by 68%, from 11.1 to 3.6% of DW, in *C. reinhardtii* and 64%, from 8.4 to 3.0% of DW, in *P. tricornutum*. The carbon contents of both *C. reinhardtii* and *P. tricornutum* increased by 1.2-fold following N-starvation (**Figure 1**). In both algae, as the stress levels gradually rose, a sustaining accumulation of TAG occurred.

During normal growth of *C. reinhardtii* and *P. tricornutum*, the primary fatty acyl groups of the former consisted of 16:0, 16:4n3 and 18:3n3, and those of the latter consisted of 16:0, 16:1n7, 16:3n4 and 20:5n3 (eicosapentaenoic acid, EPA). Each of the fatty acids accounted for more than 10% of the total lipids (**Figures 2A,B**). During Stage I of TAG accumulation (less than 24 h for *C. reinhardtii* and 72 h for *P. tricornutum* in this study), the fatty acid compositions of the two algal cells varied notably as the nitrogen stress levels grew (**Figures 2A,B**). At the end of Stage I, the relative abundances of 16:0, 18:1n9, 18:1n7 and 18:2n6 increased by 1.3-, 2.3-, 1.7- and 1.8-fold in *C. reinhardtii*, respectively. Inversely, 16:4n3 and 18:3n3 decreased to 40 and 70% of the initial levels, respectively. In *P. tricornutum*, both 16:0 and 16:1n7 rose up to 1.6-fold of the initial levels and 16:3n4 and EPA sharply declined to 20 and 30% after 72 h of N-depletion, respectively. At this point, these two microalgae accumulated TAGs up to 17% for *C. reinhardtii* and 20% for *P. tricornutum* based on DW (**Figures 2A,B**). During Stage II (longer than 24 h for *C. reinhardtii* and 72 h for *P. tricornutum* in this study), the relative fatty acid percentages of these two algae were almost unaltered; however, TAG substantially accumulated up to 43% for *C. reinhardtii* and 32% for *P. tricornutum* based on DW (**Figures 2A,B**).

Quantification of TAG Using the Relative Abundance of CFA in *C. reinhardtii* and *P. tricornutum*

To obtain quantitative models of TAG during the two stages, the relative abundances of fatty acids and TAG levels were first correlated in *C. reinhardtii* and *P. tricornutum* that were subjected to nitrogen stress. During Stage I, linear fits were observed between the relative percentages of 16:0, 16:4n3, 18:1n9 as well as 18:3n3 and the TAG contents in *C. reinhardtii*, and the relevance coefficients r^2 were 0.93, 0.92, 0.91, and 0.96, respectively (**Figure 3A**). 16:0 and 18:1n9 were found to be positively correlated with the amounts of TAG and 16:4n3 and 18:3n3 were on the contrary (**Figure 3A**). During stage II, the TAG level exceeded 17% of DW and the proportions of the four fatty acids of total lipids were maintained at 28 ± 1%, 4 ± 0%, 13 ± 1% and 13 ± 1%, respectively (**Figure 3A**). Obviously, the above linear models were no longer applicable. Similarly, in *P. tricornutum*, four fatty acids, 16:0, 16:1n7, 16:3n4 and EPA, were shown to be linearly related to the TAG contents (**Figure 3B**) and the r^2 values were all more than 0.90 during Stage I. A positive relationship existed between 16:0 as well as 16:1n7, and TAG, and there was a negative correlation between 16:3n4 as well as EPA, and TAG in *P. tricornutum* (**Figure 3B**). Beyond these limitations, the four fatty acyl groups were stable at 39 ± 1%, 40 ± 1%, 1 ± 0% and 6 ± 0%, respectively (**Figure 3B**). These linear correlations indicated that 16:0, 16:4n3, 18:1n9 as well as 18:3n3 of *C. reinhardtii*, and 16:0, 16:1n7, 16:3n4 as well as EPA of *P. tricornutum* were CFAs to quantify TAG, but it was only limited to Stage I of nitrogen stress in both two algae.

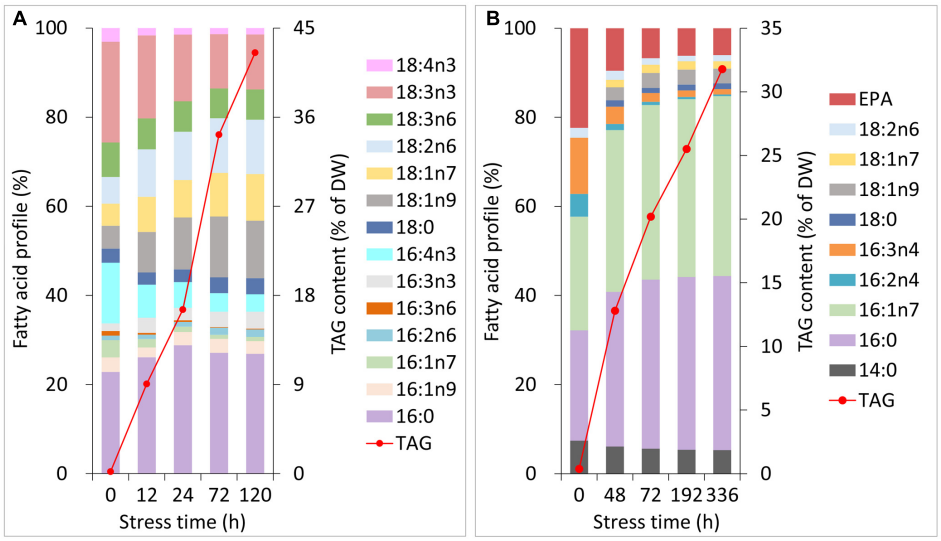

FIGURE 2 | Changes in the fatty acid profiles and TAG contents of *C. reinhardtii* **(A)** and *P. tricornutum* **(B)** under N-deprived conditions. Data are means of two biological replicates with two technical replicates (n = 4) from one independent cultivation.

Quantification of TAG Using the Absolute Amount of CFA in *C. reinhardtii* and *P. tricornutum*

To further rapidly quantify TAG also using CFA during Stage II in nitrogen-deprived *C. reinhardtii* and *P. tricornutum*, the individual CFA content based on DW was correlated with the TAG content. The individual CFA identified for Stage I was quantified in terms of the internal standard and the accurate microalgal biomass, which was calculated according to Equation 2 (see Materials and Methods). The absolute amounts of 16:0 and 18:1n9 of *C. reinhardtii* and 16:0 and 16:1n7 of *P. tricornutum* all showed linear fits with the increased TAG levels during both Stage I and II (**Figures 4A,B**). The relevance coefficients of 16:0 and 18:1n9 with TAG for *C. reinhardtii* were 0.94 and 0.97 (**Figure 4A**), and the coefficients for 16:0 and 16:1n7 with TAG for *P. tricornutum* were both 0.98 (**Figure 4B**). However, by contrast, the polyunsaturated CFAs of Stage I, including 16:4n3 and 18:3n3 of *C. reinhardtii* as well as 16:3n4 and EPA of *P. tricornutum*, exhibited no such fits with TAG. Therefore, using the linear equations in **Figure 4**, the TAG contents (x) could only be determined quickly and precisely by the continuously increasing saturated or monounsaturated CFAs (y).

DISCUSSION

Linear Correlation between TAG and CFA during Distinct Stages of Nitrogen Stress in Microalgae

In microalgae, the neutral lipid, TAG, has been verified to possess CFA for quantification and the relative abundance of CFA can be used to linearly quantify TAG within certain limits under stress conditions (Shen et al., 2016). However, TAG consecutively accumulates as stress level increases, and it is inconsistent with the variation of fatty acid profile, i.e., gradual alteration followed by invariability, in stress-induced microalgae (Breuer et al., 2012). Thus, it is necessary to define applicability and expand coverage of the CFA-based TAG quantification method established in our previous work (Shen et al., 2016). To expand its application range, the correlations between TAG and CFA were further explored over the entire period of nitrogen stress in two oleaginous microalgae *C. reinhardtii* and *P. tricornutum*.

Under stress condition, microalgae usually encompasses gradual chloroplast degradation and remodeling of the lipidome, accompanied by substantial accumulation of TAG (Zienkiewicz et al., 2016); all these alterations affect the fatty acid compositions of microalgae prominently. In this study, the fatty acid profile of algal biomass changed gradually and then remained constant upon nitrogen starvation, i.e., Stage I and Stage II, which agreed with the previous report (Breuer et al., 2012). Thus, TAG accumulation underwent two stages in terms of the fatty acid profile and the constant fatty acid profile became the determinant to distinguish Stage I and Stage II of nitrogen stress. At the turning point, the TAG levels of *C. reinhardtii* and *P. tricornutum* reached up to 17 and 20% of DW, respectively (**Figure 3**). The results in this study confirmed that the TAG quantification method based on the relative abundance of CFA (Shen et al., 2016) was only applied to Stage I. More importantly, it was the absolute amount of saturated or monounsaturated CFA, e.g., 16:0 and 18:1n9 of *C. reinhardtii* and 16:0 and 16:1n7 of *P. tricornutum*, instead of the relative abundance, to be linearly correlated to TAG content over the entire period of nitrogen deprivation. In addition, the polyunsaturated CFA could be used to quantify TAG only at Stage I and only when the relative abundance was available.

In this study, the proportions of TAG in total lipids exhibited gradual increases from 6 to 81% for *C. reinhardtii* and from 4

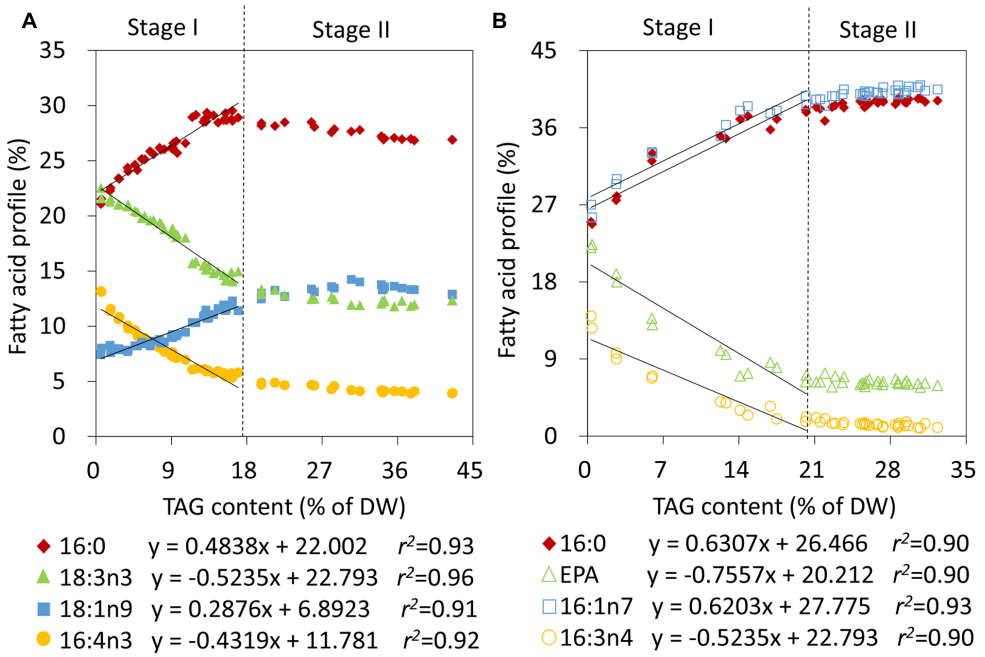

FIGURE 3 | Correlation analyses of the relative abundances of fatty acids and TAG contents in *C. reinhardtii* **(A)** and *P. tricornutum* **(B)** under nitrogen deprivation. The sampling time points were 30 for *C. reinhardtii* **(A)** and 21 for *P. tricornutum* **(B)**. Solid lines indicated the linear fits between TAG contents and the relative abundances of CFAs at Stage I and dashed lines indicated the boundary of Stage I and Stage II. In the linear equations, the variable "x" is the TAG content, "y" is the relative fatty acid percentage, and "r^2" is the correlation coefficient of x and y. The linear equations were derived from individual results of 19 time points (n = 38) within 24 h of nitrogen starvation for *C. reinhardtii* and 7 time points (n = 14) within 72 h of nitrogen starvation for *P. tricornutum*. Each time point was derived from two biological replicates of a single cultivation, and each data point was drawn from an individual result rather than the mean of the two biological replicates (n = 60, **A**; n = 42, **B**).

to 83% for *P. tricornutum* in response to nitrogen starvation (**Supplementary Figure S1**). In these two microalgae, TAGs were mainly composed of saturated and monounsaturated fatty acyls (Supplementary Tables S1, S2), which were presumed to be *de novo* synthesized (Liu et al., 2013). These newly synthesized fatty acids were mostly diverted into TAG following N-depletion. Thus, the concurrent increases of the absolute amounts of 16:0 and 18:1n9 of *C. reinhardtii* and 16:0 and 16:1n7 of *P. tricornutum* as well as the respective TAG contents based on dry biomass led to the formation of the linear correlations during the entire stage of nitrogen stress. It also demonstrated that the quantitative saturated or monounsaturated CFA was the authentic CFA, which could be utilized to quantify TAG at any levels.

Apart from a slight increase of 18:3n3 of *C. reinhardtii*, the contents of all of the polyunsaturated CFAs, 16:4n3 of *C. reinhardtii* and 16:3n4 and EPA of *P. tricornutum*, based on DW were almost invariable (**Figure 4**), which agreed well with previously reported results (Boyle et al., 2012; Remmers et al., 2017). These polyunsaturated CFAs were primarily located in photosynthetic membranes and played crucial roles in stabilizing photosystems (Petroutsos et al., 2014). A portion of polyunsaturated fatty acids was transferred from polar lipids to TAG when subjected to adverse conditions (Remmers et al., 2017), which could protect them from peroxidation. These factors contributed to stabilizing the amount of polyunsaturated fatty acids following nitrogen stress, yet they were no longer qualified to be CFAs for TAG quantification during Stage II.

Normally, *de novo* fatty acid synthesis together with various membrane lipids turnover contributes to TAG biosynthesis (Goold et al., 2016). In this study, no obvious alterations in acyl compositions of the major lipids, MGDG, DGDG and DGTS, were found during Stage I and Stage II of TAG accumulation in nitrogen-deprived *C. reinhardtii* as a whole (**Supplementary Figure S2**). However, in contrast to the greatly increased TAG, the levels of the three major lipids varied slightly (**Supplementary Figure S3**) in stress-induced *C. reinhardtii*. At the turning point of TAG accumulation (24 h of nitrogen deprivation), TAG levels of *C. reinhardtii* were almost equal to the polar lipid levels. During Stage I, TAG accumulation appeared to be intimately correlated with contribution of various polar lipids, especially the newly synthesized DGDG and DGTS (**Supplementary Figure S3**). It is likely that more than one pathway involving distinct membrane lipids differentially participated in TAG assembly during Stage I, which resulted in a notable variation in the lipid profile. As TAG level was further elevated, TAG accumulation entered into Stage II and the fatty acid profile was no longer altered. During Stage II, TAG dramatically accumulated up to the level that was much more than that of polar lipids, and thus TAG formation was mainly

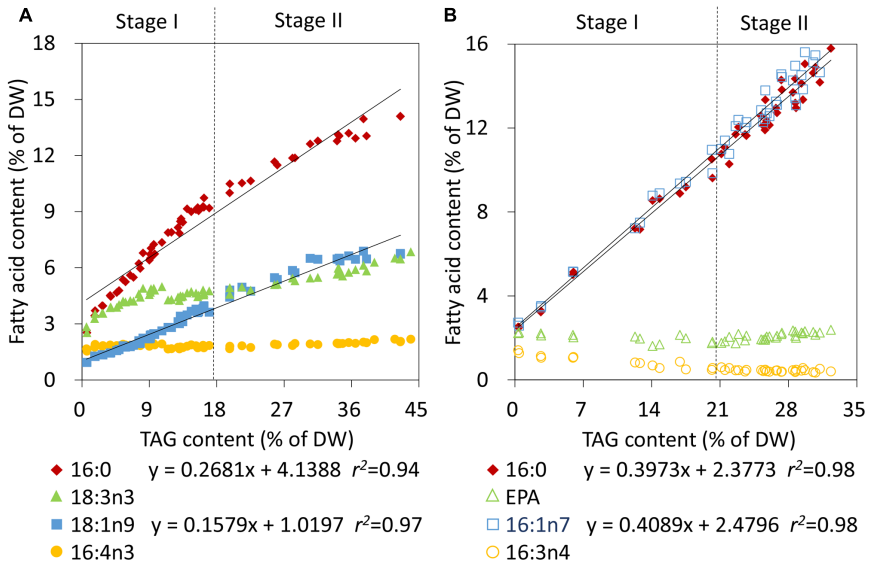

FIGURE 4 | Correlation analyses of the fatty acid contents and TAG contents in *C. reinhardtii* **(A)** and *P. tricornutum* **(B)** under nitrogen deprivation. The sampling time points were 30 for *C. reinhardtii* **(A)** and 21 for *P. tricornutum* **(B)**. Solid lines indicated the linear fits between TAG contents and the absolute amounts of CFAs during the entire phase of nitrogen starvation, including Stage I and Stage II, and dashed lines indicated the boundary of Stage I and Stage II. In the linear equations, the variable "x" is the TAG content, "y" is the CFA content, and "r^2" is the correlation coefficient of x and y. The linear equations were derived from individual results of 30 time points (n = 60) for *C. reinhardtii* and 21 time points (n = 42) for *P. tricornutum*. Each time point was derived from two biological replicates of a single cultivation, and each data point was drawn from an individual result rather than the mean of the two biological replicates (n = 60, **A**; n = 42, **B**).

attributed to the *de novo* biosynthesis, instead of turnover of membrane lipids. These findings suggested that the TAG biosynthesis pathways reached equilibrium. Therefore, Stage II was a period of lipid homeostasis for microalgae, which implied a balanced status of multiple TAG biosynthetic pathways. Overall, the turnover of membrane lipids together with the *de novo* biosynthesis pathway differentially contributes to TAG biosynthesis during different stages of TAG accumulation in microalgae. This could help understand the origin of CFAs and the distinct TAG biosynthesis mechanisms, which provides insights into their linear correlation with TAG content in the algal cell.

Principle of the CFA-Based Method to Quantify TAG in Microalgae

The current study validated two sets of correlations between CFA and TAG levels, and the correlations were applied to two stages of TAG accumulation for two model microalgae *C. reinhardtii* and *P. tricornutum*. First, it was necessary to identify the TAG accumulation stage based on the microalgal fatty acid profiles, which just required direct transesterification. Or, it could be judged in terms of the known stress time, i.e., short or long-term stress. Subsequently, the appropriate method for TAG quantification was confirmed to rapidly evaluate TAG accumulation in microalgae. If the fatty acid profile was coincided with that of Stage I, there was just a need to calculate TAG content using linear equation of that and the relative abundance of any CFA in **Figure 3**. If the fatty acid profile matched with that of Stage II, it was required to perform the transesterification process again and additional operations, including the accurate additions of fresh or dry algal biomass and internal standard of known weight, were necessary to calculate TAG content using linear equation of that and the absolute amount of any CFA in **Figure 4**. Alternatively, the absolute amount of the saturated or monounsaturated CFA, i.e., 16:0 and 18:1n9 of *C. reinhardtii* and 16:0 and 16:1n7 of *P. tricornutum*, can always be used to quantify TAG during both Stage I and Stage II of nitrogen stress. In this case, the relative abundance of CFA can be neglected, but the accurate additions of algal biomass and internal standard of known weight is necessary for each determination.

No matter which linear equation is used, TAG content can be rapidly determined without either prior lipid extraction or succeeding lipid separation using SPE column or TLC plate and it only needs one-step transesterification and GC-FID analysis, which is in favor of the algal lipid researchers to monitor TAG accumulation in real-time. This approach requires less than 1.5 h for one determination. If one wishes to track the TAG contents over a period of time, it is feasible to perform direct transesterification using fresh cells and GC-FID analysis in the meantime. Additionally, the algal samples for TAG quantification can be fresh or dry cells and a minimum of biomass equivalent to 30 μg lipids can meet demands as reported by our previous study (Liu et al., 2015), which is much less than the classical TLC versus GC-FID method. As to the emerging LC-MS method, TAG is a mixture of various components and it is both time-consuming and expensive to separate and detect many molecular species of TAG using HPLC and MS; the accurate quantification of the mixture also needs complicated

data treatment even a quality control correction in terms of TLC-GC analysis (Jouhet et al., 2017). In comparison, direct transesterification coupled with GC detection of certain fatty acids is quicker and simpler. Overall, this extended CFA approach utilizes a single fatty acid to quantify TAG mixtures and can facilitate high-throughput mutant screening for algae to a certain extent, which not only simplifies the process but also ensures its accuracy.

It is worth noting that the fatty acyl profiles of microalgae from distinct labs are probably different, and thus, the TAG amounts quantified using CFAs might be somewhat different due to distinct culture conditions and microalgal species specificities. Therefore, it is preferable to establish the corresponding quantitative relationships between CFA and TAG for the targeted strains cultured under the designated conditions, which is convenient for researchers to quickly assess the TAG levels and facilitate relevant biochemical or physiological studies.

As a whole, the present work is to establish distinct linear equations of TAG and CFA across distinct stages of TAG accumulation with emphasis on extensive application, though our previous work is to identify CFAs for TAG quantification and confirm correlation between CFA and TAG content with emphasis on the concept of "CFA." This study not only expands coverage of TAG quantification based on distinct linear equations, but also applies to an alga mutant that enhances oil biosynthesis, i.e., *sta6* of a starchless *C. reinhardtii* mutant, which both increase impact of the CFA approach. The successful application of this method on the mutant shows its usefulness for the potential forward genetics study, which could also be expanded to other mutant algal species.

To further increase impact of the CFA approach for TAG quantification, we checked the correlations of TAG and CFA under phosphate deprivation for *Nannochloropsis oceanica* and high salt stress conditions (HS medium, photoautotraphic conditions) for *sta6* of *C. reinhardtii*. The results revealed that the excellent linear relationships also existed between TAG and CFA and the linear correlation coefficients were all more than 0.90 under both the two stress conditions (**Supplementary Figures S4**, **S5**), which further confirmed validity and wide use of the CFA method. While these linear correlations were consistent with that under nitrogen stress, they were not completely the same due to the fact that TAG accumulation mechanisms differed among various stress conditions. Beyond that, the linear correlations of TAG contents and the absolute amounts of CFAs (16:0 and 18:1) were also verified in the reported studies of Lohman et al. (2014) and Wase et al. (2017). Thus, the CFA method works not only for the nitrogen induced TAG production, but also for other stress conditions, e.g., high salt, phosphate starvation, different inorganic carbon regimes (Lohman et al., 2014) and even the various chemical activators (Wase et al., 2017). Based on our present study and the published data, the linear correlation of TAG and CFA is proved to be available for more than one stress condition, although the corresponding linear equation for TAG quantification is case by case under distinct stress conditions.

CONCLUSION

An extended approach to quantify distinct levels of TAG using CFA was successfully applied to two oleaginous microalgae, *C. reinhardtii* and *P. tricornutum*. It not only defines the application range of the linear correlation between TAG and the relative abundance of CFA, but also expands coverage of TAG quantification in microalgae. The absolute amount of saturated or monounsaturated CFA is verified to be linearly correlated with TAG content over the entire period of nitrogen stress. This approach utilizes a single fatty acid to quantify TAG mixtures, and is rapid, simple and precise. Moreover, it can be widely applied to various microalgal species with variable TAG levels, monitor TAG accumulation in real-time and facilitate high-throughput mutant screening for microalgae.

AUTHOR CONTRIBUTIONS

MY and SX conceived and designed the research. MY performed the experiments and analyzed data. MY and SX wrote the manuscript. YF and P-CW participated in algal cultivations. Y-DC designed the photobioreactors and illumination systems. P-LS provided technical assistance. SX and Z-YC supervised specific experiments. All authors agreed on the manuscript.

FUNDING

This work was supported by the National Natural Science Foundation of China (21576253, 31470432 and 4140060435).

ACKNOWLEDGMENT

We are very grateful to Dr. Xi Xie from Liaoning Ocean and Fisheries Science Research Institute for his great assistance with data analyses and valuable discussions.

SUPPLEMENTARY MATERIAL

The Supplementary Material for this article can be found online at: https://www.frontiersin.org/articles/10.3389/fpls.2017.01949/full#supplementary-material

FIGURE S1 | Time course alterations of the fatty acyl contents, TAG contents and the proportions of TAG in total lipids of *C. reinhardtii* **(A,B)** and *P. tricornutum* **(C,D)** following nitrogen starvation. The average values of duplicate culture replicates are shown. A total of 30 time points are shown for *C. reinhardtii* **(A)** and 21 time points for *P. tricornutum* **(B)**.

FIGURE S2 | Variations of acyl compositions of the major lipids, MGDG **(A)**, DGDG **(B)**, DGTS **(C)**, and TAG **(D)**, in nitrogen-deprived *C. reinhardtii*. MGDG, DGDG and DGTS denote monogalactosyldiacylglycerol, digalactosyldiacylglycerol and diacylglycerol-*N, N, N*-trimethylhomoserine, respectively. The sampling time points are set as 0, 4, 6, 24, 48, and 72 h, respectively.

FIGURE S3 | Variations of the major lipids contents in nitrogen-deprived *C. reinhardtii*. MGDG, DGDG and DGTS denote monogalactosyldiacylglycerol, digalactosyldiacylglycerol and diacylglycerol-*N, N, N*-trimethylhomoserine, respectively. The sampling time points are set as 0, 4, 6, 24, 48, and 72 h, respectively.

FIGURE S4 | Correlation analyses of the relative abundances **(A)** and the absolute contents **(B)** of CFAs and TAG contents in *C. reinhardtii* under high salt stress conditions. The HS medium under high salt stress conditions refers to Li et al. (2010). The other parameters are the same as that of nitrogen-deprived *C. reinhadtii*. The sampling time points are set as 0, 24, 48, and 72 h, respectively.

FIGURE S5 | Correlation analyses of the relative abundances **(A)** and the absolute contents **(B)** of CFAs and TAG contents in *Nannochloropsis oceanica* under phosphate deprivation conditions. The culture conditions under phosphate deprivation for *N. oceanica* are the same as that under nitrogen stress for *P. tricornutum*. The sampling time points are set as 0, 7, and 14 days following phosphate starvation, and 7 days following phosphate recovery (after 14 days of phosphate starvation), respectively.

REFERENCES

Allen, J. W., DiRusso, C. C., and Black, P. N. (2014). Triglyceride quantification by catalytic saturation and LC–MS/MS reveals an evolutionary divergence in regioisometry among green microalgae. *Algal Res.* 5, 23–31. doi: 10.1016/j.algal.2014.04.003

Bligh, E. G., and Dyer, W. J. (1959). A rapid method of total lipid extraction and purification. *Can. J. Biochem. Physiol.* 37, 911–917. doi: 10.1139/y59-099

Boyle, N. R., Page, M. D., Liu, B., Blaby, I. K., Casero, D., Kropat, J., et al. (2012). Three acyltransferases and nitrogen-responsive regulator are implicated in nitrogen starvation-induced triacylglycerol accumulation in *Chlamydomonas*. *J. Biol. Chem.* 287, 15811–15825. doi: 10.1074/jbc.M111.334052

Breuer, G., Lamers, P. P., Martens, D. E., Draaisma, R. B., and Wijffels, R. H. (2012). The impact of nitrogen starvation on the dynamics of triacylglycerol accumulation in nine microalgae strains. *Bioresour. Technol.* 124, 217–226. doi: 10.1016/j.biortech.2012.08.003

Daboussi, F., Leduc, S., Marechal, A., Dubois, G., Guyot, V., Perezmichaut, C., et al. (2014). Genome engineering empowers the diatom *Phaeodactylum tricornutum* for biotechnology. *Nat. Commun.* 5:3831. doi: 10.1038/ncomms4831

Danielewicz, M., Anderson, L. A., and Franz, A. K. (2011). Triacylglycerol profiling of marine microalgae by mass spectrometry. *J. Lipid Res.* 52, 2101–2108. doi: 10.1194/jlr.D018408

Feng, D., Chen, Z., Xue, S., and Zhang, W. (2011). Increased lipid production of the marine oleaginous microalgae *Isochrysis zhangjiangensis* (Chrysophyta) by nitrogen supplement. *Bioresour. Technol.* 102, 6710–6716. doi: 10.1016/j.biortech.2011.04.006

Goold, H., Cuine, S., Legeret, B., Liang, Y., Brugiere, S., Auroy, P., et al. (2016). Saturating light induces sustained accumulation of oil in plastidal lipid droplets in *Chlamydomonas reinhardtii*. *Plant Physiol.* 171, 2406–2417. doi: 10.1104/pp.16.00718

Guillard, R. R. L. (1975). "Culture of phytoplankton for feeding marine invertebrates," in *Proceedings of the 1st Conference on Culture of Marine Invertebrate Animals Greenport: Culture of Marine Invertebrate Animals*, eds W. L. Smith and M. H. Chanley (Boston, MA: Springer), 29–60.

Harris, E. H. (2009). "Chapter 8 - *Chlamydomonas* in the laboratory," in *The Chlamydomonas Sourcebook,* 2nd Edn), eds D. B. Stern and G. B. Witman (London: Academic Press), 241–302.

He, X. N., Allen, J., Black, P. N., Baldacchini, T., Huang, X., Huang, H., et al. (2012). Coherent anti-stokes Raman scattering and spontaneous Raman spectroscopy and microscopy of microalgae with nitrogen depletion. *Biomed. Opt. Express* 3, 2896–2906. doi: 10.1364/BOE.3.002896

Jouhet, J., Lupette, J., Clerc, O., Magneschi, L., Bedhomme, M., Collin, S., et al. (2017). LC-MS/MS versus TLC plus GC methods: consistency of glycerolipid and fatty acid profiles in microalgae and higher plant cells and effect of a nitrogen starvation. *PLOS ONE* 12:e0182423. doi: 10.1371/journal.pone.0182423

Kobayashi, N., Noel, E. A., Barnes, A., Rosenberg, J. N., Dirusso, C., Black, P., et al. (2013). Rapid detection and quantification of triacylglycerol by HPLC–ELSD in *Chlamydomonas reinhardtii* and *Chlorella* strains. *Lipids* 48, 1035–1049. doi: 10.1007/s11745-013-3828-9

Li, Y., Han, D., Hu, G., Dauvillee, D., Sommerfeld, M., Ball, S., et al. (2010). *Chlamydomonas* starchless mutant defective in ADP-glucose pyrophosphorylase hyper-accumulates triacylglycerol. *Metab. Eng.* 12, 387–391. doi: 10.1016/j.ymben.2010.02.002

Liu, B., Vieler, A., Li, C., Jones, A. D., and Benning, C. (2013). Triacylglycerol profiling of microalgae *Chlamydomonas reinhardtii* and *Nannochloropsis oceanica*. *Bioresour. Technol.* 146, 310–316. doi: 10.1016/j.biortech.2013.07.088

Liu, J., Liu, Y., Wang, H., and Xue, S. (2015). Direct transesterification of fresh microalgal cells. *Bioresour. Technol.* 176, 284–287. doi: 10.1016/j.biortech.2014.10.094

Lohman, E. J., Gardner, R. D., Halverson, L. D., Peyton, B. M., and Gerlach, R. (2014). Carbon partitioning in lipids synthesized by *Chlamydomonas reinhardtii* when cultured under three unique inorganic carbon regimes. *Algal Res.* 5, 171–180. doi: 10.1016/j.algal.2014.08.001

Merchant, S. S., Prochnik, S., Vallon, O., Harris, E. H., Karpowicz, S. J., Witman, G. B., et al. (2007). The *Chlamydomonas* genome reveals the evolution of key animal and plant functions. *Science* 318, 245–250. doi: 10.1126/science.1143609

Miglio, R., Palmery, S., Salvalaggio, M., Carnelli, L., Capuano, F., and Borrelli, R. (2013). Microalgae triacylglycerols content by FT-IR spectroscopy. *J. Appl. Phycol.* 25, 1621–1631. doi: 10.1007/s10811-013-0007-6

Na, J., Lee, H. S., Oh, Y., Park, J., Ko, C. H., Lee, S., et al. (2011). Rapid estimation of triacylglycerol content of *Chlorella* sp. by thermogravimetric analysis. *Biotechnol. Lett.* 33, 957–960. doi: 10.1007/s10529-011-0522-y

Patil, P. D., Reddy, H. K., Muppaneni, T., Schaub, T., Holguin, F. O., Cooke, P., et al. (2013). *In situ* ethyl ester production from wet algal biomass under microwave-mediated supercritical ethanol conditions. *Bioresour. Technol.* 139, 308–315. doi: 10.1016/j.biortech.2013.04.045

Petroutsos, D., Amiar, S., Abida, H., Dolch, L., Bastien, O., Rebeille, F., et al. (2014). Evolution of galactoglycerolipid biosynthetic pathways - from cyanobacteria to primary plastids and from primary to secondary plastids. *Prog. Lipid Res.* 54, 68–85. doi: 10.1016/j.plipres.2014.02.001

Remmers, I. M., Martens, D. E., Wijffels, R. H., and Lamers, P. P. (2017). Dynamics of triacylglycerol and EPA production in *Phaeodactylum tricornutum* under nitrogen starvation at different light intensities. *PLOS ONE* 12:e0175630. doi: 10.1371/journal.pone.0175630

Scranton, M. A., Ostrand, J. T., Fields, F. J., and Mayfield, S. P. (2015). *Chlamydomonas* as a model for biofuels and bio-products production. *Plant J.* 82, 523–531. doi: 10.1111/tpj.12780

Shen, P., Wang, H., Pan, Y., Meng, Y., Wu, P., and Xue, S. (2016). Identification of characteristic fatty acids to quantify triacylglycerols in microalgae. *Front. Plant Sci.* 7:162. doi: 10.3389/fpls.2016.00162

Siaut, M., Cuiné, S., Cagnon, C., Fessler, B., Nguyen, M., Carrier, P., et al. (2011). Oil accumulation in the model green alga *Chlamydomonas reinhardtii*: characterization, variability between common laboratory strains and relationship with starch reserves. *BMC Biotechnol.* 11:7. doi: 10.1186/1472-6750-11-7

Wang, H., Yao, C., Liu, Y., Meng, Y., Wang, W., Cao, X., et al. (2014). Identification of fatty acid biomarkers for quantification of neutral lipids in marine microalgae *Isochrysis zhangjiangensis*. *J. Appl. Phycol.* 27, 249–255. doi: 10.1007/s10811-014-0300-z

Wang, T., Ji, Y., Wang, Y., Jia, J., Li, J., Huang, S., et al. (2014). Quantitative dynamics of triacylglycerol accumulation in microalgae populations at single-cell resolution revealed by Raman microspectroscopy. *Biotechnol. Biofuels* 7, 58–58. doi: 10.1186/1754-6834-7-58

Wase, N., Tu, B., Allen, J. W., Black, P. N., and Dirusso, C. C. (2017). Identification and metabolite profiling of chemical activators of lipid accumulation in green algae. *Plant Physiol.* 174, 00433.02017. doi: 10.1104/pp.17.00433

Wijffels, R. H., and Barbosa, M. J. (2010). An outlook on microalgal biofuels. *Science* 329, 796–799. doi: 10.1126/science.1189003

Zienkiewicz, K. J., Du, Z. Y., Ma, W., Vollheyde, K., and Benning, C. (2016). Stress-induced neutral lipid biosynthesis in microalgae - molecular, cellular and physiological insights. *Biochim. Biophys. Acta* 1861, 1269–1281. doi: 10.1016/j.bbalip.2016.02.008

Conflict of Interest Statement: The authors declare that the research was conducted in the absence of any commercial or financial relationships that could be construed as a potential conflict of interest.

frontiers in Plant Science

ORIGINAL RESEARCH
published: 21 September 2017
doi: 10.3389/fpls.2017.01594

Biofilm Attached Cultivation of *Chlorella pyrenoidosa* Is a Developed System for Swine Wastewater Treatment and Lipid Production

Pengfei Cheng[1,2†], *Yuanzhu Wang*[3†], *Tianzhong Liu*[4] *and Defu Liu*[5*]

[1] Poyang Lake Eco-economy Research Center, Jiujiang University, Jiujiang, China, [2] School of Water Resources and Hydropower Engineering, Wuhan University, Wuhan, China, [3] School of Water Conservancy and Environment, China Three Gorges University, Yichang, China, [4] Qingdao Institute of Bioenergy and Bioprocess Technology, Chinese Academy of Sciences, Qingdao, China, [5] School of Architectural and Environment, Hubei University of Technology, Wuhan, China

OPEN ACCESS

Edited by:
Yuval Kaye,
Carnegie Institution for Science (CIS), United States

Reviewed by:
Abdulsamie Hanano, Atomic Energy Commission of Syria, Syria
Jian Li Yang, Zhejiang University, China

***Correspondence:**
Defu Liu
dfliu@189.cn

[†]*These authors have contributed equally to this work.*

Specialty section:
This article was submitted to Plant Biotechnology, a section of the journal Frontiers in Plant Science

Received: *16 June 2017*
Accepted: *30 August 2017*
Published: *21 September 2017*

Citation:
Cheng P, Wang Y, Liu T and Liu D (2017) Biofilm Attached Cultivation of Chlorella pyrenoidosa Is a Developed System for Swine Wastewater Treatment and Lipid Production. Front. Plant Sci. 8:1594. doi: 10.3389/fpls.2017.01594

This study showed the new potential of using soluble contents and heavy metals in swine wastewater as nutrient supplements for the algae *Chlorella pyrenoidosa* with biofilm attached method. Algae with biofilm attached cultivation grew well in unpasteurized wastewater reaching a biomass productivity of 5.03 g m^{-2} d^{-1}, lipid content of 35.9% and lipid productivity of 1.80 g m^{-2} d^{-1}. *Chlorella* grew in BG11 medium delivered lower values for each of the aforementioned parameters. The FAMEs compositions in the algae paste were mainly consisted of C16:0, C18:2, and C18:3. Algae removed NH_4^+–N, total phosphorus (TP), and COD by 75.9, 68.4, and 74.8%, respectively. Notably, Zn^{2+}, Cu^+, and Fe^{2+} were removed from wastewater with a ratio of 65.71, 53.64, and 58.89%, respectively. Biofilm attached cultivation of *C. pyrenoidosa* in swine wastewater containing heavy metals could accumulate considerable biomass and lipid, and the removal ratio of NH_4^+–N, TP, COD, and as well as heavy metal were high. Treatment of wastewater with biofilm attached cultivation showed an increasingly popular for the concentration of microalgae and environmental sustainability.

Keywords: ***Chlorella pyrenoidosa*, swine wastewater, biofilm attached cultivation, heavy metals, lipid**

INTRODUCTION

Large quantities of waste continuously produced from the intensive livestock industries worldwide represent an increasingly concerning threat to the environment, especially when they were not treated properly. Excessive nutrients in the piggery wastewater, such as, nitrogen and phosphorus, will cause eutrophication in natural water bodies (Cai et al., 2013; Ayre et al., 2017). Compared with municipal domestic sewage-based wastewater, swine wastewater, which is often derived from manure, may contain very high amounts of N and P and may also contain toxic metals (Sturm and Lamer, 2011; Zhou et al., 2012). The principle in wastewater treatment is the reduction of nutrient and toxic metal to acceptable limits prior to discharge and reuse (Miranda et al., 2017). The majority of examples for wastewater treatment technologies were based on chemical or physical methods that were not economical for livestock wastewater treatment (Xu et al., 2015; Li et al., 2016).

As we known, microalgae are considered promising for production of biofuels and higher value products, but require a lot of nutrients in their growth, resulting in high operation costs and possibly adverse environmental effects due to nutrient leakage into the environment (Mata et al., 2010; Borowitzka and Moheimani, 2013; Shah et al., 2016). Therefore, application of wastewater rich in nutrients, such as, nitrogen and phosphorus, for fertilizer-driven microalgal cultivation is a promising approach to enhance economic and environmental sustainability (Mulbry et al., 2008). In particular, the genus *Chlorella* is commonly used in the wastewater treatment system due to their high tolerance to soluble organic compounds.

Nitrogen and phosphorus are removed from wastewater in two separate processes in conventional wastewater treatment. Nitrogen is usually converted into N_2 gas through coupled nitrification–denitrification, whereas phosphorus is precipitated with metal salts. By contrast, nitrogen and phosphorus could be removed from wastewater in a single process with the use of microalgae (Christenson and Sims, 2011; Abdelaziz et al., 2013; Beuckels et al., 2015). Microalgae absorb nitrogen and phosphorus from swine wastewater and convert these nutrients into biomass. Kothari et al. (2012) found that *Chlorella pyrenoidosa* could remove about 80–85% total phosphorus (TP) and 60–80% of total nitrogen (TN) from dairy wastewater. Markou et al. (2012) also found that the maximum removal of chemical oxygen demand (COD) was 73.18%, while phenols, phosphorus, and nitrates in some runs were completely removed when cultivating *Arthrospira platensis* in olive-oil mill wastewater.

However, studies of microalgae-based wastewater treatment were generally based on commercial microalgae cultivation systems, such as, open ponds or closed photobioreactors (PBRs), which exhibited relatively low biomass productivity, high water requirements and high liquid transportation and cumbersome and higher costs in harvesting (Ozkan et al., 2012; Berner et al., 2015). This research, we introduced a novel cultivation system, which was called "biofilm attached cultivation" by Liu et al. (2013). Unlike traditional cultivation methods based on suspended cultures of cells in aqua-medium, the biofilm attached cultivation is a different technology in which the algal cells are immobilized and settled on artificial supporting materials in high density. In brief, microalgal cells are attached to a supporting structure to form an artificial "leaf" and multiple of these leaves are vertically inserted into a glass chamber in this system (Cheng et al., 2013; Liu et al., 2013). Biofilm attached cultivation of microalgae in wastewater separated algae cells from wastewater instead of concentrating or filtering, and the treated wastewater can be recycled immediately. However, there were rarely reports that investigated the feasibility of using wastewater as nutrient supplements for biofilm attached cultivation of microalgae.

In this study, an integrated approach which combined freshwater microalgae *C. pyrenoidosa* biofilm attached cultivation with heavy metals rich swine wastewater treatment was investigated. The objectives of our study were: (1) to determine a feasibility study with undiluted piggery wastewater for algal cultivation, (2) to specify the productivities of biomass, lipids, and FAMEs, and (3) to reveal relevant nutrient and heavy metals removal abilities.

MATERIALS AND METHODS

Algal Strain and Inoculum Preparation

The microalgae strain *C. pyrenoidosa* which was acclimated in poultry wastewater, was obtained from Hubei University of Technology. As we mentioned before, in preparing the inoculum for biofilm attached bioreactors, the alga was first cultivated in glass bubbling columns (diameter = 0.05 m) until the exponential growth phase was reached (approximately 5 days). The glass columns contained 0.6 L of algal broth and were continuously illuminated by cold-white fluorescent lamps (NFL28-T5, NVC, China) with a light intensity of 100 ± 10 μmol $m^{-2}s^{-1}$. The broth temperature was 20 ± 2°C. CO_2 enriched air (1% v/v) was continuously injected into the bottom of the columns with a speed of 1 vvm (0.7 L/min for each column) to agitate the algal broth as well as supply carbon (Cheng et al., 2013).

Culture Medium and Photobioreactor

In this research, the algae cultivated in glass bubbling columns and biofilm attached cultivation system (control) was grown in a BG11 medium (Chiu et al., 2015), each liter of which contains 1.5 g $NaNO_3$, 0.075 g $MgSO_4{\cdot}7H_2O$, 0.036 g $CaCl_2{\cdot}2H_2O$, 0.04 g $KH_2PO_4{\cdot}H_2O$, 0.02 g Na_2CO_3, 6.0×10^{-3} g citric acid, 1.0×10^{-3} g Na_2EDTA, 6.0×10^{-3} g ferric ammonium citrate, 2.22×10^{-4} g $ZnSO_4{\cdot}7H_2O$, 6.9×10^{-5} g $CuSO_4{\cdot}5H_2O$, 1.81×10^{-3} g $MnCl_2{\cdot}4H_2O$, 3.9×10^{-4} g $Na_2MoO_4{\cdot}2H_2O$, 4.94×10^{-5} g $Co(NO_3)_2{\cdot}6H_2O$, and 2.86×10^{-3} g H_3BO_3.

The biofilm attached cultivation system applied in this research was similar to the type 1 reactor used by Liu et al. (2013) and to that described by Cheng et al. (2014) (**Figure 1**). In brief, a glass chamber comprising a glass plate and attached algal biofilm disks was placed on an iron rack with a certain tilt angle against the horizontal plane. The medium was propelled (1.2 L in total, approximately 10 ml min^{-1}) by a peristaltic pump (TP12DC 12V, Guangzhou JU PlasFitting Technology Co., Ltd., China) to facilitate circulation inside the system. Cold-white fluorescent lamps provided illumination at 100 ± 10 μmol $m^{-2}s^{-1}$ as measured inside the chamber at the position of the cultivated algae cells. Continuous air was injected into the glass chamber with a speed of 0.1 vvm and the temperature inside the glass chamber was 20 ± 2°C during the experiments. The culture time of 8 days for *C. pyrenoidosa* with biofilm attached culture was proved well in our trial test.

Culture of *Chlorella pyrenoidosa* with Swine Wastewater

Swine wastewater from a private farm in Wuhan of Hubei province, China, was used as a medium to cultivate *C. pyrenoidosa*. Pre-treatment was carried out by sedimentation and filtration with a filter cloth to remove large and non-soluble particulates. After filtration, the wastewater was not autoclaved and undiluted but used directly as a medium for algal cultivation in the biofilm attached PBR. The culture conditions for control group (BG11 medium) and the raw swine wastewater

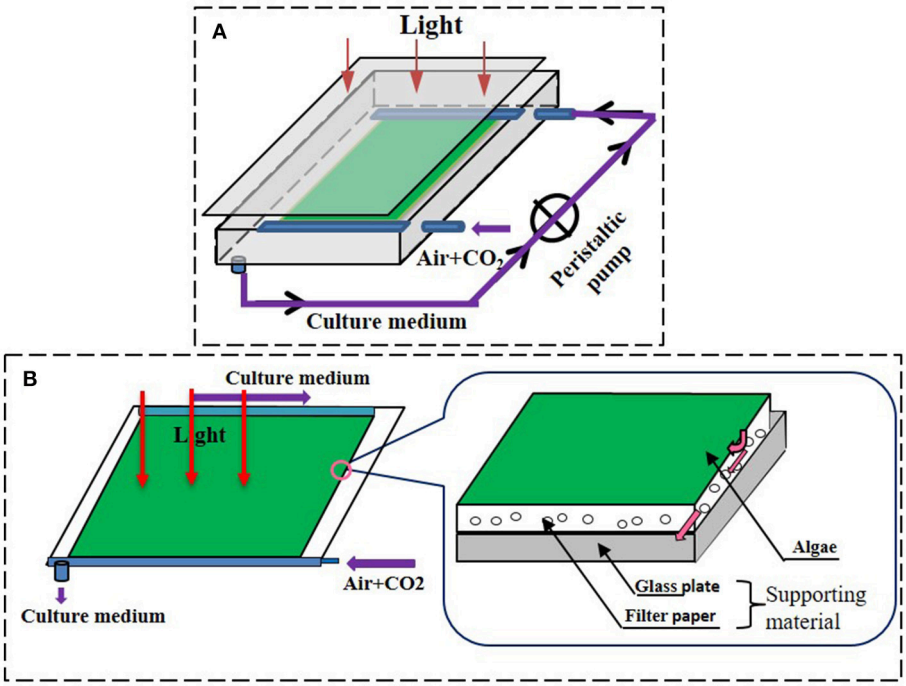

FIGURE 1 | The schematic diagrams of attached cultivation devices. **(A)** Attached cultivation module of the photobioreactor, the residual medium was recycling. The medium was propelled to the system by a peristaltic pump when it flowed through the chamber during the cultivation. **(B)** The detailed structure of the cultivation surface of the attached photobioreactor. Permission to use and adapted from Cheng et al. (2014).

were identical to those described the above section of biofilm attached cultivation system. The characteristics of the raw swine wastewater are summarized in **Table 1**. Remarkably, the wastewater contained heavy metals of Zn^{2+}, Cu^{+}, and Fe^{2+}.

Analytical Procedures

Biomass Estimation

The biomass was determined with the gravimetric method (Liu et al., 2013). During the experiments, two algae disks would be collected every 2 days; cells from the filter membrane were flushed with distilled water and then filtered to a pre-weighed 0.45 μm GF/C filter membrane (Whatman, England; DW_0). The membrane was oven dried at 80°C for about 24 h and then cooled down to room temperature to measure dry weight (DW_1). Finally, their average was used. The DW was calculated as follows:

$$DW = (DW_1 - DW_0)/0.001$$

where 0.001 represented the footprint area of the "algal disk" (m^2).

Nutrients Analysis in Wastewater

A volume of 5 mL of recirculating medium was collected every 2 days from the attached PBRs for nutrient removal analysis. The samples were first centrifuged at 1,500 g for 10 min, and then the supernatants were filtered using a 0.45 mm nylon membrane filter. The filtrates were appropriately diluted and analyzed for COD, NH_4^+–N, and TP, parallel sample was made. The COD was measured using the standard potassium dichromate method based on the Chinese National Standard GB11914-1989 with a Speed Digester (Yao et al., 2015). Potentiometric analysis using a selective electrode method was used to measure ammonia (N–NH_3) (APHA, 2012). TP were measured according to Standard Methods (Eaton et al., 2005; Hach, 2008).

Heavy Metal Elements Alterations

A volume of 50 mL of culture medium was gathered, respectively, at the second day, the fourth day, the sixth day, and the last day according to the limiting of the broth, and was examined the concentration of heavy metal of copper, zinc, iron with atom absorption spectrographic methods (PinAAcle 900T, USA).

Lipid Extraction

The attached algal cells were harvested by washing down with de-ionized water and centrifugation at 3,800 g for 10 min (Allegra X-22R, Beckman coulter, USA). The algal pellets were washed three times with de-ionized water to remove any attached salt. Then the total lipid was measured according to Bligh and Dyer's method (Bligh and Dyer, 1959) and Cheng et al. (2013).

FAMEs Content Analysis of Algae Biodiesel

FAMEs content analysis was according to Chen et al. (2012) and Wang et al. (2016). Briefly, algae powder was suspended in 2 mL 0.4 M KOH methanol solution, and was then heated at 70°C for 30 min in a water bath. After cooling, 2 mL 0.6 M H_2SO_4-methanol solution and 1 mL 14% BF_3-methanol solution

TABLE 1 | The characteristics and features of the raw piggery wastewater.

Parameter (mg L^{-1})	Fe^{2+}	Cu^{+}	Zn^{2+}	TP	NH_4^+–N	SS	COD	BOD
	1.8 ± 0.1	2.2 ± 0.2	2.8 ± 0.1	36.3 ± 1.2	402 ± 2.6	720 ± 4.2	601 ± 3.4	728 ± 2.2

Data are means ± standard deviations of three replicates.

(Sigma-Aldrich, USA) were added, the mixture was heated in water bath at 70°C for 30 min again. After cooling, the fatty acid methyl esters (FAMEs) were extracted with 2 mL *n*-hexane, then centrifuged at 4,000 rpm for 5 min. The *n*-hexane layer was transferred to a vial. The prepared sample was (0.5 mg) was dissolved in heptane (1 mL) containing heptadecanoic acid methyl ester ($C_{18}H_{37}COOCH_3$, 50 μg) as internal standard for FAMEs analysis on a Varian 450GC (Varian Inc., USA) equipped with a flame ionization detector (FID) and Agilent HP-5 GC Capillary Column (30 m × 0.25 mm × 0.25 μm). Nitrogen was used as carrier gas. The injector temperature was set at 280°C with an injection volume of 2 μL under split mode (10:1). The detector temperature was set at 280°C. The individual FAMEs were identified by chromatographic comparison with authentic standards (Sigma).

All experiments were performed in duplicate, and average values were reported. Results were analyzed with EXCEL (Microsoft Office Enterprise, 2010) and SPSS 11.5 for Windows (SPSS Inc., 2007); ANOVA was performed when applicable.

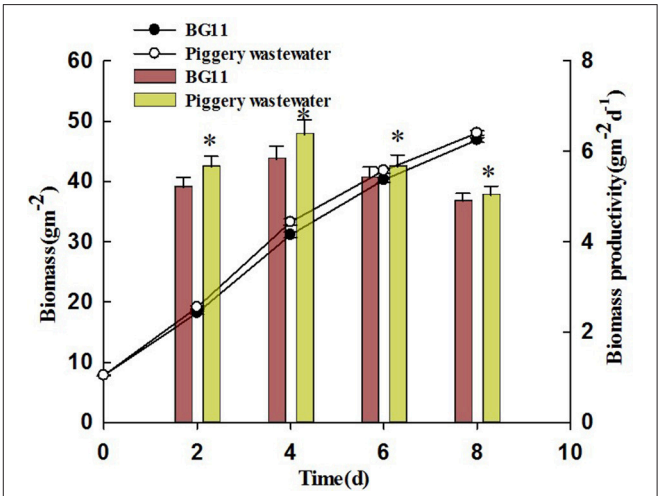

FIGURE 2 | The accumulation of biomass of *Chiarella pyrenoidosa* in BG 11 (control), piggery wastewater with biofilm attached cultivation. The algal cells were cultivated in attached culture for 8 days under continuous illumination of 1 00 ± 10 μmol m^{-2} s^{-1}. *Indicates significant differences among treatments ($P < 0.05$), Error bars are standard deviations.

RESULTS

Accumulation of Biomass of *Chlorella pyrenoidosa* with Biofilm Attached Cultivation

The growth curves of *C. pyrenoidosa* in swine wastewater for 8 days were showed in **Figure 2**. For the first 2 days, the growth was almost identical with that in BG11. After that, *C. pyrenoidosa* grew faster in swine wastewater. By the end of experiment, biomass and biomass productivity were 48.02 g m^{-2} and 5.03 g m^{-2} d^{-1}, respectively, for the wastewater treatment. They were higher than that of control treatment (BG11). A smaller yet still statistically significant increase was also found under the swine wastewater for biomass productivity (repeated measures one-way ANOVA) corresponding to a mean increase of 7.3% of control.

Conventionally, in the lag state, algal cells need to adapt to the new environment since the nutrients contained in the wastewater are different from those found inside the BG11 medium. In this study, the microalgae cultivated in the biofilm attached PBR with the COD concentration of 601 mg L^{-1} had a short lag time and could quickly adapt to the environment.

Lipid Productivity and Analysis of the Fatty Acid Profile

The lipid content of *C. pyrenoidosa* in the two treatments was shown in **Figure 3**. The lipid content of the algae in the treatment with BG11 and swine wastewater was similar, reaching 34.6 and 35.9% and corresponded to a lipid productivity of 1.69 and 1.80 g m^{-2} d^{-1}, respectively. So, there were no statistically different between the two treatments.

The compositional distribution of fatty acids extracted from the microalgae is shown in **Table 2**. In the present study, the FAMEs compositions of *C. pyrenoidosa* mainly consisted of C16:0 (palmitic acid methyl ester), C18:2 (octadecadienoic acid methyl ester), and C18:3 (octadecatrienoic acid methyl ester). The highest overall FAMEs yield was obtained in piggery wastewater with C18:3 (43.39% of the total fatty acids) as the most abundant fatty acid, which was higher than in BG11 medium (32.14% of the total fatty acids). Linoleic acid (C18:2) content reached 37.38% of the total fatty acids in wastewater, only 25.47% in BG11 medium. Nevertheless, the fraction of oleic acid was higher with BG11 (27.22% of the total fatty acids) than when using swine wastewater as a source of nutrients (4.43% of the total fatty acids). The fraction of palmitic acid methyl ester (C16:0) in the two treatments was similar, corresponding to 8.63% in wastewater and 9.30% in BG11. When the algae cells cultivated in BG11 media were transferred to the swine wastewater, polyunsaturated fatty acid content increased from 57.61 to 81.17%, however, the amount of monounsaturated fatty acids decreased from 27.82 to 5.08%. The unsaturated FAMEs for C16:1, C18:2, and C18:3 in biofilm attached cultures with piggery wastewater were predominant in the FAMEs profile.

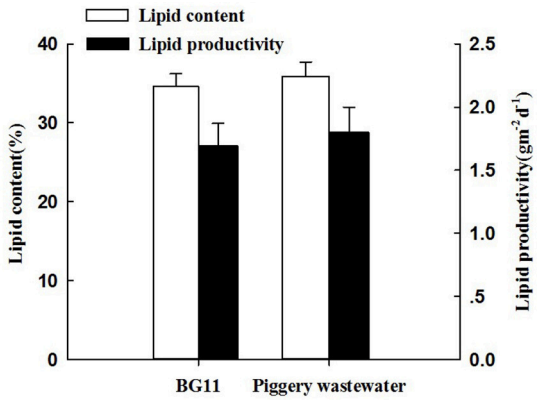

FIGURE 3 | The lipid content and lipid productivity of *Chlorella pyrenoidosa* in the treatment of BG 11 (control) and piggery wastewater with biofilm attached cultivation. The algal cells were cultivated in biofihn attached culture for 8 days under continuous illumination of 100 ± 10 μmol m^{-2} s^{-1}. Error bars are means ± standard deviations of three replicates.

TABLE 2 | Effect of piggery wastewater and BG11 medium on the fatty acids composition as % of total fatty acids of *Chlorella Pyrenoidosa* with biofilm attached cultivation for 8 days.

The content of fatty acids composition (%)	Piggery wastewater	BG11 medium
C13:0	0.10	0.04
C14:0	0.94	0.91
C15:0	0.41	0.27
C16:0	8.63	9.30
C16:1	0.65	0.60
C17:0	0.75	0.57
C18:0	2.75	3.38
C18:1	4.43	27.22
C18:2	37.78	25.47
C20:0	0.15	0.10
C18:3	43.39	32.14
SFAs	13.73	14.57
MUFAs	5.08	27.82
PUFAs	81.17	57.61

Nitrogen, Phosphorus, and COD Removal Capability

Figures 4, **5** describe the removals of NH_4^+–N, TP, and COD achieved with treatment of piggery wastewater by microalgae cultivation. In this study, the cultivation of *C. pyrenoidosa* in the form of a biofilm receiving wastewater as a source of nutrients decreased the initial NH_4^+–N concentration from 409 to 98 mg L^{-1}, and TP concentration from 35 to 10 mg L^{-1}, and the initial COD concentration from 601 to 152 mg L^{-1}. This corresponded to a removal ratio of NH_4^+–N, TP, and COD of 75.9, 68.4, and 74.8%, respectively.

The typical N/P ratio for optimal conditions for microalgae biomass production was 8:1 (US DOE, 2008); however, the N/P ratios in our swine wastewater were higher than that of values (**Table 1**). Current literature has reported that algae can assimilate NH_4^+–N, nitrate, and simple organic nitrogen such as, urea, acetic acid, and amino acids in wastewater; however, the concentration of NH_4^+–N of <300 mg L^{-1} in the accessible paper (Beuckels et al., 2015).

Heavy Metal Elements Disposal Ratio

The swine wastewater in this study was detected some of high concentration of heavy metals ions. **Table 1** showed that the concentration of Zn^{2+} in swine wastewater reached 2.8 mg L^{-1}, followed by Cu^+ and Fe^{2+} (2.2 and 1.8 mg L^{-1}, respectively). Heavy metals removal from swine wastewater by microalgae with attached culture has been tested (**Figure 6**). As shown in **Figure 6A**, the metal concentrations (Zn^{2+}, Cu^+, and Fe^{2+}) decreased sharply after only 2 days of cultivation. The reduction rate greatly decreased in the following days. By the end of experiment, residual quantity of Zn^{2+}, Cu^+ and Fe^{2+} were still detected reaching concentrations of 0.96, 1.02, and 0.74 mg L^{-1}, respectively (**Figure 6A**).

This result indicated the high removal ratio of Zn^{2+} (65.71%), Cu^+ (53.64%), and Fe^{2+} (58.89%) with the attached cultivation of *Chlorella* (**Figure 6B**). Our results are supported from Carrilho and Gilbert (2000) who revealed that biosorption of algae was rapid and accumulation of metals happened within short time (**Figure 6A**).

DISCUSSION

Ayre et al. (2017) reported that many microalgae species can grow in diluted digested piggery wastewater, and they utilize the abundant N, P, and other organic carbon in the water. *Chlorella* sp. was the dominant algae species in a wastewater treatment study. However, nearly all experiments were performed on piggery wastewater diluted with either synthetic media or water to reduce the toxicity of organic components (Min et al., 2011; Zhu et al., 2011). Min et al. (2011) and Zhu et al. (2011) also cultivated *Chlorella* sp. in swine wastewater with relatively high COD in a pilot-scale PBR, however, in their experiment the biomass productivity and initial NH_4^+–N concentration of wastewater were lower than our experiment (**Figure 2**). Flynn (1991) reported that ammonium assimilation causes a rapid and reversible inactivation of nitrate transport which influences growth of microalgae.

The dilution of swine wastewater for microalgae growth would be limited by the high cost of clean water consumption, sewage volume, need for artificial nutrients, and other inconvenient operations. Therefore, developing an efficient process that allow algae to grow well under undiluted piggery slurry is very important, rendering the application of microalgae-based technology feasible and economical for full-scale wastewater treatment and biodiesel production. This study aimed at investigating the feasibility of tested microalgae in undiluted slurry of piggery wastewater, and the microalgae treated with the biofilm attached culture method grew well in undiluted slurry.

Feng et al. (2012) and Rodolfi et al. (2009) proved that lipid accumulation can be raised through increasing light intensity. The wastewater had a darker color than the BG11; however,

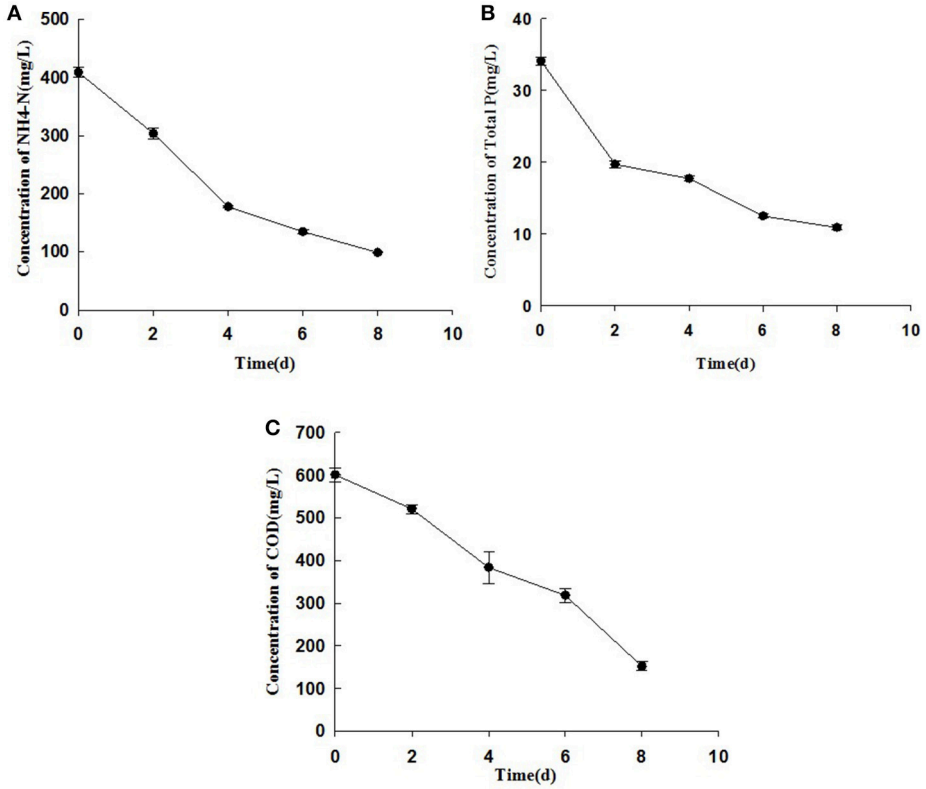

FIGURE 4 | The changes of concentrations of NH^{4+}–N **(A)**, TP **(B)**, and COD **(C)** of cultivation broth by *Chiarella pyrenoidosa* with biofilm attached cultivation. The algal cells were cultivated in biofilm attached culture for 8 days under continuous illumination of 100 ± 10 μmol m^{-2} s^{-1}. Error bars are means ± standard deviations of three replicates.

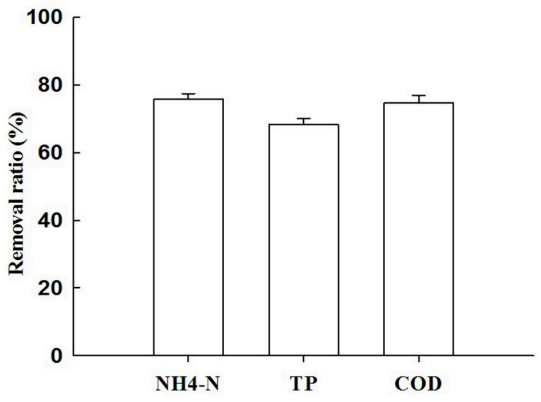

FIGURE 5 | The removal ratio ofNH^{4+}–N, TP, and COD with treatment ofpiggery wastewater by *Chiarella pyrenoidosa* biofilm attached cultivation. The algal cells were cultivated in biofilm attached culture for 8 days under continuous illumination of 100 ± 10 μmol m^{-2} s^{-1}. Error bars are means ± standard deviations of three replicates.

lipid accumulation for the swine wastewater treatment was not inhibited in biofilm attached cultivation. This might be because the algal cells cultivated with attached PBR are generally immobilized and fixed onto supporting materials in high density and separated with swine wastewater. *Chlorella* sp. are known to have high content of lipids, which have the potential to be converted to biofuels that can be used mixed to—or in substitution to traditional fossil fuels. Beal et al. (2012) reported the cost of algal biofuel production was mainly related to algal culture (77%), harvesting (12%), and lipid extraction phases (7.9%). It was obvious that the utilization of wastewater as a substitute for algae nutrients would significantly reduce the operational cost of algae cultivation (Cai et al., 2013).

The environmental and cultural conditions have been reported by previous research to have an effect on lipid content and fatty acid (Petkov and Garcia, 2007; Li et al., 2011). So, it was not surprising to observe the different FAMEs profiles in our study (**Table 2**). Not all lipids can be converted to FAMEs, such as, glycolipids and phospholipids and long-chain carbon (Li et al., 2011). However, *C. pyrenoidosa* cultivated in swine wastewater was found to have shorter carbon chains for fatty acids in our study. The degree of unsaturation of fatty acids is due to the metals toxicity more than to favoritism of piggery wastewater. They mainly contained 16–18 carbons (**Table 2**), which were ideal for biodiesel conversion (Huang et al., 2010). Integration of microalgal cultivation with wastewater for biodiesel production is a promising choice and could enhance the economic and environmental sustainability (Lee and Lee, 2002).

The high NH_4^+–N content in wastewater represents a growth inhibitory factor for microalgae because it may contribute to changes in pH value of the culture medium. Tam and Wong (1996) showed that the growth of *Chlorella* sp. was reduced at NH_4^+–N concentrations higher than 700 mg L^{-1} with a pH level below 7. Chiu et al. (2015) reported that the TP concentration for biomass productivity was lower than 100 mg L^{-1}. The consumed phosphorus of swine wastewater was mainly assimilated by algal cells. The effects of NH_4^+–N and TP concentrations in wastewater on the *Chlorella* biomass production and productivity are similar (Chiu et al., 2015). The consumed COD in this study with attached cultivation of *Chlorella* were higher than the reported that of 73.18% COD removal ratio with *Arthrospira (Spirulina) platensis* cultivated in 25% olive oil mill wastewater (Markou et al., 2012).

The main physicochemical approaches to remove heavy metal ions from wastewaters include ion exchange, chemical precipitation, electrokinetic, membrane processing, and adsorption (Lee and Pandey, 2012; Goharshadi and Moghaddam, 2015). The incomplete removal of heavy metal ions and high costs of chemicals are the main limiting factors in the development of physicochemical approaches. However, biosorption of heavy metal ions in wastewater with proper microalgae species could offer an ecologically safer, cheaper, and more efficient means. Indeed, algae could be used to absorb toxic and radioactive metal ions and to recover precious metals (Pohl and Schimmack, 2006). And polysaccharides and proteins present in algae cell walls contain the most number of metal binding sites (Schiewer and Volesky, 2000). However, factors including concentration of metal ions, algae biomass, pH, temperature, and presence of competing ions affect the biosorption of heavy metals ions by algae. Algal cell walls are the first barrier against biosorption of heavy metal ions. Given the different distribution and abundance of cell wall compositions in different algal strains, the biosorption capacity for metal ions would vary depend on the considered algal strain.

Chlorella can effectively grow and utilize nutrients in swine wastewater, reducing the content of metal ions in this research. **Table 3** compared of the growth, lipid production, and cultivation parameters of microalgae in wastewater for

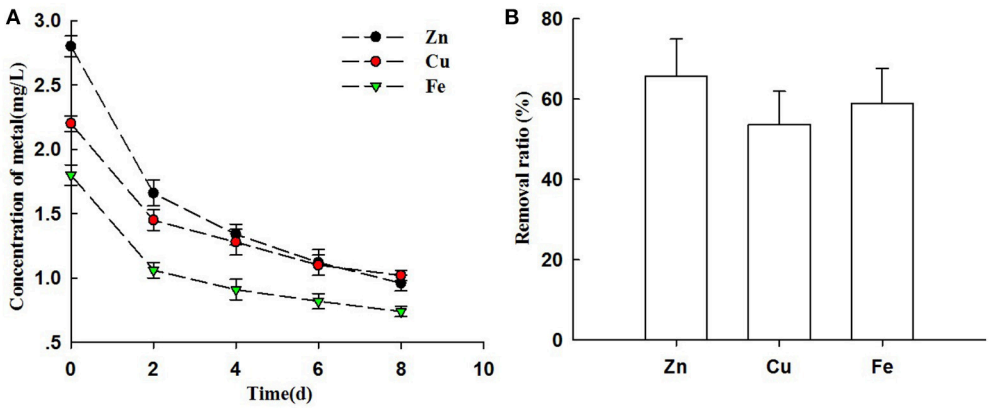

FIGURE 6 | Heavy metals ions removal from piggery wastewater by biofihn attached culture (**A**) The changes of concentrations of Zn^{2+}, Cu^+, and Fe^{2+} of cultivation broth by *Chlorella pyrenoidosa* with biofilm attached cultivation. (**B**) The removal ratio of Zn^{2+}, Cu^+, and Fe^{2+} with treatment of piggery wastewater by *Chlorella pyrenoidosa* biofilm attached cultivated. The algal cells were cultivated in biofilm attached culture for 8 days under continuous illumination of 100 ± 10 μmol m^{-2} s^{-1}. Error bars are means ± standard deviations of three replicates.

TABLE 3 | Comparison of growth, lipid production and cultivation parameters of microalgae in wastewater for different cultivation methods.

Wastewater source	Algae	Biomass	Lipid content (%)	NH_4–N (mg L^{-1})	TP (mg L^{-1})	COD (mg L^{-1})	Cultivation systems	Reference
Piggery wastewater	*Chlorella Pyrenoidosa*	48.02 g m^{-2}	35.9	409	35	601	Attached photobioreactor	This study
50% Piggery wastewater	*Chlorella zofingiensis*	2.01 g L^{-1}	34.8	–	146	–	Tubular bubble column photobioreactors	Zhu et al., 2011
Municipal wastewater	*Scenedesmus* sp.	0.78 g L^{-1}	12.7	27.7	7.3	273.5	Erlenmeyer flasks	Sacristán de Alva et al., 2013
10% Dairy wastewater	*Chlorella zofingiensis* G1	0.14 g L^{-1}	17.9	5	15	–	ponds	Huo et al., 2012
Digested dairy manure	*Chlorella* sp.	1.39 g L^{-1}	10.1	100	18	–	Erlenmeyer flasks	Wang et al., 2010

"–" Means was not studied.

different cultivation methods. It could be observed that most of study concerned of algae-based treatment diluted wastewater (Ji et al., 2013), which would increase cost in practice. In addition, few papers focused on the question of heavy metal pollution of piggery wastewater, which recently has attracted growing attention to agricultural pollution (Zeraatkar et al., 2016). The cultivation scale of most recent studies was limited to the laboratory bench—or pilot plant scale. The significant question to consider is what kind of cultivation system could be more economically viable and environmental-friendly for large scale production of microalgal biomass. As a result of the difficulty of construction and the condition of vast land area, most of the PBRs and ponds used in recent studies are not economically convenient for large-scale microalgal biomass production. Therefore, the efforts on novel cultivation system are very important in the future research (Wang et al., 2015).

In summary, *C. pyrenoidosa* could accumulate considerable biomass and lipid in swine wastewater with biofilm attached culture. A major portion of FAMEs compositions were ideal for biodiesel conversion. The removal of $NH4^+$–N, TP, COD and, as well as heavy metal pollution of wastewater with *C. pyrenoidosa* by biofilm attached culture can be a remarkable solution for swine wastewater resource utilization.

AUTHOR CONTRIBUTIONS

PC and DL proposed the idea and hypothesis. PC drafted the manuscript. YW carried out the experiment design and carried out the biofilm attached cultivation of *C. pyrenoidosa* in undiluted swine wastewater. TL performed the statistical analysis and helped to draft and revise the manuscript. All authors read and approved the final manuscript for publication.

ACKNOWLEDGMENTS

This work was supported by the National Natural Science Foundation of China (31560724), China Postdoctoral Science Foundation (2017T100583, 2016M600616), Natural Science and Technology Major Special Program of China (2014ZX07104-005-02), and Collaborative Innovation Center for Major Ecological Security Issues of Jiangxi Province and Monitoring Implementation (JXS-EW-00).

REFERENCES

Abdelaziz, A. E. M., Leite, G. B., and Hallenbeck, P. C. (2013). Addressing the challenges for sustainable production of algal biofuels: I. Algal strains and nutrient supply. Environ. Technol. 34, 1783–1805. doi: 10.1080/09593330.2013.827748

APHA (2012). *Standard Methods for the Examination for Water and Wastewater, 22nd Edn*. Toronto, ON.

Ayre, J. M., Moheimani, N. R., and Borowitzka, M. A. (2017). Growth of microalgae on undiluted anaerobic digestate of piggery effluent with high ammonium concentrations. *Algal Res.* 24, 218–226. doi: 10.1016/j.algal.2017.03.023

Beal, C. M., Hebner, R. E., Webber, M. E., Ruoff, R. S., Seibert, A. F., and King, C. W. (2012). Comprehensive evaluation of algae production: experimental and target results. *Energies* 5, 1943–1981. doi: 10.3390/en5061943

Berner, F., Heimann, K., and Sheehan, M. (2015). Microalgal biofilms for biomass production. *J. Appl. Phycol.* 27, 1793–1804. doi: 10.1007/s10811-014-0489-x

Beuckels, A., Smolders, E., and Muylaert, K. (2015). Nitrogen availability influences phosphorus removal in microalgae-based wastewater treatment. *Water Res.* 77, 98–106. doi: 10.1016/j.watres.2015.03.018

Bligh, E. G., and Dyer, W. J. (1959). A rapid method of total lipid extraction and purification. *Can. J. Biochem. Physiol.* 37, 911–917. doi: 10.1139/o59-099

Borowitzka, M. A., and Moheimani, N. R. (2013). Sustainable biofuels from algae. *Mitig. Adapt. Strateg. Glob. Change* 18, 13–25. doi: 10.1007/s11027-010-9271-9

Cai, T., Park, S. Y., and Li, Y. (2013). Nutrient recovery from wastewater streams by microalgae: status and prospects. *Renew. Sust. Energy Rev.* 19, 360–369. doi: 10.1016/j.rser.2012.11.030

Carrilho, E. N. V. M., and Gilbert, T. R. (2000). Assessing metal sorption on the marine alga *Pilayellalittoralis*. *J. Environ. Monitor.* 2, 410–415. doi: 10.1039/B004128I

Chen, L., Liu, T. Z., Zhang, W., Chen, X. L., and Wang, J. F. (2012). Biodiesel production from algae oil high in free fatty acids by two-step catalytic conversion. *Bioresour. Technol.* 111, 208–214. doi: 10.1016/j.biortech.2012.02.033

Cheng, P., Ji, B., Gao, L., Zhang, W., Wang, J., and Liu, T. (2013). The growth, lipid and hydrocarbon production of *Botryococcus braunii* with attached cultivation. *Bioresour. Technol.* 138, 95–100. doi: 10.1016/j.biortech.2013.03.150

Cheng, P., Wang, J., and Liu, T. (2014). Effects of nitrogen source and nitrogen supply model on the growth and hydrocarbon accumulation of immobilized biofilm cultivation of *B. braunii*. *Bioresour. Technol.* 166, 527–533. doi: 10.1016/j.biortech.2014.05.045

Chiu, S. Y., Kao, C. Y., Chen, T. Y., Chang, Y. B., Kuo, C. M., and Lin, C. S. (2015). Cultivation of microalgal Chlorella for biomass and lipid production using wastewater as nutrient resource wastewater as nutrient resource. *Bioresour. Technol.* 184, 179–189. doi: 10.1016/j.biortech.2014.11.080

Christenson, L., and Sims, R. (2011). Production and harvesting of microalgae for wastewater treatment, biofuels, and bioproducts. *Biotechnol. Adv.* 29, 686–702. doi: 10.1016/j.biotechadv.2011.05.015

Eaton, A. D., Clesceri, L. S., and Greenberg, A. E. (2005). *Standard Methods for the Examination of Water and Wastewater*. Washington, DC: American Public Health Association/American Water Works Association/Water Environment Federation.

Feng, P., Deng, Z., Hu, Z., and Fan, L. (2012). Lipid accumulation and growth of *Chlorella zofingiensis* in flat plate photobioreactors outdoors. *Bioresour. Technol.* 102, 10577–10584. doi: 10.1016/j.biortech.2011.08.109

Flynn, J. (1991). Algal carbon–nitrogen metabolism: a biochemical basis for modelling the interactions between nitrate and ammonium uptake. *J. Plankton Res.* 13, 373–387. doi: 10.1093/plankt/13.2.373

Goharshadi, E. K., and Moghaddam, M. B. (2015). Adsorption of hexavalent chromium ions from aqueous solution by graphene nanosheets: kinetic and thermodynamic studies. *Int. J. Environ. Sci. Technol.* 12, 2153–2160. doi: 10.1007/s13762-014-0748-z

Hach (2008). *Procedure Manual*. Loveland, CO: Hach.

Huang, G. H., Chen, F., Wei, D., Zhang, X. W., and Chen, G. (2010). Biodiesel production by microalgal biotechnology. *Appl. Energy* 87, 38–46. doi: 10.1016/j.apenergy.2009.06.016

Huo, S., Wang, Z., Zhu, S., Zhou, W., Dong, R., and Yuan, Z. (2012). Cultivation of *Chlorella zofingiensis* in bench-scale outdoor ponds by regulation of pH using dairy wastewater in winter, South China. *Bioresour. Technol.* 121, 76–82. doi: 10.1016/j.biortech.2012.07.012

Ji, M. K., Kim, H. C., Sapireddy, V. R., Yun, H. S., Abou-Shanab, R. A. I., Choi, J., et al. (2013). Simultaneous nutrient removal and lipid production from pretreated piggery wastewater by *Chlorella vulgaris* YSW-04. *Appl. Microbiol. Biotechnol.* 97, 2701–2710. doi: 10.1007/s00253-012-4097-x

Kothari, R., Pathak, V. V., Kumar, V., and Singh, D. P. (2012). Experimental study for growth potential of unicellular alga *Chlorella pyrenoidosa* on dairy waste water: an integrated approach for treatment and biofuel production. *Bioresour. Technol.* 116, 466–470. doi: 10.1016/j.biortech.2012.03.121

Lee, K., and Lee, C. G. (2002). Nitrogen removal from wastewaters by microalgae without consuming organic carbon sources. *J. Microbiol. Biotechnol.* 12, 979–985.

Lee, J. C., and Pandey, B. D. (2012). Bio-processing of solid wastes and secondary resources for metal extraction-a review. *Waste Manag.* 32, 3–18. doi: 10.1016/j.wasman.2011.08.010

Li, X., Guo, J., Dong, R., Ahring, B. K., and Zhang, W. (2016). Properties of plant nutrient: comparison of two nutrient recovery techniques using liquid fraction of digestate from anaerobic digester treating pig manure. *Sci. Total Environ.* 544, 774–781. doi: 10.1016/j.scitotenv.2015.11.172

Li, Y., Chen, Y., Chen, P., Min, M., Zhou, W., Martinez, B., et al. (2011). Characterization of a microalga *Chlorella* sp. well adapted to highly concentrated municipal wastewater for nutrient removal and biodiesel production. *Bioresour. Technol.* 102, 5138–5144. doi: 10.1016/j.biortech.2011.01.091

Liu, T., Wang, J., Hu, Q., Cheng, P., Ji, B., Liu, J., et al. (2013). Attached cultivation technology of microalgae for cost-affordable biomass feedstock production. *Bioresour. Technol.* 127, 216–222. doi: 10.1016/j.biortech.2012.09.100

Markou, G., Chatzipavlidis, I., and Georgakakis, D. (2012). Cultivation of *Arthrospira* (*Spirulina*) *platensis* in olive-oil mill wastewater treated with sodium hypochlorite. *Bioresour. Technol.* 112, 234–241. doi: 10.1016/j.biortech.2012.02.098

Mata, T. M., Martins, A. A., and Caetano, N. S. (2010). Microalgae for biodiesel production and other applications: a review. *Renew. Sust. Energy Rev.* 14, 217–232. doi: 10.1016/j.rser.2009.07.020

Min, M., Wang, L., Li, Y., Mohr, M. J., Hu, B., Zhou, W., et al. (2011). Cultivating *Chlorella* sp. in a pilot-scale photobioreactor using centrate wastewater for microalgae biomass production and wastewater nutrient removal. *Appl. Biochem. Biotechnol.* 165, 123–137. doi: 10.1007/s12010-011-9238-7

Miranda, A. F., Ramkumar, N., Andriotis, C., Holtkemeier, T., Yasmin, A., Rochfort, S., et al. (2017). Applications of microalgal biofilms for wastewater treatment and bioenergy production. *Biotechnol. Biofuels* 10, 120–143. doi: 10.1186/s13068-017-0798-9

Mulbry, W., Kondrad, S., Pizarro, C., and Kebede-Westhead, E. (2008). Treatment of dairy manure effluent using freshwater algae: algal productivity and recovery of manure nutrients using pilot-scale algal turf scrubbers. *Bioresour. Technol.* 99, 8137–8142. doi: 10.1016/j.biortech.2008.03.073

Ozkan, A., Kinney, K., Katz, L., and Berberoglu, H. (2012). Reduction of water and energy requirement of algae cultivation using an algae biofilm photobioreactor. *Bioresour. Technol.* 114, 542–548. doi: 10.1016/j.biortech.2012.03.055

Petkov, G., and Garcia, G. (2007). Which are fatty acids of the green alga *Chlorella*. *Biochem. Syst. Ecol.* 35, 281–285. doi: 10.1016/j.bse.2006.10.017

Pohl, P., and Schimmack, W. (2006). Adsorption of radionuclides (134Cs, 85Sr, 226Ra, 241Am) by extracted biomasses of cyanobacteria (Nostoc Carneum, N. Insulare, Oscillatoria Geminata and Spirulina Laxis-sima) and phaeophyceae (Laminaria digitata and L. Japonica; waste products from alginate production) at different pH. *J. Appl. Phycol.* 18, 135–143. doi: 10.1007/s10811-006-9084-0

Rodolfi, L., Zittelli, G., Bassi, N., Padovani, G., Biondi, N., Bonini, G., et al. (2009). Microalgae for oil: strain selection, induction of lipid synthesis and outdoor mass cultivation in a low-cost photobioreactor. *Biotechnol. Bioeng.* 102, 100–112. doi: 10.1002/bit.22033

Sacristán de Alva, M., Luna-Pabello, V. M., Cadena, E., and Ortíz, E. (2013). Green microalga *Scenedesmus acutus* grown on municipal wastewater to couple nutrient removal with lipid accumulation for biodiesel production. *Bioresour. Technol.* 146, 744–748. doi: 10.1016/j.biortech.2013.07.061

Schiewer, S., and Volesky, B. (2000). "Biosorption by marine algae" in *Bioremediation,* ed J. Valdes (Berlin: Springer Netherlands), 139–169.

Shah, M. M. R., Liang, Y. M., Cheng, J. J., and Daroch, M. (2016). Astaxanthin-producing green microalga *Haematococcus pluvialis*: from single cell to high value commercial products. *Front. Plant Sci.* 7:531. doi: 10.3389/fpls.2016.00531

Sturm, B. S. M., and Lamer, S. L. (2011). An energy evaluation of coupling nutrient removal from wastewater with algal biomass production. *Appl. Energy* 88, 3499–3506. doi: 10.1016/j.apenergy.2010.12.056

Tam, N. F. Y., and Wong, Y. S. (1996). Effect of ammonia concentrations on growth of *Chlorella vulgaris* and nitrogen removal from media. *Bioresour. Technol.* 57, 45–50. doi: 10.1016/0960-8524(96)00045-4

US DOE (2008). *Algal Biofuels. Biomass Program*. Washington, DC: Department of Energy.

Wang, J. F., Liu, J. L., and Liu, T. Z. (2015). The difference in effective light penetration may explain the superiority in photosynthetic efficiency of attached cultivation over the conventional open pond for microalgae. *Biotechnol. Biofuels* 8, 1–17. doi: 10.1186/s13068-015-0240-0

Wang, L., Li, Y., Chen, P., Min, M., Chen, Y., Zhu, J., et al. (2010). Anaerobic digested dairy manure as a nutrient supplement for cultivation of oil-rich green microalgae *Chlorella* sp. *Bioresour. Technol.* 101, 2623–2628. doi: 10.1016/j.biortech.2009.10.062

Wang, T., Ge, H. Y., Liu, T. T., Tian, X. W., Wang, Z. J., Guo, M. J., et al. (2016). Salt stress induced lipid accumulation in heterotrophic culture cells of *Chlorella protothecoides*: mechanisms based on the multi-level analysis of oxidative response, key enzyme activity and biochemical alteration. *J. Biotechnol.* 228, 18–27. doi: 10.1016/j.jbiotec.2016.04.025

Xu, J., Zhao, Y. J., Zhao, G. H., and Zhang, H. (2015). Nutrient removal and biogas upgrading by integrating freshwater algae cultivation with piggery anaerobic digestate liquid treatment. *Appl. Microbiol. Biotechnol.* 99, 6493–6501. doi: 10.1007/s00253-015-6537-x

Yao, N., Liu, Z., Chen, Y., Zhou, Y., and Xie, B. (2015). A novel thermal sensor for the sensitive measurement of chemical oxygen demand. *Sensors* 15, 20501–20510. doi: 10.3390/s150820501

Zeraatkar, A. K., Ahmadzadeh, H., Talebi, A. F., Moheimani, N. R., and McHenry, M. K. (2016). Potential use of algae for heavy metal bioremediation, a critical review. *J. Environ. Manage.* 181, 817–831. doi: 10.1016/j.jenvman.2016.06.059

Zhou, W., Min, M., Li, Y., Hu, B., Ma, X., Cheng, Y., et al. (2012). A hetero-photoautotrophic two-stage cultivation process to improve wastewater nutrient removal and enhance algal lipid accumulation. *Bioresour. Technol.* 110, 448–455. doi: 10.1016/j.biortech.2012.01.063

Zhu, L., Li, Z., and Ketola, T. (2011). Biomass accumulations and nutrient uptake of plants cultivated on artificial floating beds in China's rural area. *Ecol. Eng.* 37, 1460–1466. doi: 10.1016/j.ecoleng.2011.03.010

Conflict of Interest Statement: The authors declare that the research was conducted in the absence of any commercial or financial relationships that could be construed as a potential conflict of interest.

frontiers in Plant Science

ORIGINAL RESEARCH
published: 03 August 2017
doi: 10.3389/fpls.2017.01347

Knock-Down of the IFR1 Protein Perturbs the Homeostasis of Reactive Electrophile Species and Boosts Photosynthetic Hydrogen Production in *Chlamydomonas reinhardtii*

*Deepak Venkanna[1], Christian Südfeld[1], Thomas Baier[1], Sarah V. Homburg[2], Anant V. Patel[2], Lutz Wobbe[1] and Olaf Kruse[1]**

[1] Faculty of Biology, Center for Biotechnology (CeBiTec), Bielefeld University, Bielefeld, Germany, [2] Faculty of Engineering and Mathematics, Fermentation and Formulation of Biologicals and Chemicals, Bielefeld University of Applied Sciences, Bielefeld, Germany

OPEN ACCESS

Edited by:
Jianhua Fan, Carnegie Institution for Science (CIS), United States

Reviewed by:
Wenqiang Yang, Carnegie Institution for Science, United States
Conrad Mullineaux, Queen Mary University of London, United Kingdom

***Correspondence:**
Olaf Kruse
olaf.kruse@uni-bielefeld.de

Specialty section:
This article was submitted to Plant Biotechnology, a section of the journal Frontiers in Plant Science

Received: *13 June 2017*
Accepted: *19 July 2017*
Published: *03 August 2017*

Citation:
Venkanna D, Südfeld C, Baier T, Homburg SV, Patel AV, Wobbe L and Kruse O (2017) Knock-Down of the IFR1 Protein Perturbs the Homeostasis of Reactive Electrophile Species and Boosts Photosynthetic Hydrogen Production in Chlamydomonas reinhardtii. Front. Plant Sci. 8:1347. doi: 10.3389/fpls.2017.01347

The protein superfamily of short-chain dehydrogenases/reductases (SDR), including members of the atypical type (aSDR), covers a huge range of catalyzed reactions and *in vivo* substrates. This superfamily also comprises isoflavone reductase-like (IRL) proteins, which are aSDRs highly homologous to isoflavone reductases from leguminous plants. The molecular function of IRLs in non-leguminous plants and green microalgae has not been identified as yet, but several lines of evidence point at their implication in reactive oxygen species homeostasis. The *Chlamydomonas reinhardtii* IRL protein IFR1 was identified in a previous study, analyzing the transcriptomic changes occurring during the acclimation to sulfur deprivation and anaerobiosis, a condition that triggers photobiological hydrogen production in this microalgae. Accumulation of the cytosolic IFR1 protein is induced by sulfur limitation as well as by the exposure of *C. reinhardtii* cells to reactive electrophile species (RES) such as reactive carbonyls. The latter has not been described for IRL proteins before. Over-accumulation of IFR1 in the singlet oxygen response 1 (*sor1*) mutant together with the presence of an electrophile response element, known to be required for SOR1-dependent gene activation as a response to RES, in the promoter of *IFR1*, indicate that IFR1 expression is controlled by the SOR1-dependent pathway. An implication of IFR1 into RES homeostasis, is further implied by a knock-down of *IFR1*, which results in a diminished tolerance toward RES. Intriguingly, *IFR1* knock-down has a positive effect on photosystem II (PSII) stability under sulfur-deprived conditions used to trigger photobiological hydrogen production, by reducing PSII-dependent oxygen evolution, in *C. reinhardtii*. Reduced PSII photoinhibition in *IFR1* knock-down strains prolongs the hydrogen production phase resulting in an almost doubled final hydrogen yield compared to the parental strain. Finally, *IFR1*

knock-down could be successfully used to further increase hydrogen yields of the high hydrogen-producing mutant *stm6*, demonstrating that *IFR1* is a promising target for genetic engineering approaches aiming at an increased hydrogen production capacity of *C. reinhardtii* cells.

Keywords: *Chlamydomonas reinhardtii*, photobiological hydrogen production, isoflavone reductase-like proteins, short-chain dehydrogenases/reductases, reactive electrophile species, singlet oxygen response 1 (*sor1*)

INTRODUCTION

Among the most urgent challenges of our society today, are those associated to global warming, depletion of fossil fuels and a steady increase of the energy demand, which can pose a threat to economic and political stability (Organisation for Economic Co-operation and Development [OECD]/International Energy Agency [IEA], 2011). Photosynthesis-driven H_2 production by photosynthetic microbes, such as cyanobacteria and microalgae, has a perfect carbon footprint, because of its zero CO_2 emission. Within photobiological hydrogen production electrons and protons from water splitting are directed via photosynthesis toward specific H_2-evolving enzymes, the hydrogenases (Gaffron and Rubin, 1942). Microalgae exploit Fe–Fe hydrogenases, which compared to other hydrogenases are highly efficient because of their extraordinarily high turnover number (Volgusheva et al., 2013; Lubitz et al., 2014). However, due to its oxygen sensitivity (Ghirardi et al., 1997), oxygenic photosynthesis cannot be directly coupled to hydrogen production in green microalgae. Therefore, photobiological hydrogen production has to be split into a two-stage process, which can be achieved by the experimental protocol proposed by Melis et al. (2000). This protocol relies on biomass generation under sulfur-replete conditions in the first stage and subsequent withdrawal of sulfur to trigger photoinhibition of photosystem II, resulting in a continuous decline of photosynthetic oxygen evolution, while mitochondrial respiration remains relatively unaffected by the lack of sulfur in the medium. In sealed culture flasks, this cultivation regime helps establishing anaerobic conditions, which are a prerequisite for the induction of the hydrogenase pathway (Ghysels and Franck, 2010). In *Chlamydomonas reinhardtii*, sulfur deprivation results in a strong down-regulation of the Calvin cycle and photosynthetic light reactions, based on a rapid decrease of Rubisco levels (Zhang et al., 2002) and an impaired PSII repair cycle, which relies on the *de novo* synthesis of the PSII subunit D1, which is restricted by the limited availability of sulfur-containing amino acids under these conditions (Wykoff et al., 1998). Although a massive decline in water-splitting activity is a prerequisite for the establishment of anaerobic conditions, which enable hydrogen production via the oxygen-sensitive hydrogenase enzyme, several studies clearly demonstrated that residual PSII activity and linear electron transport toward the hydrogenase are indispensable for efficient hydrogen production in *C. reinhardtii* (Antal et al., 2003; Volgusheva et al., 2013; Baltz et al., 2014; Steinbeck et al., 2015). The *C. reinhardtii* mutant *stm6* (Schönfeld et al., 2004) displays an enhanced hydrogen production capacity (Kruse et al., 2005) and its increased rate of mitochondrial oxygen consumption (Uhmeyer et al., 2017), was proposed to protect PSII during sulfur deprivation by accelerating the establishment of anaerobic conditions (Volgusheva et al., 2013), where irreversible, oxygen-dependent photoinhibition (Vass et al., 1992) cannot occur. Besides the PSII-dependent pathway of hydrogen production, starch degradation and subsequent glycolysis can provide NADH, which can be used to feed electrons into the photosynthetic electron transport chain without the need for water-splitting at PSII (Chochois et al., 2009; Baltz et al., 2014). Therefore, larger starch reserves present in *stm6* compared to wild type strains also contribute to the higher hydrogen production capacity seen for this mutant (Kruse et al., 2005; Doebbe et al., 2010). Cyclic electron flow (CEF) around photosystem I competes with electron delivery to the hydrogenase and a reduced CEF activity of *stm6* is another important aspect of its phenotype, which should significantly contribute to the elevated hydrogen production potential (Kruse et al., 2005). In addition to its photobiological production, hydrogen can also be produced under dark fermentative conditions in *C. reinhardtii* (Grossman et al., 2011).

With the aim to generate *C. reinhardtii* strains producing increased amounts of hydrogen upon exposure to sulfur limitation, several strategies have already been applied, which mainly targeted the oxygen sensitivity of the hydrogenase, the competition between CEF and hydrogen production, the efficiency of light conversion in the antenna and cellular starch contents (for review see Dubini and Ghirardi, 2015). Transcriptomics conducted with *C. reinhardtii* cells subjected to hydrogen production conditions could be another strategy to identify novel gene targets for the optimization of hydrogen production via genetic engineering (Nguyen et al., 2011; Toepel et al., 2013).

In a previous study (Nguyen et al., 2011), a transcript encoding the protein IFR1 (Cre11.g477200; NmrA-like) accumulated strongly in hydrogen-producing cells of *C. reinhardtii*. NmrA-like proteins belong to the protein superfamily of atypical short-chain dehydrogenases/reductases (aSDRs), which also contains isoflavone reductase-like (IRL) proteins (Moummou et al., 2012). IRL proteins from higher plants such as OsIRL from rice, were proposed to be implicated in ROS homeostasis, as OsIRL expression is induced by ROS and an overexpression confers enhanced ROS tolerance (Kim et al., 2010). SDRs and aSDRs including IRL proteins remain poorly characterized in microalgae thus far (Moummou et al., 2012). Therefore, we analyzed the function of IFR1 by applying a forward genetics strategy based

on the use of artificial microRNA (amiRNA)-mediated knock-down of IFR1 in two distinct *C. reinhardtii* strains and subsequent analysis of the resulting phenotype, with a special focus on photosynthetic hydrogen production.

MATERIALS AND METHODS

Chemicals

3-(3,4-Dichlorophenyl)-1,1-dimethylurea (DCMU), 2,5-Dibromo-6-isopropyl-3-methyl-1,4-Benzoquinone (DBMIB), 2E-Hexenal, Hydrogen peroxide (H_2O_2), Methyl Viologen (MV), Neutral red (NR), and Rose Bengal (RB) were purchased from Sigma-Aldrich.

Strains and Growth Conditions

Chlamydomonas reinhardtii wild type CC124 (137c mt−), 4A+ (137c background) and mutant CC4604- sor1 (mt+) (Fischer et al., 2012) were obtained from the Chlamydomonas Center. UVM4, a UV mutant derived from CC4350 (cw15 arg7-8 mt+) known to efficiently express nuclear transgenes (Neupert et al., 2009) was kindly provided by R. Bock (MPI for Molecular Plant Physiology, Potsdam-Golm). The MOC1 knock-out mutant *stm6* was generated via random insertion of plasmid pArg7.8 (Debuchy et al., 1989), carrying the *Arg7* gene, into the nuclear genome of the arginine auxotrophic strain, *CC1618*. The *MOC1*-complemented strain *B13* (Schönfeld et al., 2004) was generated by co-transforming *stm6* with a 37-kb *Moc1*-containing cosmid isolated from a cosmid library and the *Cry1* gene as a dominant selectable marker conferring resistance to emetine (plasmid p613; Nelson et al., 1994). All strains were grown photoheterotrophically in TAP (tris acetate phosphate) medium (Harris, 1989) at 25°C with continuous white light of 100 μmol m^{-2} s^{-1}. Experiments were performed by using the cells from mid-log phase. For hydrogen production, cells were harvested and washed three times with TAP-S medium. The cells were finally suspended in TAP-S to the tune of ∼25 μg/ml of chlorophyll. Hydrogen setup and gas measurement was carried out as described previously (Doebbe et al., 2010). After 20 h of anaerobic conditions, the effect of DCMU on H_2 production was assessed by adding 20 μM DCMU to the sealed bioreactors. Quantitative analysis of RES and ROS stress tolerance was evaluated by growing 2×10^6 cells/ml in TAP at 100 μmol m^{-2} s^{-1} with following chemicals: 5 μM DBMIB, 500 μM 2*E*-Hexenal, 4 μM RB, 15 μM NR, 0.5 μM MV and 7 mM H_2O_2. Cell growth was determined by analyzing OD_{680} and cell count (Z2 cell and particle counter, Beckman Coulter) at 0 and 24 h and 10 μl of culture was spotted on TAP agar plate for recovery.

Generation of IRL Knock-Down Strains

The artificial microRNA sequence for generating IRL knock-down was designed with a web based tool WMD3[1]. The amiRNA sequences were generated to target exons 2 (*forward*: ctagtCAGGTCCAGGAGATTGATATAtctcgctgatcggcaccatg gggtggtggtgatcagcgcaTATAACAATCTCCTGGACCTGg; reverse: ctagcCAGGTCCAG GAGATTGTTATAtagcgctgatcaccaccacccc catggtgccgatcagcgagaTATATCAATCTCCTGGACCTGa) and 4 (forward: ctagtGAGCACGCTATTAAGGTCGTAtctcgctgatcgg caccatgg gggtggtggtgatcagcgctaTACGGTCTTA-ATAGCGTGCT Cg and *reverse*: ctagcGAGCACGC TATTAAGACCGTAtagcgct gatcaccaccacccccatggtgccgatcagcgagaTACGACCTTAATAG GT GCTCa) of the coding region and cloned into vector pChlamiRNAi3int (Molnar et al., 2009). CC124 was transformed by electroporation (Jaeger et al., 2017) and *stm6* was transformed via glass beads as mentioned previously (Kindle, 1990). Transformants were selected on paromomycin (10 μg/ml) TAP agar plates and transferred to sulfur depleted medium for screening.

[1]http://wmd3.weigelworld.org

Antibody and Recombinant Protein Production

The polyclonal antiserum directed against a 17 aa polypeptide IFR1 was raised in rabbit (Agrisera, Sweden). To heterologously express IFR1 in *Escherichia coli*, a codon optimized full length *IFR1* coding sequence (phytozome: Transcript Cre11.g477200.t1.2) was synthesized *de novo* (Genscript, United States) and cloned between the *Nde*I and *Xho*I restriction sites of expression vector pET-24a(+) (Novagen), enabling streptag-based affinity purification.

RNA Extraction and Quantitative Real Time PCR

Real-time RT-PCR was performed with DNaseI (RQ1 RNase -free DNase, Promega)-digested total RNA samples which was subjected to reverse transcription and PCR amplification using the SensiFAST^{TM} SYBR No-ROX One-Step Kit (BIOLINE, Germany). SYBR Green I fluorescence was recorded on a DNA Engine Opticon (Bio-RAD, Germany). Per sample 100 ng total RNA were used and *RPL13* (Gene ID: 5718254) as well as RACK1 (GeneID: 5723548) served as housekeeping genes. The following primers were used within the study: *IFR1* (5′-ATGGC GACTAAGAAGCACAC-3′ and 5′-CGAAGCCTGCTCATTGT AGT-3′), *RPL13* (5′-ATTCTTGCCGGGCAGCAGATTGTG-3′ and 5′-TTGCGCAGGAAG CGGTCATACTTC-3′) and *RACK1* (5′-TCAACATCACCAGCAAGAAGG-3′ and 5′-CTGGGCAT TTACAGGGAGTG-3′). Relative mRNA expression levels were calculated according to Pfaffl (Pfaffl, 2001).

SDS-PAGE and Immunoblotting

Cells were pelleted (3000 × g, 3 min) and suspended in lysis buffer (60 mM Tris pH 6.8, 2% SDS, 10% glycerol and freshly added 1 mM Pefabloc). Total proteins were extracted via freeze-thaw cycle in liquid N_2 and quantified by Lowry assay (BioRAD). The proteins were separated by a 12% Tris-glycine SDS-PAGE and blotted on to a nitrocellulose membrane. After overnight blocking (5% Milk powder in TBST with 0.1% Tween), the membrane was incubated at room temperature for 1.5 h with IFR1-specific antiserum (1:2500), washed and then incubated for 1 h with a peroxidase-conjugated anti-rabbit antibody (Agrisera, Sweden) for chemiluminescence detection (ECL: GE Healthcare).

Signals were visualized using the FUSION-FX7 detection system (Peqlab, Germany). Protein bands were quantified with MyImageAnalysis software (ThermoFisher Scientific).

Chlorophyll Fluorescence Analyses

To determine the maximum quantum yield (F_v/F_m), 2 ml samples of a culture were incubated in the dark and aerated for 20 min. Chlorophyll fluorescence changes were recorded during a 10 min induction curve with actinic light (800 μmol photons m^{-2} s^{-1}) using a Mini PAM (Waltz) and F_v/F_m calculated according to the following equation (Maxwell and Johnson, 2000):

$$\frac{F_v}{F_m} = \frac{F_m - F_0}{F_m}$$

Construction of Fusion Protein and Confocal Microscopy

The IFR1 coding sequence, codon-optimized for the nuclear codon bias of *C. reinhardtii* was cloned into vector pOpt-mVenus_Paro (Lauersen et al., 2015) by using the *Nde*I::*Bgl*II and *Eco*RV::*Eco*RI restriction sites to obtain C-terminal and N-terminal fusions, respectively. Fluorescence imaging was accomplished with a confocal laser scanning microscope (LSM780, Carl Zeiss GmbH, Germany) with specific filters for chlorophyll and mVenus as described before (Lauersen et al., 2015).

Statistical Analysis

The significance of results was evaluated with a student's two-tailed *t*-test for independent samples. The significance threshold was set between $p < 0.05$ to $p < 0.1$. Error bars represent standard error (SE) and in case of box plots the whiskers represent variability within the first and third quartile.

RESULTS

IFR1 Is an Atypical Short-Chain Dehydrogenase that Accumulates in the Cytosol of *C. reinhardtii* as a Response to Abiotic Stress

A previous study (Nguyen et al., 2011), demonstrated that a transcript encoding a putative isoflavone reductase (IFR1) accumulated significantly in hydrogen-producing cells of *C. reinhardtii*. An NCBI-BLAST search using the amino acid sequence of IFR1 (Phytozome locus name Cre11.g477200; *C. reinhardtii* v5.5) revealed that this protein contains a conserved phenylcoumaran benzylic ether reductase (PCBER) like domain (specific hit/e-value $1.55e^{-68}$). PCBERs are NADPH-dependent aromatic alcohol reductases, and are described as atypical members of the short-chain dehydrogenase/reductase (SDR) family (Min et al., 2003). Atypical SDRs possess an N-terminus characteristic of NAD(P)-binding proteins and a small C-terminal domain presumed to be involved in substrate binding (Filling et al., 2002; Persson et al., 2003; Kavanagh et al., 2008). In contrast to classical SDRs, they do not have the conserved active site tyrosine residue typically found in SDRs and contain an atypical glycine-rich NADP-binding motif reading GXGXXG or G[GA]XGXXG (Supplementary Figure S1). The amino acid sequence of IFR1 shows identities to other members of the protein family in the range of 20–30% (Supplementary Table S1), with the highest similarity found for isoflavone reductases (Babiychuk et al., 1995) and IRL proteins (Petrucco et al., 1996) (Supplementary Figure S1 and Table S1).

The *C. reinhardtii IFR1* gene encodes a 32 kDa protein whose localization was predicted to be cytosolic by the *in silico* prediction tool PredAlgo (Tardif et al., 2012). To confirm that IFR1 indeed resides in the cytosol, IFR1 was C- and N- terminally fused with YFP (mVenus variant; Kremers et al., 2006) and expressed in the *C. reinhardtii* cell line UVM4 (Neupert et al., 2009). Two strains, stably expressing either full length IFR1-YFP (C) or IFR1-YFP (N) were identified via immunoblots (Supplementary Figure S2; C and N). YFP fluorescence could be detected in both strains expressing YFP, either N- or C- terminally fused to IFR1 (**Figure 1**; N and C), while the parental control strain (PCS) only emitted red chlorophyll auto-fluorescence from the cup-shaped structure representing the chloroplast. Superimposition of the chlorophyll and YFP fluorescence demonstrated that the YFP-tagged IFR1 variants displayed a distribution of the YFP signal identical to that observed in the control strain (Cyto), expressing YFP in the cytosol (Lauersen et al., 2015). YFP-tagging of IFR1 in conjunction with confocal laser-scanning microscopy demonstrated that the localization of IFR1 is indeed cytosolic.

In a previous study (Nguyen et al., 2011) we compared the transcriptomes of the *C. reinhardtii* wild type (wt) cc406 and the high hydrogen production mutant *stm6glc4* (Doebbe et al., 2007) [derived from *stm6* (Kruse et al., 2005)] during photosynthetic hydrogen production triggered by sulfur deprivation (Melis et al., 2000). The transcriptome data revealed that within the peak hydrogen production phase, *IFR1* transcripts accumulated to a high extent (∼10–40-fold compared to sulfur-replete condition) in both strains. In order to confirm that the accumulation of IFR1 transcript is indeed translated into elevated protein amounts, we analyzed protein samples taken at distinct points from a hydrogen-producing culture of a *C. reinhardtii* wild type (**Figure 2A**). A strong induction of IFR1 protein expression was observed in the wild type under S-deprived anaerobic H_2 production conditions. IFR1 accumulation started before the onset of anaerobiosis and H_2 production conditions (from 24 h onward), indicating that sulfur deprivation rather than anaerobiosis is required for IFR1 induction. An inspection of published RNAseq data sets using AlgaePath (Zheng et al., 2014) revealed that sulfur deprivation alone triggers *IFR1* mRNA accumulation [∼8-fold induction 6 h after withdrawal of sulfur; González-Ballester et al., 2010; gene expression omnibus (GEO) series GSE17970]. An even stronger induction was observed within a transcriptome study analyzing the modulation of the *C. reinhardtii* transcriptome in response to nitrogen depletion (∼46-fold after 48 h; Miller et al., 2010; GSE24367), but IFR1 protein expression could not be detected under nitrogen-deplete conditions (data not shown), demonstrating that IFR1 accumulation is not generally observed as a response

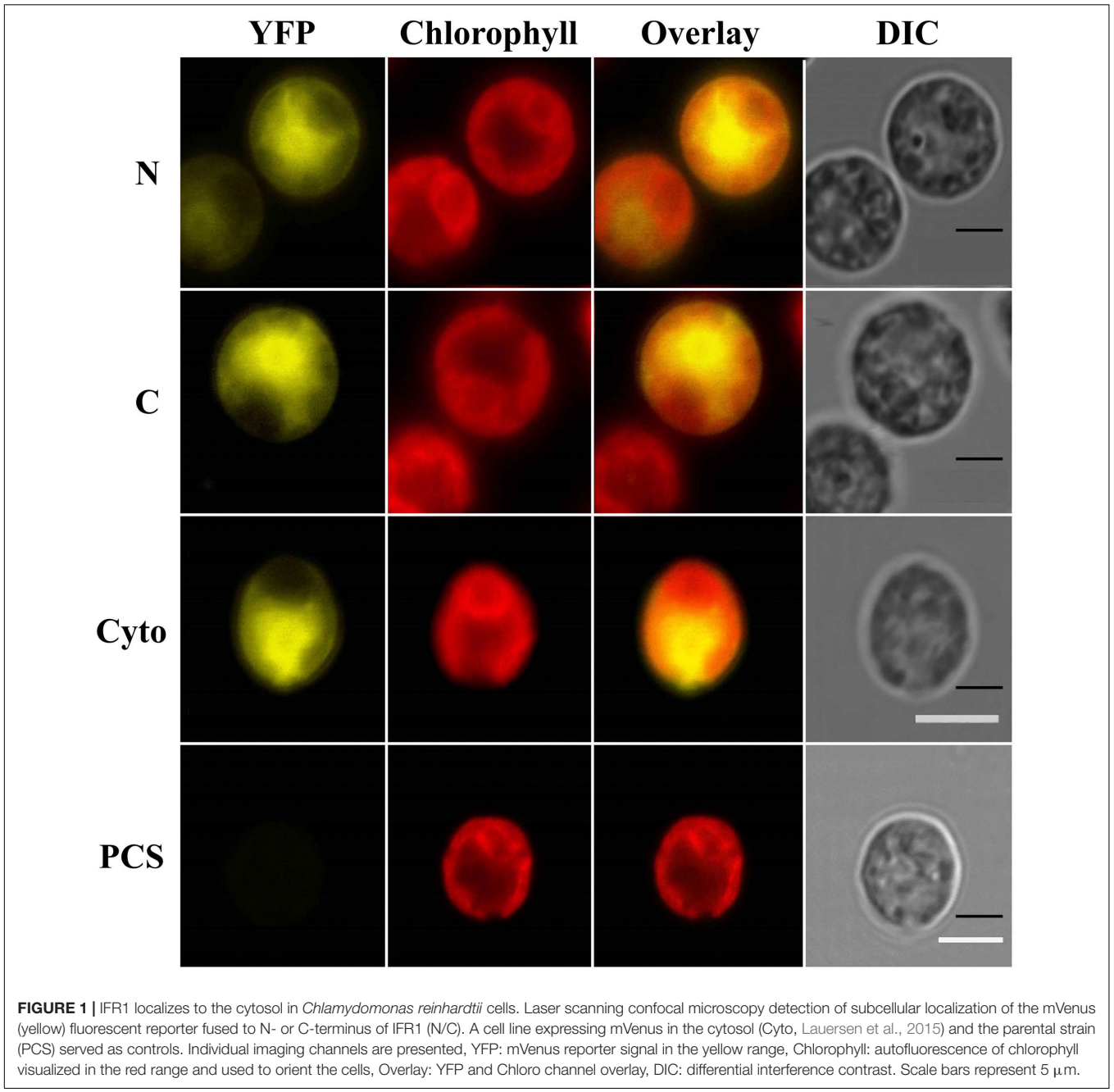

FIGURE 1 | IFR1 localizes to the cytosol in *Chlamydomonas reinhardtii* cells. Laser scanning confocal microscopy detection of subcellular localization of the mVenus (yellow) fluorescent reporter fused to N- or C-terminus of IFR1 (N/C). A cell line expressing mVenus in the cytosol (Cyto, Lauersen et al., 2015) and the parental strain (PCS) served as controls. Individual imaging channels are presented, YFP: mVenus reporter signal in the yellow range, Chlorophyll: autofluorescence of chlorophyll visualized in the red range and used to orient the cells, Overlay: YFP and Chloro channel overlay, DIC: differential interference contrast. Scale bars represent 5 μm.

to macronutrient limitation. While effects of carbon dioxide limitation on *IFR1* transcript accumulation were comparably small (∼2-fold; Fang et al., 2012; GSE33927), exposure of wild type *C. reinhardtii* cells to hydrogen peroxide led to a rapid accumulation of IFR1 transcript (∼19-fold within 1 h; Blaby et al., 2015; GSE34826). In addition, a previous transcriptome study indicated that *IFR1* belongs to the set of genes overexpressed in the mutant *singlet oxygen resistant 1* (*sor1*), which shows a constitutively higher expression of genes implicated in the detoxification of reactive oxygen and electrophile species [9.8 in *sor1* vs. 0 in parental (4A+); Fischer et al., 2012; GSE33548]. Overexpression of IFR1 mRNA in *sor1* vs. its parental strain (4A+) could be confirmed by RTqPCR experiments [median 17.8; lower quartile (Q1) 13.9; upper quartile (Q3) 25.4; IFR1 mRNA level in 4A+ set to 1; **Figure 2B**]. The higher mRNA level was also translated into higher IFR1 protein amounts found in *sor1* (**Figure 2C**; 48 and 72 h; sor1 vs. 4A+). Analysis of the IFR1 promoter region led to the identification of an 8 bp palindromic motif (CAACGTTG) (**Figure 2D**) which was identified as an electrophile response element (ERE) in nuclear promoters of *C. reinhardtii* genes overexpressed in the mutant *sor1* and whose expression is

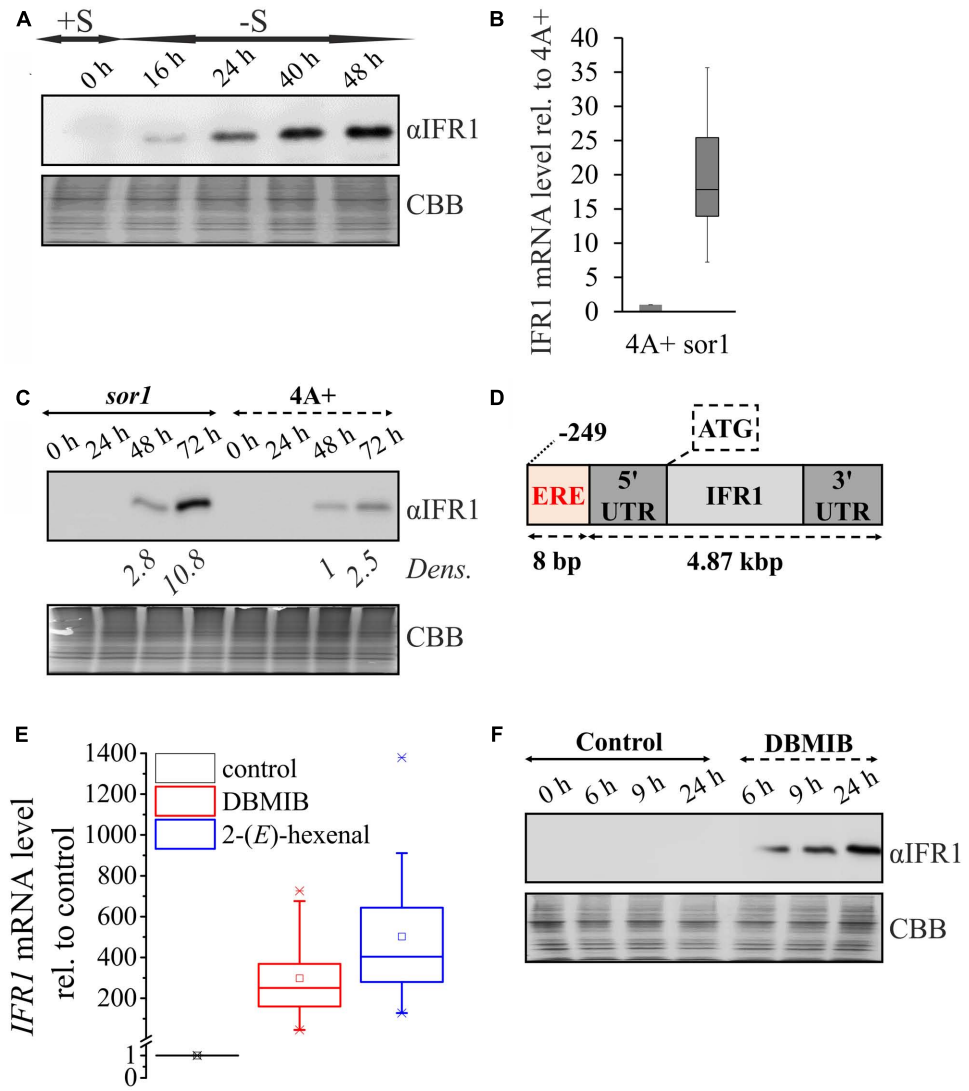

FIGURE 2 | IFR1 accumulation is triggered by the SOR1-dependent pathway. **(A)** Samples were taken before (0 h, +S) and during the course of hydrogen production induced by sulfur deprivation of a wild type cell line (16–48 h; –S). IFR1 accumulation was analyzed with an IFR1-specific antiserum (αIFR1) and equal protein loading confirmed by colloidal Coomassie staining (CBB). **(B)** Comparison of *IFR1* mRNA levels in the *sor1* mutant (Fischer et al., 2012) and its parental strain (4A+) with samples taken in the late exponential phase. mRNA levels were determined by RTqPCR and the *IFR1* transcript level in 4A+ was set to 1. Median and interquartile range shown in the box-and-whisker diagram are derived from two biological replicates, each including nine technical replicates (n = 18). **(C)** Representative immunoblot (αIFR1) showing IFR1 accumulation during growth of mutant *sor1* and its parental strain (4A+) in nutrient-replete TAP medium for 3 days. Relative band intensities (*Dens.*) determined by densitometric scanning of immunblot signals are given relative to the band intensity of the 4A+ sample at $t_{48\,h}$ (set to 1). **(D)** Position of the octanucleotide motif CAACGTTG described to represent an electrophile response element (ERE; Fischer et al., 2012) implicated in the genetic response to reactive electrophile species (RES) and SOR1-dependent signaling relative to the start codon (ATG) of the 4.87 kbp IFR1 gene, comprising exons, introns and untranslated regions (UTRs). **(E)** *IFR1* mRNA levels determined by RTqPCR following dark treatment of WT cell cultures with DBMIB (5 μM) and 2-(*E*)-hexenal (500 μM) for 24 h. The mRNA level of the solvent control sample was set to 1. Median and interquartile range shown in the box-and-whisker diagram are derived from two biological replicates, each including six technical replicates (n = 12). **(F)** Immunoblot (αIFR1) showing IFR1 accumulation distinct time points (6–24 h) after the addition of DBMIB (5 μM) or only solvent (Control) to a liquid TAP culture of the *C. reinhardtii* wild type CC124 and subsequent dark incubation for 24 h.

activated by reactive electrophile species (RES) (Fischer et al., 2012).

Indeed, treatment of *C. reinhardtii* WT cultures with the RES-compounds DBMIB (2,5-Dibromo-6-isopropyl-3-methyl-1,4-benzoquinone) and 2-(*E*)-hexenal triggered a strong accumulation of *IFR1* mRNA [median fold-induction vs. control: 250.5 for DBMIB and 403.5 for 2-(*E*)-hexenal; **Figure 2E**]. In contrast to DBMIB, 2-(*E*)-hexenal is a RES (oxylipin) that occurs naturally in high light-stressed cells of *C. reinhardtii* (Roach et al., 2017) and is formed from polyunsaturated fatty acids via peroxidation and subsequent enzymatic cleavage (Mosblech et al., 2009). Addition of DBMIB to sulfur-replete cultures of a *C. reinhardtii* WT in the dark induced a strong accumulation of IFR1 protein (**Figure 2F**). However, IFR1 protein expression

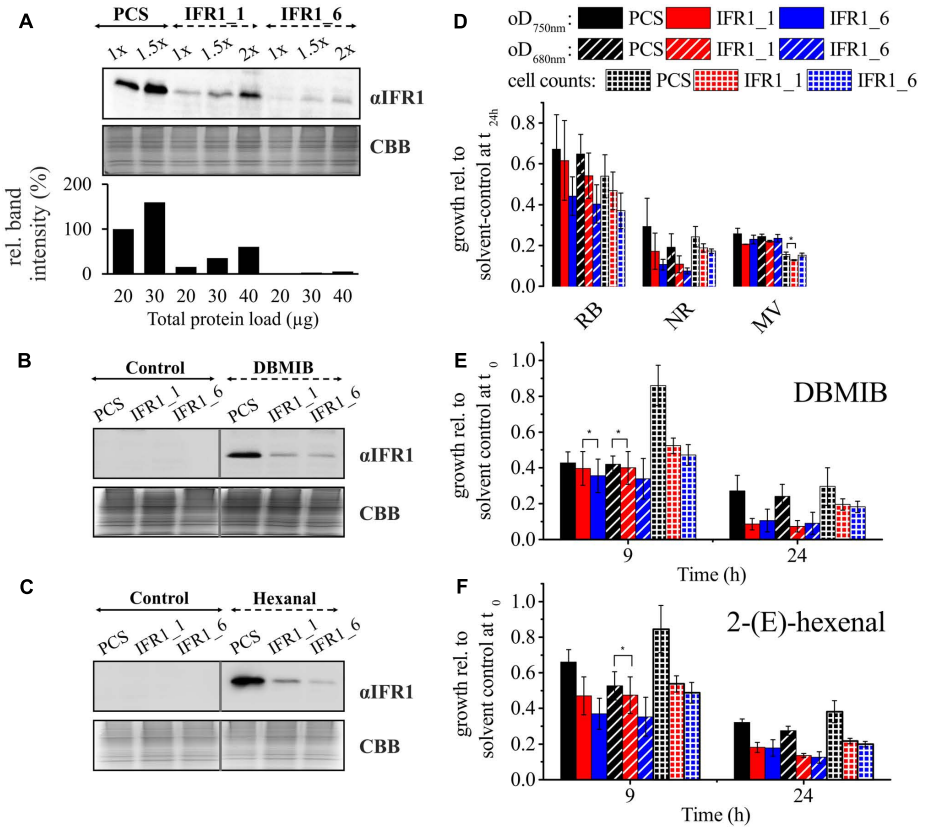

FIGURE 3 | IFR1 knock-down causes diminished tolerance toward RES in *C. reinhardtii*. **(A)** Immunodetection of IFR1 protein (αIFR1) in the parental strain (PCS; wild type CC124) and IFR1 knock-down strains (IFR1_1 and IFR1_6) detected after 48 h of cultivation in sulfur deplete medium. A colloidal Coomassie stained gel (CBB) served as loading control. Different amounts of proteins were used and band intensities (lower bar diagram) determined by densitometric analysis (1x PCS set to 100%). **(B,C)** IFR1 accumulation in PCS and IFR1 knock-down strains grown for 24 h in TAP supplemented with DBMIB (5 µM) or 2-(E)-hexenal (500 µM). **(D)** Growth inhibition by reactive oxygen species determined for the PCS and the two IFR1 knock-down strains during 24 h of growth in TAP supplemented with 4 µM rose Bengal (RB), 15 µM neutral red (NR), or 0.5 µM methyl viologen (MV). Optical densities (determined at 680 and 750 nm) and cell counts are given relative to the untreated/solvent-control sample (set to 1). Error bars indicate standard errors derived from three biological replicates including technical replicates ($n = 3$). Asterisks indicate significant differences between PCS and knock-down strains according to a two-tailed Student's *t*-test ($p < 0.05$). **(E,F)** Growth inhibition following treatment of PCS and IFR1 knock-down strains with 5 µM DBMIB and 500 µM 2-(E)-hexenal for 9 or 24 h in TAP medium. Standard errors are derived from three biological replicates, including technical replicates ($n = 3$). Except for the data indicated by asterisks ($p > 0.05$) differences between PCS and knock-down strains were significant according to a two-tailed Student's *t*-test ($p < 0.05$).

could not be observed (data not shown) in TAP grown cultures supplemented with DCMU [3-(3,4-Dichlorophenyl)-1,1-dimethylurea; PSII forward electron inhibitor; Metz et al., 1986], indicating that inhibition of photosynthetic electron transport by DCMU or DBMIB can be excluded and noted effects can be mainly attributed to DBMIB's action as a reactive electrophile.

A Knock-Down of IFR1 Causes Diminished RES-Tolerance

To functionally characterize IFR1 of *C. reinhardtii*, we applied a reverse genetics approach, employing a nuclear expression vector for the expression of artificial microRNAs (amiRNA) (Molnar et al., 2009). Screening of transformants based on immunoblots with the IFR1-specific antiserum led to the identification of two knock-down strains. When grown in S-deplete medium, IFR1_1 and IFR1_6 accumulated ∼65 and ∼95% less IFR1 protein, respectively as compared to the parental strain (**Figure 3A**).

Diminished accumulation of IFR1 in both knock-down strains was also observed, when cells were treated with the RES compound DBMIB (**Figure 3B**). In line with the strong *IFR1* transcript accumulation observed after treatment with 2-(*E*)-hexenal (**Figure 2E**), addition of this compound to liquid cultures triggered a strong accumulation of IFR1 protein in the parental strain, which was diminished in knock-down strains (**Figure 3C**). Prompted by the finding that IFR1 protein accumulates following the exposure of *C. reinhardtii* cells to RES and the reported requirement of IRL proteins for oxidative stress tolerance in higher plants (Babiychuk et al., 1995; Kim et al., 2010), we analyzed the tolerance of IFR1 knock-down strains toward various compounds which either act as reactive oxygen/electrophile species (ROS/RES) or induce their cellular accumulation (**Figures 3D–F**). To this end, compounds inducing ROS-stress [rose bengal (RB); neutral red (NR), and methyl viologen (MV)] or acting as

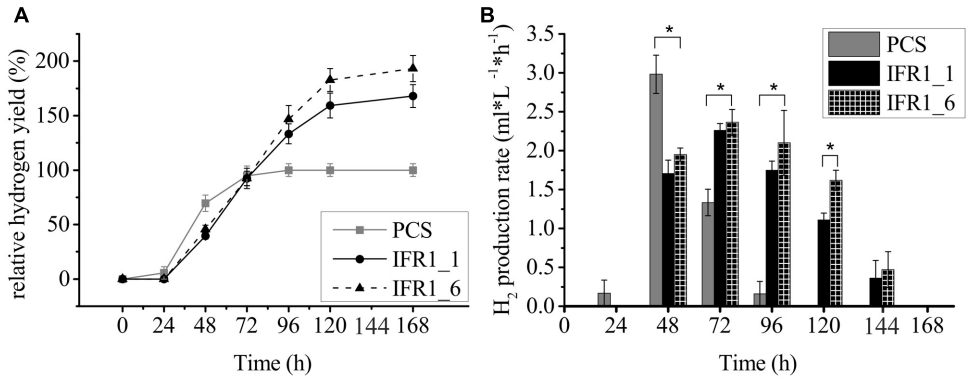

FIGURE 4 | Prolonged hydrogen production in IFR1 knock-down strains compared to the wild type. **(A)** Time course of hydrogen production for the parental strain (PCS) and IFR1 knock-down strains. Hydrogen yields in the knock-down strains are given relative to the final yield of the parental strain (set to 100%). Each data curve represents an average of three biological replicates including three technical triplicates ($n = 9$) with error bars representing the standard error. **(B)** H_2 production rates during the course of hydrogen production. Error bars indicate the standard error ($n = 9$) and asterisks indicate differences between PCS and knock-down strains which are significant according to a two-tailed Student's *t*-test (*$p < 0.05$).

RES [DBMIB and 2-(*E*)-hexenal] were added to the cultures and the growth retarding-effect was quantified after 24 h via measurement of optical densities ($oD_{680\ nm/750\ nm}$) and cell densities based on cell counting. The cultures were also spotted on TAP agar plates for recovery (Supplementary Figure S3). Significant differences reflected by all growth parameters applied could not be observed regarding the susceptibility of knock-down strains vs. parental strain toward methyl viologen, which triggers superoxide formation *in vivo* (Babbs et al., 1989) (**Figure 3D**; MV). Although neutral red and rose bengal, which act as photosensitizers and trigger the formation of singlet oxygen in live cells (Fischer et al., 2004), exerted a greater growth-inhibiting effect on both knock-down strains (**Figure 3D**), differences between the parental and IFR1 knock-down strains were not statistically significant according to a two-tailed Student's *t*-test ($p < 0.05$). In contrast, statistically robust ($p < 0.05$; two-tailed Student's *t*-test) differences could be seen when cells were treated for 24 h with DBMIB or 2-(*E*)-hexenal (**Figures 3E,F**), which caused a more pronounced growth inhibition in the knock-down strains. At least when cell counts were used as a growth parameter, a significantly higher susceptibility of knock-down strains toward RES could already be seen 9 h after the addition of DBMIB or 2-(*E*)-hexenal. A diminished availability of IFR1 in *C. reinhardtii* therefore reduces the tolerance toward RES.

Prolonged Hydrogen Production by IFR1 Knock-Down Mutants

IFR1 protein accumulates strongly in hydrogen producing cultures following sulfur-depletion (**Figure 2A**), indicating a potential role of this protein during the acclimation to sulfur depletion or anaerobiosis. The effect of *IFR1* knock-down was assessed by measuring H_2 production of the knock-down strains (**Figure 4A**). Parental strain, IFR1_1 and IFR1_6 were grown in sulfur-replete TAP medium to a mid-log phase and transferred to sulfur-deplete TAP medium by adjusting them to the same starting chlorophyll concentration (∼25 μg/ml). Hydrogen production was first notable 48 h after the onset of sulfur depletion and at the beginning hydrogen yields in the PCS exceeded those of the knock-down strains by ∼35–40%. During the course of H_2 production, production rates declined in the PCS from 48 h onward, while rates in the knock-down strains increased toward $t_{72\,h}$ and started declining notably beyond the time point $t_{120\,h}$ (**Figure 4B**). The H_2 production phase in PCS ceased at 96 h with a production phase (time between the first detection and the end of H_2 production) of 3 days as compared to 5 days by *IFR1* knock-down strains. Although the highest rate of hydrogen production (2.98 ± 0.25 ml L^{-1} h^{-1}) was reached in the PCS strain, the prolonged hydrogen production in the knock-down strains eventually led to final hydrogen yields that were about $68 \pm 10\%$ (SE) (IFR1-1) and $93 \pm 12\%$ (IFR1-6) higher than the yield from the wild type.

Prolonged H_2 Production in IFR1 Knock-Down Strains Results from a Sustained PSII Activity

One of the reasons for a prolonged hydrogen production in the course of sulfur starvation, could be a high residual PSII activity, which is required for efficient hydrogen production (Volgusheva et al., 2013; Steinbeck et al., 2015). Indeed, both IFR1 knock-down strains displayed a higher residual activity of PSII, measured as the maximum quantum yield of dark-adapted cells (F_v/F_m), following the exposure to sulfur limitation under aerobic conditions (**Figure 5A**; $-S/+O_2$; Fv/Fm; $t_{72-168\,h}$). The knock-down strain IFR1_6 was then selected for more detailed analyses regarding differences in PSII stability between knock-down and parental strain under hydrogen production conditions (sulfur deprivation under anaerobic conditions). Also during the course of hydrogen production, the knock-down of IFR1 causes an

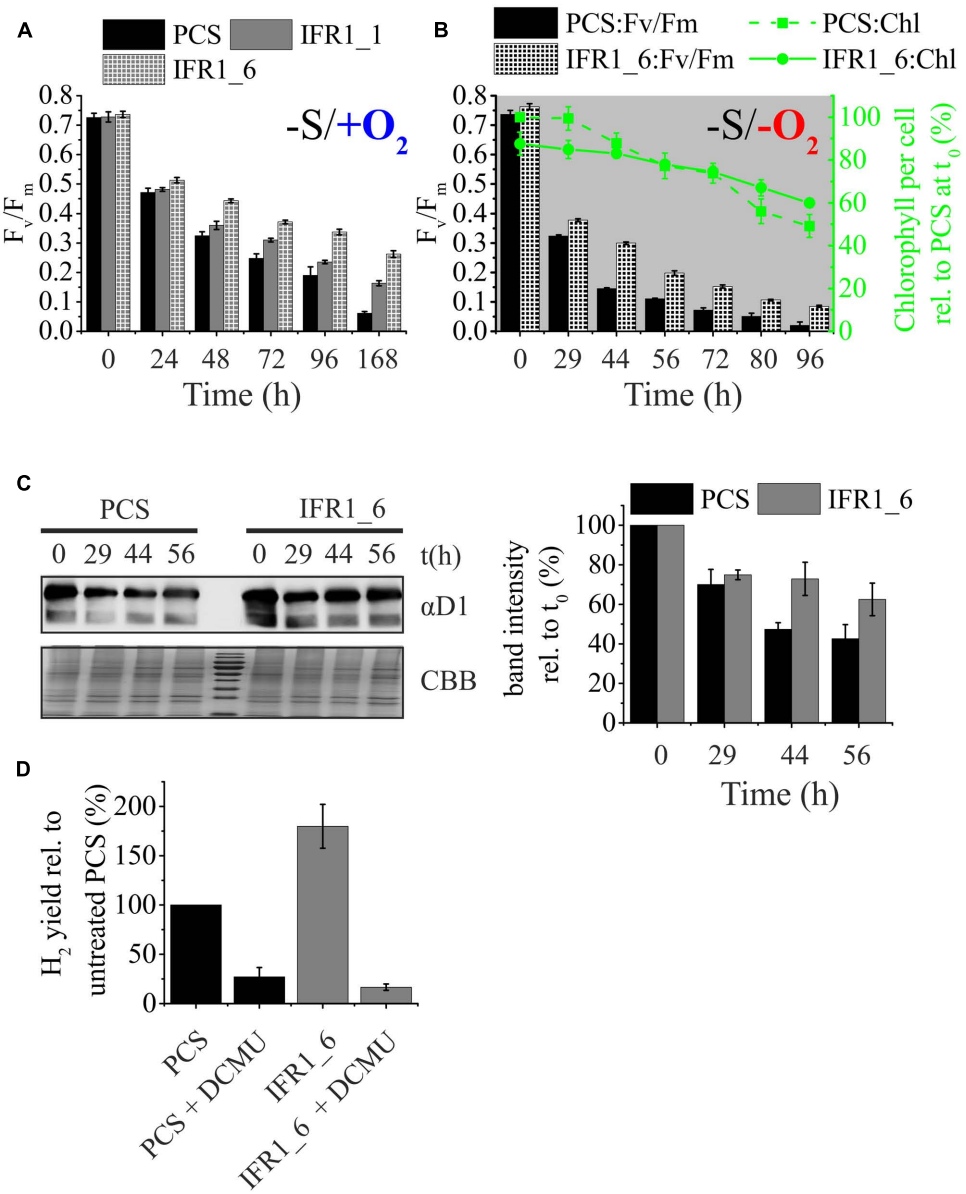

FIGURE 5 | Contribution of PSII and photosynthetic/respiration (P/R) rates on hydrogen production. **(A)** Maximum quantum yield (F_v/F_m) of dark-adapted cells of the parental strain (PCS) and IFR1 knock-down strains (IFR1_1/IFR1_6) before (t_0) and after exposure to sulfur limitation (t_{24}–$t_{168\,h}$) and aerobic conditions. Error bars indicate the standard error from three biological replicates ($n = 3$). **(B)** Time course of the maximum quantum yield (F_v/F_m; left y-axis) and the cellular chlorophyll content (right y-axis) during photosynthetic hydrogen production of the parental strain (PCS) and one of the IFR1 knock-down strains (IFR1_6). Chlorophyll data were normalized to the chlorophyll content of PCS at t_0 (set to 100%). Standard errors derived from three biological replicates ($n = 3$) are indicated as error bars. Except for t_0, the differences between PCS and IFR1_6 in regard to F_v/F_m were significant according to a two-tailed Student's *t*-test ($p < 0.05$). **(C)** Representative immunoblot showing the immunodetection of PSII subunit D1 (upper left panel; αD1) in samples of the parental strain (PCS) and IFR1_6 taken at indicated times during a hydrogen production experiment. A colloidal Coomassie stain (lower left panel; CBB) served as a loading control. Results from densitometric scanning (right panel) of blot signals are given relative to the D1 signal intensity determined for t_0 (set to 100%). Error bars indicate standard errors (three biological replicates; $n = 3$). **(D)** Relative H_2 yields obtained with the parental control strain (PCS) (black bars) and knock-down strain IFR1_6 (gray bars) in the absence or presence of 20 μM DCMU. Hydrogen yields determined for the untreated PCS were set to 100%. Error bars represent standard error ($n = 6$).

increased stability of PSII, as seen by higher F_v/F_m values from time point $t_{29\,h}$ onward (**Figure 5B**; $-S/-O_2$; left y-axis; PCS vs. IFR1_6). The lowered susceptibility of PSII toward photoinhibition in the IFR1_6 was also reflected by a lower relative decrease in the cellular chlorophyll content (~30% vs. 50% in PCS; **Figure 5B**; right y-axis; green curves). In good agreement with the higher residual PSII activity found in IFR1 knock-down strains (**Figures 5A,B**), the cellular content of the PSII core subunit D1 declined more slowly within the course of hydrogen production in

knock-down strain IFR1_6 compared to its parental strain (**Figure 5C**).

Specific inhibition of PSII with DCMU was used to confirm if the electrons for prolonged H_2 production indeed originated from residual PSII activity. DCMU was added directly into the H_2 bioreactors 30 h after the onset of sulfur deprivation. DCMU blocks the PSII-dependent pathway of hydrogen production based on residual water-splitting activity and linear electron transport toward the hydrogenase enzyme and inhibits H_2 production substantially, as reported before (Kruse et al., 2005; Volgusheva et al., 2007; Scoma et al., 2014). H_2 production dropped in both strains upon addition of DCMU (**Figure 5D**), but the relative effect of DCMU on hydrogen production was much stronger in the IFR1 knock-down strain (73% reduction in PCS vs. 163% reduction in IFR1_6). Furthermore total hydrogen production in strain IFR1_6 (16.6 ± 3.2%) was lower than the production observed for the parental strain (27.1 ± 9.4%), when DCMU was added to inhibit PSII. It can thus be concluded that the increased hydrogen production capacity caused by a knock-down of IFR1 mainly results from an enhanced activity of the PSII-dependent pathway, especially during the later stages of the hydrogen production pathway, when PSII activity in IFR1 knock-down strains exceeds the respective activity seen in the parental strain (**Figures 5A–C**).

IFR1 Knock-Down Can Be Applied as a Tool to Further Enhance Hydrogen Production in a Strain with a High Starting Capacity

To test whether the knock-down of *IFR1* can be applied as a tool to improve the hydrogen production capacity in various *C. reinhardtii* strains, we selected the strain *stm6*, known to produce high amounts of hydrogen (Kruse et al., 2005; Doebbe et al., 2010; Nguyen et al., 2011). One of the created *IFR1* knock-down strains, *stm6_IFR1kd*, displayed an IFR1 accumulation diminished to ∼20% of the IFR1 level found in the parental strain *stm6* (**Figure 6A**; αIFR1; 1X *stm6* vs. 1X *stm6_IFRkd*). Confirming the results obtained with knock-down strains derived from a wild type cell line (**Figure 4**), an IFR1 knock-down in the background of strain *stm6* also had a tremendous impact on the time course of hydrogen production and the overall production capacity (**Figure 6B**). The onset of hydrogen production in strain *stm6_IFRkd* (**Figure 6B**; gray curve) was delayed by ∼20 h compared to the parental strain (black curve), but hydrogen production in the knock-down strain reached a plateau phase only at time point 168 h, while the parental strain reached this phase already before $t_{120\,h}$. A prolonged hydrogen production phase together with an increased H_2 productivity rate (up to 3.07 ml· L^{-1}·h^{-1} at $t_{72\,h}$), indicated by a steeper slope of the *stm6_IFRkd* curve, resulted in a final hydrogen yield of the knock-down strain which was 70% higher than the respective yield obtained with the parental strain.

In analogy to what has been observed for the *IFR1* knock-down strains derived from a wild type, PSII activity (F_v/F_m;

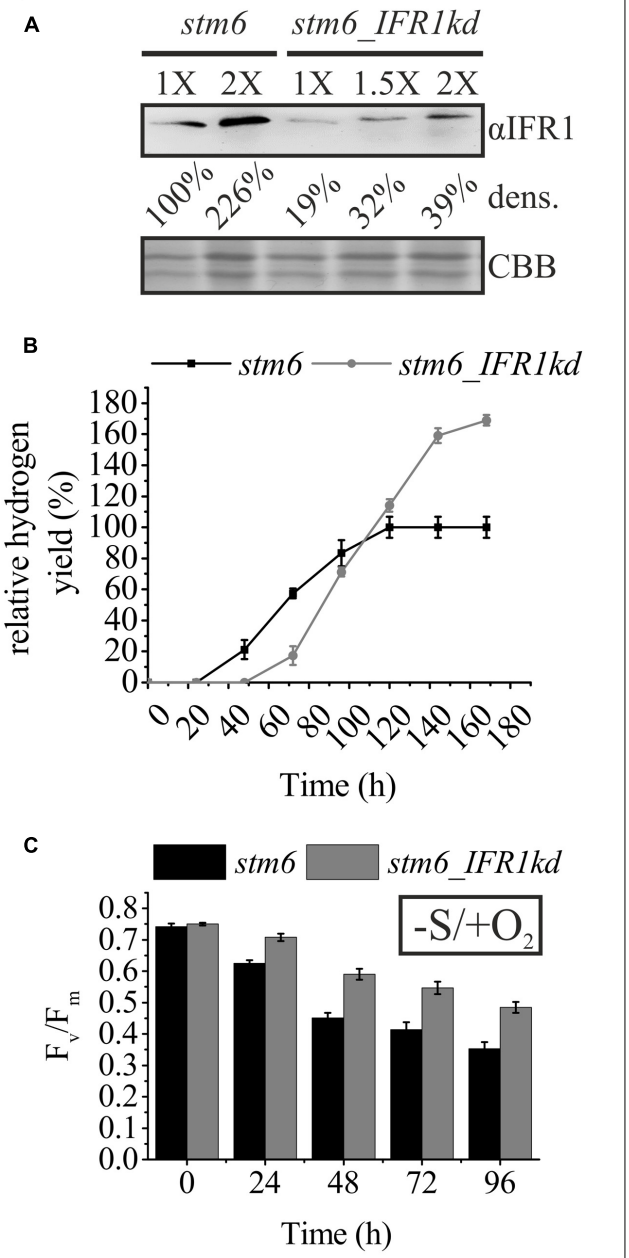

FIGURE 6 | Knock-down of IFR1 in the boosts hydrogen production in the high hydrogen producer mutant *stm6.* **(A)** Immunoblot analysis of IFR1 accumulation in *stm6* and *stm6_IFR1kd* cultivated under sulfur-limiting conditions. Different amounts of total protein (1X; 1.5X; and 2X) were used for immunodetection of IFR1 (αIFR1) with a colloidal Coomassie stain (CBB) serving as a loading control. Results from densitometric signal analysis (dens.) are indicated. **(B)** Relative time-dependent H_2 yields of the *stm6* parental strain (black curve) and *stm6_IFR1kd* (gray curve) with the final yield in *stm6* set to 100%. Error bars represent the standard error (three biological replicates including technical triplicates, $n = 9$). **(C)** Maximum quantum yield of PSII determined after dark incubation (Fv/Fm) determined in cultures of *stm6* (black bars) and *stm6_IFR1kd* (gray bars) exposed to sulfur starvation. Standard errors, shown as error bars are derived from three biological replicates including technical duplicates ($n = 6$). Except for t_0, differences between *stm6* and *stm6_IFR1kd* were significant according to a two-tailed Student's *t*-test ($p < 0.05$).

Figure 6C) declined more slowly in *stm6_IFRkd* vs. *stm6* when cells were cultivated under aerobic sulfur-limiting conditions (0.48 ± 0.01 in *stm6_IFRkd* vs. 0.35 ± 0.02 in *stm6* at $t_{96\,h}$). In summary, these results demonstrate again that a diminished IFR1 level boosts hydrogen production in *C. reinhardtii* and that this effect is based on a sustained residual PSII activity which extends the hydrogen production phase significantly. The correlation between cellular amounts of IFR1 and hydrogen production capacity is further underscored by the diminished hydrogen yields obtained with the *sor1* mutant (Supplementary Figure S4), which overexpresses IFR1 (**Figures 2B,C**), in comparison to its parental strain (4A+).

DISCUSSION

In silico analyses performed with the amino acid sequence of IFR1 revealed that this protein represents an atypical member of the short-chain dehydrogenase/reductase (SDR) superfamily. Several SDRs including IFR1 from *C. reinhardtii* have been suggested to be referred to as NmrA-like family proteins (family designation SDR48A) according to a nomenclature initiative of Persson et al. (2009). Most of these SDRs including IFR1, however, share significantly higher percent identities with isoflavone reductases (*Arabidopsis thaliana* IFR; ∼29% identity to IFR1), IRL proteins (*Zea mays* IRL; ∼29%), phenylcoumaran benzylic ether reductases (PCBER; ∼28%) or eugenol synthases (EGS; ∼24%) from higher plants than with the N metabolite repression protein A (NmrA; ∼20%) from *Aspergillus (Emericella) nidulans* (Supplementary Figure S1 and Table S1). A wide-scale bioinformatics study on SDRs in plant genomes suggested a distinct SDR family for IFR, PCBER and eugenol synthase (family designation SDR460A) and although IFR1 was 1 of 15 *C. reinhardtii* proteins that could not be assigned to any SDR family during that study, a high homology of IFR1 to members of the SDR460A family was claimed, however (Moummou et al., 2012).

In the legume alfalfa (*Medicago sativa*), isoflavone reductase (IFR) catalyzes the stereospecific reduction of 2′-hydroxyformononetin to yield (3R)-vestitone (Dewick, 1977; Paiva et al., 1991) as part of the biosynthesis pathway for the isoflavonoid (−)-medicarpin (Guo and Paiva, 1995). Isoflavonoids and IFRs are almost entirely confined to legumes and, although flavonoids have been identified as sex pheromones in *Chlamydomonas eugamentos* (Birch et al., 1953), no isoflavonoids or IFRs have been reported in *C. reinhardtii* (May et al., 2008; Annamalai and Nallamuthu, 2014). Several IFR-like (IRL) proteins have been cloned from non-leguminous plants (Babiychuk et al., 1995; Petrucco et al., 1996; Shoji et al., 2002; Kim et al., 2003; Hua et al., 2013). Despite their high homology toward IFR proteins, IRL proteins do not accept 2′-hydroxyformononetin as a substrate (Petrucco et al., 1996) and for several higher plant IRLs their specific induction by abiotic stresses such as exposure to reactive oxygen species (Kim et al., 2010) or UV light (Lers et al., 1998) has been demonstrated. For the IRL proteins from maize and rice, a strong negative correlation between cellular glutathione (GSH) levels and the expression level of IRLs was shown (Petrucco et al., 1996). Sulfur depletion, which triggers the accumulation of maize IRL, is a condition known to cause a strong decline of GSH levels in green algae (Salbitani et al., 2015) and higher plants (Kopriva and Rennenberg, 2004). As observed within the present study, *C. reinhardtii* IFR1 also accumulates upon sulfur limitation, whereas its expression is low under stress-free conditions (**Figure 2A**).

In further analogy to IRL proteins from maize and rice, expression of the *C. reinhardtii IFR1* gene is also induced by reactive oxygen species such as hydrogen peroxide (Blaby et al., 2015). Molecular details on the expression regulation of higher plant *IRL* genes have thus far remained obscure, whereas for IFR1 the present study provides strong evidence for the function of an ERE (Fischer et al., 2012) as a *cis*-regulatory *IFR1* promoter sequence required for the accumulation of IFR1 following exposure to reactive electrophiles (**Figures 2B–F**, **3C**). The ERE *cis*-regulatory element (CAACGTTG) was identified as a palindromic sequence overrepresented in the −70 to −340 bp promoter region of genes overexpressed in the *singlet oxygen resistant 1* (*sor1*) mutant and the ERE of *IFR1* lies within this region (−249 bp; **Figure 2D**). It was shown to be required for the induction and overexpression of ROS/RES-defense genes (glutathione-*S*-transferase 1; *GSTS1*) by the lipophilic RES-compound DBMIB in mutant *sor1*. Reporter constructs containing the ERE responded more strongly and much faster to lipophilic RES than to hydrophilic chemicals producing ROS. From this and other results it was therefore concluded that ERE activation via ROS is indirect and based on lipid peroxidation triggered by ROS and generating lipophilic RES such as malondialdehyde (Fischer et al., 2012). Among a variety of ROS- and RES-generating chemicals tested, *GSTS1* reporter constructs containing ERE elements responded most strongly to DBMIB and 2-(*E*)-hexenal (Fischer et al., 2012), and IFR1 transcript (**Figure 2E**) and protein (**Figures 2F**, **3B,C**) accumulates upon treatment of *C. reinhardtii* cells with these compounds. Furthermore, IFR1 mRNA and protein over-accumulate in the *sor1* mutant (**Figures 2B,C**).

In addition to their strong effects on IFR1 expression, the growth-retarding effect of DBMIB and 2-(*E*)-hexenal is more prominent in IFR1 knock-down strains than in their parental strain (**Figures 3E,F**). It is therefore tempting to speculate, that the short-chain dehydrogenase/reductase (SDR) IFR1 might be involved in the detoxification of these compounds, since (SDRs) have already been shown to act as cytosolic aldehyde reductases (CytADRs) in *A. thaliana* (Yamauchi et al., 2011). In principle, highly reactive 2-alkenals from lipid peroxidation can be detoxified either by reduction of the aldehyde group or by reduction of the α, β-unsaturated bond (Mano et al., 2005; Yamauchi et al., 2011). CytADRs catalyze the latter reaction and represent typical SDRs while IFR1 is an atypical SDR (aSDR) according to its NAD(P)H binding motif of the G-X-X-G-X-X-G type (Supplementary Figure S1). Alignment of the IFR1

amino sequence with those of CytADRs from *A. thaliana* revealed percent identities in the range of 19–21%, whereas a *C. reinhardtii* SDR (Cre12.g549852) whose expression is induced by 2-(*E*)-hexenal (Fischer et al., 2012) shows a higher degree of identity to CytADRs (23–25% identity; Supplementary Table S1). In *A. thalinana*, enzymes reducing reactive carbonyls have been identified within the medium-chain dehydrogenase/reductase (MDR) superfamily, NADB_Rossmann (SDR) superfamily and aldo-keto reductase (AKR) superfamily (Yamauchi et al., 2011), but aSDRs implicated in the detoxification of reactive carbonyls have not been identified so far. *In vitro* assays based on NADPH consumption monitored via absorbance change at 340 nm with recombinant IFR1 and 2-(E)-hexenal (data not shown) did not indicate that this compound could represent a substrate *in vivo*.

Apart from the treatment of cell cultures with lipophilic RES, sulfur deprivation is a condition that is associated with IFR1 accumulation (**Figure 2A**). In microalgae sulfur limitation is known to cause the formation of reactive oxygen species (Salbitani et al., 2015), which could in turn trigger lipid peroxidation resulting in the production of reactive carbonyls/RES (Mosblech et al., 2009; Roach et al., 2017). At the same time, the withdrawal of sulfur diminishes the glutathione pool size (Salbitani et al., 2015) and a large pool of reduced glutathione (GSH) protects cellular components (e.g., amino groups from DNA bases or within proteins) against modification by RES via scavenging as GSH-conjugates and subsequent detoxification (Mueller and Berger, 2009). It is therefore possible that *IFR1* induction under sulfur-deplete conditions proceeds via the accumulation of RES, originating from −S-triggered ROS formation and simultaneous impairment of GSH-dependent scavenging, and an activation of the SOR1-dependent pathway. This could also provide an explanation for the finding that nitrogen limitation does not induce IFR1 accumulation, because at least in higher plants, effects of nitrogen deficiency on foliar GSH levels are rather small compared to those exerted by sulfur withdrawal (Koprivova et al., 2000).

Although IFR1 does not seem to be involved in the direct detoxification of RES, a diminished amount of IFR1 reduces RES tolerance in *C. reinhardtii* (**Figures 3E,F**), indicating that IFR1 is somehow implicated in the regulation of RES homeostasis. The precise *in vivo* function of IFR1 within the context of RES homeostasis in *C. reinhardtii* can, however, not be depicted at the moment. Since *in vivo* substrate identification based on *in silico* analyses of SDRs and aSDRs is not feasible, future research on IFR1 will have to comprise the cumbersome screening of compound libraries (Bhatia et al., 2015).

Intriguingly, a knock-down of IFR1 in *C. reinhardtii* boosts hydrogen production (**Figures 4**, **6**). In *C. reinhardtii*, the production of hydrogen can be triggered by sulfur deprivation in air-tight cultures (Melis et al., 2000). A strong down-regulation of the Calvin–Benson cycle is thought to over-reduce the photosynthetic electron transport chain, a condition which promotes the formation of ROS. ROS damage the photosynthetic apparatus, especially photosystem II, and a diminished activity of the PSII repair cycle in the absence of sulfur further contributes to a strong decline in PSII activity, which in turn gradually decreases the oxygen content of cultures, because mitochondrial respiration is less affected by sulfur deprivation (Ghysels and Franck, 2010). A strong decline of PSII activity could also be noted under sulfur limitation in the present study (**Figures 5A,B**, **6C**) and remarkable differences were seen between parental strains and IFR1 knock-down mutants. Interestingly, in strains expressing lower amounts of IFR1, PSII was less susceptible to −S-induced photoinhibition, as could be seen as higher F_v/F_m values (**Figures 5A,B**, **6C**) and a slower decline in the levels of D1 protein (**Figure 5C**), constituting the PSII core complex. The increased stability of PSII in knock-down strains caused a prolonged hydrogen production phase in strains with diminished IFR1 levels. Therefore, the data from the present study nicely underscore the importance of residual water-splitting activity for −S-induced hydrogen production, which was also observed in previous studies (Volgusheva et al., 2013).

The simultaneous occurrence of a higher RES sensitivity and increased stability of PSII as important phenotypic characteristics of *IFR1* knock-strains first seems counterintuitive. In this context, however, it must be emphasized that RES should not be merely viewed as cytotoxic compounds that need be rapidly removed from the cellular metabolism in order to prevent cell damage. Numerous studies indicate a role of RES as important signaling molecules which represent a central component of abiotic stress responses (Yamauchi et al., 2015; Muench et al., 2016). For instance, 2-(*E*)-hexenal has been shown to be a strong inducer of genetic programs activated as part of abiotic stress responses (Copolovici et al., 2012; Yamauchi et al., 2015) and this compound is formed under photooxidative stress conditions [e.g., as experienced by plants devoid of non-photochemical quenching mechanisms (Loreto et al., 2006)]. The PSII-damaging effect of 2-(*E*)-hexenal was found to be rather subtle in higher plants (Yamauchi et al., 2015). Therefore, the more pronounced growth retarding effect of 2-(*E*)-hexenal seen for *IFR1* knock-down strains might be based on mechanisms other than PSII inhibition. Overall, it seems feasible that perturbation of RES-dependent signaling could also result in a higher stress tolerance of cells (e.g., by a diminished threshold for the activation of stress response mechanisms or even their constitutive activation).

As a novel finding, manipulation of RES homeostasis in *C. reinhardtii* can be used to increase photosynthetic hydrogen production. Although the precise molecular function of IFR1 in *Chlamydomonas* is difficult to depict at the moment, the regulation of IFR1 expression via a characterized ERE, its strong over-accumulation in the *sor1* mutant and the lowered RES tolerance indicate that IFR1 is a factor required for RES-dependent signaling or RES handling in this microalga (**Figures 2B–D**, **3E,F**). IFR1 will thus represent an important tool for future studies regarding the role of RES in abiotic stress responses of *C. reinhardtii*.

AUTHOR CONTRIBUTIONS

DV performed most of the experiments; DV, SH, CS, and TB performed and designed experiments; DV, LW, AP, and OK

conceived the project and wrote the article with contributions of all the authors.

FUNDING

This work is supported by the Ministry of Innovation, Science, Research and Technology of the State of North Rhine-Westphalia (MIWFT) as part of the research cooperation "MoRitS - Model-based Realization of intelligent Systems in Nano- and Biotechnologies" (grant no. 321 - 8.03.04.03 - 2012/02).

ACKNOWLEDGMENT

We are grateful to the Center for Biotechnology (CeBiTec) at Bielefeld University for access to the Technology Platforms.

SUPPLEMENTARY MATERIAL

The Supplementary Material for this article can be found online at: http://journal.frontiersin.org/article/10.3389/fpls.2017.01347/full#supplementary-material

REFERENCES

Andrianopoulos, A., Kourambas, S., Sharp, J. A., Davis, M. A., and Hynes, M. J. (1998). Characterization of the *Aspergillus nidulans nmra* gene involved in nitrogen metabolite repression. *J. Bacteriol.* 180, 1973–1977.

Annamalai, J., and Nallamuthu, T. (2014). Antioxidant potential phytochemicals from methanol extract of *Chlorella vulgaris* and *Chlamydomonas reinhardtii*. *J. Algal Biomass Util.* 5, 60–67.

Antal, T. K., Krendeleva, T. E., Laurinavichene, T. V., Makarova, V. V., Ghirardi, M. L., Rubin, A. B., et al. (2003). The dependence of algal H_2 production on Photosystem II and O_2 consumption activities in sulfur-deprived *Chlamydomonas reinhardtii* cells. *Biochim. Biophys. Acta* 1607, 153–160. doi: 10.1016/j.bbabio.2003.09.008

Babbs, C. F., Pham, J. A., and Coolbaugh, R. C. (1989). Lethal hydroxyl radical production in paraquat-treated plants. *Plant Physiol.* 90, 1267–1270. doi: 10.1104/pp.90.4.1267

Babiychuk, E., Kushnir, S., Belles-Boix, E., Van Montagu, M., and Inze, D. (1995). *Arabidopsis thaliana* NADPH oxidoreductase homologs confer tolerance of yeasts toward the thiol-oxidizing drug diamide. *J. Biol. Chem.* 270, 26224–26231. doi: 10.1074/jbc.270.44.26224

Baltz, A., Dang, K.-V., Beyly, A., Auroy, P., Richaud, P., Cournac, L., et al. (2014). Plastidial expression of type II NAD(P)H dehydrogenase increases the reducing state of plastoquinones and hydrogen photoproduction rate by the indirect pathway in *Chlamydomonas reinhardtii*. *Plant Physiol.* 165, 1344–1352. doi: 10.1104/pp.114.240432

Bhatia, C., Oerum, S., Bray, J., Kavanagh, K. L., Shafqat, N., Yue, W., et al. (2015). Towards a systematic analysis of human short-chain dehydrogenases/reductases (SDR): ligand identification and structure-activity relationships. *Chem. Biol. Interact.* 234, 114–125. doi: 10.1016/j.cbi.2014.12.013

Birch, A. J., Donovan, F. W., and Moewus, F. (1953). Biogenesis of flavonoids in *Chlamydomonas eugametos*. *Nature* 172, 902–904. doi: 10.1038/172902a0

Blaby, I. K., Blaby-Haas, C. E., Perez-Perez, M. E., Schmollinger, S., Fitz-Gibbon, S., Lemaire, S. D., et al. (2015). Genome-wide analysis on *Chlamydomonas reinhardtii* reveals the impact of hydrogen peroxide on protein stress responses and overlap with other stress transcriptomes. *Plant J.* 84, 974–988. doi: 10.1111/tpj.13053

Chochois, V., Dauvillee, D., Beyly, A., Tolleter, D., Cuine, S., Timpano, H., et al. (2009). Hydrogen production in *Chlamydomonas*: photosystem II-dependent and -independent pathways differ in their requirement for starch metabolism. *Plant Physiol.* 151, 631–640. doi: 10.1104/pp.109.144576

Copolovici, L., Kannaste, A., Pazouki, L., and Niinemets, U. (2012). Emissions of green leaf volatiles and terpenoids from *Solanum lycopersicum* are quantitatively related to the severity of cold and heat shock treatments. *J. Plant Physiol.* 169, 664–672. doi: 10.1016/j.jplph.2011.12.019

Debuchy, R., Purton, S., and Rochaix, J. D. (1989). The argininosuccinate lyase gene of *Chlamydomonas reinhardtii*: an important tool for nuclear transformation and for correlating the genetic and molecular maps of the ARG7 locus. *EMBO J.* 8, 2803–2809.

Dewick, P. M. (1977). Biosynthesis of pterocarpan phytoalexins in *Trifolium pratense*. *Phytochemistry* 16, 93–97. doi: 10.1016/0031-9422(77)83020-3

Doebbe, A., Keck, M., La Russa, M., Mussgnug, J. H., Hankamer, B., Tekçe, E., et al. (2010). The interplay of proton, electron, and metabolite supply for photosynthetic H(2) production in *Chlamydomonas reinhardtii*. *J. Biol. Chem.* 285, 30247–30260. doi: 10.1074/jbc.M110.122812

Doebbe, A., Rupprecht, J., Beckmann, J., Mussgnug, J. H., Hallmann, A., Hankamer, B., et al. (2007). Functional integration of the *HUP1* hexose symporter gene into the genome of *C. reinhardtii*: impacts on biological H_2 production. *J. Biotechnol.* 131, 27–33. doi: 10.1016/j.jbiotec.2007.05.017

Dubini, A., and Ghirardi, M. L. (2015). Engineering photosynthetic organisms for the production of biohydrogen. *Photosynth. Res.* 123, 241–253. doi: 10.1007/s11120-014-9991-x

Fang, W., Si, Y., Douglass, S., Casero, D., Merchant, S. S., Pellegrini, M., et al. (2012). Transcriptome-wide changes in *Chlamydomonas reinhardtii* gene expression regulated by carbon dioxide and the CO_2-concentrating mechanism regulator CIA5/CCM1. *Plant Cell* 24, 1876–1893. doi: 10.1105/tpc.112.097949

Filling, C., Berndt, K. D., Benach, J., Knapp, S., Prozorovski, T., Nordling, E., et al. (2002). Critical residues for structure and catalysis in short-chain dehydrogenases/reductases. *J. Biol. Chem.* 277, 25677–25684. doi: 10.1074/jbc.M202160200

Fischer, B. B., Krieger-Liszkay, A., and Eggen, R. I. L. (2004). Photosensitizers neutral red (Type I) and rose bengal (Type II) cause light-dependent toxicity in *Chlamydomonas reinhardtii* and induce the *Gpxh* gene via increased singlet oxygen formation. *Environ. Sci. Technol.* 38, 6307–6313. doi: 10.1021/es049673y

Fischer, B. B., Ledford, H. K., Wakao, S., Huang, S. G., Casero, D., Pellegrini, M., et al. (2012). *SINGLET OXYGEN RESISTANT 1* links reactive electrophile signaling to singlet oxygen acclimation in *Chlamydomonas reinhardtii*. *Proc. Natl. Acad. Sci. U.S.A.* 109, E1302–E1311. doi: 10.1073/pnas.1116843109

Gaffron, H., and Rubin, J. (1942). Fermentative and photochemical production of hydrogen in algae. *J. Gen. Physiol.* 26, 219–240. doi: 10.1085/jgp.26.2.219

Ghirardi, M. L., Togasaki, R. K., and Seibert, M. (1997). Oxygen sensitivity of algal H_2-production. *Appl. Biochem. Biotechnol.* 6, 141–151. doi: 10.1007/BF02920420

Ghysels, B., and Franck, F. (2010). Hydrogen photo-evolution upon S deprivation stepwise: an illustration of microalgal photosynthetic and metabolic flexibility and a step stone for future biotechnological methods of renewable H_2 production. *Photosynth. Res.* 106, 145–154. doi: 10.1007/s11120-010-9582-4

González-Ballester, D., Casero, D., Cokus, S., Pellegrini, M., Merchant, S. S., and Grossman, A. R. (2010). RNA-seq analysis of sulfur-deprived *Chlamydomonas* cells reveals aspects of acclimation critical for cell survival. *Plant Cell* 22, 2058–2084. doi: 10.1105/tpc.109.071167

Grossman, A. R., Catalanotti, C., Yang, W., Dubini, A., Magneschi, L., Subramanian, V., et al. (2011). Multiple facets of anoxic metabolism and hydrogen production in the unicellular green alga *Chlamydomonas reinhardtii*. *New Phytol.* 190, 279–288. doi: 10.1111/j.1469-8137.2010.03534.x

Guo, L., and Paiva, N. L. (1995). Molecular cloning and expression of alfalfa (*Medicago sativa* L.) vestitone reductase, the penultimate enzyme in medicarpin biosynthesis. *Arch. Biochem. Biophys.* 320, 353–360. doi: 10.1016/0003-9861(95)90019-5

Harris, E. H. (1989). *The Chlamydomonas Sourcebook: A Comprehensive Guide to Biology and Laboratory Use*. San Diego, CA: Academic Press.

Hua, C., Linling, L., Feng, X., Yan, W., Honghui, Y., Conghua, W., et al. (2013). Expression patterns of an isoflavone reductase-like gene and its possible roles in secondary metabolism in *Ginkgo biloba*. *Plant Cell Rep.* 32, 637–650. doi: 10.1007/s00299-013-1397-2

Jaeger, D., Hübner, W., Huser, T., Mussgnug, J. H., and Kruse, O. (2017). Nuclear transformation and functional gene expression in the oleaginous microalga *Monoraphidium neglectum*. *J. Biotechnol.* 249, 10–11. doi: 10.1016/j.jbiotec.2017.03.011

Kavanagh, K. L., Jörnvall, H., Persson, B., and Oppermann, U. (2008). Medium- and short-chain dehydrogenase/reductase gene and protein families: the SDR superfamily: functional and structural diversity within a family of metabolic and regulatory enzymes. *Cell Mol. Life Sci.* 65, 3895–3906. doi: 10.1007/s00018-008-8588-y

Kim, S. G., Kim, S. T., Wang, Y., Kim, S. K., Lee, C. H., Kim, K. K., et al. (2010). Overexpression of rice isoflavone reductase-like gene (*OsIRL*) confers tolerance to reactive oxygen species. *Physiol. Plant.* 138, 1–9. doi: 10.1111/j.1399-3054.2009.01290.x

Kim, S. T., Cho, K. S., Kim, S. G., Kang, S. Y., and Kang, K. Y. (2003). A rice isoflavone reductase-like gene, OsIRL, is induced by rice blast fungal elicitor. *Mol. Cells* 16, 224–231.

Kindle, K. L. (1990). High-frequency nuclear transformation of *Chlamydomonas reinhardtii*. *Proc. Natl. Acad. Sci. U.S.A.* 87, 1228–1232. doi: 10.1073/pnas.87.3.1228

Kopriva, S., and Rennenberg, H. (2004). Control of sulphate assimilation and glutathione synthesis: interaction with N and C metabolism. *J. Exp. Bot.* 55, 1831–1842. doi: 10.1093/jxb/erh203

Koprivova, A., Suter, M., den Camp, R. O., Brunold, C., and Kopriva, S. (2000). Regulation of sulfate assimilation by nitrogen in Arabidopsis. *Plant Physiol.* 122, 737–746. doi: 10.1104/pp.122.3.737

Kremers, G. J., Goedhart, J., van Munster, E. B., and Gadella, T. W. Jr. (2006). Cyan and yellow super fluorescent proteins with improved brightness, protein folding, and FRET Forster radius. *Biochemistry* 45, 6570–6580. doi: 10.1021/bi0516273

Kruse, O., Rupprecht, J., Bader, K. P., Thomas-Hall, S., Schenk, P. M., Finazzi, G., et al. (2005). Improved photobiological H_2 production in engineered green algal cells. *J. Biol. Chem.* 280, 34170–34177. doi: 10.1074/jbc.M503840200

Lauersen, K. J., Kruse, O., and Mussgnug, J. H. (2015). Targeted expression of nuclear transgenes in *Chlamydomonas reinhardtii* with a versatile, modular vector toolkit. *Appl. Microbiol. Biotechnol.* 99, 3491–3503. doi: 10.1007/s00253-014-6354-7

Lers, A., Burd, S., Lomaniec, E., Droby, S., and Chalutz, E. (1998). The expression of a grapefruit gene encoding an isoflavone reductase-like protein is induced in response to UV irradiation. *Plant Mol. Biol.* 36, 847–856. doi: 10.1023/A:1005996515602

Loreto, F., Barta, C., Brilli, F., and Nogues, I. (2006). On the induction of volatile organic compound emissions by plants as consequence of wounding or fluctuations of light and temperature. *Plant Cell Environ.* 29, 1820–1828. doi: 10.1111/j.1365-3040.2006.01561.x

Louie, G. V., Baiga, T. J., Bowman, M. E., Koeduka, T., Taylor, J. H., Spassova, S. M., et al. (2007). Structure and reaction mechanism of basil eugenol synthase. *PLoS ONE* 2:e993. doi: 10.1371/journal.pone.0000993

Lubitz, W., Ogata, H., Rudiger, O., and Reijerse, E. (2014). Hydrogenases. *Chem Rev.* 114, 4081–4148. doi: 10.1021/cr4005814

Mano, J., Belles-Boix, E., Babiychuk, E., Inze, D., Torii, Y., Hiraoka, E., et al. (2005). Protection against photooxidative injury of tobacco leaves by 2-alkenal reductase. Detoxication of lipid peroxide-derived reactive carbonyls. *Plant Physiol.* 139, 1773–1783. doi: 10.1104/pp.105.070391

Maxwell, K., and Johnson, G. N. (2000). Chlorophyll fluorescence-a practical guide. *J. Exp. Bot.* 51, 659–668. doi: 10.1093/jxb/51.345.659

May, P., Wienkoop, S., Kempa, S., Usadel, B., Christian, N., Rupprecht, J., et al. (2008). Metabolomics- and proteomics-assisted genome annotation and analysis of the draft metabolic network of *Chlamydomonas reinhardtii*. *Genetics* 179, 157–166. doi: 10.1534/genetics.108.088336

Melis, A., Zhang, L., Forestier, M., Ghirardi, M. L., and Seibert, M. (2000). Sustained photobiological hydrogen gas production upon reversible inactivation of oxygen evolution in the green alga *Chlamydomonas reinhardtii*. *Plant Physiol.* 122, 127–136. doi: 10.1104/pp.122.1.127

Metz, J. G., Pakrasi, H. B., Seibert, M., and Arntzer, C. J. (1986). Evidence for a dual function of the herbicide-binding D1 protein in photosystem II. *FEBS Lett.* 205, 269–274. doi: 10.1016/0014-5793(86)80911-5

Miller, R., Wu, G., Deshpande, R. R., Vieler, A., Gartner, K., Li, X., et al. (2010). Changes in transcript abundance in *Chlamydomonas reinhardtii* following nitrogen deprivation predict diversion of metabolism. *Plant Physiol.* 154, 1737–1752. doi: 10.1104/pp.110.165159

Min, T., Kasahara, H., Bedgar, D. L., Youn, B., Lawrence, P. K., Gang, D. R., et al. (2003). Crystal structures of pinoresinol-lariciresinol and phenylcoumaran benzylic ether reductases and their relationship to isoflavone reductases. *J. Biol. Chem.* 278, 50714–50723. doi: 10.1074/jbc.M308493200

Molnar, A., Bassett, A., Thuenemann, E., Schwach, F., Karkare, S., Ossowski, S., et al. (2009). Highly specific gene silencing by artificial microRNAs in the unicellular alga *Chlamydomonas reinhardtii*. *Plant J.* 58, 165–174. doi: 10.1111/j.1365-313X.2008.03767.x

Mosblech, A., Feussner, I., and Heilmann, I. (2009). Oxylipins: structurally diverse metabolites from fatty acid oxidation. *Plant Physiol. Biochem.* 47, 511–517. doi: 10.1016/j.plaphy.2008.12.011

Moummou, H., Kallberg, Y., Tonfack, L. B., Persson, B., and van der Rest, B. (2012). The plant short-chain dehydrogenase (SDR) superfamily: genome-wide inventory and diversification patterns. *BMC Plant Biol.* 12:219. doi: 10.1186/1471-2229-12-219

Mueller, M. J., and Berger, S. (2009). Reactive electrophilic oxylipins: pattern recognition and signalling. *Phytochemistry* 70, 1511–1521. doi: 10.1016/j.phytochem.2009.05.018

Muench, M., Hsin, C. H., Ferber, E., Berger, S., and Mueller, M. J. (2016). Reactive electrophilic oxylipins trigger a heat stress-like response through HSFA1 transcription factors. *J. Exp. Bot.* 67, 6139–6148. doi: 10.1093/jxb/erw376

Nelson, J. A., Savereide, P. B., and Lefebvre, P. A. (1994). The CRY1 gene in *Chlamydomonas reinhardtii*: structure and use as a dominant selectable marker for nuclear transformation. *Mol. Cell. Biol.* 14, 4011–4019. doi: 10.1128/MCB.14.6.4011

Neupert, J., Karcher, D., and Bock, R. (2009). Generation of *Chlamydomonas* strains that efficiently express nuclear transgenes. *Plant J.* 57, 1140–1150. doi: 10.1111/j.1365-313X.2008.03746.x

Nguyen, A. V., Toepel, J., Burgess, S., Uhmeyer, A., Blifernez, O., Doebbe, A., et al. (2011). Time-course global expression profiles of *Chlamydomonas reinhardtii* during photo-biological H_2 production. *PLoS ONE* 6:e29364. doi: 10.1371/journal.pone.0029364

Organisation for Economic Co-operation and Development [OECD]/International Energy Agency [IEA] (2011). *OECD Green Growth Studies: Energy*. Available at: http://www.oecd.org/greengrowth/greening-energy/49157219.pdf

Paiva, N. L., Edwards, R., Sun, Y., Hrazdina, G., and Dixon, R. A. (1991). Stress responses in alfalfa (*Medicago sativa* L.) 11. Molecular cloning and expression of alfalfa isoflavone reductase, a key enzyme of isoflavonoid phytoalexin biosynthesis. *Plant Mol. Biol.* 17, 653–667. doi: 10.1007/BF00037051

Persson, B., Kallberg, Y., Bray, J. E., Bruford, E., Dellaporta, S. L., Favia, A. D., et al. (2009). The SDR (short-chain dehydrogenase/reductase and related enzymes) nomenclature initiative. *Chem. Biol. Interact.* 178, 94–98. doi: 10.1016/j.cbi.2008.10.040

Persson, B., Kallberg, Y., Oppermann, U., and Jornvall, H. (2003). Coenzyme-based functional assignments of short-chain dehydrogenases/reductases (SDRs). *Chem. Biol. Interact.* 14, 271–278. doi: 10.1016/S0009-2797(02)00223-5

Petrucco, S., Bolchi, A., Foroni, C., Percudani, R., Rossi, G. L., and Ottonello, S. (1996). A maize gene encoding an NADPH binding enzyme highly homologous to isoflavone reductases is activated in response to sulfur starvation. *Plant Cell* 8, 69–80. doi: 10.1105/tpc.8.1.69

Pfaffl, M. W. (2001). A new mathematical model for relative quantification in real-time RT-PCR. *Nucleic Acids Res.* 29:e45. doi: 10.1093/nar/29.9.e45

Roach, T., Baur, T., Stoggl, W., and Krieger-Liszkay, A. (2017). *Chlamydomonas reinhardtii* responding to high light: a role for 2-propenal (acrolein). *Physiol. Plant.* doi: 10.1111/ppl.12567 [Epub ahead of print].

Salbitani, G., Vona, V., Bottone, C., Petriccione, M., and Carfagna, S. (2015). Sulfur deprivation results in oxidative perturbation in *Chlorella sorokiniana* (211/8k). *Plant Cell Physiol.* 56, 897–905. doi: 10.1093/pcp/pcv015

Schönfeld, C., Wobbe, L., Borgstadt, R., Kienast, A., Nixon, P. J., and Kruse, O. (2004). The nucleus-encoded protein MOC1 is essential for mitochondrial light acclimation in *Chlamydomonas reinhardtii*. *J. Biol. Chem.* 279, 50366–50374. doi: 10.1074/jbc.M408477200

Scoma, A., Durante, L., Bertin, L., and Fava, F. (2014). Acclimation to hypoxia in *Chlamydomonas reinhardtii*: Can biophotolysis be the major trigger for long-term H_2 production? *New Phytol.* 204, 890–900. doi: 10.1111/nph.12964

Shoji, T., Winz, R., Iwase, T., Nakajima, K., Yamada, Y., and Hashimoto, T. (2002). Expression patterns of two tobacco isoflavone reductase-like genes and their possible roles in secondary metabolism in tobacco. *Plant Mol. Biol.* 50, 427–440. doi: 10.1023/A:1019867732278

Steinbeck, J., Nikolova, D., Weingarten, R., Johnson, X., Richaud, P., Peltier, G., et al. (2015). Deletion of proton gradient regulation 5 (PGR5) and PGR5-Like 1 (PGRL1) proteins promote sustainable light-driven hydrogen production in *Chlamydomonas reinhardtii* due to increased PSII activity under sulfur deprivation. *Front. Plant Sci.* 6:892. doi: 10.3389/fpls.2015.00892

Tardif, M., Atteia, A., Specht, M., Cogne, G., Rolland, N., Brugiere, S., et al. (2012). PredAlgo: a new subcellular localization prediction tool dedicated to green algae. *Mol. Biol. Evol.* 29, 3625–3639. doi: 10.1093/molbev/mss178

Toepel, J., Illmer-Kephalides, M., Jaenicke, S., Straube, J., May, P., Goesmann, A., et al. (2013). New insights into *Chlamydomonas reinhardtii* hydrogen production processes by combined microarray/RNA-seq transcriptomics. *Plant Biotechnol. J.* 11, 717–733. doi: 10.1111/pbi.12062

Uhmeyer, A., Ballottari, M., Cecchin, M., and Wobbe, L. (2017). Impaired mitochondrial transcription termination disrupts the stromal redox poise in *Chlamydomonas*. *Plant Physiol.* 174, 1399–1419. doi: 10.1104/pp.16.00946

Vass, I., Styring, S., Hundal, T., Koivuniemi, A., Aro, E., and Andersson, B. (1992). Reversible and irreversible intermediates during photoinhibition of photosystem II: stable reduced QA species promote chlorophyll triplet formation. *Proc. Natl. Acad. Sci. U.S.A.* 89, 1408–1412. doi: 10.1073/pnas.89.4.1408

Volgusheva, A., Styring, S., and Mamedov, F. (2013). Increased photosystem II stability promotes H2 production in sulfur-deprived *Chlamydomonas reinhardtii*. *Proc. Natl. Acad. Sci. U.S.A.* 110, 7223–7228. doi: 10.1073/pnas.1220645110

Volgusheva, A. A., Zagidullin, V. E., Antal, T. K., Korvatovsky, B. N., Krendeleva, T. E., Paschenko, V. Z., et al. (2007). Examination of chlorophyll fluorescence decay kinetics in sulfur deprived algae *Chlamydomonas reinhardtii*. *Biochim. Biophys. Acta* 1767, 559–564. doi: 10.1016/j.bbabio.2007.04.006

Wykoff, D. D., Davies, J. P., Melis, A., and Grossman, A. R. (1998). The regulation of photosynthetic electron transport during nutrient deprivation in *Chlamydomonas reinhardtii*. *Plant Physiol.* 117, 129–139. doi: 10.1104/pp.117.1.129

Yamauchi, Y., Hasegawa, A., Taninaka, A., Mizutani, M., and Sugimoto, Y. (2011). NADPH-dependent reductases involved in the detoxification of reactive carbonyls in plants. *J. Biol. Chem.* 286, 6999–7009. doi: 10.1074/jbc.M110.202226

Yamauchi, Y., Kunishima, M., Mizutani, M., and Sugimoto, Y. (2015). Reactive short-chain leaf volatiles act as powerful inducers of abiotic stress-related gene expression. *Sci. Rep.* 5:8030. doi: 10.1038/srep08030

Zhang, L., Happe, T., and Melis, A. (2002). Biochemical and morphological characterization of sulfur-deprived and H_2-producing *Chlamydomonas reinhardtii* (green alga). *Planta* 214, 552–561. doi: 10.1007/s004250100660

Zheng, H.-Q., Chiang-Hsieh, Y.-F., Chien, C.-H., Hsu, B.-K. J., Liu, T.-L., Chen, C.-N. N., et al. (2014). AlgaePath: comprehensive analysis of metabolic pathways using transcript abundance data from next-generation sequencing in green algae. *BMC Genomics* 15:196. doi: 10.1186/1471-2164-15-196

Conflict of Interest Statement: The authors declare that the research was conducted in the absence of any commercial or financial relationships that could be construed as a potential conflict of interest.

Advantages of publishing in Frontiers

OPEN ACCESS
Articles are free to read for greatest visibility and readership

FAST PUBLICATION
Around 90 days from submission to decision

HIGH QUALITY PEER-REVIEW
Rigorous, collaborative, and constructive peer-review

TRANSPARENT PEER-REVIEW
Editors and reviewers acknowledged by name on published articles

Frontiers
Avenue du Tribunal-Fédéral 34
1005 Lausanne | Switzerland

Visit us: www.frontiersin.org
Contact us: info@frontiersin.org | +41 21 510 17 00

REPRODUCIBILITY OF RESEARCH
Support open data and methods to enhance research reproducibility

DIGITAL PUBLISHING
Articles designed for optimal readership across devices

FOLLOW US
@frontiersin

IMPACT METRICS
Advanced article metrics track visibility across digital media

EXTENSIVE PROMOTION
Marketing and promotion of impactful research

LOOP RESEARCH NETWORK
Our network increases your article's readership